USGS-OFR-95-698

U. S. DEPARTMENT OF THE INTERIOR

U. S. GEOLOGICAL SURVEY

SEISMIC IMAGING OF KILAUEA VOLCANO AND LOIHI SEAMOUNT: 1994 ONSHORE-OFFSHORE EXPERIMENT DATA FROM THE HAWAIIAN VOLCANO OBSERVATORY SEISMIC NETWORK

By

Laura S. L. Kong[1], Paul G. Okubo[1], Spahr C. Webb[2], Fred K. Duennebier[3],

Mark A. McDonald[2], Wayne C. Crawford[2], and John A. Hildebrand[2]

Open-File Report 95-698

[1] U. S. Geological Survey, Hawaiian Volcano Observatory, P. O. Box 51, Hawaii National Park, HI 96718

[2] Scripps Institution of Oceanography, Marine Physical Laboratory, A-0205, 9500 Gilman Drive, La Jolla, CA 92093-0205

[3] University of Hawaii, School of Ocean and Earth Science and Technology, 2525 Correa Rd., Honolulu, HI 96822

Hawaii National Park, Hawaii
1995

CONTENTS

FIGURES

TABLES

ABSTRACT

An active-source offshore-onshore seismic experiment was conducted in February, 1994, to constrain the three-dimensional seismic velocity structure of Kilauea volcano, Mauna Loa's southern flank, and Loihi Seamount. The collaborative project, between the U. S. Geological Survey / Hawaiian Volcano Observatory (USGS/HVO), the University of California at San Diego / Scripps Institute of Oceanography (UCSD/SIO), and the University of Hawaii at Manoa / School of Ocean and Earth Science and Technology (UH/SOEST), was also conducted as a feasibility study to investigate the efficiency of seismic energy propagation from a marine source to land stations. In this experiment, 200 km of seismic lines were collected using a 4-element air gun array (2775 cu in, 45.5 liters) fired at 100-150 m intervals. Three lines were shot between the coast and over Loihi Seamount, two lines across the summit of Loihi, one line parallel to the shore, and a single line was shot from the present coastal lava entry point seaward over the submarine portion of the south flank. Line lengths ranged up to 45 km. The data were recorded by the 52-station permanent HVO seismic network supplemented by three portable seismometers on land, and four ocean-bottom instruments, 10 sonobuoys, and a 6-channel seismic streamer at sea. This report describes the experiment, provides locations and times of the seismic shooting, documents procedures followed to reduce the HVO seismic network data, and includes record sections for all useable data recorded by the HVO network. Data recorded by the temporary receivers deployed on land and at sea are presented in a companion Open File Report. Data from the HVO network demonstrate that P wave energy is clearly identifiable on a majority of Kilauea's seismic stations out to 40-50 km range, and coherently detectable out to ranges as great at 95 km. The results of this study imply that with a larger air gun source, we can expect to observe first-arriving energy to distances enabling us to seismically image the volcanoes, oceanic crust, and uppermost mantle.

INTRODUCTION

The Hawaiian Islands are located at the southern end of the Hawaiian-Emperor volcanic chain, a chain of more than 107 individual volcanoes stretching 6000 km across the northern Pacific Ocean (*Clague and Dalrymple*, 1987). Active volcanism is centered on the island of Hawaii beneath Kilauea and Mauna Loa volcanoes, and on Loihi Seamount, located about 35 km to the south and the youngest expression of the Hawaiian hot spot (Figure 1). Recent GLORIA surveys verify that slumps and landslide debris avalanches extend far out onto the sea floor from the flanks of Hawaiian volcanoes (*Moore et al.*, 1989). On the island of Hawaii, there are at least seven major landslides, including the Hilina slump, a 100-km wide, active landslide involving most of the south flank of Kilauea, and its active Hilina Fault System, a major dislocation feature in the slump (Figure 1).

When magma intrudes into the volcano's rift zones, lateral stresses accumulate in its adjacent flanks and are eventually released through large earthquakes that move the flank seaward. The most seismically-hazardous flanks are those adjacent to active rift zones, such as the south flank of Kilauea and the flanks of Mauna Loa (Figure 2). Measurements of lateral slip along a detachment surface, and gravitational subsidence along normal faults of the unbuttressed south flank of Kilauea, reveal movements of 6-10 cm/yr (*Owen et al.*, 1993, *Delaney et al.*, 1993). After the 1975 Kalapana earthquake (M 7.2), geodetic data indicated that much of the south coast had subsided up to 3.5 m and moved seaward as much as 8 m, and that a 30-km segment of the Hilina fault system had been reactivated (*Lipman et al.*, 1985). The distribution of seismicity and earthquake faulting suggested that the movement occurs along slip surfaces within the brittle edifice and along a ~10-km deep decollement zone thought to contain either viscous magma (*Swanson et al.*, 1976, *Clague and Denlinger*, 1994), and/or ocean-derived sedimentary material (*Nakamura*, 1980). The depth and thickness of this zone are still poorly known.

Although the measured displacements of the unbuttressed south flank of Kilauea are directed uniformly seaward, the pattern of vertical and horizontal movement also shows the response of the summit caldera and rift zones to the movement of magma (e.g., *Delaney et al.*, 1990, 1993). The long-term deformation or slumping therefore results not only from the gravitational instability of the volcano flank and the episodic large-scale contributions from earthquakes, but also from the inflation of the summit reservoir, forceful injection into the rift zones, and readjustment of the volcano after large earthquakes and to the basaltic loading from eruptions (*Swanson et al.*, 1976; *Lipman et al.*, 1985; *Tilling and Dvorak*, 1993).

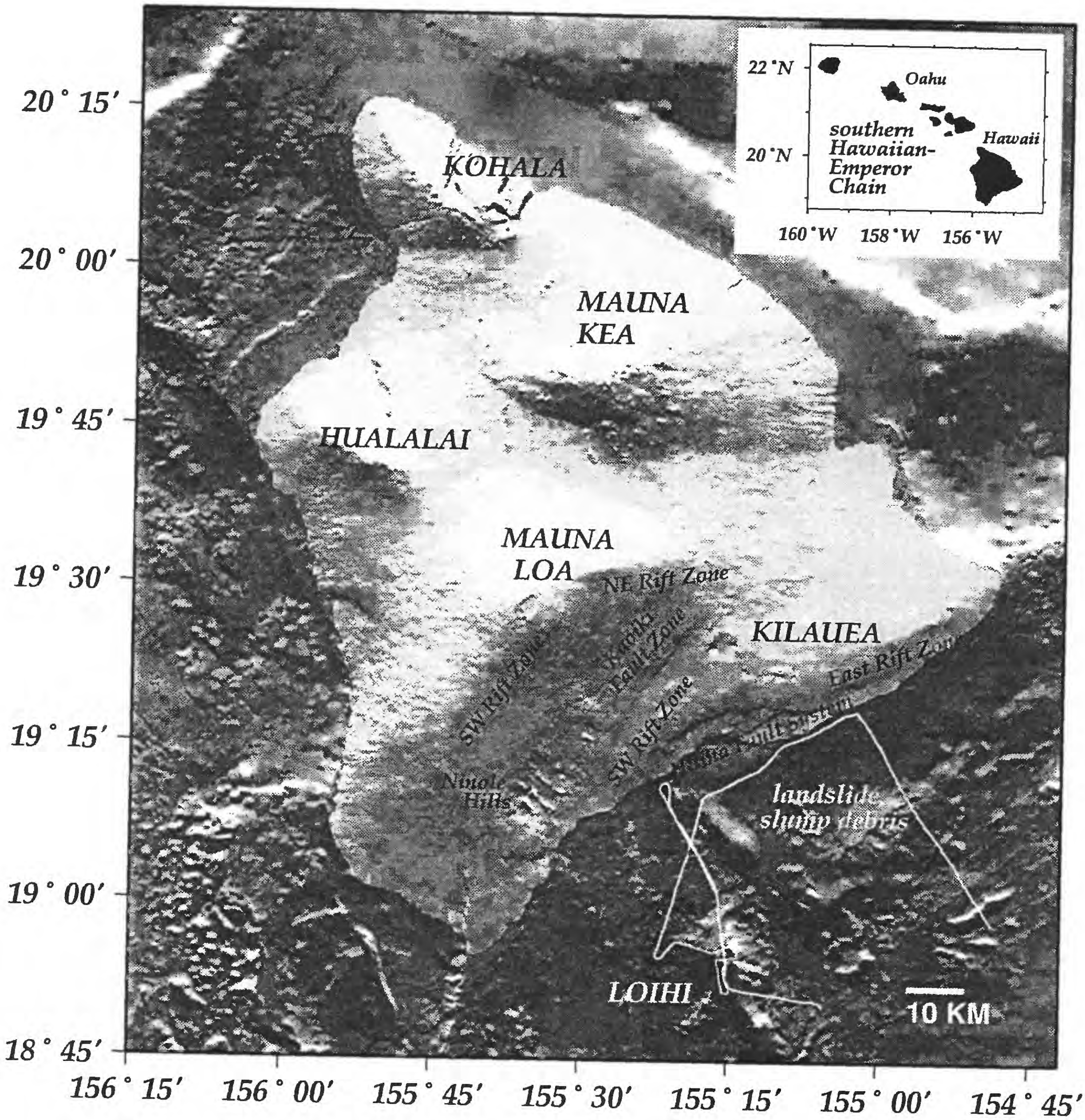

Figure 1. Shaded relief map of the island of Hawaii showing the locations of the five major volcanoes and active fault systems associated with Kilauea and Mauna Loa volcanoes. Shot lines from 1994 experiment shown in white. Bathymetry compilation provided by J. R. Smith and T. Duennebier.

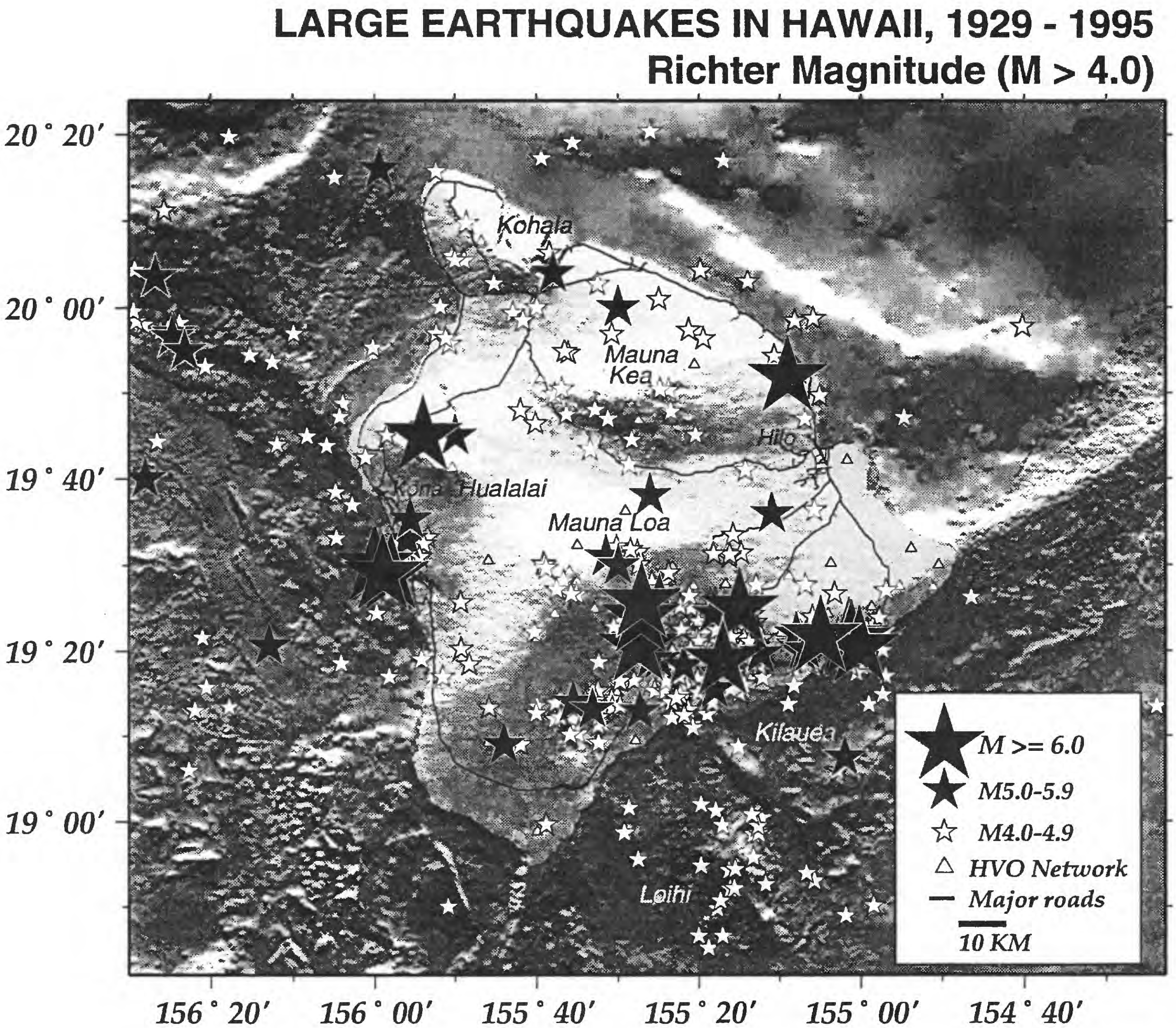

Figure 3. Moderate to large earthquakes instrumentally-recorded on the island of Hawaii since 1929 (M > 4). Tectonic earthquakes associated with movements of the flanks of the active Kilauea and Mauna Loa volcanoes represent the main seismic hazard in Hawaii. The last damaging lithospheric earthquake occurred north of Hilo in 1973 (M6.2). Bathymetry compilation provided by J. R. Smith and T. Duennebier.

OBJECTIVES

While several active-source seismic experiments have been conducted to determine the crustal structure of Hawaii island, most of these have been at intermediate scales and/or have characterized the structure by a simple plane-layered velocity function. Refraction studies (*Ryall and Bennett*, 1968; *Hill*, 1969; *Zucca and Hill*, 1980; *Zucca et al.*, 1982), conducted more than 15 years ago, were only able to map regional structures because of limitations in source and receiver availability; only explosives were used at 2-10 km shot intervals and receiver spacing ranged from 500 m to 10's of km. These studies are thus unable to distinguish details in the volcano-tectonic models that are now being proposed for Kilauea's south flank. In addition, a number of seismic tomography studies have been carried out using earthquake sources to determine the velocity structure beneath Kilauea volcano (*Ellsworth and Koyanagi*, 1977; *Thurber*, 1984; *Rowan and Clayton*, 1993). While these studies had the advantage of tens of thousands of sources, resolution was poor in important parts of the imaged volume because of the non-uniform spatial distribution of seismicity.

To resolve the continuity of structures smaller than several hundreds of meters, an active-source offshore-onshore seismic experiment was conducted in February, 1994, to investigate the efficiency of seismic energy propagation from a marine source to land-based stations, and to obtain data to constrain the three dimensional (3-D) seismic velocity structure of Kilauea volcano, Mauna Loa's southern flank, and Loihi Seamount (*Kong et al.*, 1994, Figure 3).

Results from the 1994 Kilauea-Loihi Crustal Imaging Experiment will be used, in conjunction with earthquake hypocentral locations, focal mechanisms, deformation, geological data, and previous seismic refraction and tomography results, to derive a model for the slippage of Kilauea's south flank. A seismic image of the decollement zone will address the causes of the large earthquakes, and the geometry and topography of this zone may shed light on understanding the relationships between gravitational sliding, small-magnitude seismicity, large earthquakes, and volcanism in this dynamic environment.

DATA ACQUISITION

During the Kilauea-Loihi Crustal Imaging Experiment (*Kong et al.*, 1994), 200 km of seismic shot lines were collected over a 29-hour time period during a four-day cruise in February, 1994 (Table 1). The seismic lines were shot with a 4-element air gun array (2775 cu in) digitally fired at 1-minute intervals at ship speed ranging from 3.5-5 kts (110-140 m shot spacing) from *the R/V Moana Wave* (Figure 3). Using Global Positioning System (GPS) navigation and timing, three seismic lines were shot between

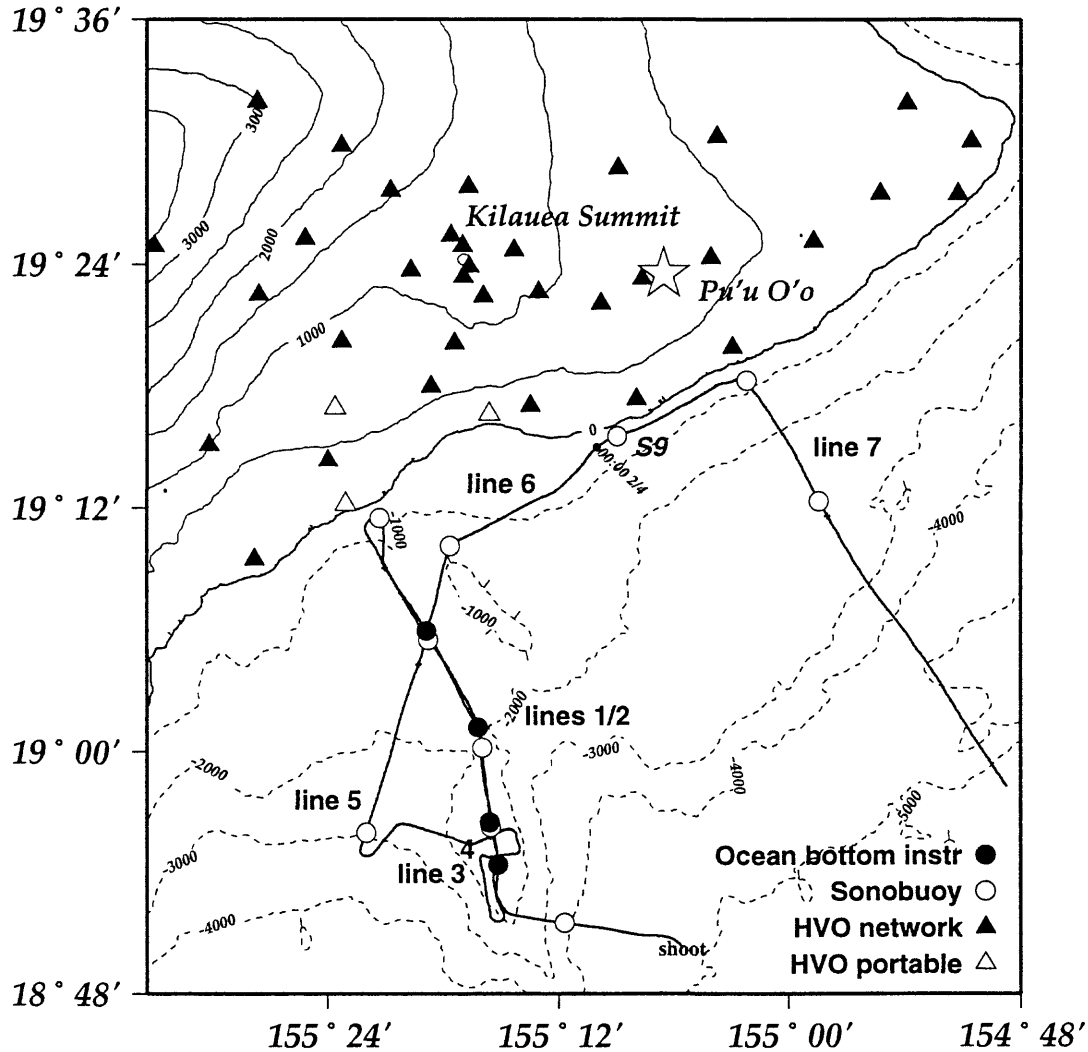

Figure 3. Shot lines and receivers for the 1994 Kilauea-Loihi Crustal Imaging Experiment. Elevation and water depth in meters.

Table 1. Seismic Source, Shooting Schedule, and Line Locations

SOURCE:	4 Air Guns (total 2775 cu. in., 45.5 liters), with 4 Floats (35' tow cable) (port to starboard guns: 760, 640, 550, 825 cu. in.) (gun tow cable : 90', 100', 104', 103'6")
SHOOTING:	Start: 0249Z 3Feb94 (1438 HST), Line 1 (2 guns for 1st 1.75 hrs) Stop: 0745Z 4Feb94 (2145 HST), Line 7 Total Shooting Time: 28.9 hrs Nominal Ship Speed: 3.5-4.0 kts Shot Interval / Shot Spacing: 1 minute / 108-123 m Total Length of Shot Lines: 200 km
TIMING & NAVIGATION:	Computer-based Digital Firing System Kinemetrics Truetime GPS shipboard clock for shot times/ship locations

SHOT LINES:

	Start			End			
Line	Time (Z)	Lat (N)	Lon (W)	Time	Lat (N)	Lon (W)	Location
1	3Feb 0249	18° 51.93'	155°14.40'	0832	19° 10.76'	155°21.96'	Loihi to shore (SN)
2a	0832	19° 10.76'	155°21.96'	0900	19° 11.15'	155°21.12'	turn to line 2
2	0900	19° 11.15'	155°21.12'	1408	18° 51.94'	155°14.83'	Shore to Loihi (NS)
3a	1408	18° 51.94'	155°14.83'	1501	18° 54.74'	155°16.04'	transit to line 3
3	1501	18° 54.74'	155°16.04'	1529	18° 54.95'	155°14.21'	Cross-Loihi (WE)
4a	1529	18° 54.95'	155°14.21'	1542	18° 55.88'	155°14.20'	transit to line4
4	1542	18° 55.88'	155°14.20'	1613	18° 55.43'	155°16.51'	Cross-Loihi (EW)
5a	1613	18° 55.43'	155°16.51'	1743	18° 55.01'	155°22.28'	transit to line 5
5	1743	18° 55.01'	155°22.28'	2132	19° 10.00'	155°17.68'	SW to shore
6	3 Feb 2132	19° 10.00'	155°17.68'	4 Feb 0156	19° 18.40'	155° 2.53'	Along-shore (WE)
7	0156	19° 18.40'	155° 2.53'	0745	18° 58.25'	154°48.73'	South Flank (NS)

Hawaiian Standard Time = Greenwich Mean Time - 10 the coast and over Loihi Seamount (Lines 1, 2, 5), two lines across the summit of Loihi (Lines 3 and 4), one line parallel to the shore (Line 6), and a single line was shot from the present coastal lava entry point seaward over the submarine portion of the south flank (Line 7). Lines 1 and 2 were 37 km long, Lines 3 and 4 across the summit 4 km long, Lines 5 and 6 were 30 km, and Line 7 was 45 km in length. GPS-based ship locations (WGS 84 datum, estimated error 20-50 m) were logged on a computer for use in processing the data and creating SEG-Y station files of the shots. A shipboard GPS clock (estimated accuracy of 0.1 ms) was used to trigger the air gun system, which in turn synchronized the firing of the individual guns by calculating delays based on gun size. The data were recorded by the 52-station permanent HVO seismic network (Table 2, Figures 4 - 6) supplemented by three portable seismometers on land, and one ocean-bottom seismometer, three ocean-bottom hydrophones, 10 sonobuoys, and a 6-channel multi-channel seismic streamer at sea. The ocean bottom instrumentation was concentrated on Loihi seamount, with two instruments located on the summit and one at the base of the seamount along the north rift zone; the last instrument was located about halfway between Loihi and the shore along the shot lines in order to obtain shallow crustal velocity information in this region (Figure 3).

This report only describes data that were recorded by the Hawaiian Volcano Observatory permanent seismic network. Data recorded by the temporary receivers, which included three portable seismic recorders deployed on land, three ocean bottom hydrophones, one ocean bottom seismometer, nine sonobuoys, and multi-channel seismic data recorded on a 6-channel seismic streamer, are presented in a companion Open File Report.

The U. S. Geological Survey Hawaiian Volcano Observatory operates an extensive, short-period (1.0 Hz geophones), high-gain, permanent seismic network located on the island of Hawaii for volcano hazard mitigation purposes. The network is most dense about the active volcanoes of Kilauea and Mauna Loa, and during the 1994 experiment, consisted of 52 seismograph stations, 13 of which were three-component stations. Station locations are derived from U. S. Geological Survey, 7.5 minute topographic quadrangle sheets (1:24,000 scale), which utilize the Hawaii coordinate system map projection (zone 1, transverse Mercator based on 1866 Clark spheroid, Old Hawaiian Datum (OHD)); estimated location uncertainties are less than 100 m. Seismic data are radio-telemetered back to HVO in real time, where they are automatically processed using the Caltech-USGS Seismic Processing System (CUSP), a VAX VMS-based seismic system encompassing digitization of incoming analog data, real time subnet triggering, phase association and location of events, off-line analysis of earthquakes, and efficient and logical archival and retrieval of both triggered events and continuously-recorded data streams.

TABLE 2. HVO STATION LOCATIONS, SHOT RANGES, AND AZIMUTHS FOR LINES 1, 2, 5, 6, AND 7.

				LINE 1				LINE 2				LINE 5				LINE 6				LINE 7			
STA	LON,° W	LAT,° N	ELE,m	RANGE,km		AZIM,°		RANGE,km		AZIM,°		RANGE,km		AZIM,°		RANGE,km		AZIM,°		RANGE,km		AZIM,°	
AHU	155.26230	19.37025	1070	56.2	23.9	178	207	22.5	56.2	205	178	51.7	22.8	193	189	22.8	16.7	189	143	24.1	64.9	107	133
AIN	155.45763	19.37192	1524	60.8	23.6	158	156	23.4	60.5	152	159	51.4	28.5	170	143	28.5	33.4	143	114	44.1	81.2	99	123
CAC	155.91545	19.48509	323	98.9	67.0	134	121	67.8	98.4	119	134	85.1	74.1	138	118	74.1	82.8	118	108	93.7	129.2	102	116
CPK	155.32564	19.39192	1038	59.2	24.1	171	190	23.0	59.2	187	172	53.0	25.2	185	173	25.2	23.0	173	133	31.2	71.5	108	131
DAN	155.66461	19.35393	3003	70.3	36.9	141	122	37.7	69.9	120	141	57.5	44.1	148	118	44.1	53.5	118	102	65.5	99.2	95	115
DES	155.38564	19.33360	815	54.3	17.4	164	173	16.7	54.1	168	164	46.3	20.8	178	153	20.8	24.8	153	112	36.1	72.5	95	124
ESR	155.23613	19.40825	1177	60.4	28.9	180	208	27.5	60.4	206	181	56.4	27.5	195	193	27.5	19.0	193	157	23.2	66.0	119	138
FEF	155.14580	19.47524	691	68.5	40.3	188	215	38.7	68.7	214	189	66.4	37.6	201	205	37.6	25.1	205	185	21.7	66.2	150	148
HAB	156.24725	20.76353	92	235.9	198.9	153	152	198.8	235.6	152	154	224.8	203.5	156	151	203.5	202.6	151	146	205.1	249.6	142	143
HLP	155.30780	19.29626	707	48.4	14.4	172	205	13.1	48.4	201	172	42.7	14.4	189	174	14.4	15.7	174	109	27.8	63.5	88	125
HPU	155.45561	19.77773	3396	103.9	67.3	167	172	66.6	103.8	171	168	96.1	70.0	175	166	70.0	66.0	166	153	67.9	112.3	140	143
HSS	155.48279	19.60208	2445	85.8	48.7	163	165	48.2	85.6	164	163	77.0	52.2	171	158	52.2	51.3	158	140	56.6	99.5	125	135
HTC	155.39763	19.23576	381	44.4	7.2	158	152	7.3	44.2	139	159	35.5	13.2	176	125	13.2	24.3	125	86	38.1	68.3	78	116
HUA	155.83595	19.68441	2189	110.5	74.8	145	139	75.1	110.1	137	146	98.2	80.8	150	135	80.8	85.2	135	124	93.2	133.6	117	126
HUL	154.97597	19.41574	369	67.2	48.7	204	237	47.0	67.5	237	205	69.3	43.4	217	231	43.4	27.2	231	227	14.0	52.4	210	161
KAA	155.86862	19.26327	524	79.5	53.6	124	100	54.9	78.9	99	124	64.9	61.2	126	100	61.2	73.7	100	91	86.8	115.7	87	106
KAE	155.12981	19.28609	37	48.2	27.5	194	244	25.8	48.4	245	195	48.2	21.8	212	233	21.8	5.5	233	224	9.4	48.5	76	136
KFA	155.41695	19.41775	1579	64.2	27.1	163	169	26.6	64.0	165	164	55.8	30.7	175	155	30.7	32.2	155	125	41.2	80.7	107	128
KHU	155.61562	19.24526	1939	57.8	27.3	137	106	28.4	57.3	103	137	44.6	34.8	145	104	34.8	47.1	104	89	60.5	89.8	83	110
KII	155.76228	19.50625	1841	89.9	55.3	142	131	55.8	89.5	130	143	77.3	61.9	148	128	61.9	68.7	128	114	78.7	116.2	106	121
KKU	155.34029	19.88672	1863	114.0	78.8	175	182	77.9	114.0	181	175	107.8	80.2	182	177	80.2	73.1	177	166	71.6	116.0	154	151
KLC	155.06529	19.40275	659	62.5	40.2	197	232	38.5	62.8	231	198	62.8	35.6	211	223	35.6	20.0	223	212	11.0	55.0	168	151
KLU	154.91830	19.45491	271	73.7	56.1	207	237	54.4	74.1	237	208	76.4	50.8	219	231	50.8	34.6	231	229	21.0	55.0	218	168
KOH	155.77678	20.12506	1166	151.0	113.7	158	158	113.5	150.7	157	158	140.8	117.9	162	155	117.9	116.4	155	147	119.1	163.4	140	142
KPN	155.28728	19.33192	924	52.1	18.9	175	206	17.6	52.1	203	175	46.9	18.3	191	182	18.3	15.6	182	126	25.8	64.1	96	129
KPO	154.83913	19.49724	134	81.9	65.6	211	237	64.0	82.3	237	211	85.3	60.3	221	233	60.3	44.0	233	231	30.1	58.7	225	177
MLO	155.38564	19.49359	201	71.5	35.1	168	177	34.3	71.4	174	168	64.1	37.5	179	165	37.5	35.5	165	140	41.5	83.7	120	134
MLX	155.34229	19.45692	1475	66.6	31.1	171	185	30.1	66.6	182	171	60.1	32.6	183	171	32.6	29.5	171	141	35.6	77.6	118	134
MOK	155.59695	19.48492	4104	78.4	41.8	151	145	42.0	78.1	142	152	67.4	47.5	159	138	47.5	52.2	138	120	61.4	100.3	109	125
MPR	155.16147	19.36475	881	56.1	29.8	188	226	28.2	56.3	225	189	54.4	26.0	204	213	26.0	12.8	213	182	14.0	57.2	117	140
MTV	155.05980	19.50108	409	73.2	48.1	195	222	46.5	73.4	221	196	72.7	44.6	207	214	44.6	30.1	214	202	21.7	64.5	175	156
NAG	155.02596	19.69890	1	95.3	68.0	194	212	66.5	95.6	211	194	94.2	65.5	203	206	65.5	52.0	206	197	43.7	84.1	182	165
NPT	155.28062	19.41192	1115	60.9	27.4	176	199	26.2	60.9	197	177	55.8	27.3	190	183	27.3	21.6	183	146	27.6	69.5	115	135
OTL	155.27962	19.38659	1038	58.1	24.8	176	201	23.5	58.1	199	177	53.1	24.5	191	184	24.5	19.3	184	142	26.4	67.5	110	133
PAU	155.21564	19.37392	994	56.6	26.8	183	216	25.3	56.7	215	183	53.3	24.4	198	200	24.4	14.7	200	160	19.6	61.7	112	137
PLA	155.45847	19.53024	2992	77.4	40.3	163	166	39.8	77.2	164	163	68.8	43.9	172	157	43.9	43.7	157	135	50.2	92.1	120	132
POI	154.85097	19.45391	16	77.1	62.1	212	241	60.4	77.6	241	213	80.9	56.4	223	236	56.4	40.1	236	236	25.9	53.9	231	176
POL	155.22180	19.28060	169	46.2	18.9	182	233	17.2	46.3	233	183	43.3	14.7	201	211	14.7	6.7	211	120	19.0	55.2	81	129
PPL	155.46179	19.15527	35	39.8	10.4	144	76	12.0	39.4	73	145	28.1	17.6	160	86	17.6	32.8	86	71	47.1	71.3	69	107
RIM	155.27396	19.39525	1128	59.0	26.0	177	202	24.6	59.0	200	177	54.1	25.5	191	185	25.5	19.7	185	145	26.2	67.7	112	134
RSD	155.27528	19.45992	1270	66.2	32.7	177	197	31.5	66.2	195	177	61.2	32.6	190	184	32.6	26.0	184	154	29.8	73.0	125	138
SPT	155.66263	18.97878	244	46.3	38.3	106	55	40.0	45.5	55	106	31.4	44.0	103	62	44.0	60.2	62	60	74.6	89.5	61	91
STC	155.12514	19.38525	765	59.0	34.2	192	228	32.5	59.2	227	193	58.1	30.1	207	216	30.1	15.6	216	196	12.3	56.7	135	145
SWR	155.60229	19.45125	4048	75.5	39.2	150	141	39.5	75.1	138	150	64.1	45.2	158	134	45.2	50.9	134	116	60.9	98.7	105	123
TRA	155.54662	19.41209	3207	68.8	32.2	152	144	32.3	68.5	141	153	58.0	38.0	162	136	38.0	43.8	136	114	54.2	91.5	102	122
URA	155.29062	19.42025	1240	61.9	28.0	175	196	26.8	61.9	194	176	56.6	28.1	189	181	28.1	23.0	181	145	28.9	70.9	116	135
WAI	155.65729	19.85657	1433	118.6	81.3	158	158	81.1	118.4	157	159	108.7	85.6	164	154	85.6	84.8	154	143	88.8	132.6	133	138
WHA	155.04596	19.32859	29	55.4	37.5	202	244	35.8	55.7	244	202	57.1	31.7	217	236	31.7	15.4	236	235	2.5	46.8	172	148
WIL	155.58095	19.46609	4037	75.8	39.1	152	145	39.3	75.5	142	152	64.9	44.8	160	138	44.8	49.7	138	119	59.2	97.8	107	124
WOB	155.58078	19.53542	3396	82.7	45.6	154	150	45.6	82.4	148	155	72.2	50.8	162	144	50.8	53.8	144	126	61.9	102.3	114	128
WOO	155.49930	19.24826	909	50.6	16.0	147	119	16.9	50.2	114	148	39.2	23.3	160	113	23.3	34.9	113	90	48.4	78.6	82	113

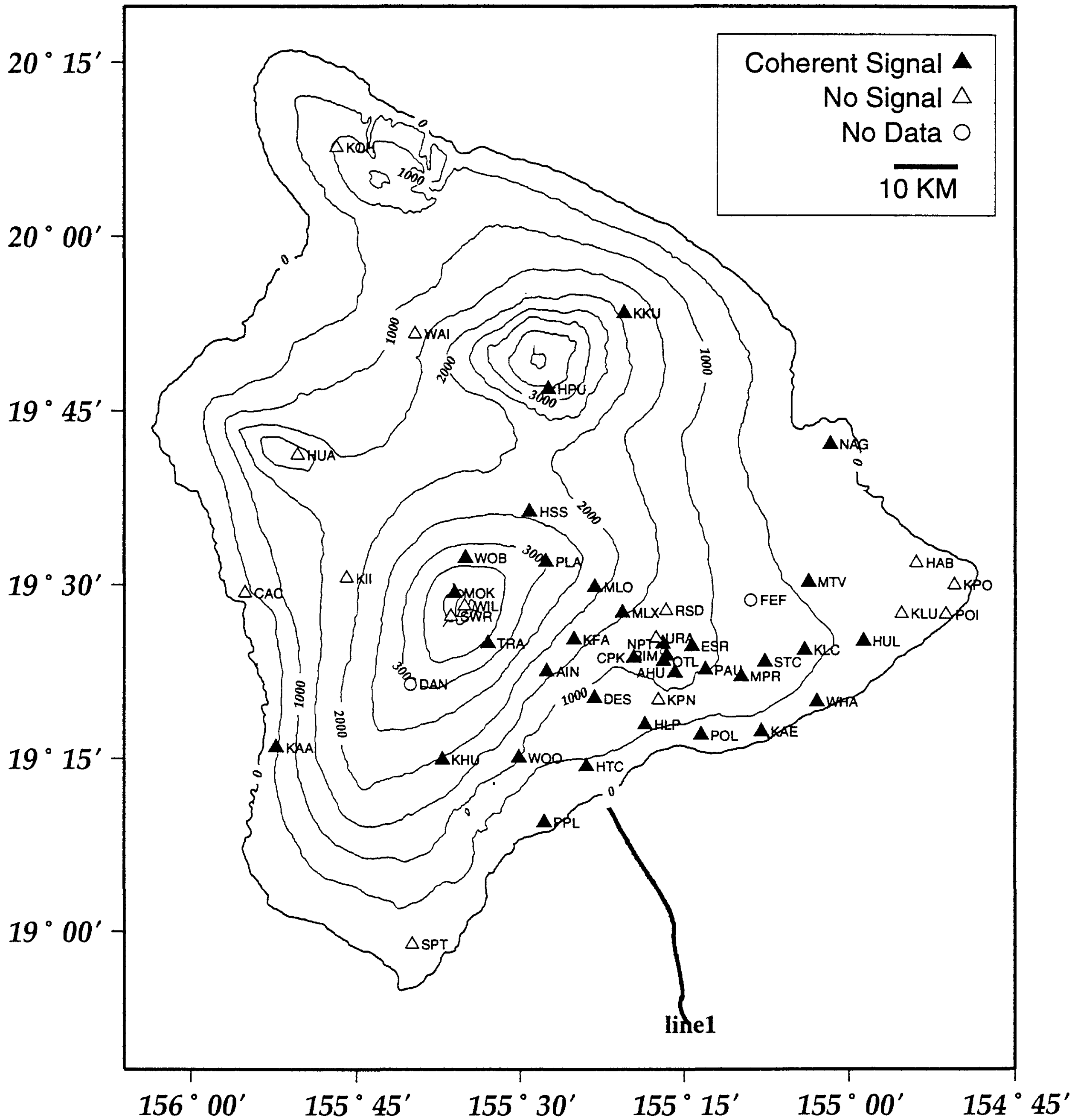

Figure 4. HVO network stations recording data from Line 1. Elevation in meters.

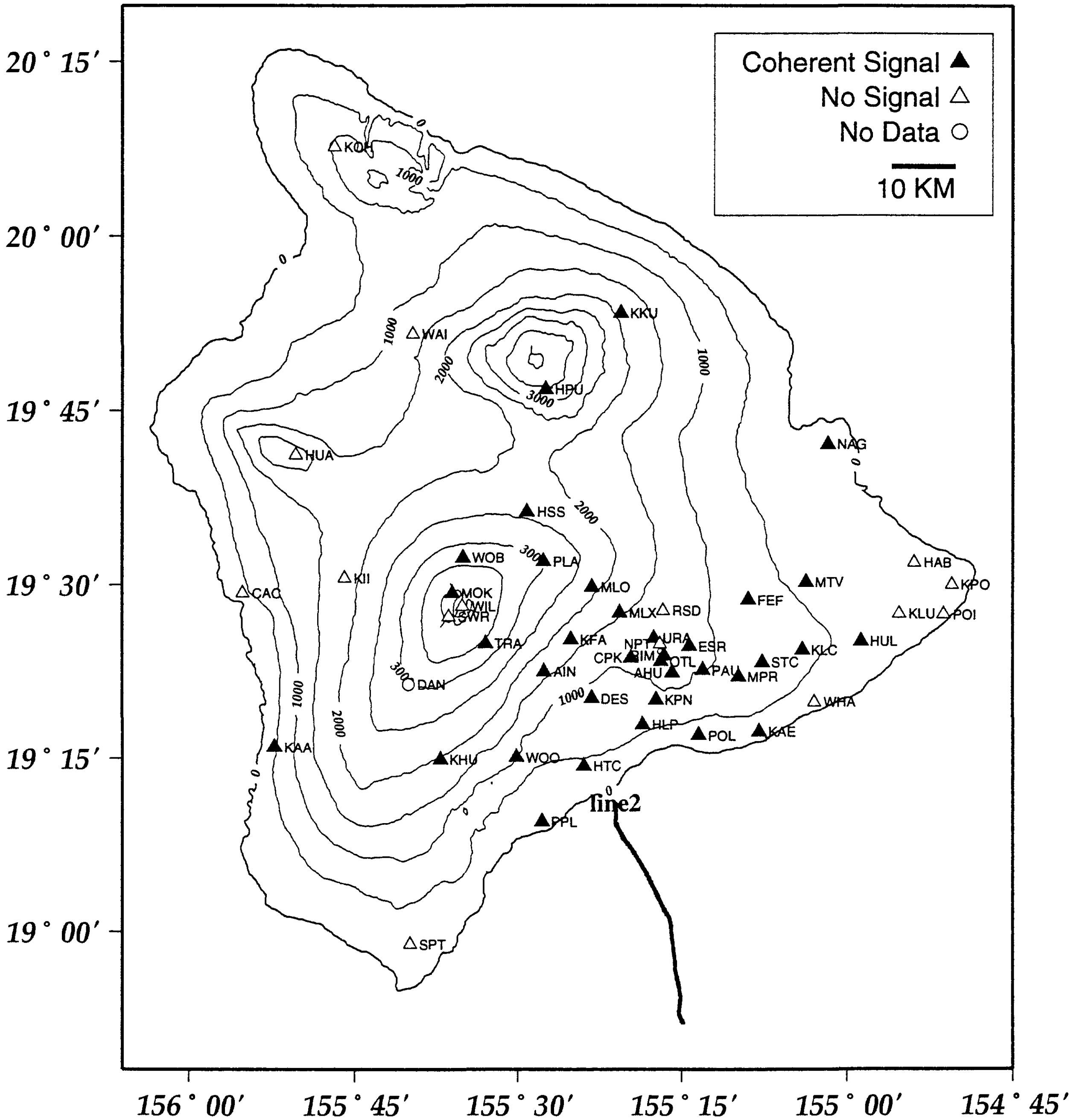

Figure 5. HVO network stations recording data from Line 2. Elevation in meters.

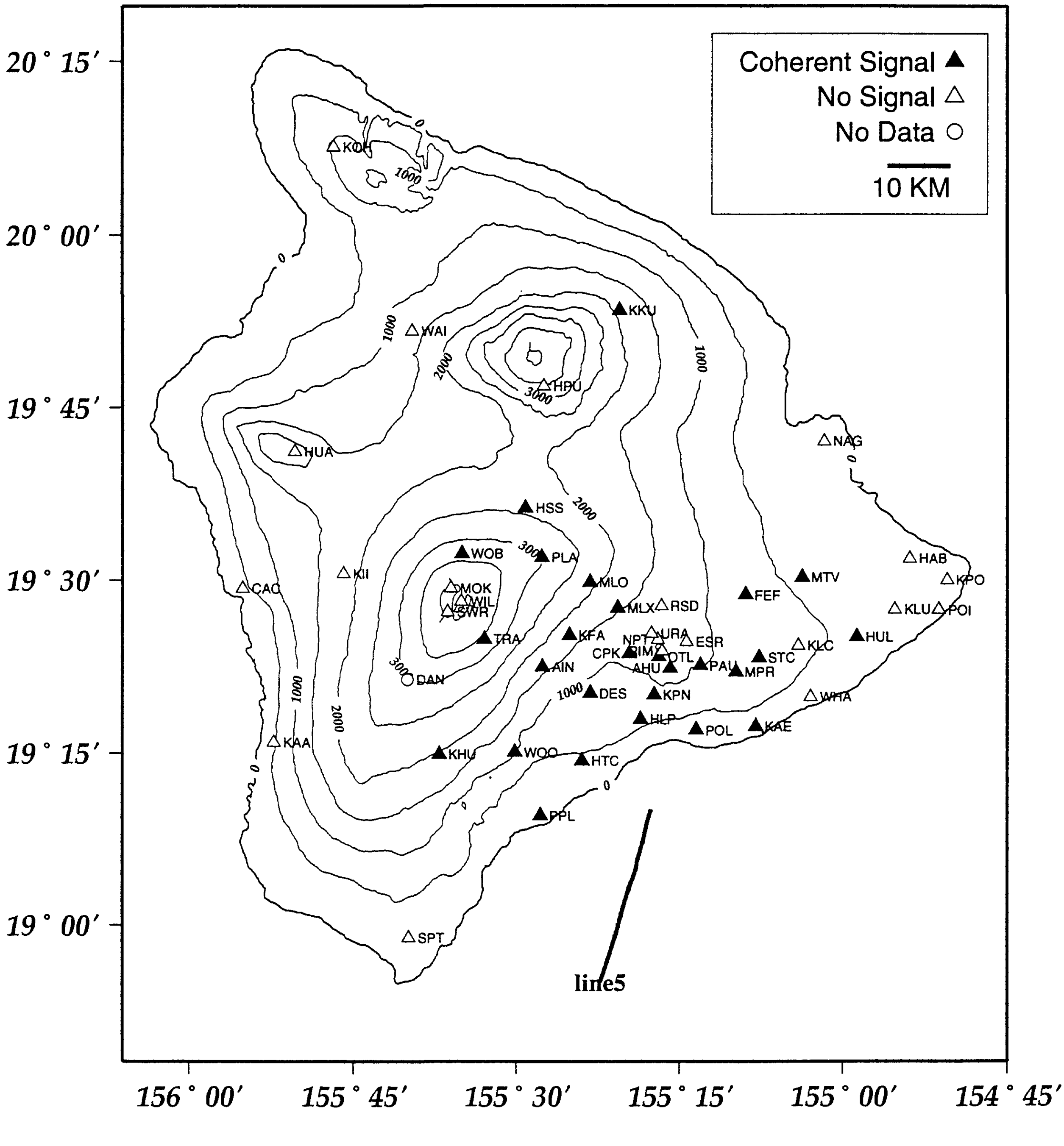

Figure 6. HVO network stations recording data from Line 5. Elevation in meters.

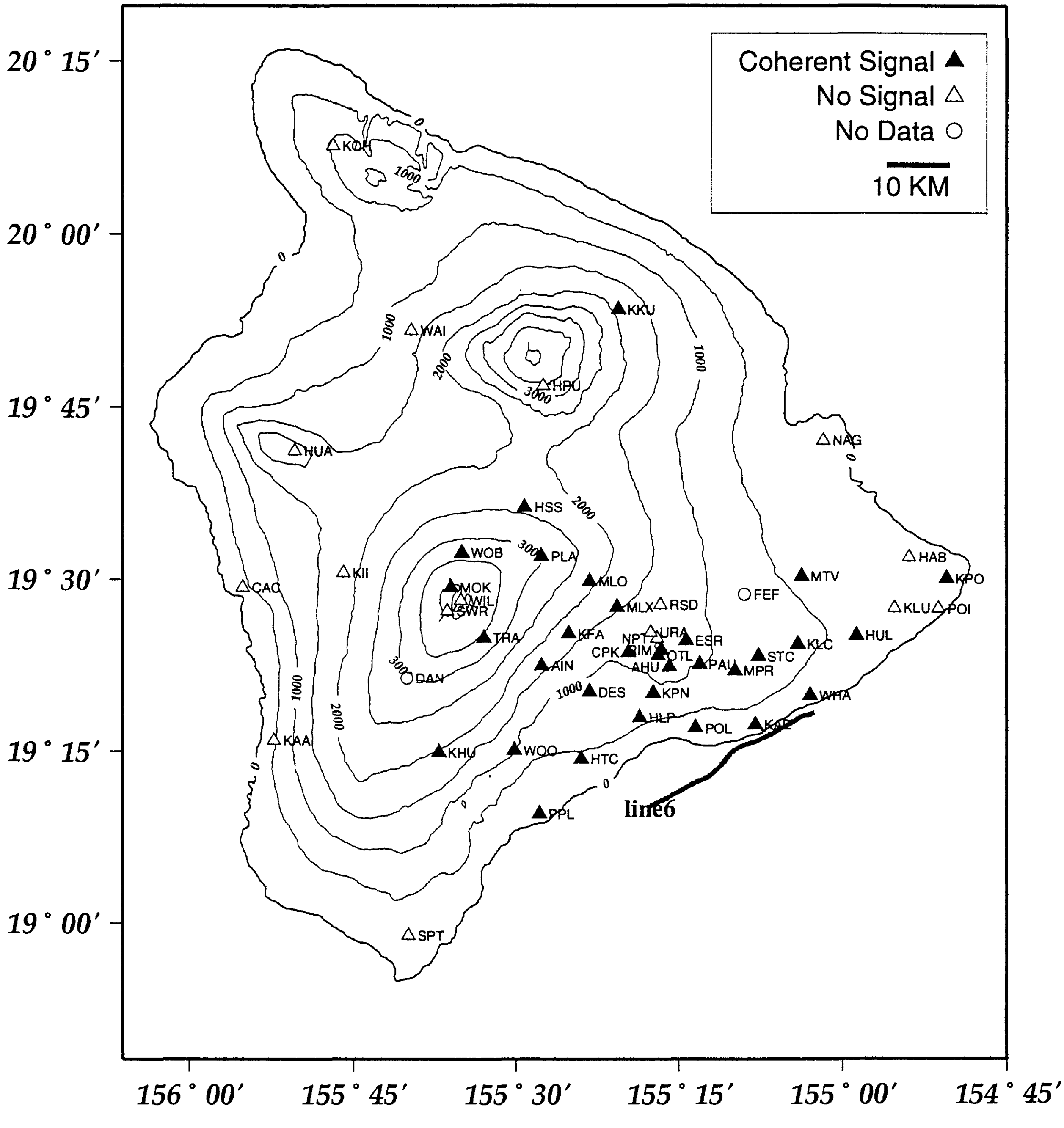

Figure 7. HVO network stations recording data from Line 6. Elevation in meters.

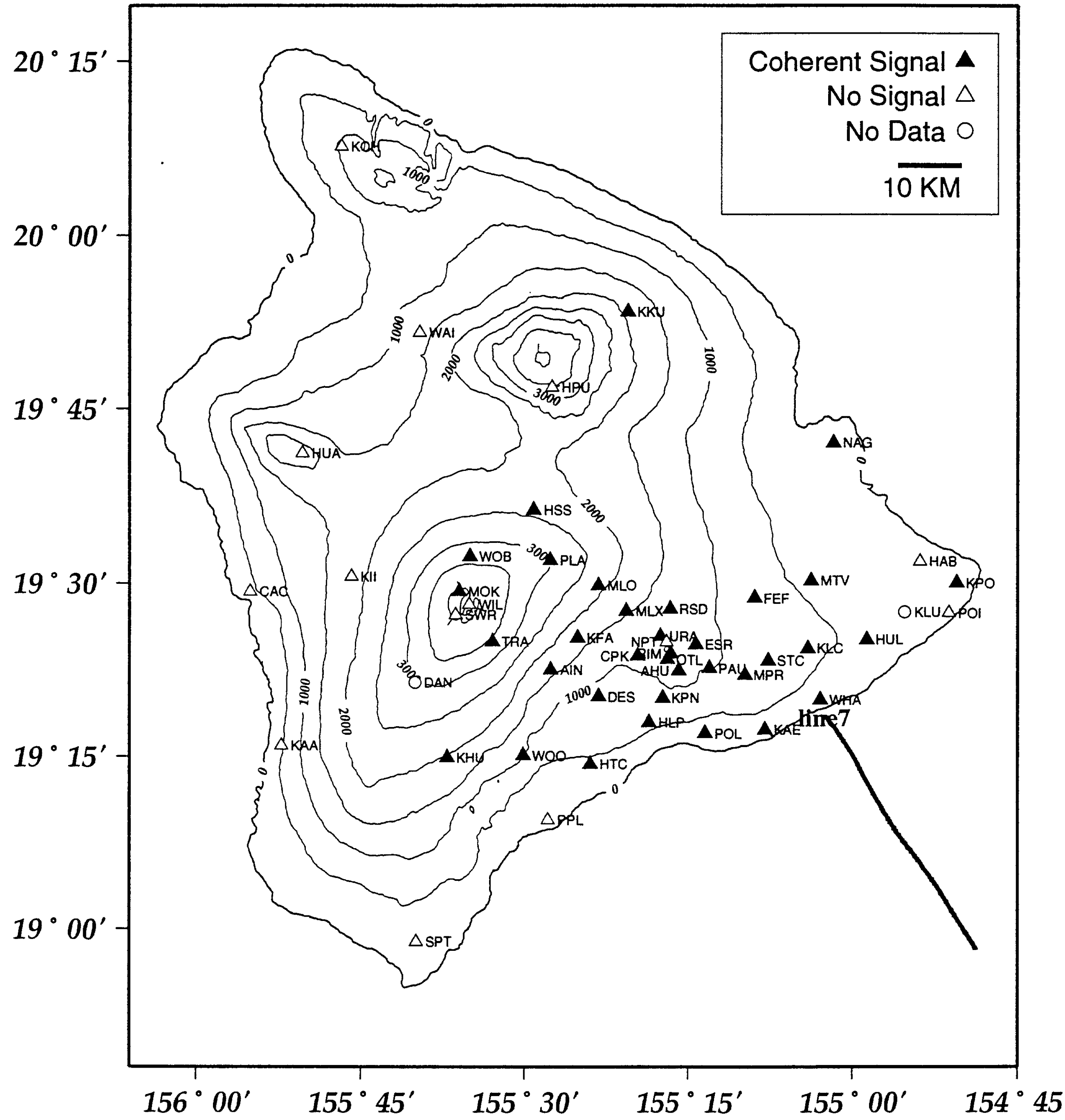

Figure 8. HVO network stations recording data from Line 7. Elevation in meters.

DATA PROCESSING

Data reduction included extraction of the CUSP digital data from each seismic line, clock corrections to shot times based on WWV-Hawaii (WWVH) and GPS time standards, data conversion to SEG-Y format, calculation of shot ranges using OHD-estimated locations for the HVO network and GPS shot locations, and plotting of the seismic data as record sections for each station. The CUSP to SEG-Y processing scheme was adapted from that described in *Brocher and Pope* (1994). Incoming data from the HVO permanent seismic network were digitized in real time at the Observatory at 100 samples-per-second using a 16-bit, 128-channel digitizer. IRIG-E time code is also recorded and decoded to assign the true clock time for the start of each file. The CUSP system archives both triggered event files to disk, and continuously-recorded data streams onto Digital Audio Tapes (DAT, SQUIRREL tapes). The 1-min shot interval in this experiment necessitated use of the SQUIRREL tapes for data playback.

Two time standards were used in the experiment, GPS for shipboard and WWVH for land-based operations. WWVH signals are broadcast from a repeater on the island of Kauai, and received at HVO where IRIG-E time-code is generated for digitization by the CUSP system; the time code generator outputs time accurate to within 1 ms of WWVH. Clock corrections were made to convert GPS shot times in Greenwich Mean Time to IRIG-E Hawaiian Standard Time using a clock drift determined from a linear fit of clock offset points recorded before and after the experiment. Comparisons were made at HVO using a Datum Model 9100 time code generator and a Kinemetrics TrueTime Satellite GPS receiver (Model 805-339). The drift was 0.000597 s/hr, and typically amounted to an addition of 0.04 s to the GPS time to arrive at the HST time. Shot times were also adjusted to account for the firing delay inherent in the digital air gun firing system. Based on observations from previous experiments utilizing the same firing system, and a comparison between the predicted ocean bottom instrument depths from the direct water wave and the observed depth from Sea Beam multi-beam bathymetry, this delay was estimated to be 50 ms.

CUSP data from the seismic shooting time period were extracted from the SQUIRREL tapes using the CUSP TISK utility, which creates time-based GRM seismogram files and MEM header information files. GRM files ranged in size from 60,000 to 530,000 VAX blocks (30 - 265 Mb), and covered 30 minutes to 4.5 hours of data; altogether, close to 3 million blocks (1.4 Gb) of data were collected from only 30 hours of continuous seismic shooting; from this, about 700 Mb of seismic shot data were extracted for record section plotting and travel time analysis. GRM files from each seismic line were then run through the SYNCH utility to read the IRIG-E time code and place file start information in the MEM file.

Next, 30 seconds of data starting from the shot time were extracted from the CUSP data and converted to SEG-Y, station-based files using the CUSP TO_SEGY utility; individual SEG-Y data files ranged in size from 2800-4200 VAX blocks (1.4 - 2.1 Mb) per station. The SEG-Y format consists of a number of shot traces, with each trace consisting of a 240-byte trace header of 2- and 4-byte integers describing the specific trace and 3001 2-byte integer data samples. The location and description of each value in the SEG-Y trace header is described by *Barry et al.* (1975), and was slightly modified by *Luetgert et al.* (1990).

During this process, the IRIG-E time code was re-read for each shot to establish to the true file start time and digitizer sample count for the trace extraction, and the sample rate based on each new SEG-Y file was updated in the header; re-reading of the time code was required because the HVO digitizer clock drifts at about 1 s/hr, and would have resulted in sample count errors of up to 30 s over the shooting period. For each station, shot data from the vertical component, and where available the horizontal components, were extracted and separate SEG-Y data files created for each component. Data for Lines 1, 2, 5, 6, and 7 were extracted; Lines 3 and 4 were not processed because these ran over the magmatically-active summit of Loihi at ranges which are not expected to show first arrivals (> 40 km). Finally, the SEG-Y and CUSP GRM and MEM files were archived by seismic line onto DAT tapes using the VAX VMS BACKUP utility.

In order to calculate shot ranges, HVO station locations, based on Old Hawaiian Datum coordinates, were first converted to the equivalent GPS location (WGS 84 datum). This correction results in shifts averaging 445 m along a N140°E azimuth. True shot locations were determined from the ship's GPS location, the average horizontal distance of the air guns behind the ship (29.75 m, from the 30.3 m average air gun cable length and 5.7 m estimated shot depth), and the ship's heading at the shot time. Ranges between the receiver and shot were then calculated and the corrected distance placed in the SEG-Y header.

Finally, record sections were plotted for each station using the VAX program RSEC90 (*Luetgert*, 1988). This program, together with a file post-processor to convert the plot file to postscript language, was used to produce time vs. distance and azimuth vs. distance plots of each seismic line as recorded by each station. Station data were input in SEG-Y format, and the plot files created in batch mode and sent to the printer. Plotted traces were bandpass filtered between 3 and 10 Hz, and each trace was scaled to a uniform maximum amplitude; for time-range plots, traces are displayed as reduced travel time sections using reduction velocities of 6 or 8 km/s. Reduction velocities of 6 and 8 km/s were selected to allow easy identification of the ranges at which Moho velocities signifying the oceanic crust-mantle boundary (PmP reflections) and crustal velocities related to the volcano-oceanic crust transition (PiP reflections), respectively, first appear. Record sections for all seismic stations that display any recognizable P wave energy are shown in Appendices A-E; no topographic or water column corrections were applied prior to plotting. in Figures 4 - 6 show station summaries of the distribution of recorded P wave energy.

DATA DESCRIPTION

A plot of the ray coverage for the 1994 seismic experiment shows good coverage for the subaerial portion of Kilauea's south flank extending about 20 km offshore, the Kaoiki fault zone, the lowermost southeastern flank of Mauna Loa volcano, and the corridor extending from the coast over Loihi seamount 35 km offshore (Figure 7). Inclusion of the thousands of shallow, intermediate, and deep earthquakes recorded over the last 25 years as well will result in a far more complete data set than was possible in previous seismic tomography studies (due to the greater spatial diversity of raypaths), giving greatly improved resolution of the three-dimensional subsurface structure of the volcano, oceanic crust, and uppermost mantle.

Preliminary playbacks of the HVO network data reveal coherent P wave energy on a majority of Kilauea's seismic stations, strong out to 40-50 km, and detectable typically out to 60-70 km (*Kong et al.*, 1994, Figures 4 - 6, e.g., Appendix A.1 (AIN), Appendix E.11 (MTV)). Rays at these ranges sample the lowermost crust and upper mantle, and pass through the postulated decollement. The maximum range at which seismic P wave energy was recorded was 110 km at station KKU on the northeast slope of Mauna Kea from Line 2 (Appendix B.8); station KKU recorded signals from all lines. Pn energy from Line 7 shots was also observed at nearly 100 km range at station WOB located on the northern summit slope of Mauna Loa (Appendix E.18). The minimum range recorded by HVO stations was less than 2 km by coastal station WHA from Lines 6 and 7 shots (Appendices D.15, E.17). The excellent signal-to-noise ratios observed at a majority of stations in this experiment prove that even a small marine source can generate enough seismic energy to achieve sufficient ray sampling for constraining three-dimensional structure. PmP reflections from the crust-mantle boundary are commonly observed between 30 and 50 km range (e.g., Appendices A.1 (AIN), B.9 (MLO), E.13 (PAU)), and PiP reflections from the volcano-crust boundary at ranges from 20-30 km (e.g., Appendices A.5 (HTC), B.2 (DES), C.7 (KPN), E.5 (HUL)). PmP is often the strongest secondary arrival and displays the largest amplitudes of all recorded arrivals at HVO network stations. Crustal Pg (e.g., Appendices B.1, E.1 (AHU)) and mantle Pn (e.g., Appendix B.4 (HSS) refractions of varying amplitude are also identifiable. S wave energy was not recorded on any of the HVO network stations.

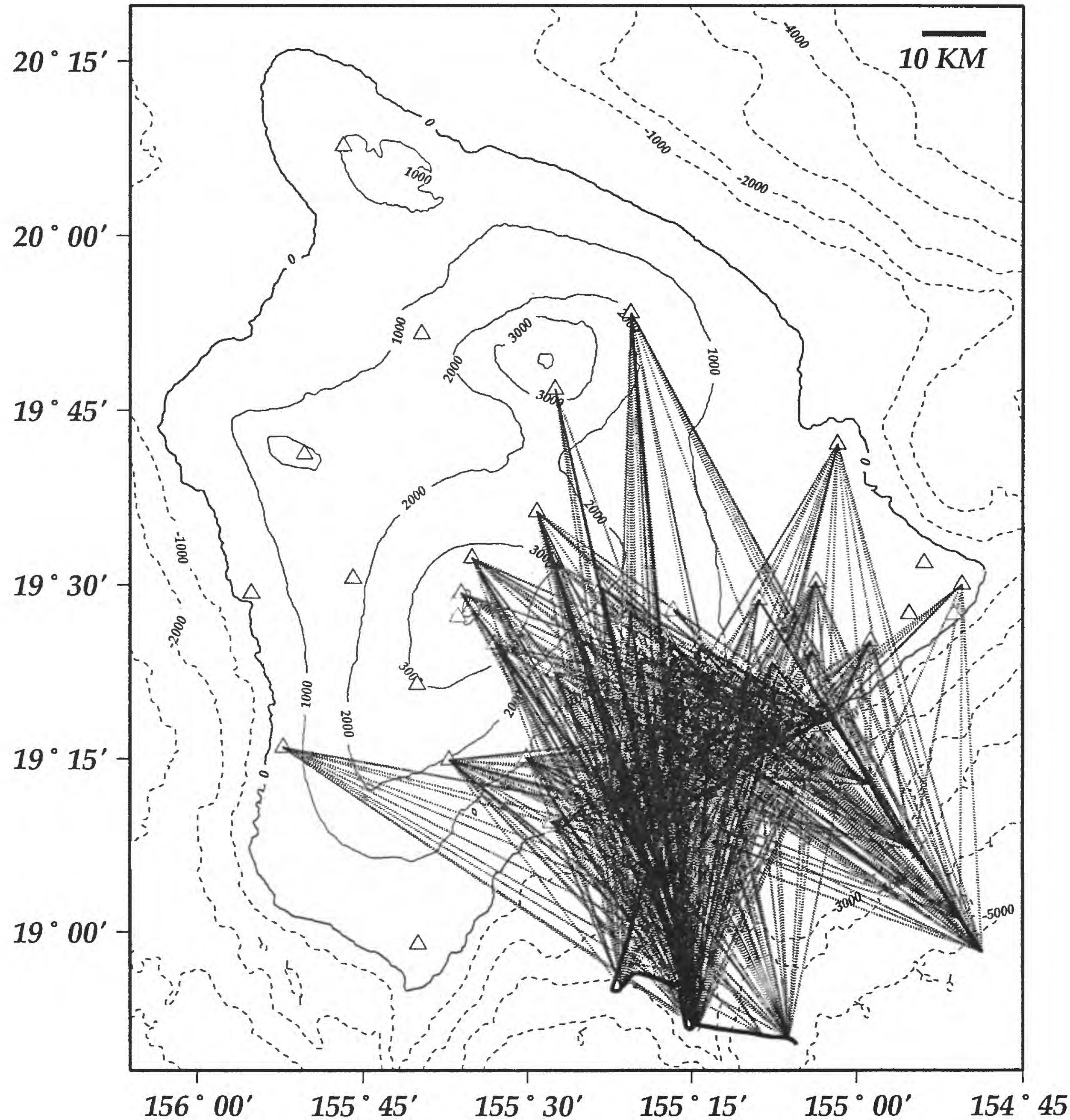

Figure 9. Representative ray coverage for 1994 Kilauea-Loihi Crustal Imaging Experiment. Ray density is greatest over the southwest rift zone and Hilina fault zone of Kilauea. Elevation and water depth in meters.

Signals were not well-detected at stations located atop Kilauea summits (Figures 4 - 6, e.g., Appendices A.12 (NPT), A.15 (RIM), C.10 (OTL), E.17 (URA)) however, because of severe attenuation in P wave energy as these waves passed through the volcanoes' magma conduit systems; stations that generally did not show any P wave energy included NPT, RIM, RSD, and URA on Kilauea. Stations located on southern rim of Mauna Loa's summit similarly did not record energy (WIL, SWR), though station MOK on the northern rim recorded energy from Lines 1 and 2 at its closest ranges (Appendices A.10, B.10), and at 75 km range from Line 7 (Appendix E.10). Station WOB located on the northern slope recorded good P wave signals at ranges up to 75 km from all lines (e.g., Appendices A.17, E.18), as well as station TRA on Mauna Loa's upper southeastern though background noise levels were relatively high on TRA (e.g., Appendices A.16, B.16, E.16).

Signals recorded from Line 6 shots can be used to map the areal dimensions of Kilauea's central magma conduit system. An attenuative P wave shadow zone at depths of perhaps 10-15 km (45-50 km range) intercepts rays passing beneath Kilauea caldera over a 15° azimuthal range (122-137°) from Line 6 shots recorded at station PLA on Mauna Loa (Appendix D.12). However, clear P wave arrivals are recorded at station AHU at all azimuths implying that the magma conduit does not extend more than three km south of Kilauea's central caldera (Appendix D.1). In general, volcano summit stations also show higher background noise levels or seismic tremor activity related to the present 13-year-old Pu'u O'o eruption.

Line 6 and 7 shots recorded at station WHA, located near the present entrance of lava into the ocean, show apparent velocities of less than 4 km/s for the uppermost crust located immediately offshore. The coastal entry has been the site of numerous subaerial bench collapses which contribute to the steep offshore slope; the multi-channel data suggest that the talus debris apron extends 10 km offshore, and that nearshore thicknesses are ~1 s two-way travel time (perhaps 1-2 km thick).

The magnitudes of recorded P wave energy at stations along Kilauea's east rift zone delineate the active eruptive rift zone. Stations located on the rift zone had higher signal-to-noise ratios than stations located just south of the rift zone. Pg energy from Line 7 shots is clearly observed in the 15-30 km range at station MPR (Makaopuhi crater, Appendix E.11) located along the southern edge of the rift zone, indicating that no attenuative material exists in the upper few kilometers to the south of the station. In contrast, only very weak energy is observed in the 23-30 km range at station FEF (Appendix E.3), which is located north of the active Pu'u O'o eruptive vent, but stronger P wave energy is received at similar ranges at station MTV (Appendix E.11), located further downrift and to the northeast of Pu'u O'o. These observations imply that the attenuative zone at depth (perhaps 5-10 km deep) does not extend beyond the Pu'u O'o cone.

Signals recorded at stations HLP and KPN located in the Hilina Region showed higher background noise levels and less coherency with range in P wave energy, presumably due to the fractured subsurface associated with the active fault system (e.g., Appendices A.3, B.9, C.3, D.3). Stations located along the coast, especially WHA, PPL, and KAE, showed slightly higher background levels at far ranges due to wind and the ocean surf noise (e.g., Appendices C.5, D.15, E.6). Station SPT located at the southernmost point of Hawaii island showed high noise levels due to the persistent winds that typically blow at 30-40 mph in this area. Stations located on the western flank of Mauna Loa (except KAA from Lines 1 and 2), Hualalai, western flank of Mauna Kea, and Kohala volcanoes did not record any P wave energy from any of the seismic lines. No P wave energy was generally also not observed on stations located on the lowermost section Kilauea's east rift zone (KLU, POI, KPO, and HAB). Signals from station DAN located along the rift zone just south of Mauna Loa's summit showed electrical interference and were not usable.

ACKNOWLEDGMENTS

We thank the Captain and crew of the *R/V Moana Wave* and *R/V Kila*, and Scientific Party of the *R/V Moana* Wave for their invaluable efforts in collecting the offshore data, and the seismic, computer, and electronics staff of the Hawaiian Volcano Observatory for their assistance in collecting and playing back the onshore data. We especially thank Perry Crampton for providing his air gun services and Jim Vaughan and Renee Ellorda for installing and running the shipboard sonobuoy receiving system. We thank Sharon Stahl, Steve Poulos, and Mike Simpson for setting up and maintaining the seagoing digital recording system, and Greg Moore for his assistance in processing the multi-channel seismic data. On land, Allan Largo and Peter Aderinto collected the Kuee temporary station data, and Ken Honma logged the GPS - WWVH clock drift. Tom Brocher, Will Kohler, and especially Alan Walters provided help in converting the CUSP data to SEGY format for plotting using Jim Luetgert's record section program. Bathymetry and elevation data were compiled by John Smith and Terri Duennebier. Costs for the experiment were shared by the USGS/HVO, by UCSD/SIO, and by UH/SOEST. Ship use during the 1994 onshore-offshore experiment was sponsored by the National Science Foundation.

APPENDIX A. RECORD SECTIONS FROM LINE 1

Vertical-component record sections for HVO seismic network stations recording seismic phases from Line 1 shots (Figure 4). Data are plotted versus distance or azimuth. Data were bandpass filtered (3 - 10 Hz), and each trace scaled to a uniform maximum amplitude. For time vs. distance plots, data were linearly reduced using velocities of 6 or 8 km/s. Reduction velocities were selected to permit identification of the ranges at which Moho (oceanic crust-mantle boundary) and crustal (volcano-oceanic crust transition) velocities first appear. No topographic or water column corrections have been applied, and the estimated 50 ms firing system delay has not been accounted for in the plots. Shot range is the distance between OHD HVO station locations and WGS 84 shot locations; true ranges, resulting in shifts averaging 445 m in the N140°E direction, are calculated in Table 2.

FIGURE *PAGE*

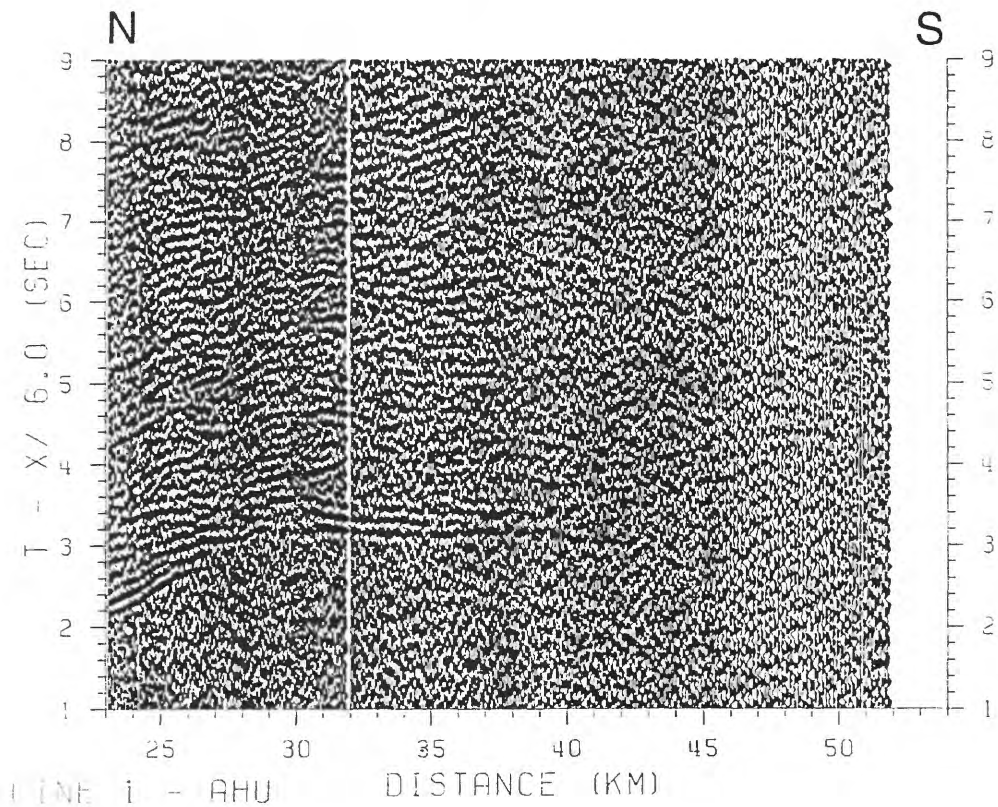
N
S
T - X/ 6.0 (SEC)
1
2
3
4
5
6
7
8
9
25
30
35
40
45
50
DISTANCE (KM)
LINE 1 - AHU

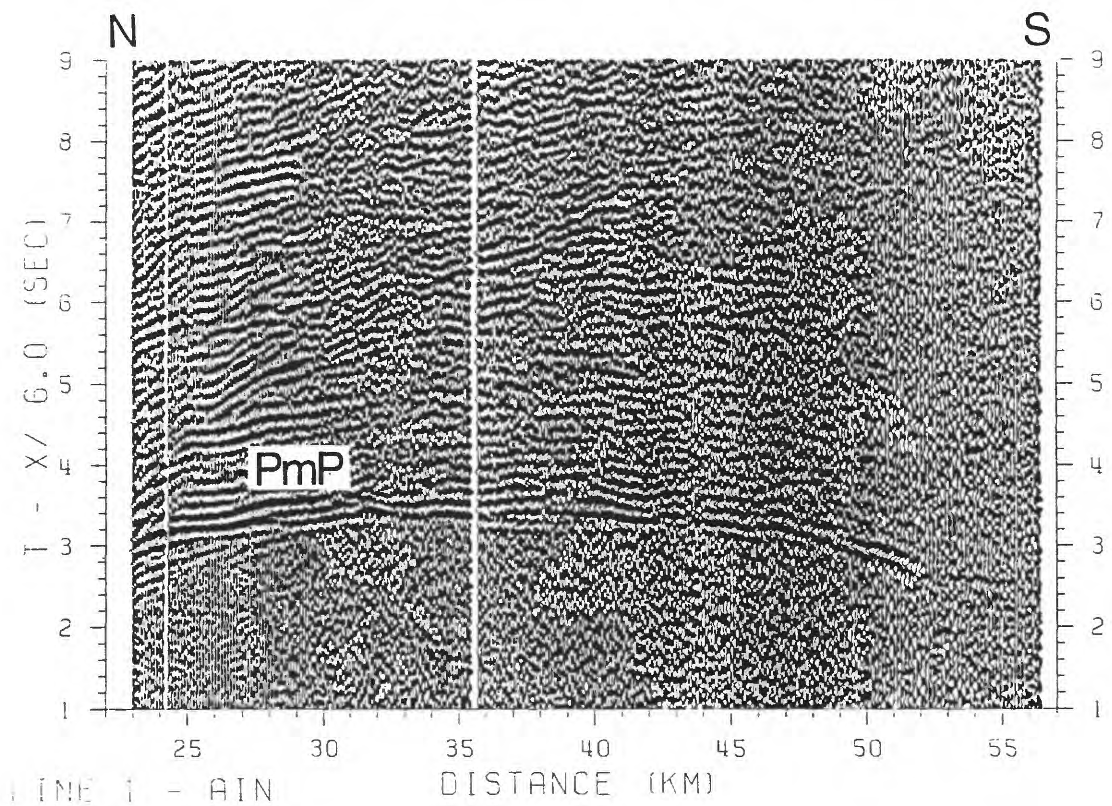
N
S
PmP
T - X/ 6.0 (SEC)
1
2
3
4
5
6
7
8
9
25
30
35
40
45
50
55
DISTANCE (KM)
LINE 1 - AIN

Appendix A.1

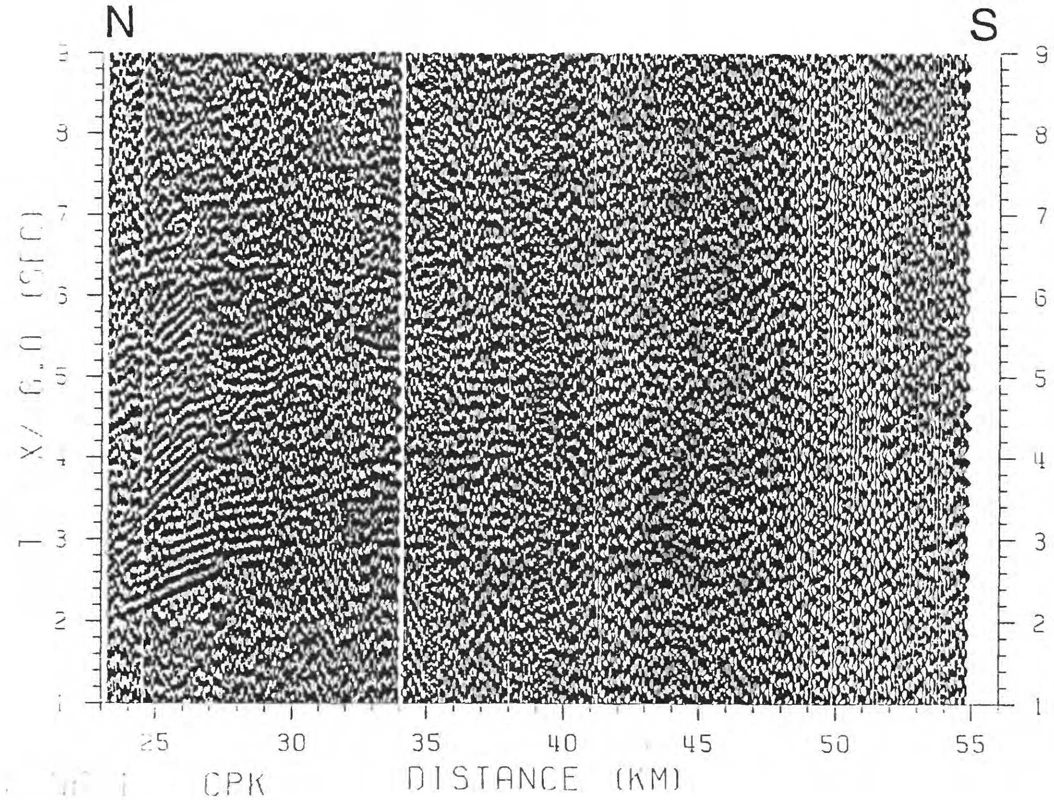
N
S
T - X/ 6.0 (SEC)
25 30 35 40 45 50 55
CPK
DISTANCE (KM)

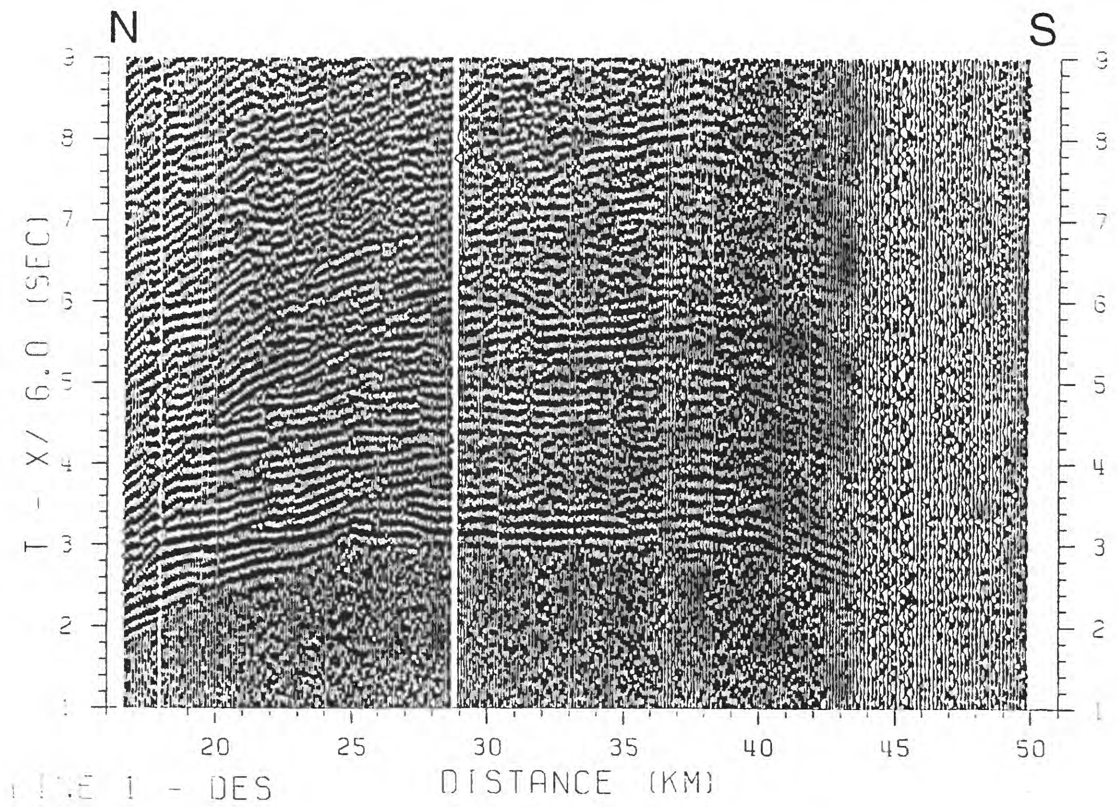
N
S
T - X/ 6.0 (SEC)
20 25 30 35 40 45 50
1 - DES
DISTANCE (KM)

Appendix A.2

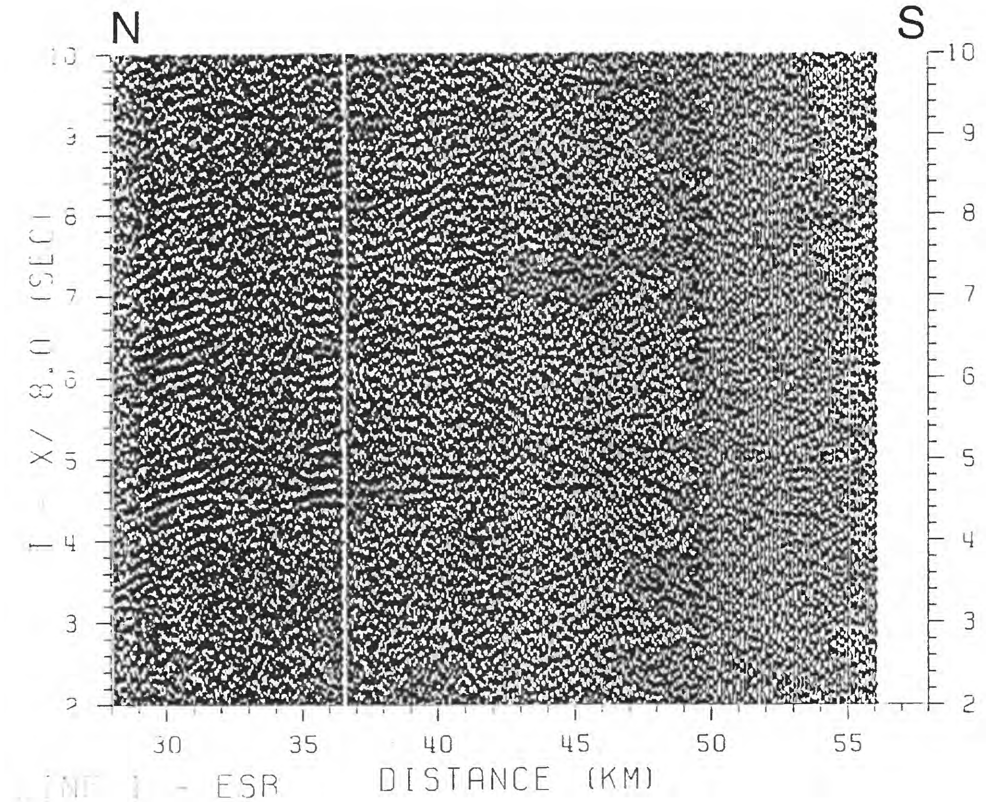
N
S
T - X/ 8.0 (SEC)
DISTANCE (KM)
LINE 1 - ESR

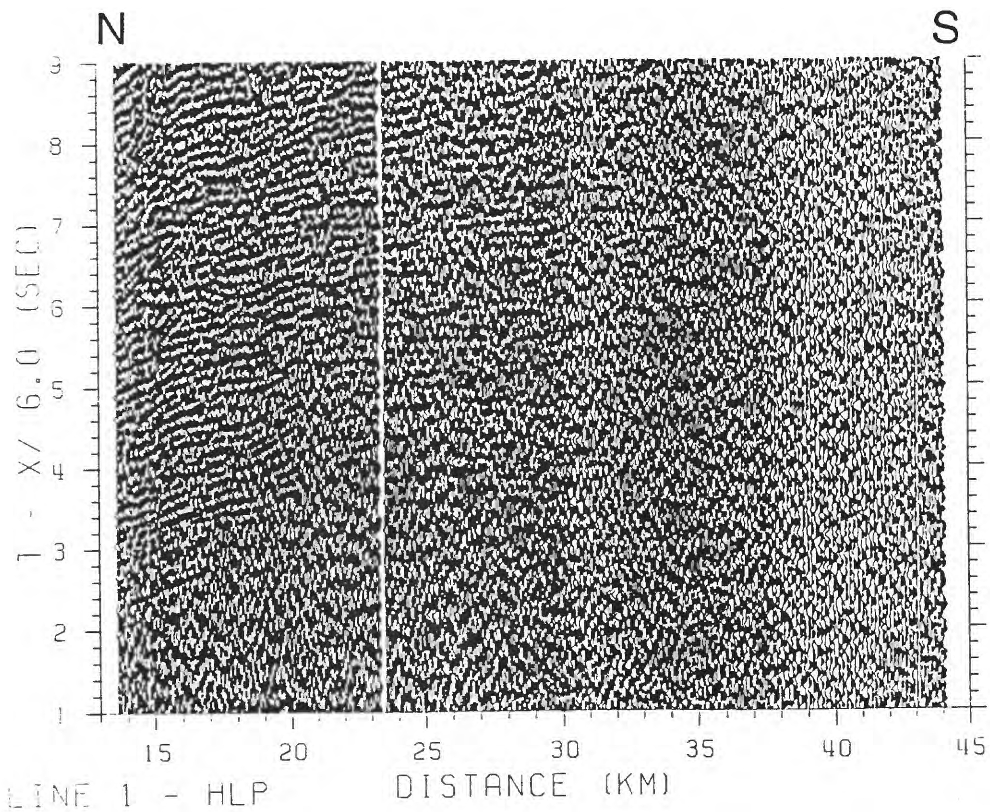
N
S
T - X/ 6.0 (SEC)
DISTANCE (KM)
LINE 1 - HLP

Appendix A.3

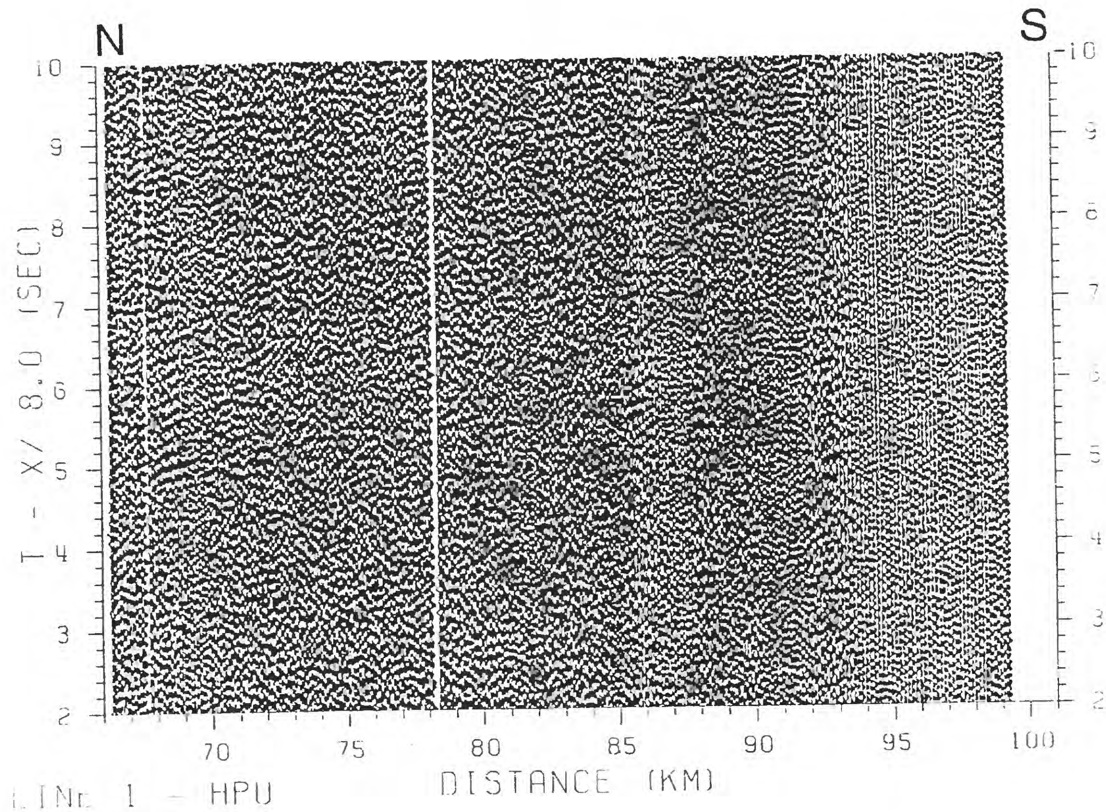
N
S
T - X/ 8.0 (SEC)
DISTANCE (KM)
LINE 1 - HPU

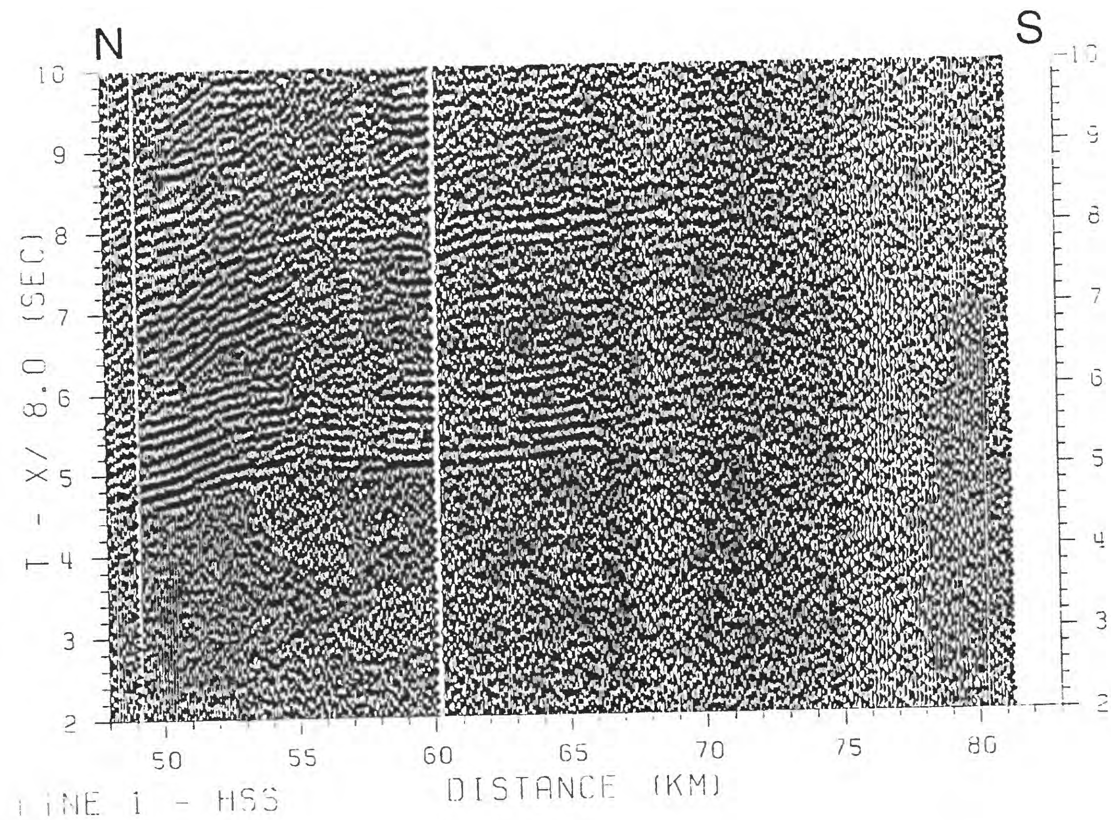
N
S
T - X/ 8.0 (SEC)
DISTANCE (KM)
LINE 1 - HSS

Appendix A.4

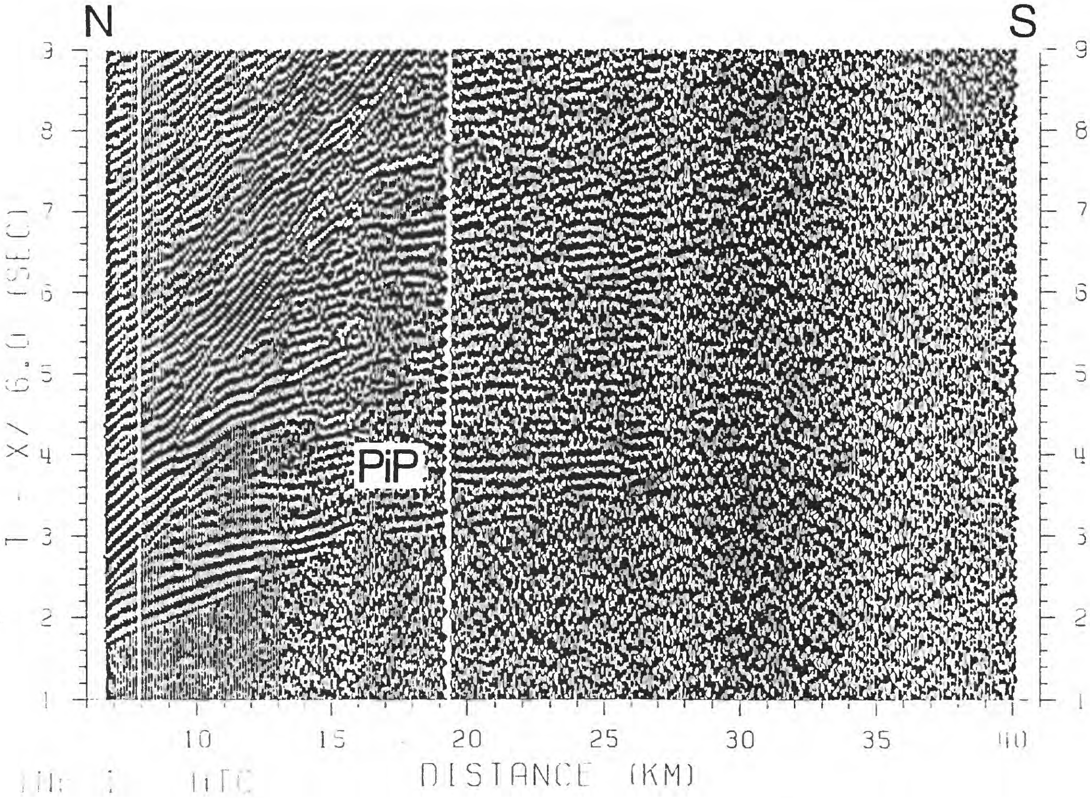

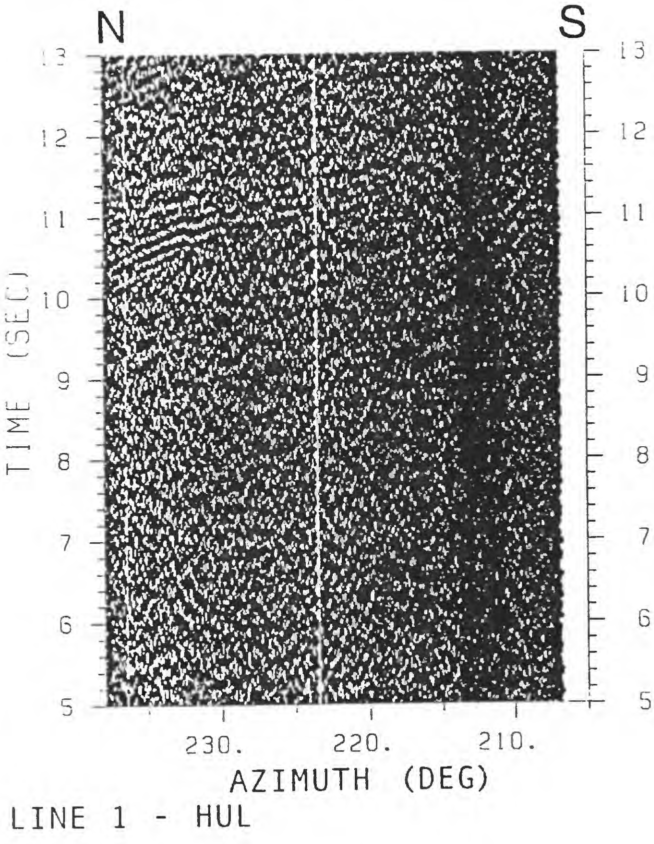

Appendix A.5

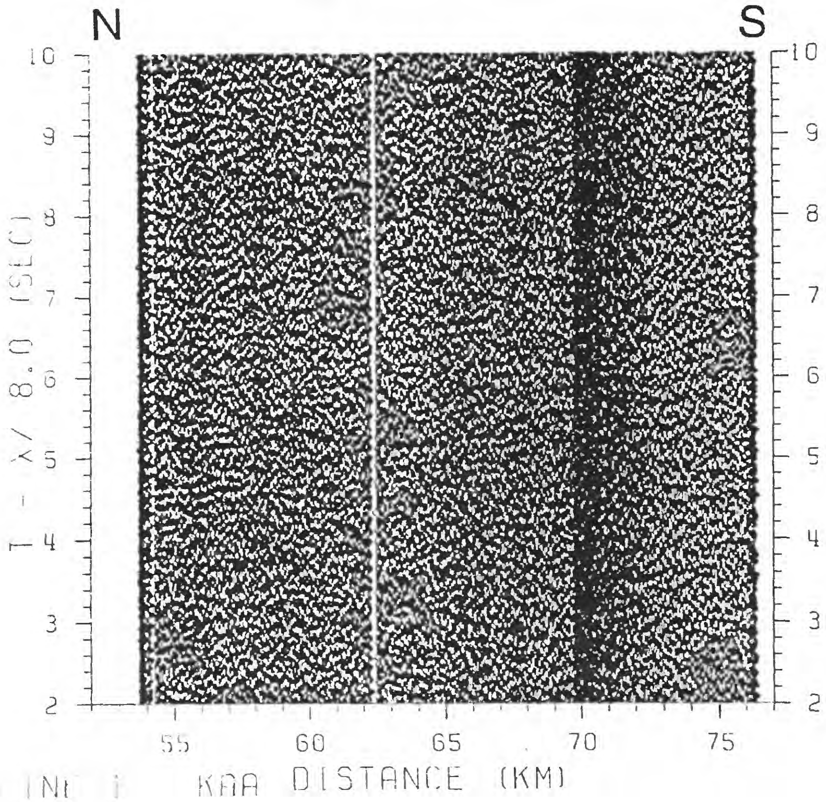
N
S
T - X/ 8.0 (SEC)
2
3
4
5
6
7
8
9
10
55
60
65
70
75
KAA DISTANCE (KM)

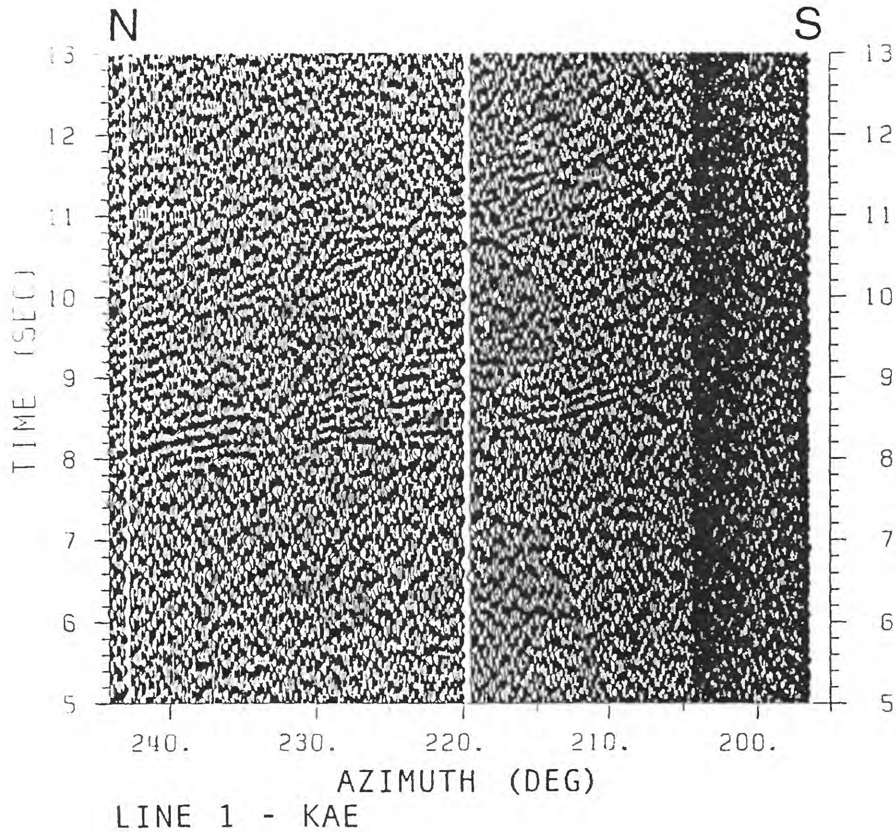
N
S
TIME (SEC)
5
6
7
8
9
10
11
12
13
240.
230.
220.
210.
200.
AZIMUTH (DEG)
LINE 1 - KAE

Appendix A.6

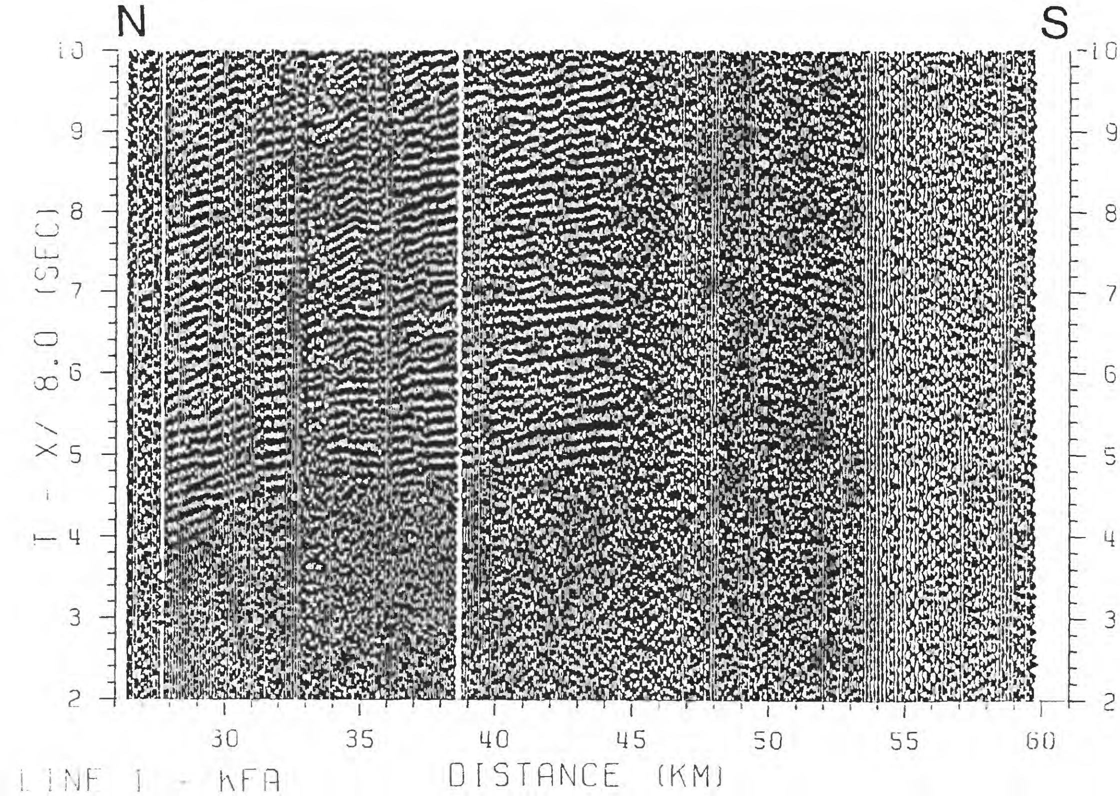
N
S
T - X/ 8.0 (SEC)
DISTANCE (KM)
LINE 1 - KFA

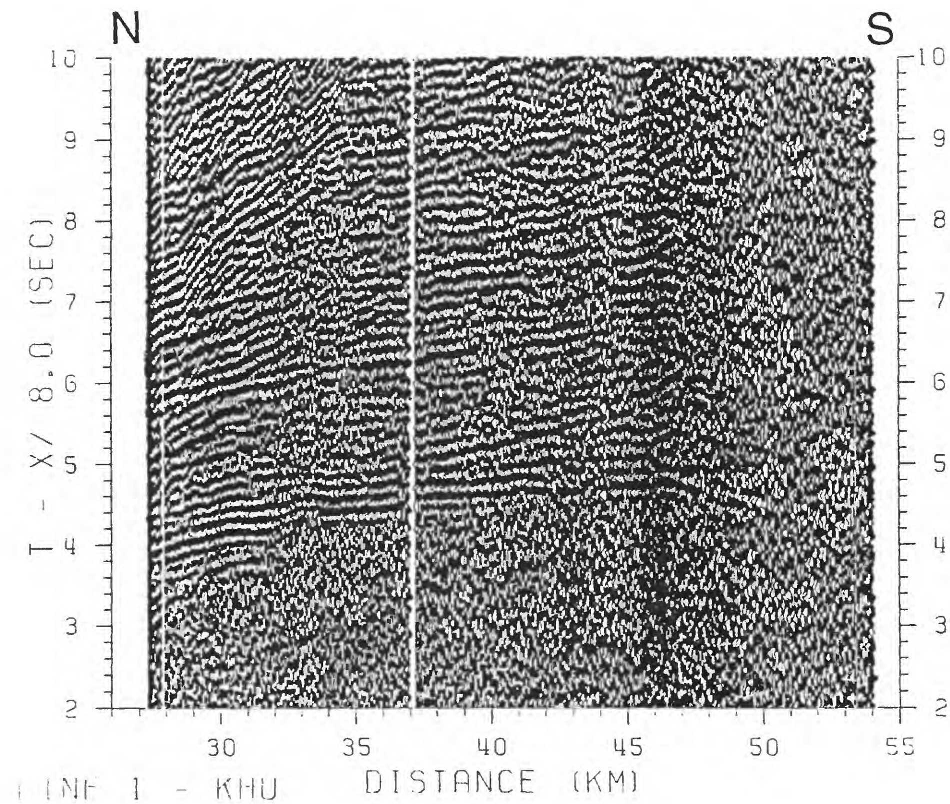
N
S
T - X/ 8.0 (SEC)
DISTANCE (KM)
LINE 1 - KHU

Appendix A.7

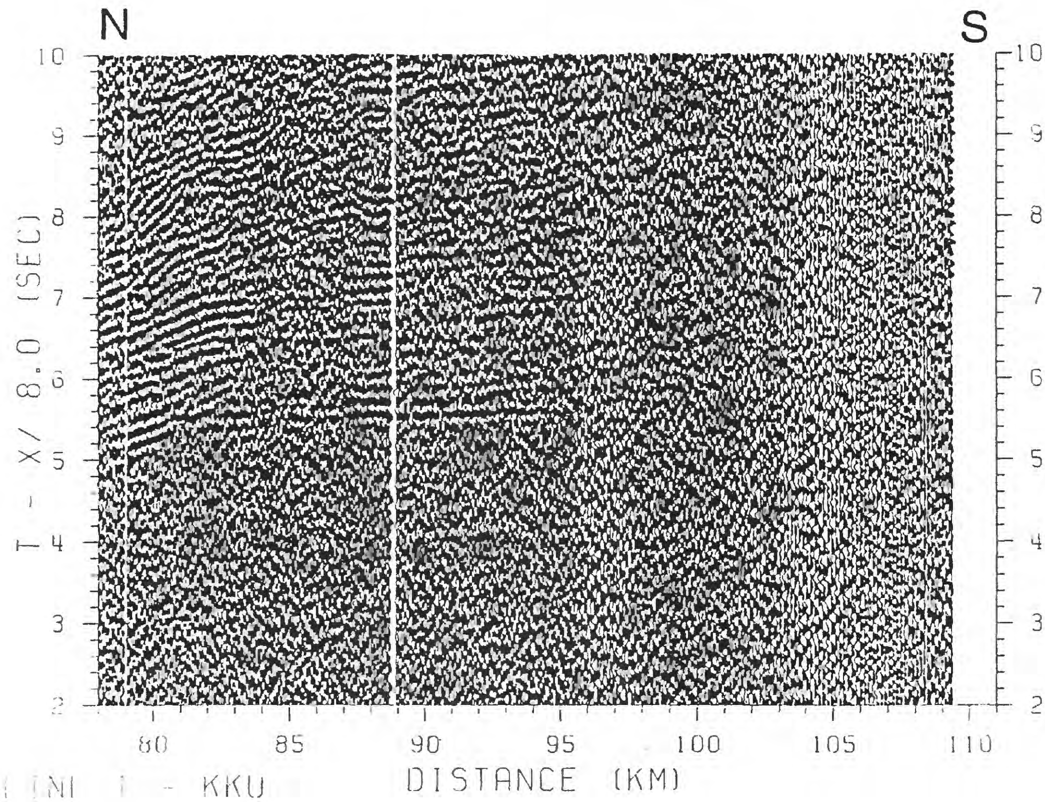
N
S
T - X/ 8.0 (SEC)
10
9
8
7
6
5
4
3
2
80
85
90
95
100
105
110
DISTANCE (KM)
LINE 1 - KKU

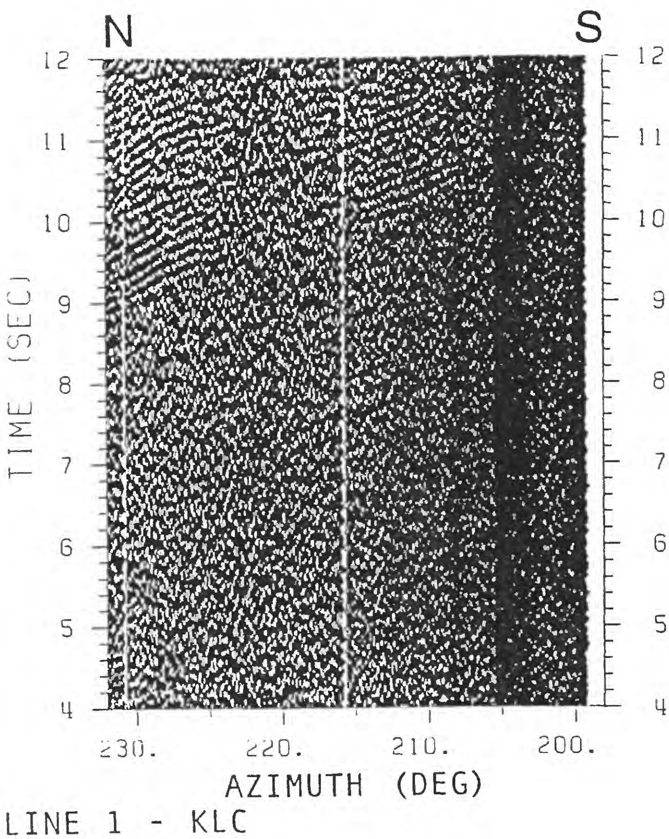
N
S
TIME (SEC)
12
11
10
9
8
7
6
5
4
230.
220.
210.
200.
AZIMUTH (DEG)
LINE 1 - KLC

Appendix A.8

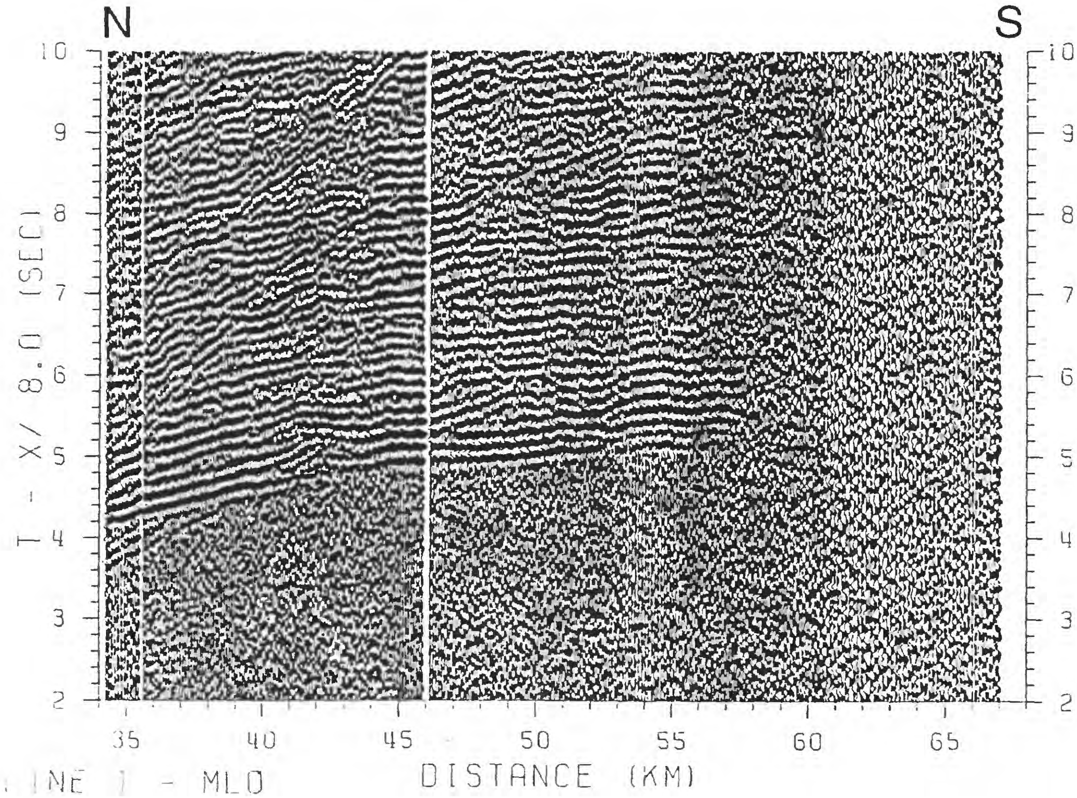

N
S
T - X/ 8.0 (SEC)
DISTANCE (KM)
LINE 1 - MLO

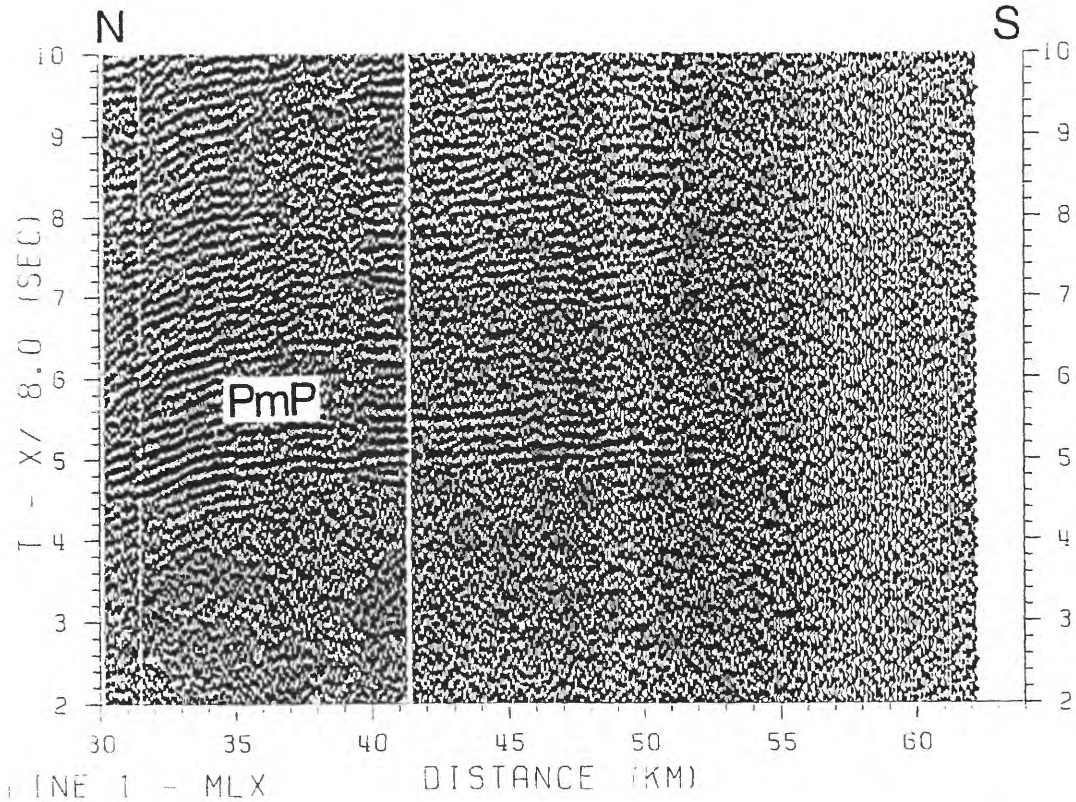

N
S
PmP
T - X/ 8.0 (SEC)
DISTANCE (KM)
LINE 1 - MLX

Appendix A.9

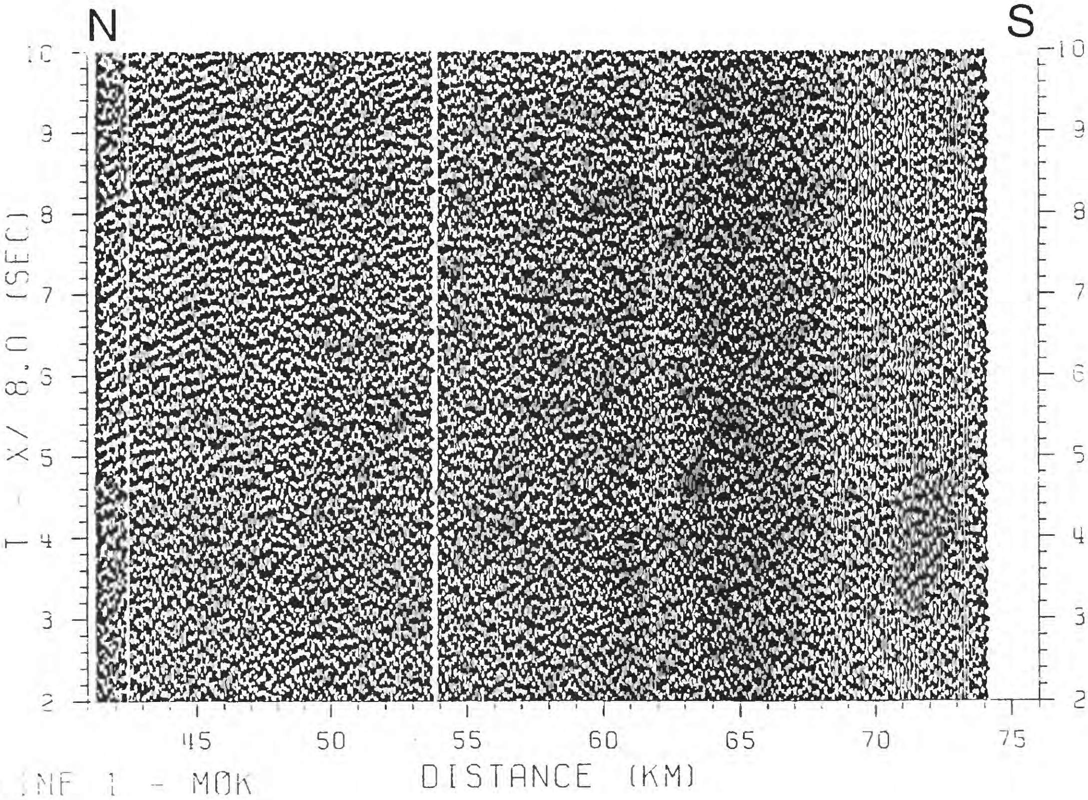

LINE 1 - MOK

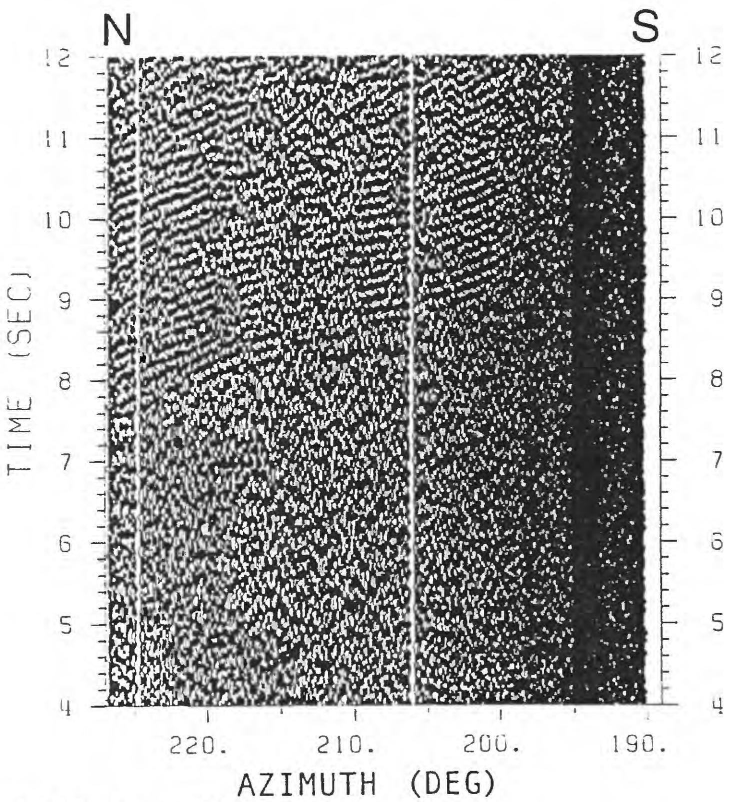

LINE 1 - MPR

Appendix A.10

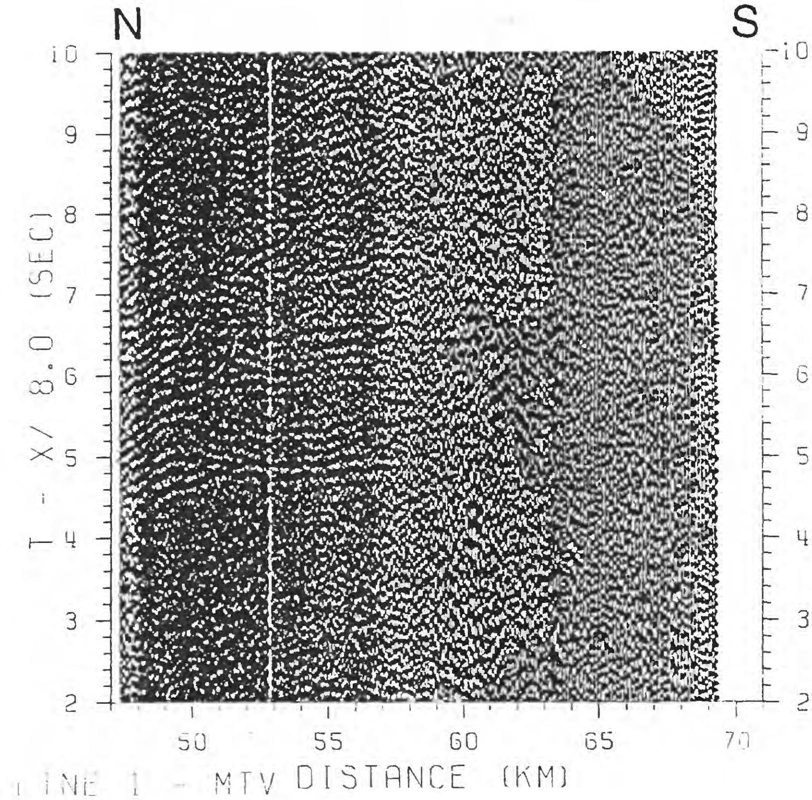

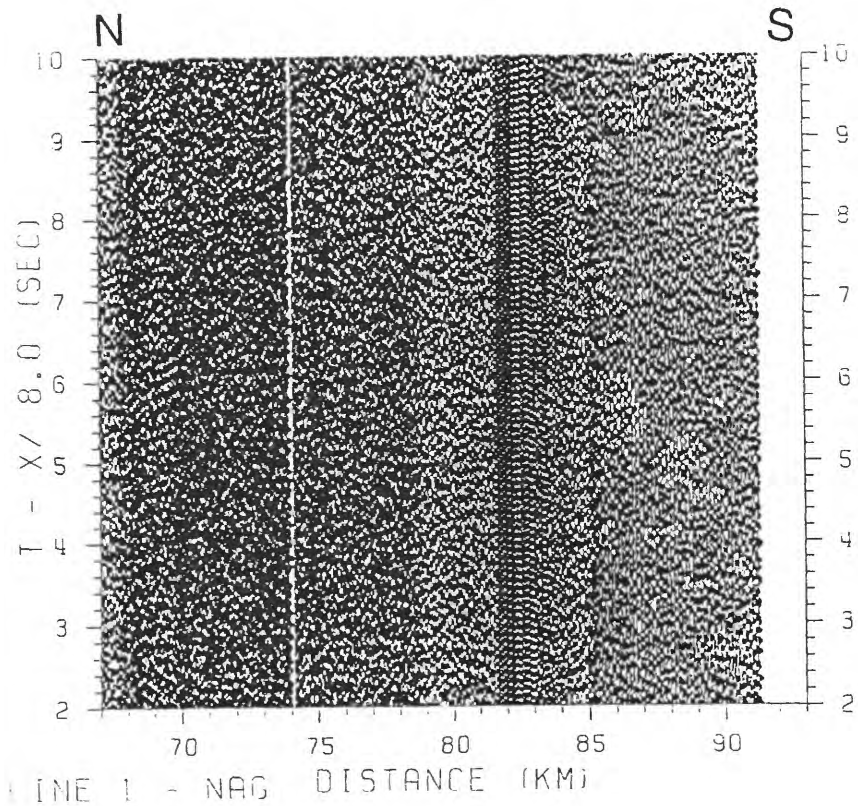

Appendix A.11

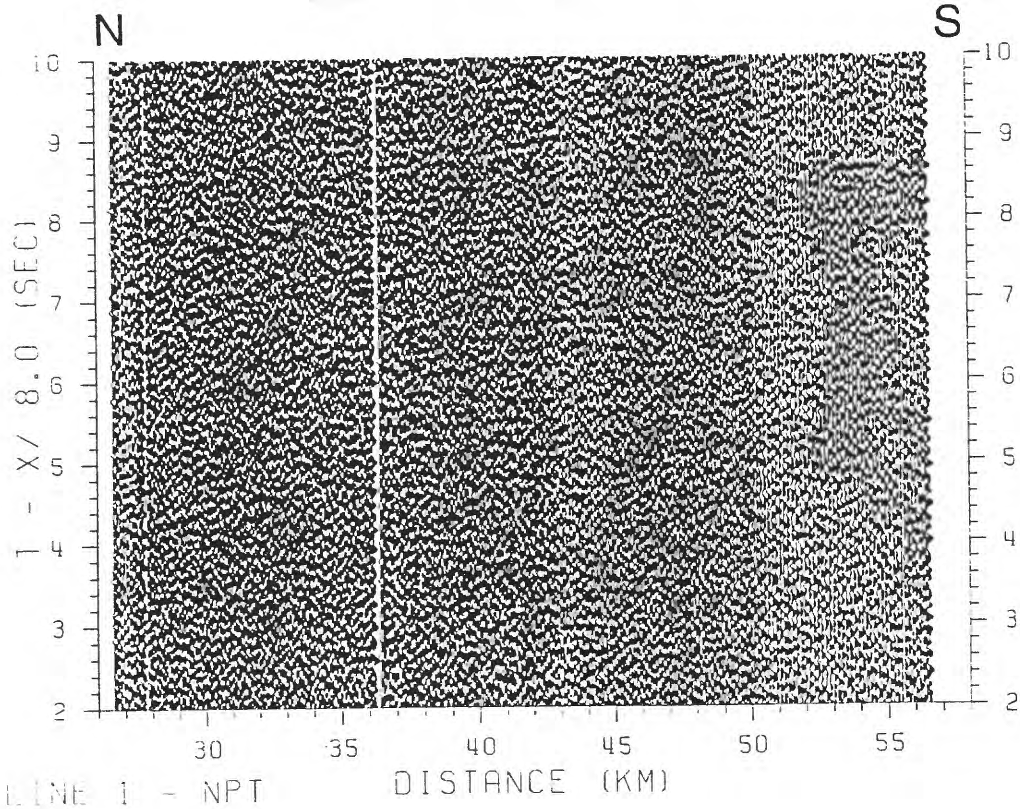

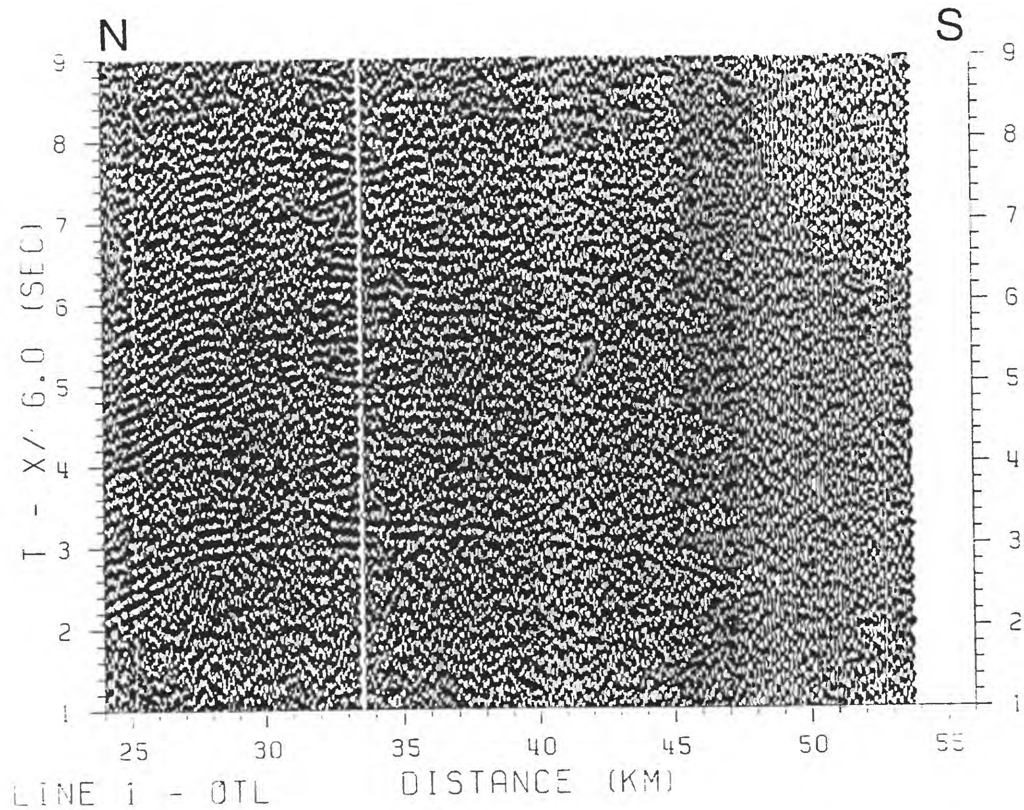

Appendix A.12

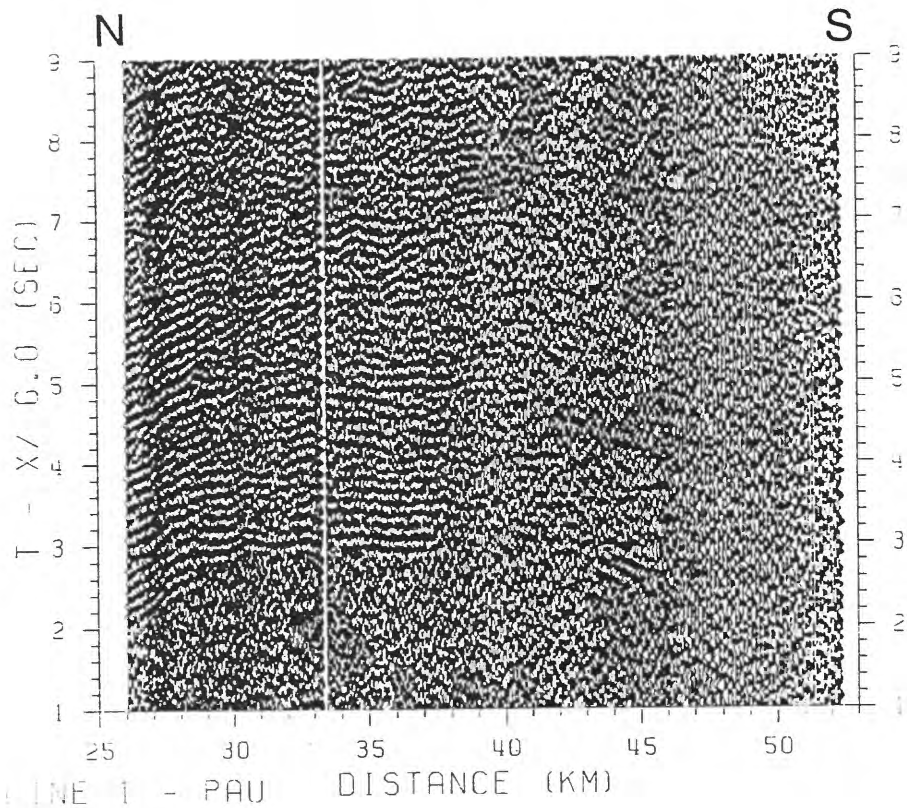

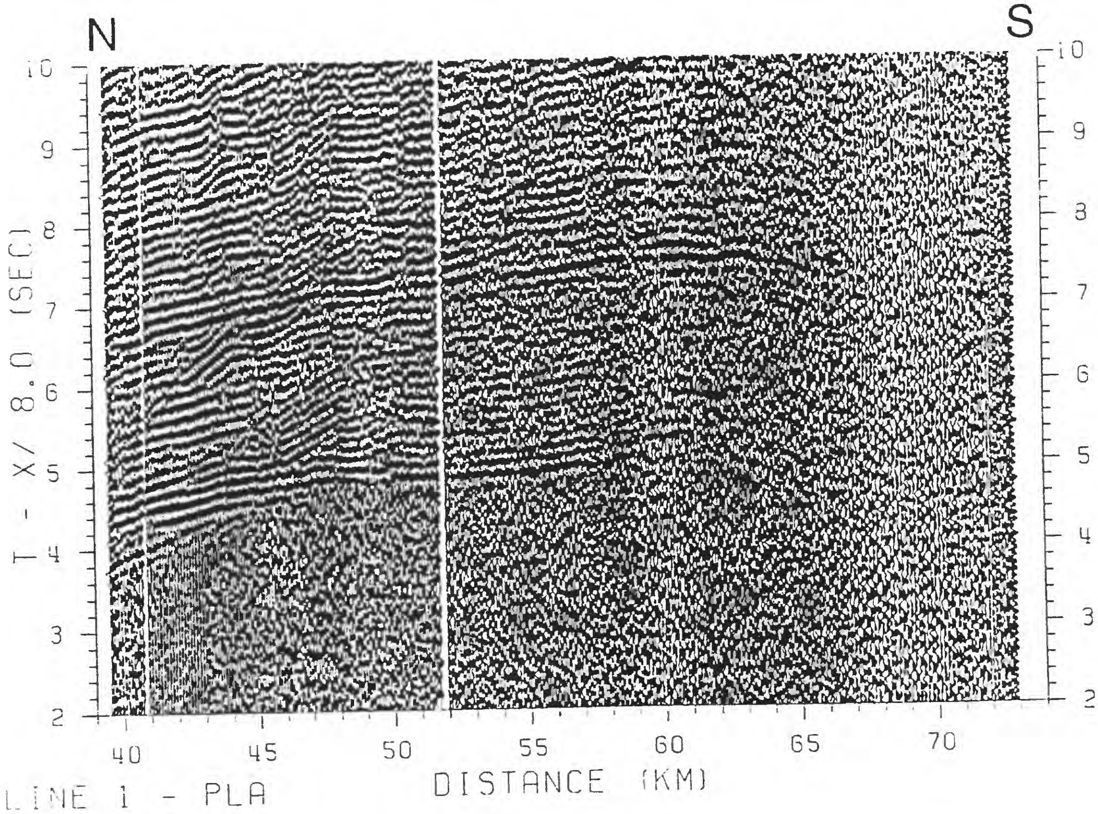

Appendix A.13

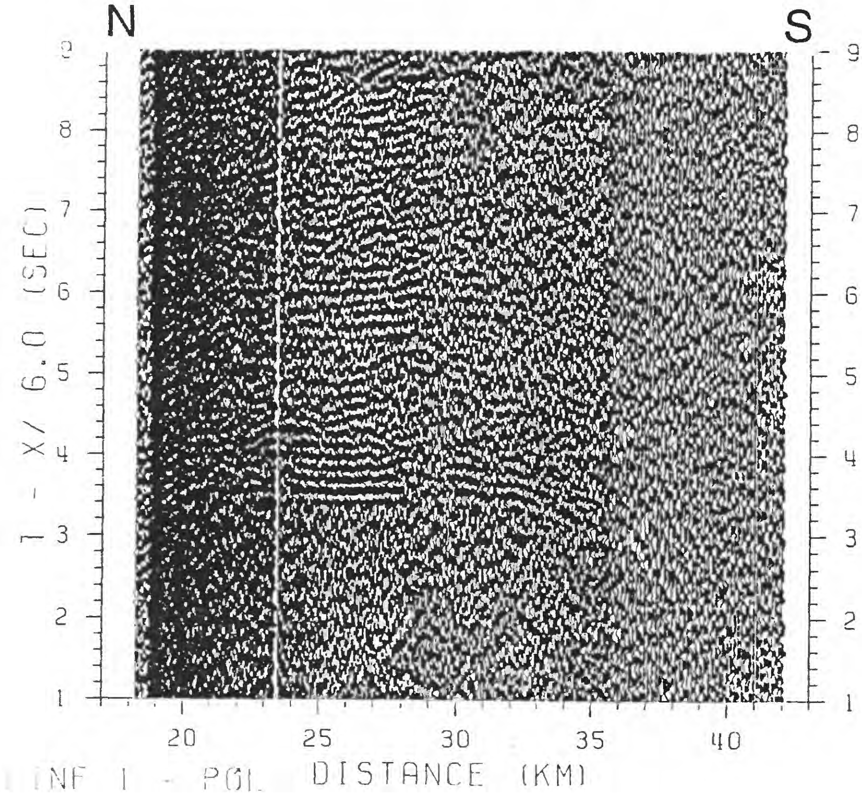

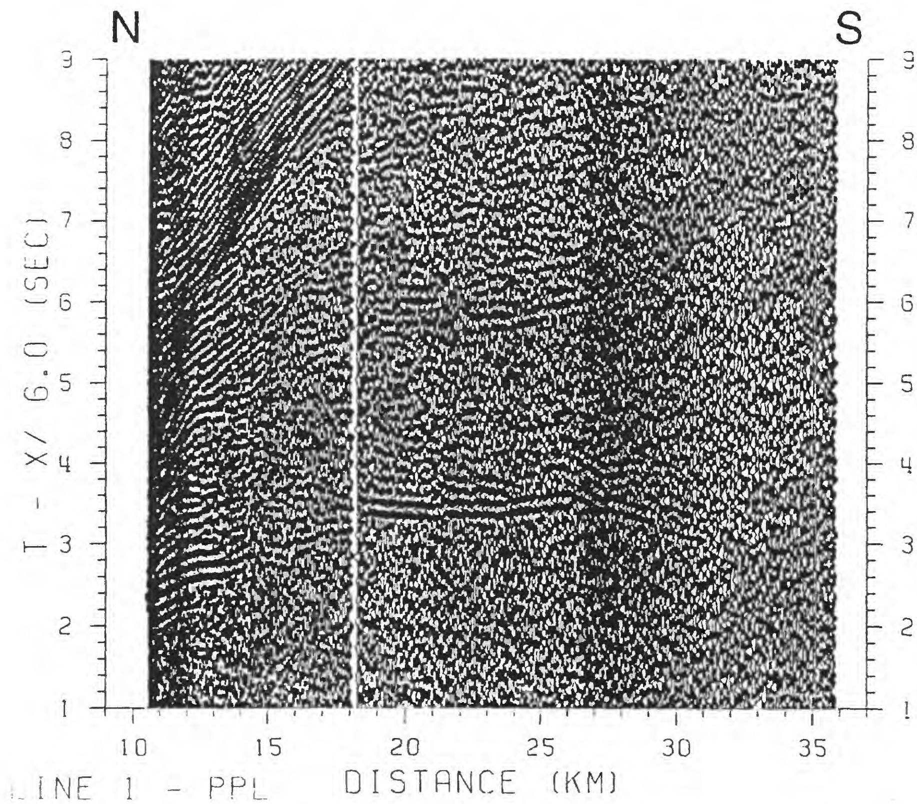

Appendix A.14

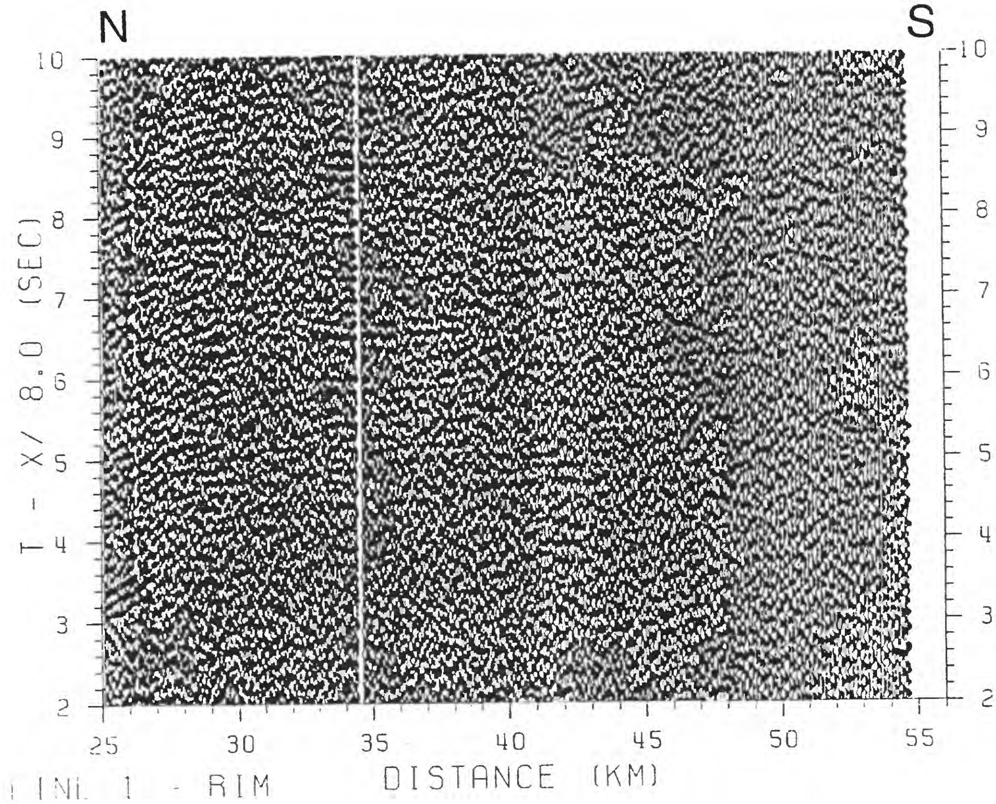

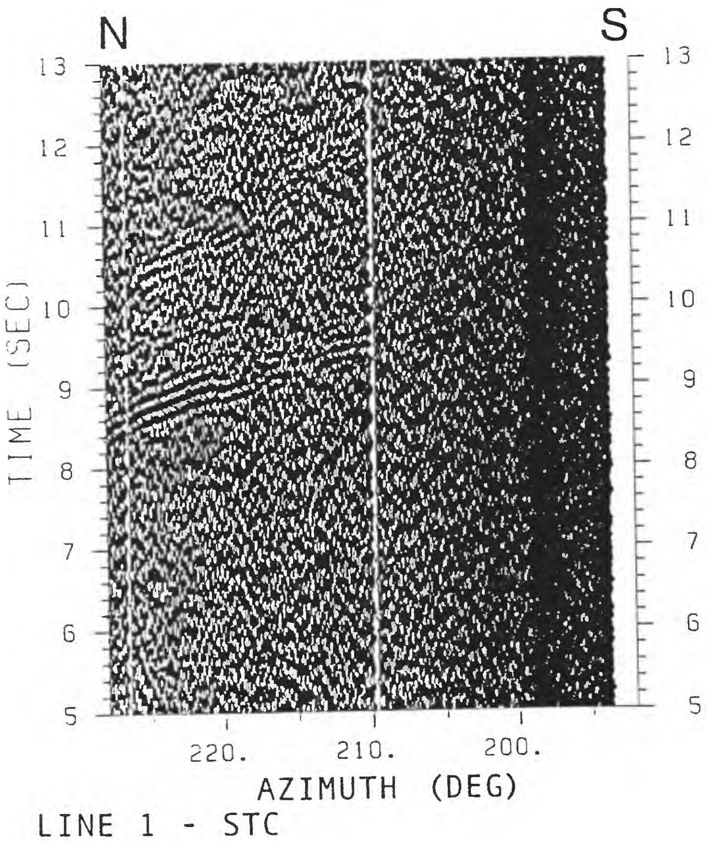

Appendix A.15

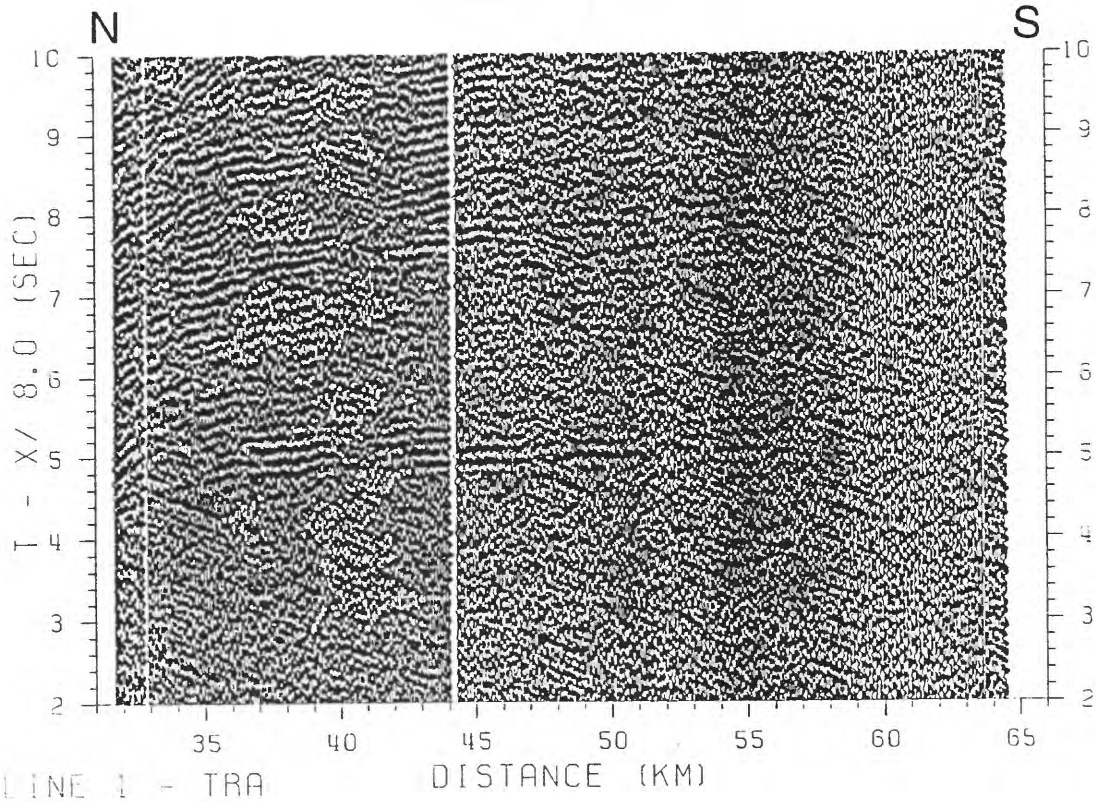

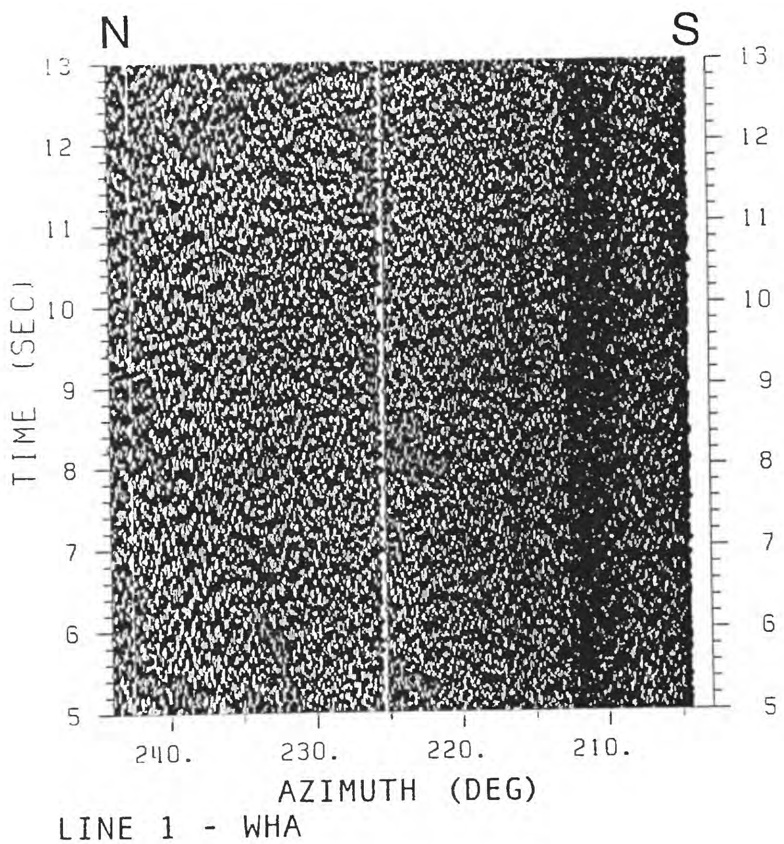

Appendix A.16

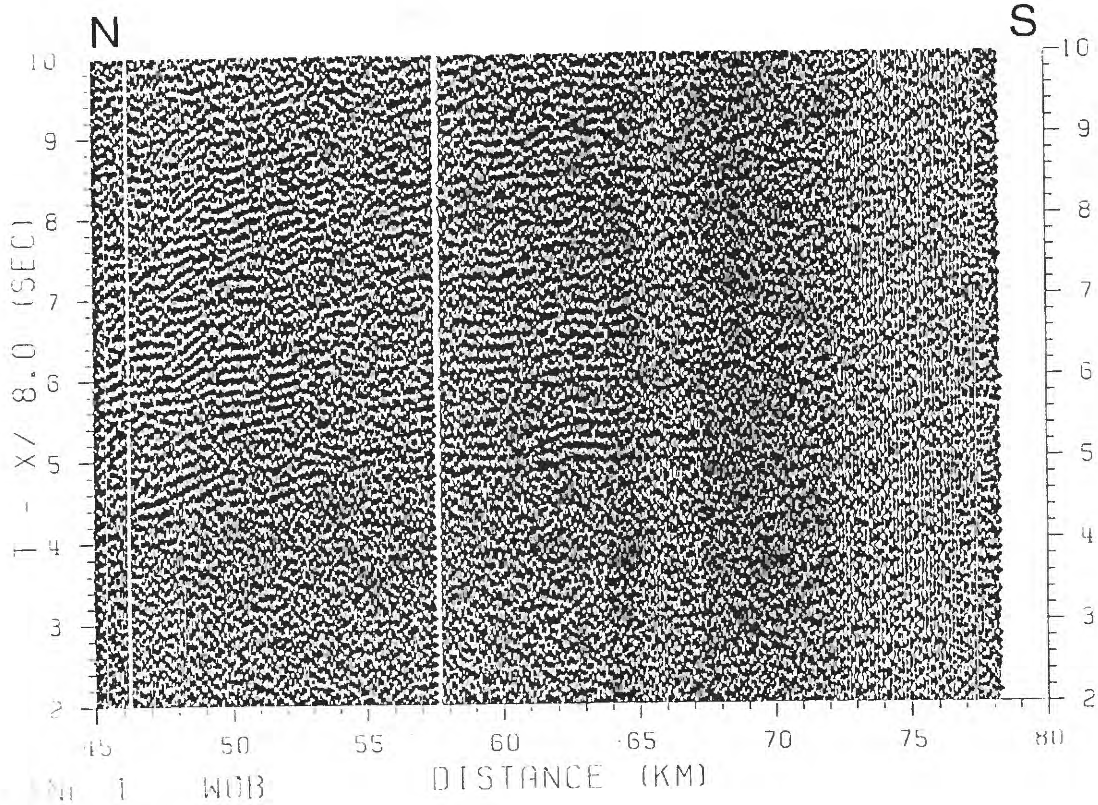

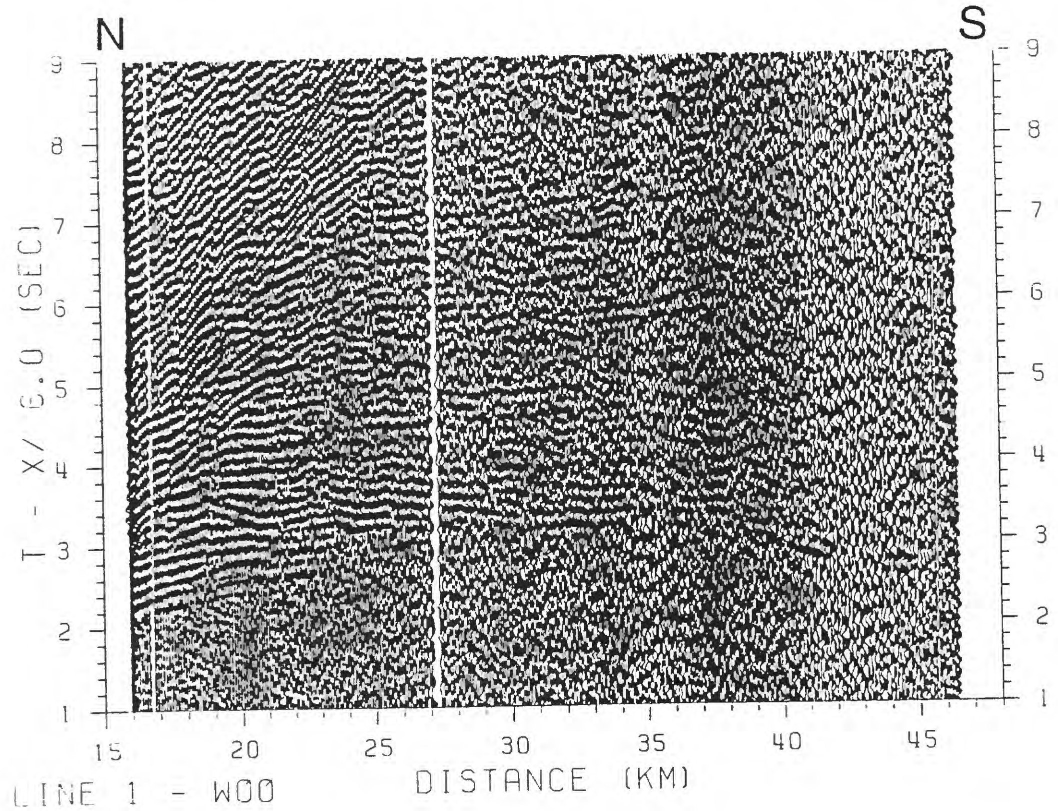

Appendix A.17

APPENDIX B. RECORD SECTIONS FROM LINE 2

Vertical-component record sections for HVO seismic network stations recording seismic phases from Line 2 shots (Figure 4). Data are plotted versus distance or azimuth. Data were bandpass filtered (3 - 10 Hz), and each trace scaled to a uniform maximum amplitude. For time vs. distance plots, data were linearly reduced using velocities of 6 or 8 km/s. Reduction velocities were selected to permit identification of the ranges at which Moho (oceanic crust-mantle boundary) and crustal (volcano-oceanic crust transition) velocities first appear. No topographic or water column corrections have been applied, and the estimated 50 ms firing system delay has not been accounted for in the plots. Shot range is the distance between OHD HVO station locations and WGS 84 shot locations; true ranges, resulting in shifts averaging 445 m in the N140°E direction, are calculated in Table 2.

FIGURE *PAGE*

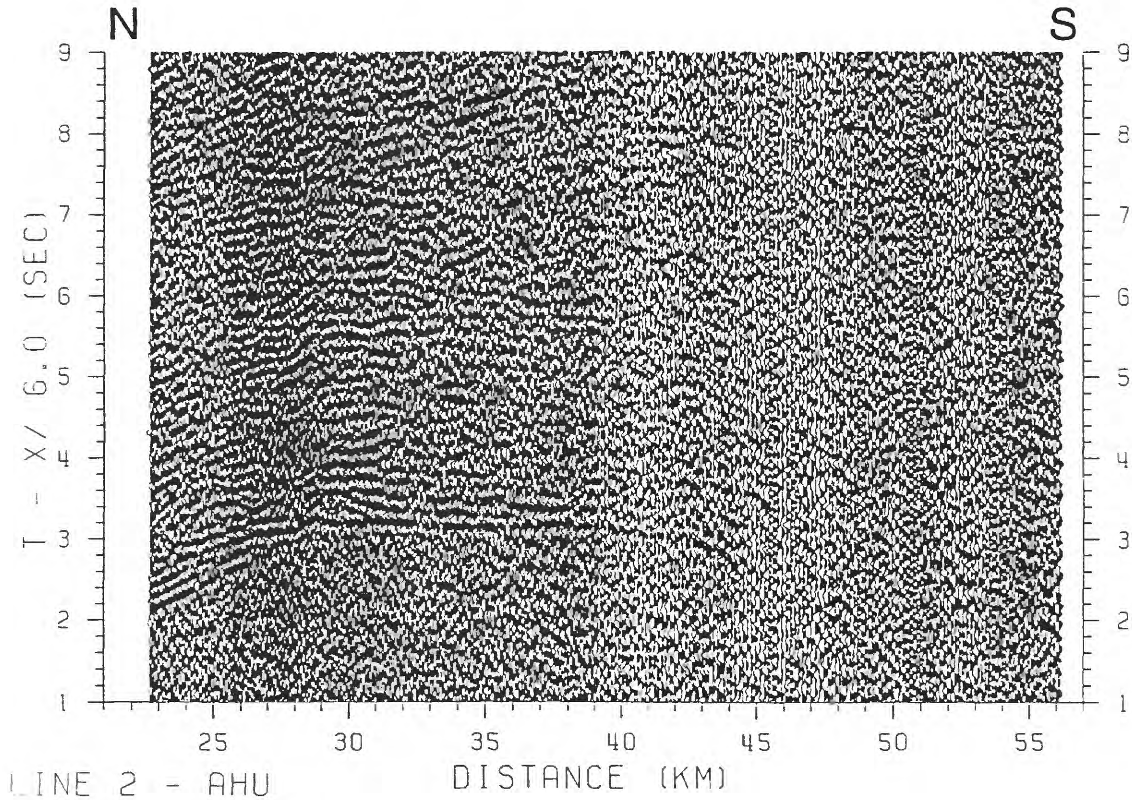
N
S
T - X/ 6.0 (SEC)
DISTANCE (KM)
LINE 2 - AHU

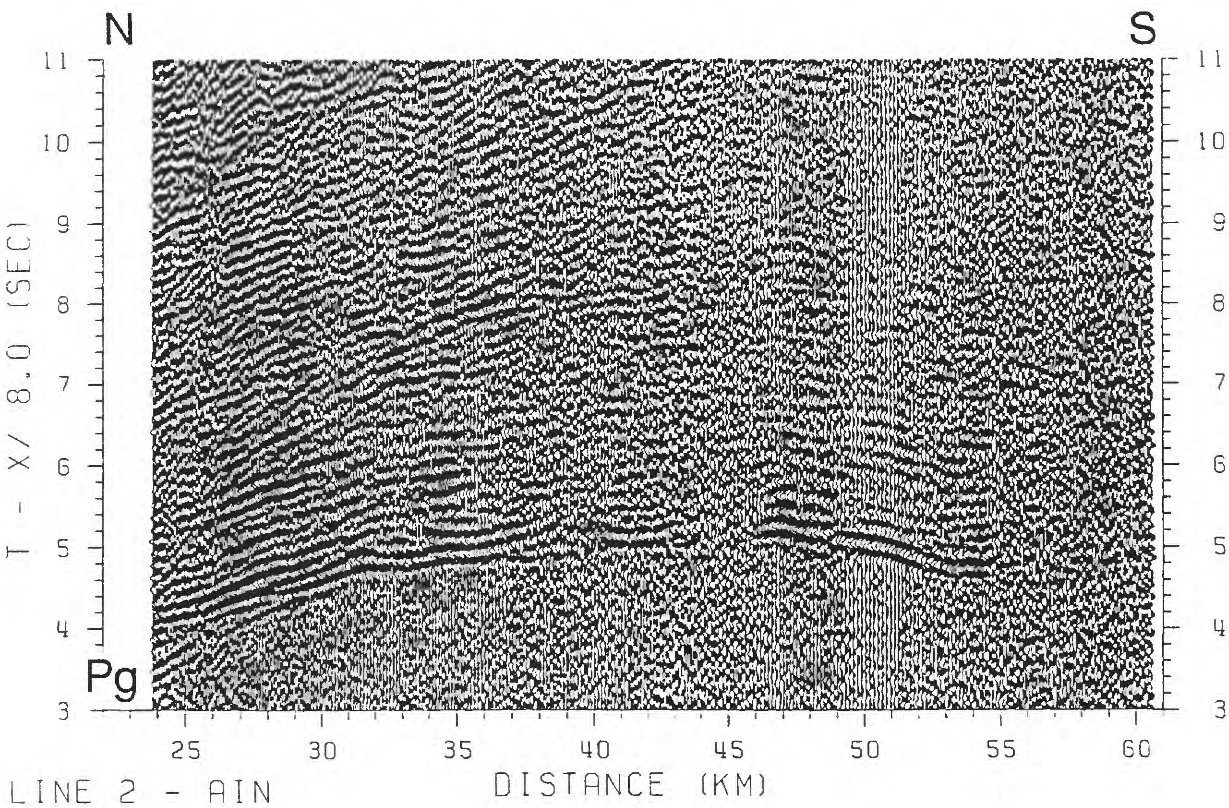
N
S
Pg
T - X/ 8.0 (SEC)
DISTANCE (KM)
LINE 2 - AIN

Appendix B.1

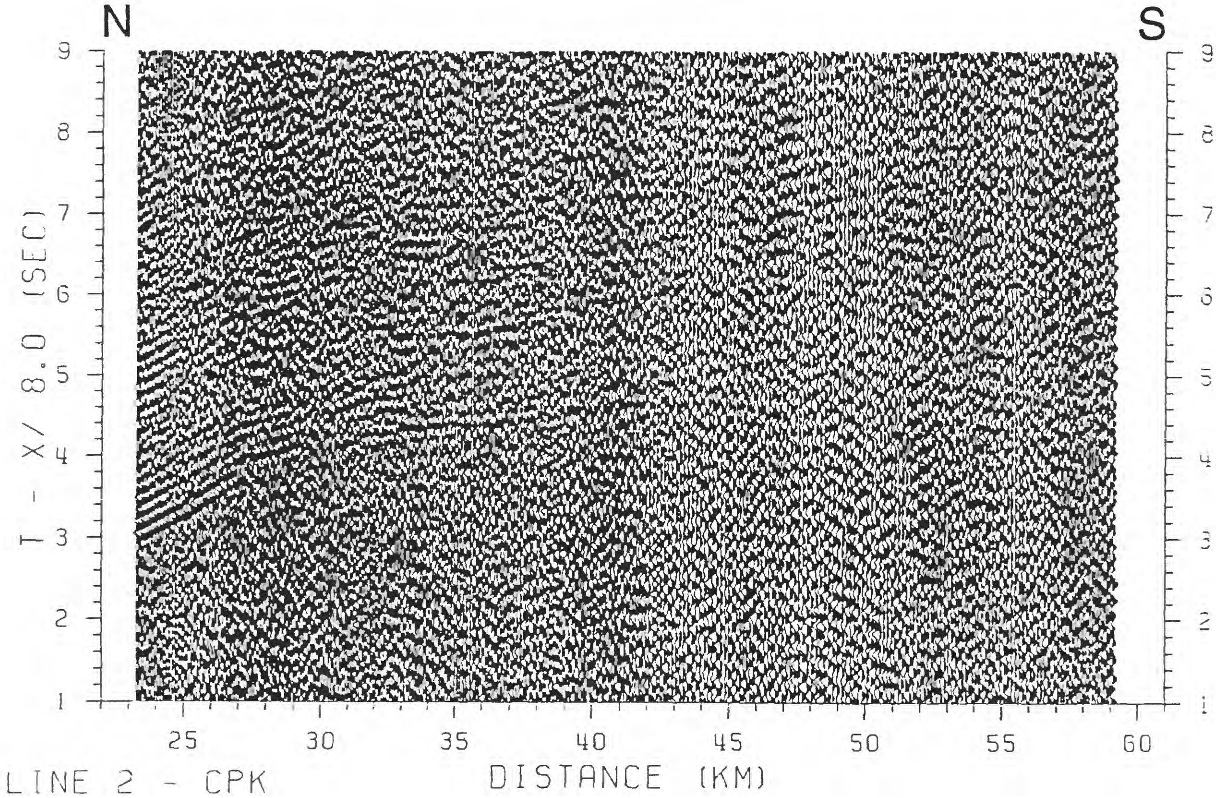

N
S
T - X/ 8.0 (SEC)
DISTANCE (KM)
LINE 2 - CPK

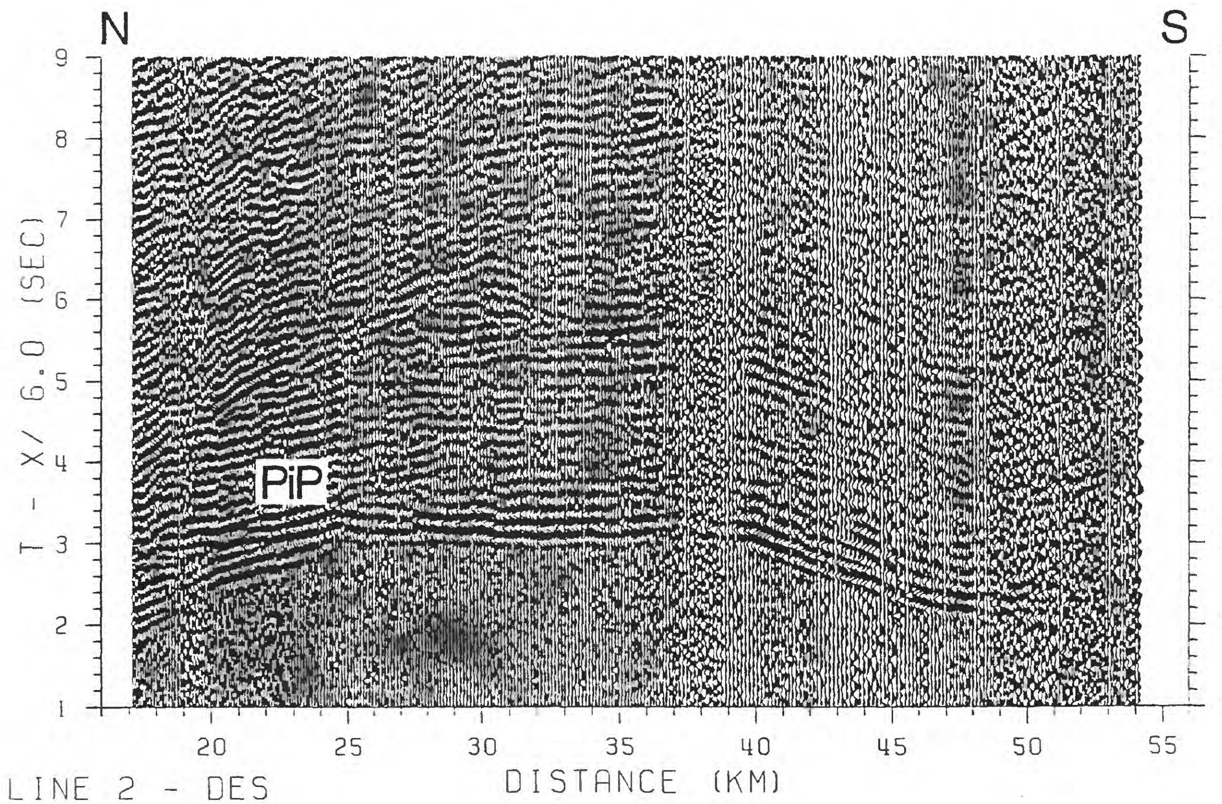

N
S
PiP
T - X/ 6.0 (SEC)
DISTANCE (KM)
LINE 2 - DES

Appendix B.2

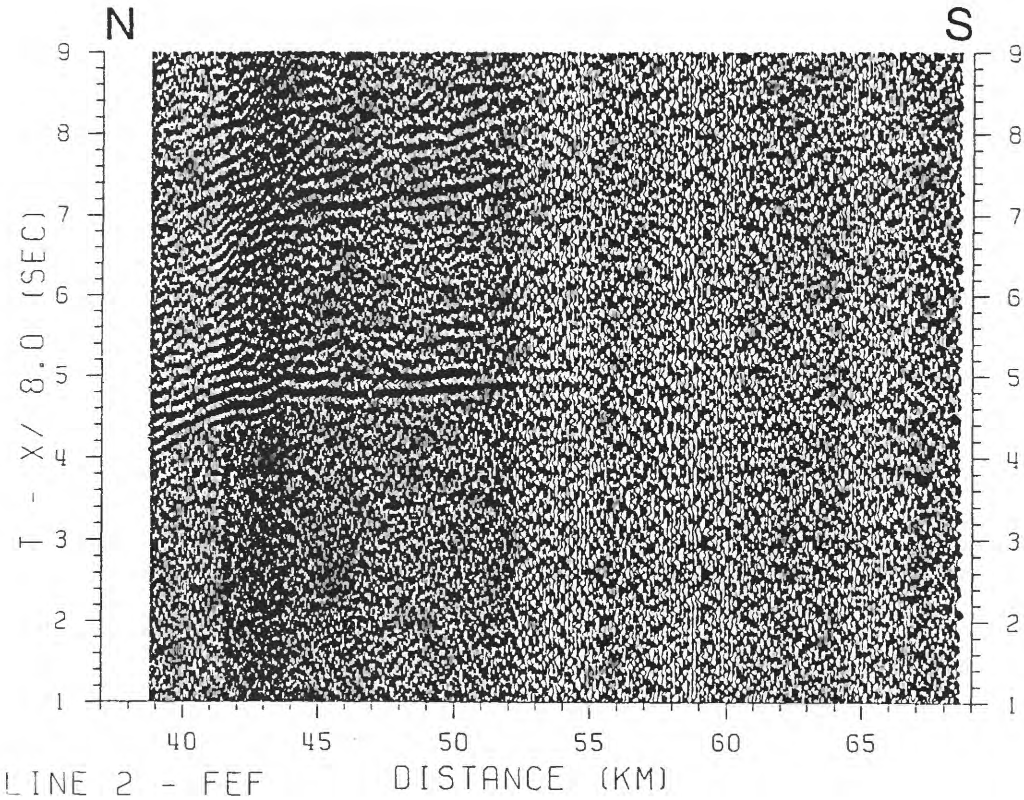
N
S
T - X/ 8.0 (SEC)
40
45
50
55
60
65
LINE 2 - FEF
DISTANCE (KM)

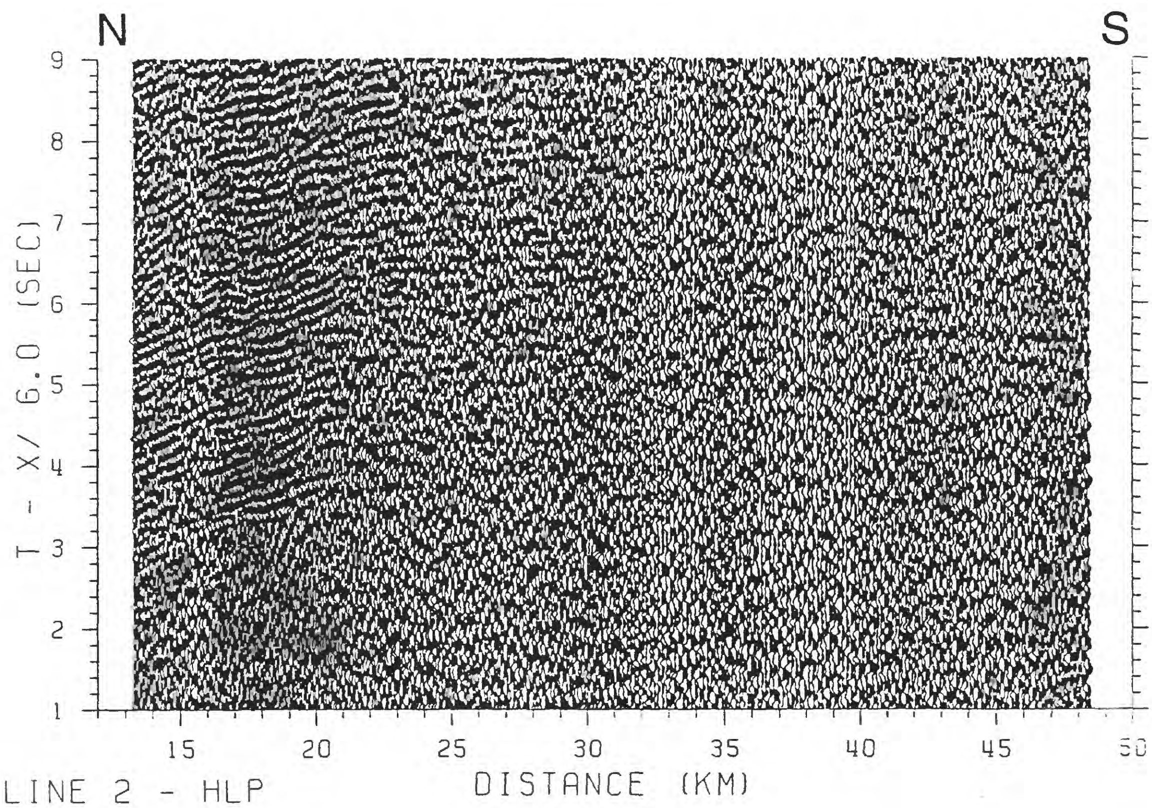
N
S
T - X/ 6.0 (SEC)
15
20
25
30
35
40
45
50
LINE 2 - HLP
DISTANCE (KM)

Appendix B.3

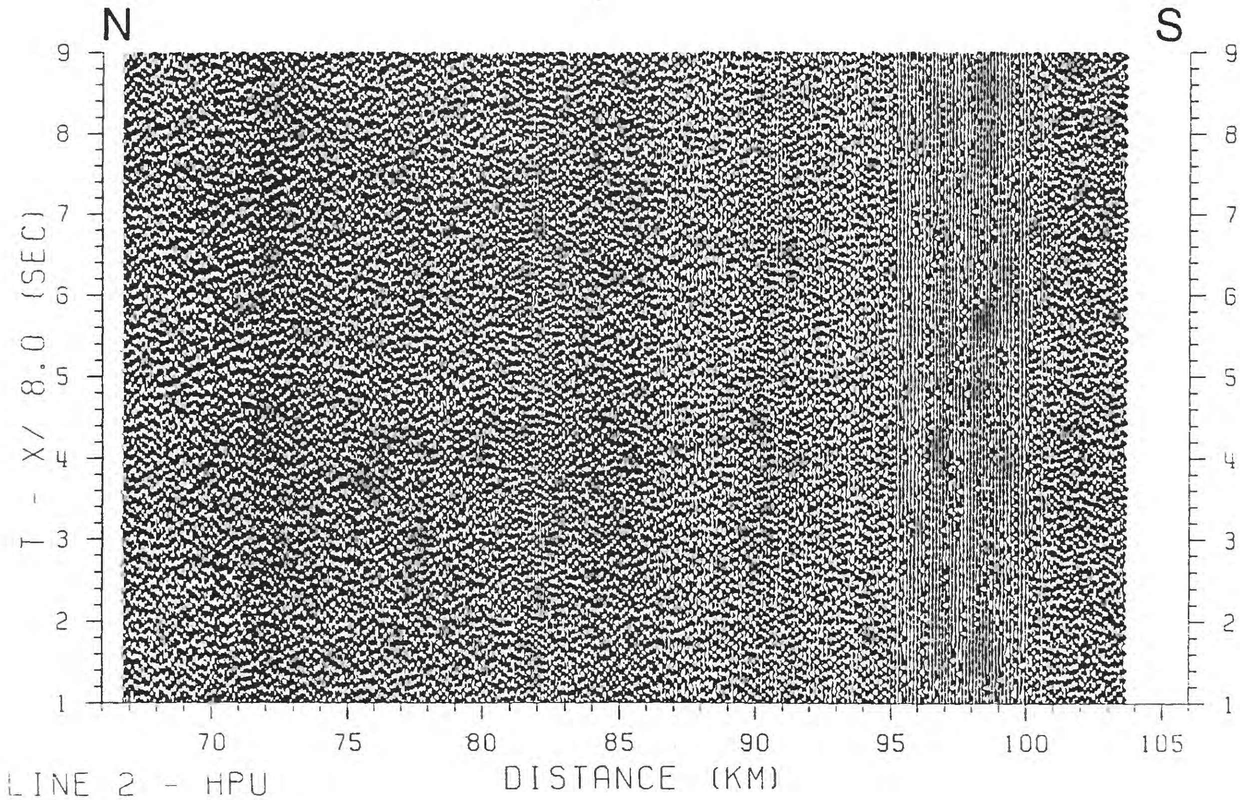
N
S
T - X/ 8.0 (SEC)
DISTANCE (KM)
LINE 2 - HPU

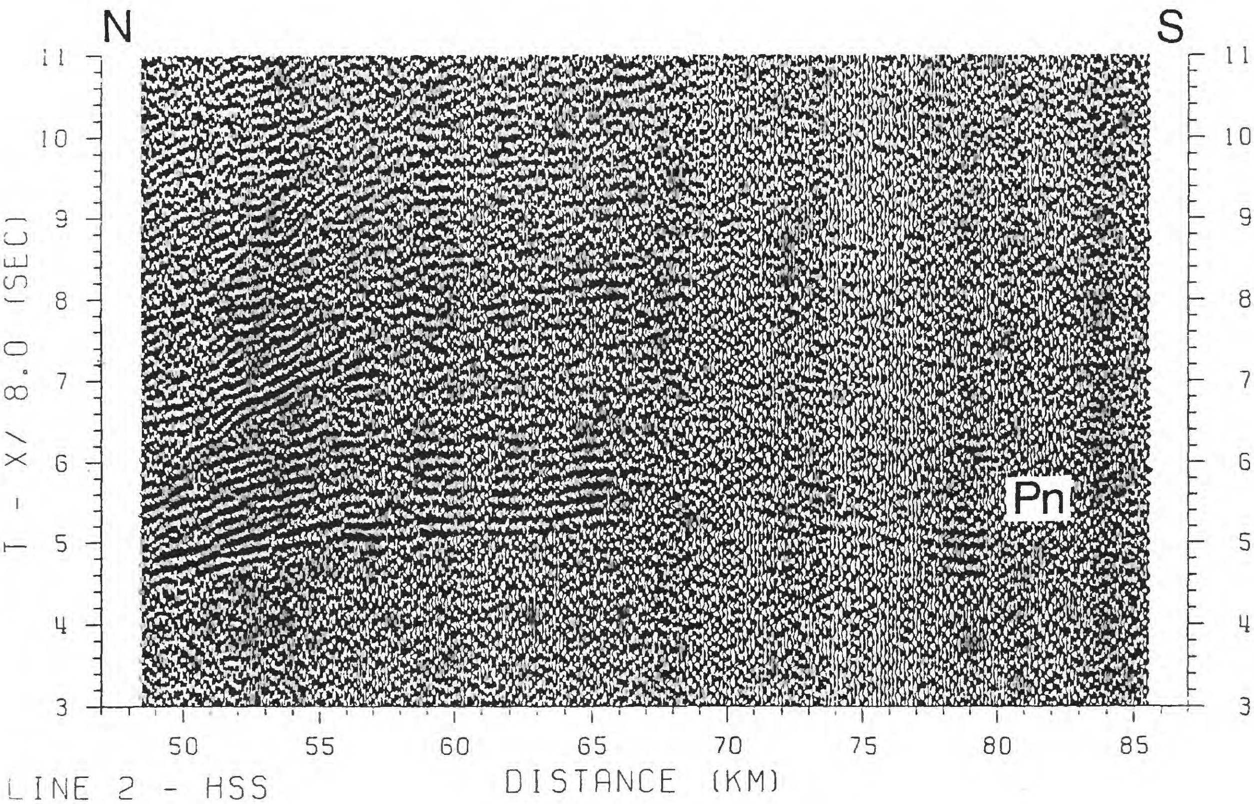
N
S
Pn
T - X/ 8.0 (SEC)
DISTANCE (KM)
LINE 2 - HSS

Appendix B.4

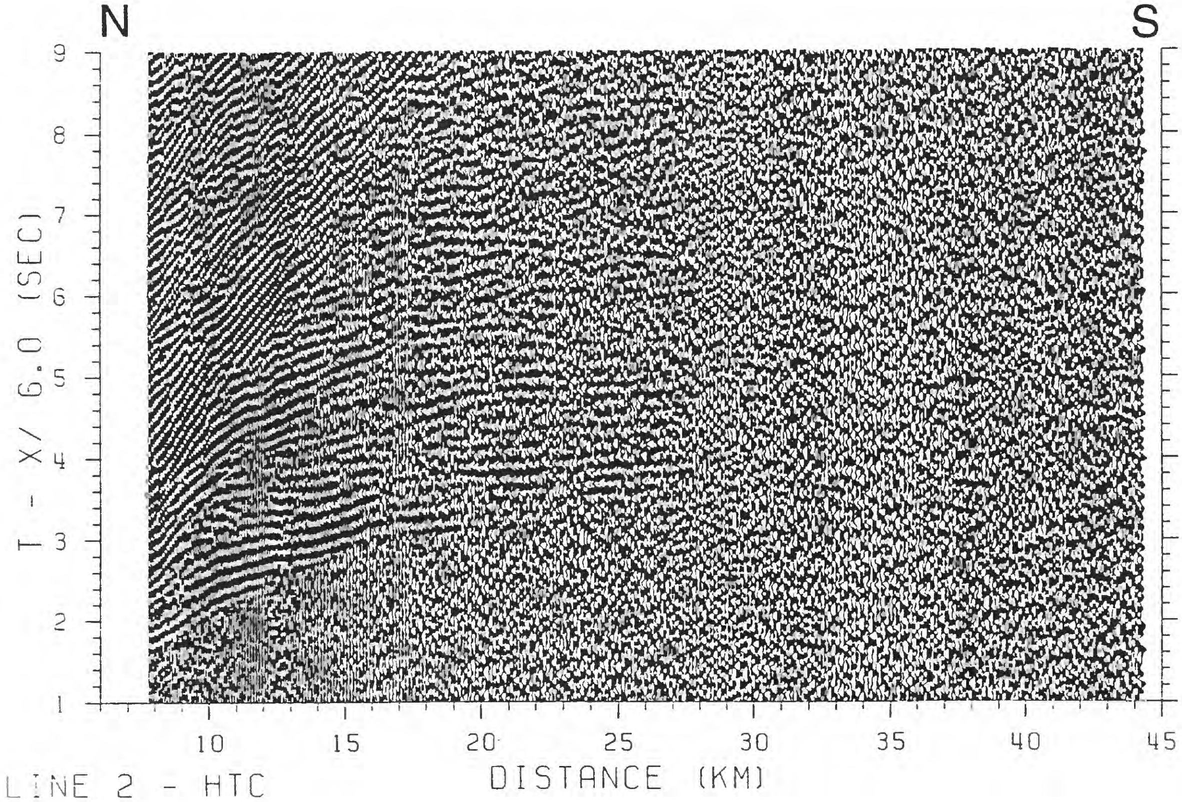
N
S
T - X/ 6.0 (SEC)
1
2
3
4
5
6
7
8
9
10
15
20
25
30
35
40
45
DISTANCE (KM)
LINE 2 - HTC

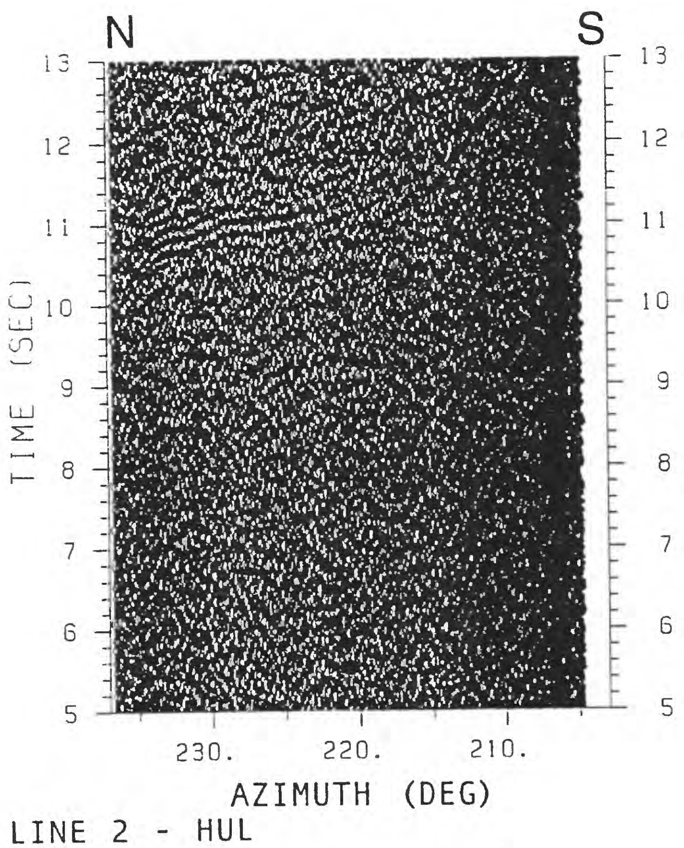
N
S
TIME (SEC)
5
6
7
8
9
10
11
12
13
230.
220.
210.
AZIMUTH (DEG)
LINE 2 - HUL

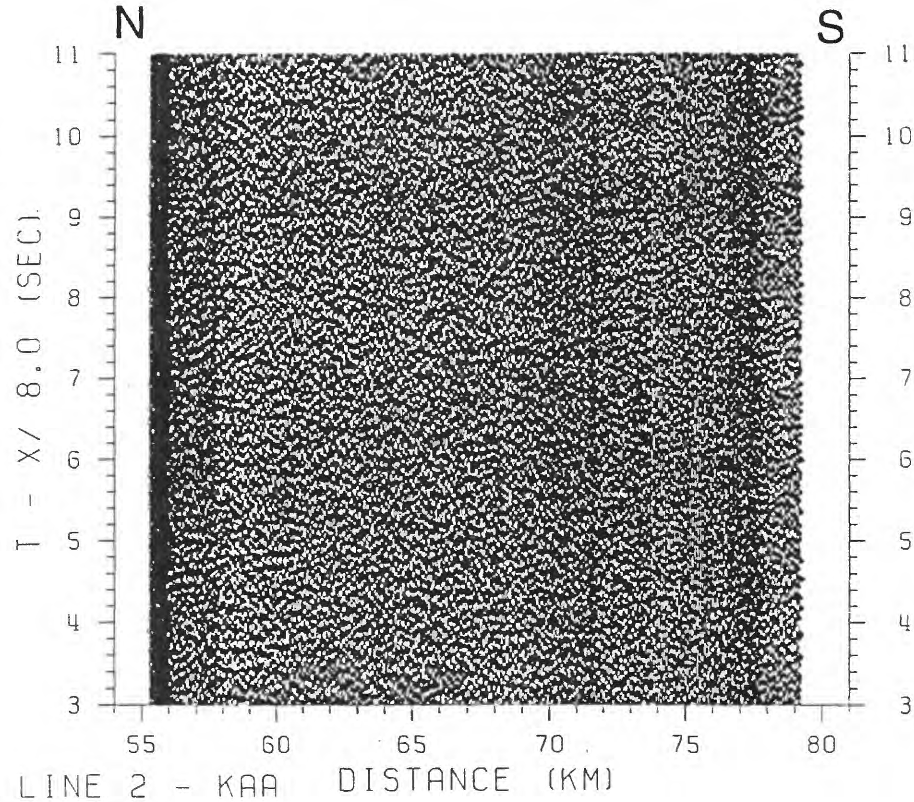
N
S
T - X/ 8.0 (SEC)
11
10
9
8
7
6
5
4
3
55
60
65
70
75
80
LINE 2 - KAA
DISTANCE (KM)

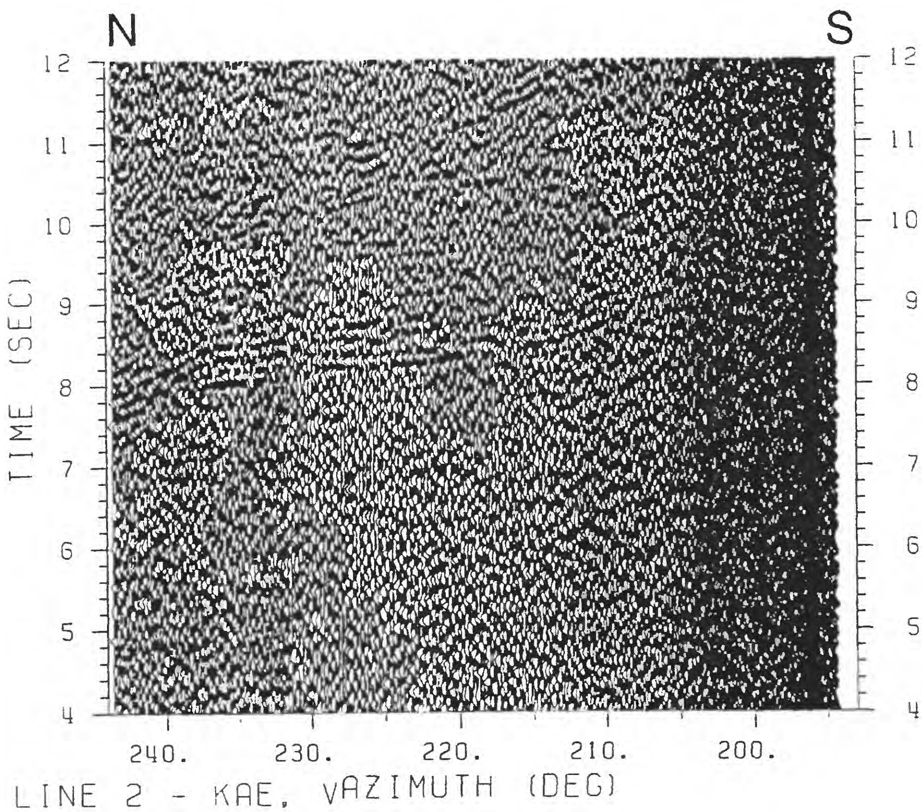
N
S
TIME (SEC)
12
11
10
9
8
7
6
5
4
240.
230.
220.
210.
200.
LINE 2 - KAE, VAZIMUTH (DEG)

Appendix B.6

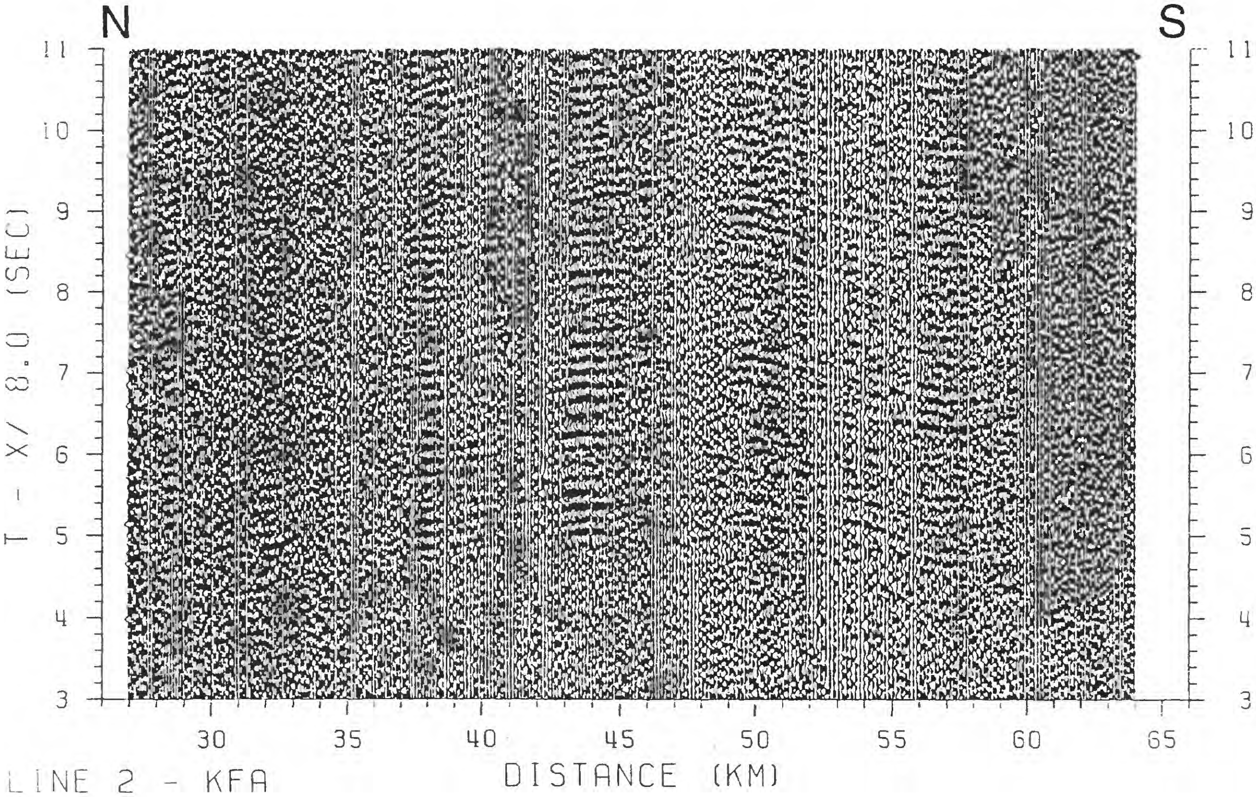
N
S
T - X/ 8.0 (SEC)
3
4
5
6
7
8
9
10
11
30
35
40
45
50
55
60
65
DISTANCE (KM)
LINE 2 - KFA

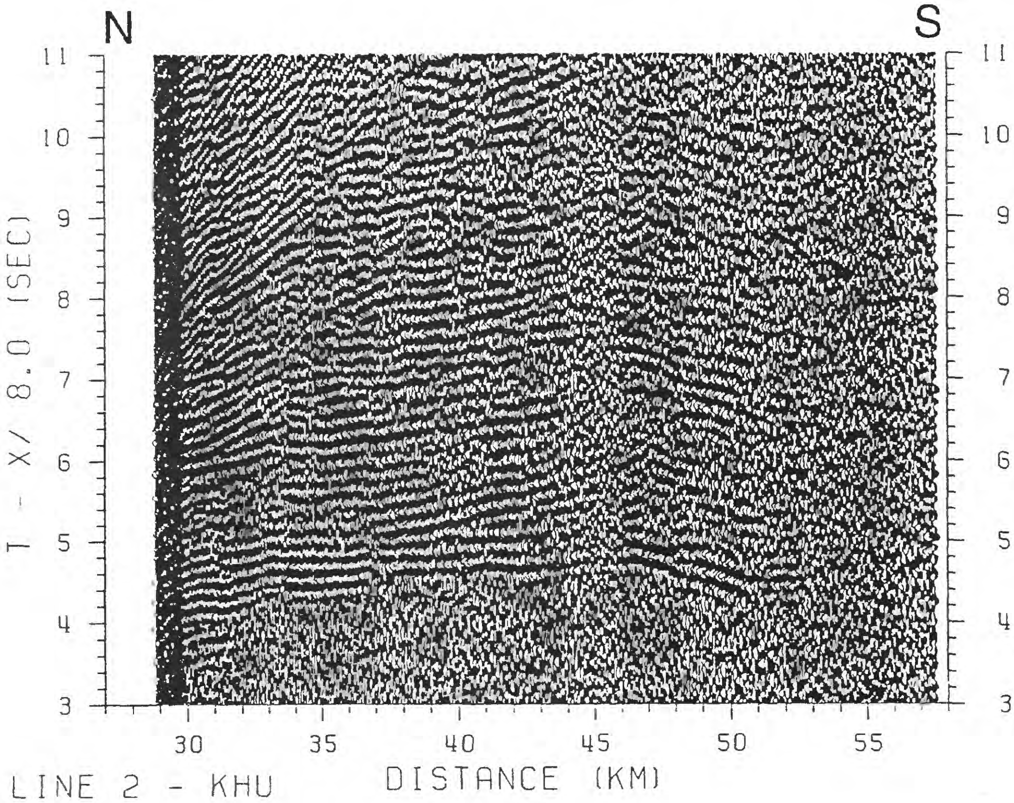
N
S
T - X/ 8.0 (SEC)
3
4
5
6
7
8
9
10
11
30
35
40
45
50
55
DISTANCE (KM)
LINE 2 - KHU

Appendix B.7

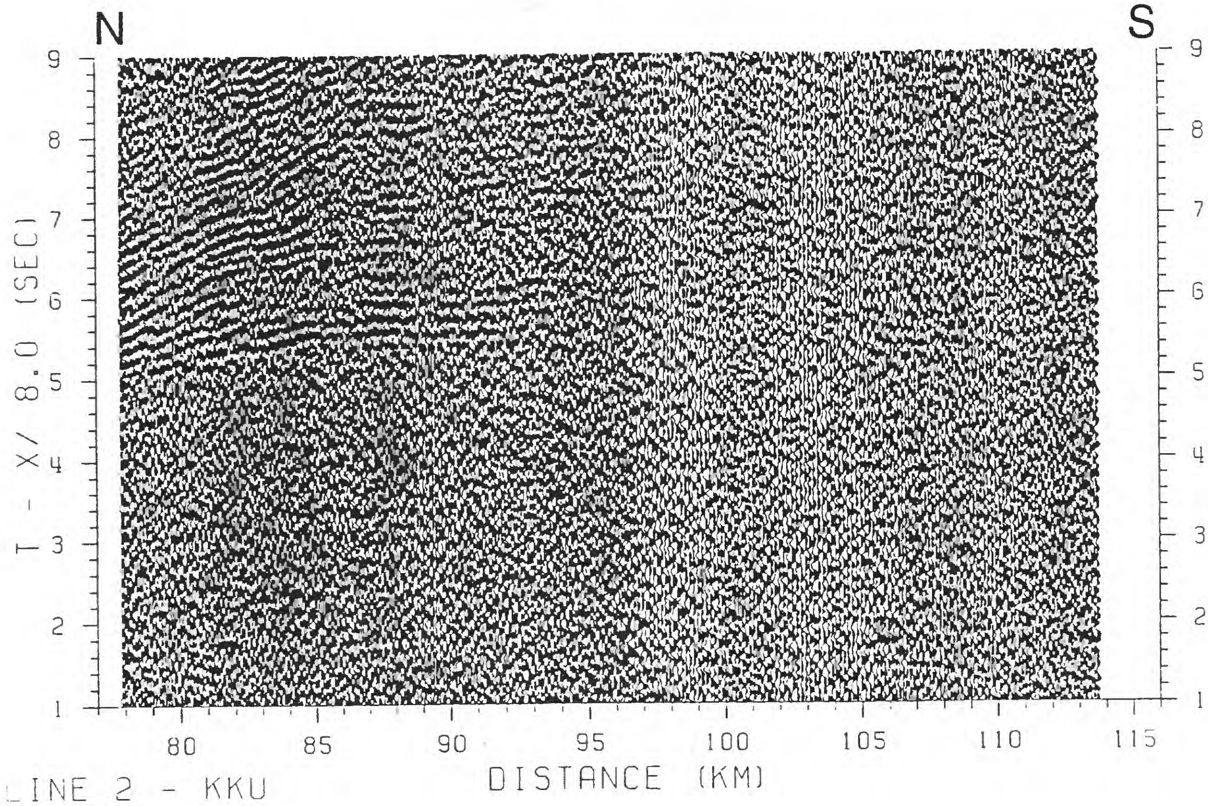

N
S
T - X/ 8.0 (SEC)
1 2 3 4 5 6 7 8 9
80 85 90 95 100 105 110 115
DISTANCE (KM)
LINE 2 - KKU

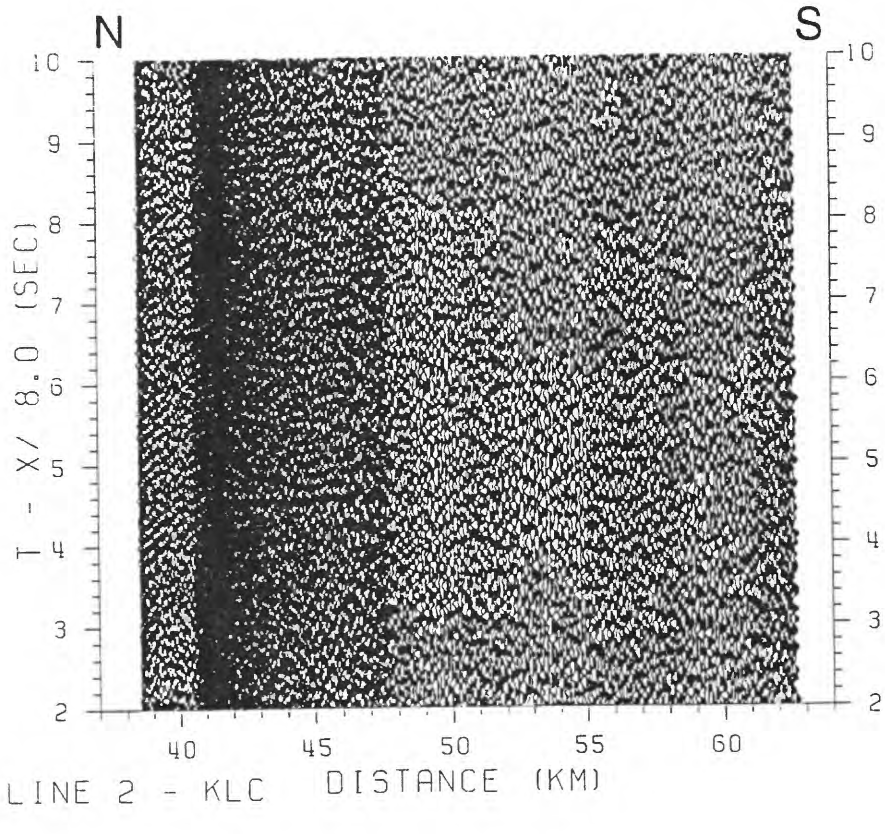

N
S
T - X/ 8.0 (SEC)
2 3 4 5 6 7 8 9 10
40 45 50 55 60
LINE 2 - KLC
DISTANCE (KM)

Appendix B.8

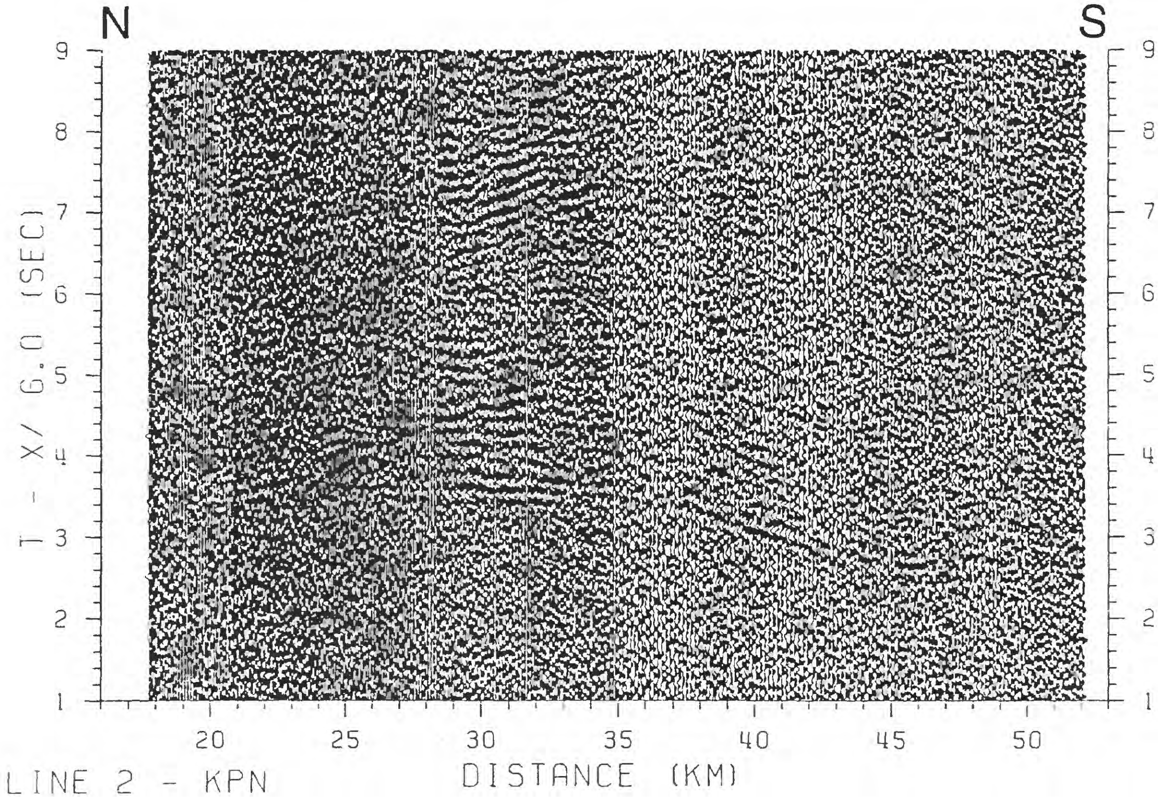
N
S
T - X/ 6.0 (SEC)
DISTANCE (KM)
LINE 2 - KPN

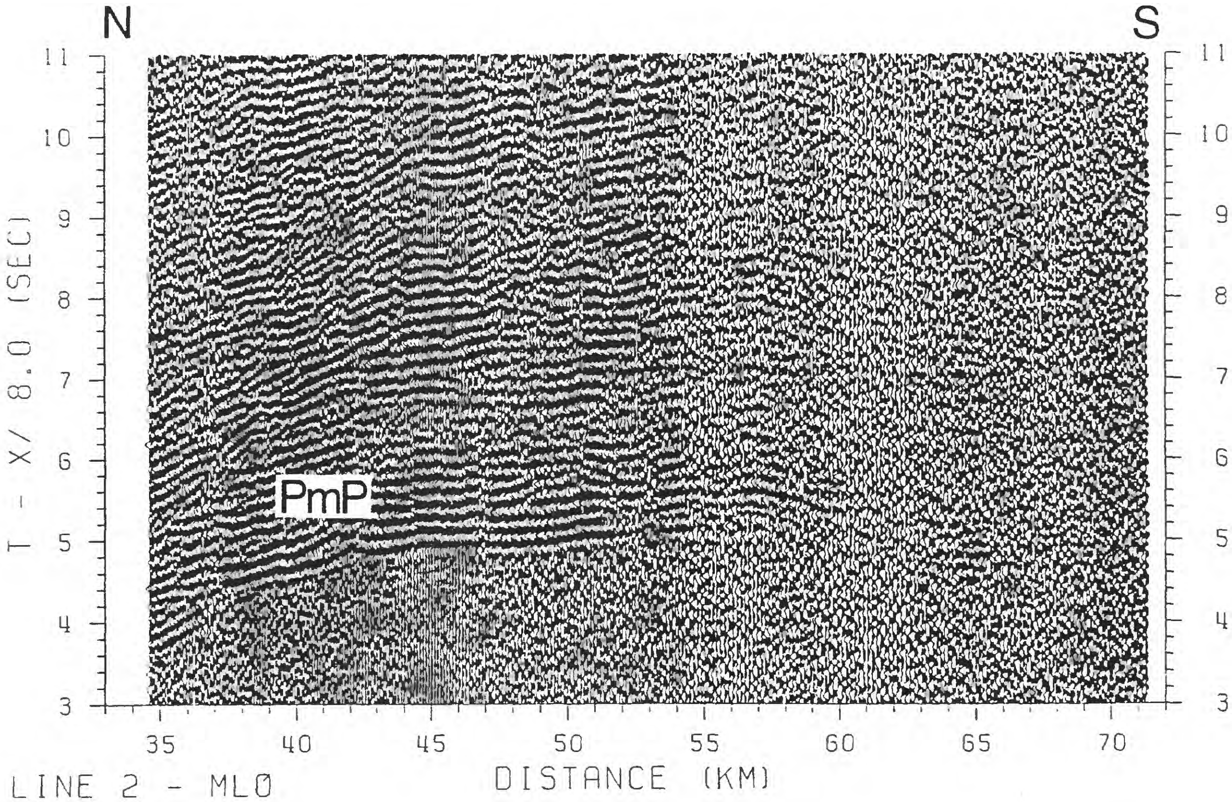
N
S
T - X/ 8.0 (SEC)
PmP
DISTANCE (KM)
LINE 2 - MLO

Appendix B.9

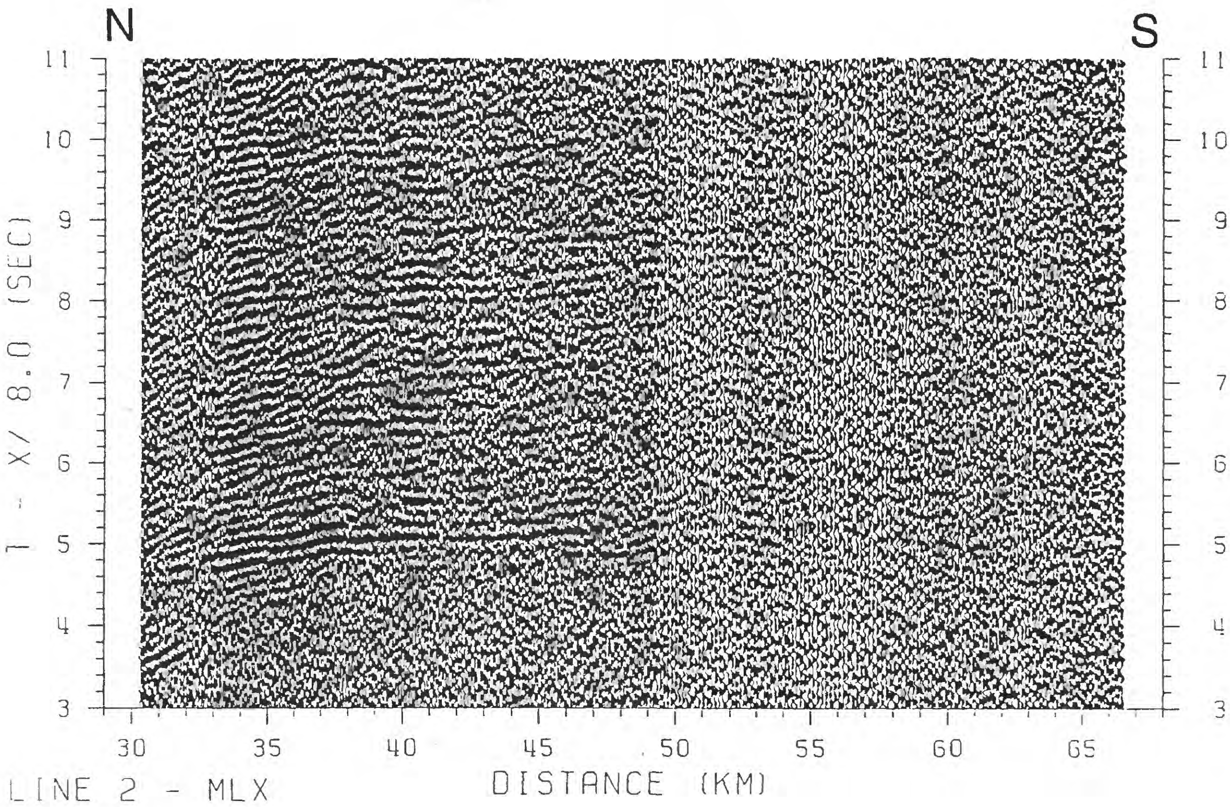

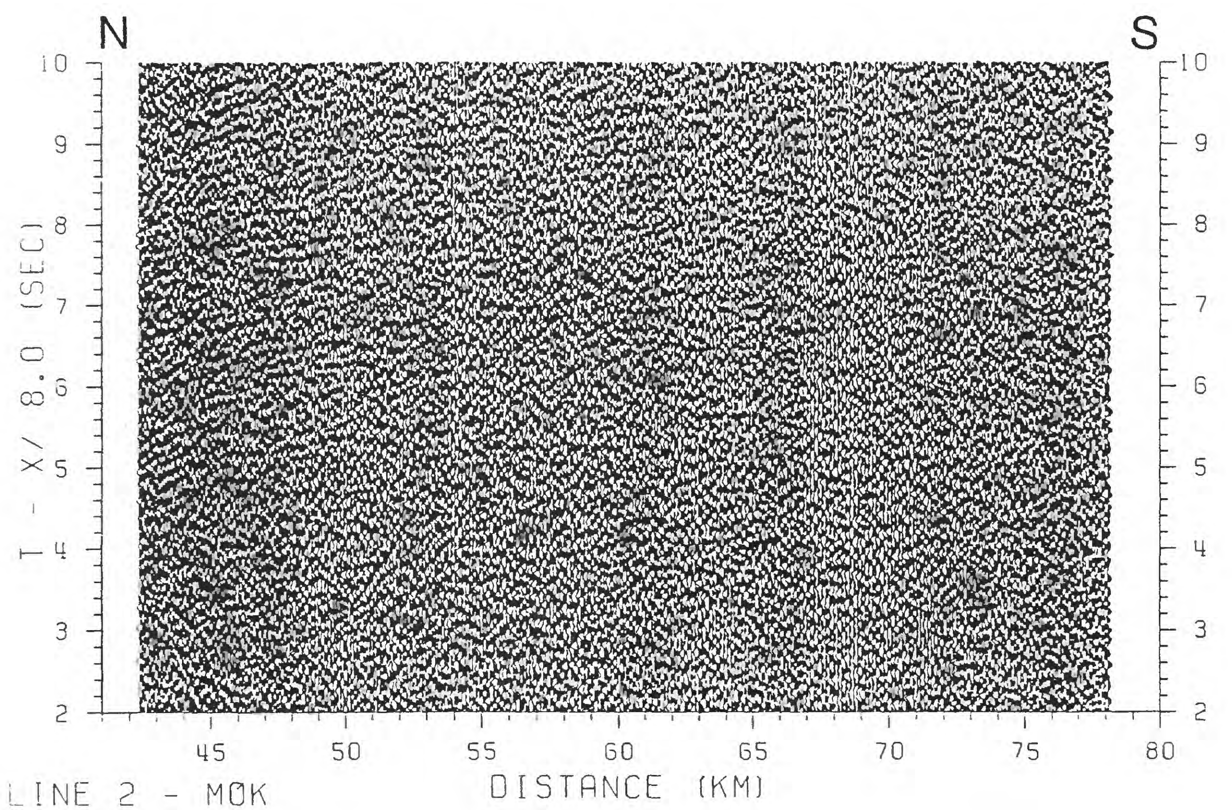

Appendix B.10

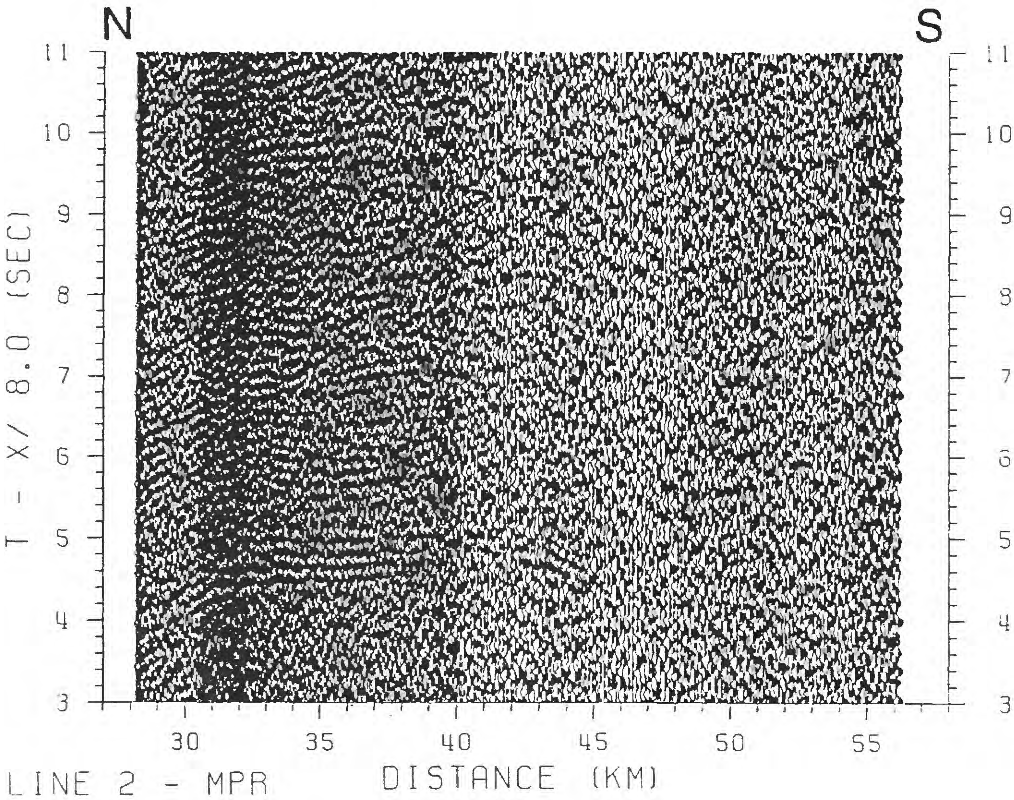

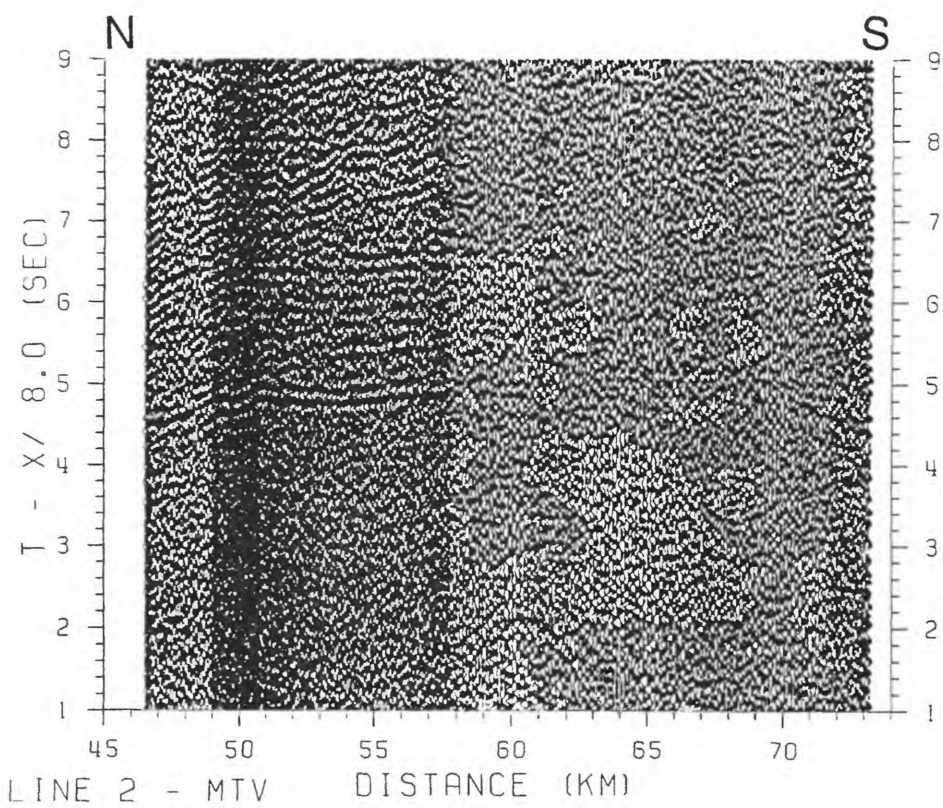

Appendix B.11

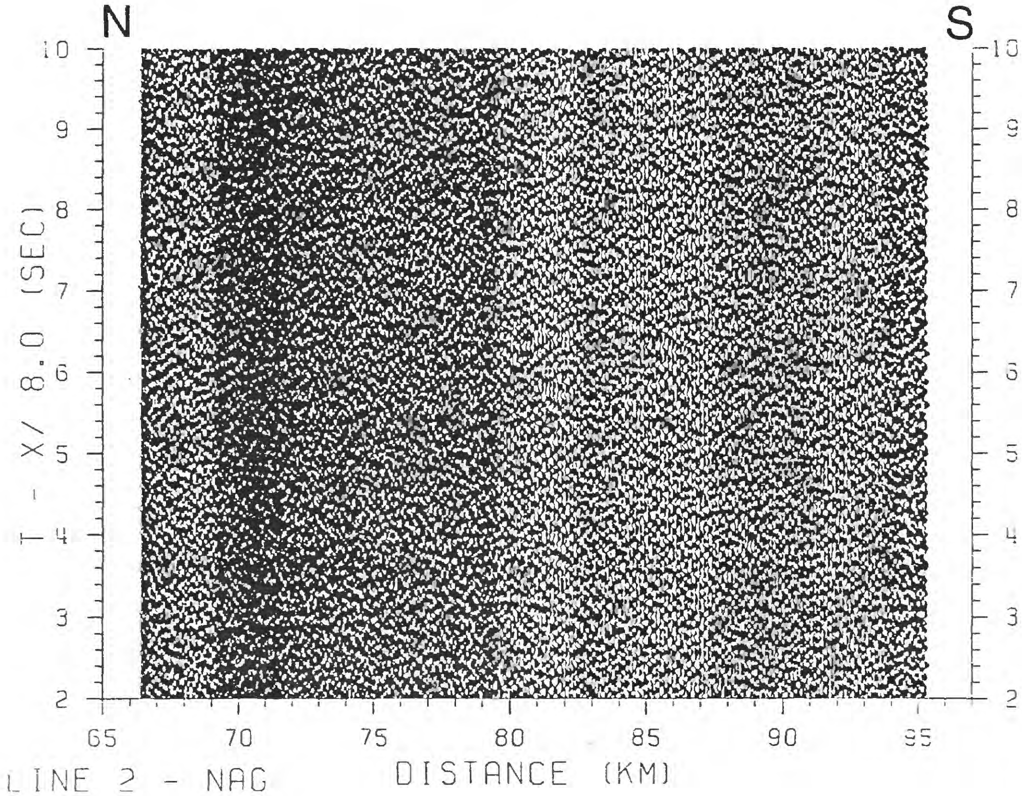

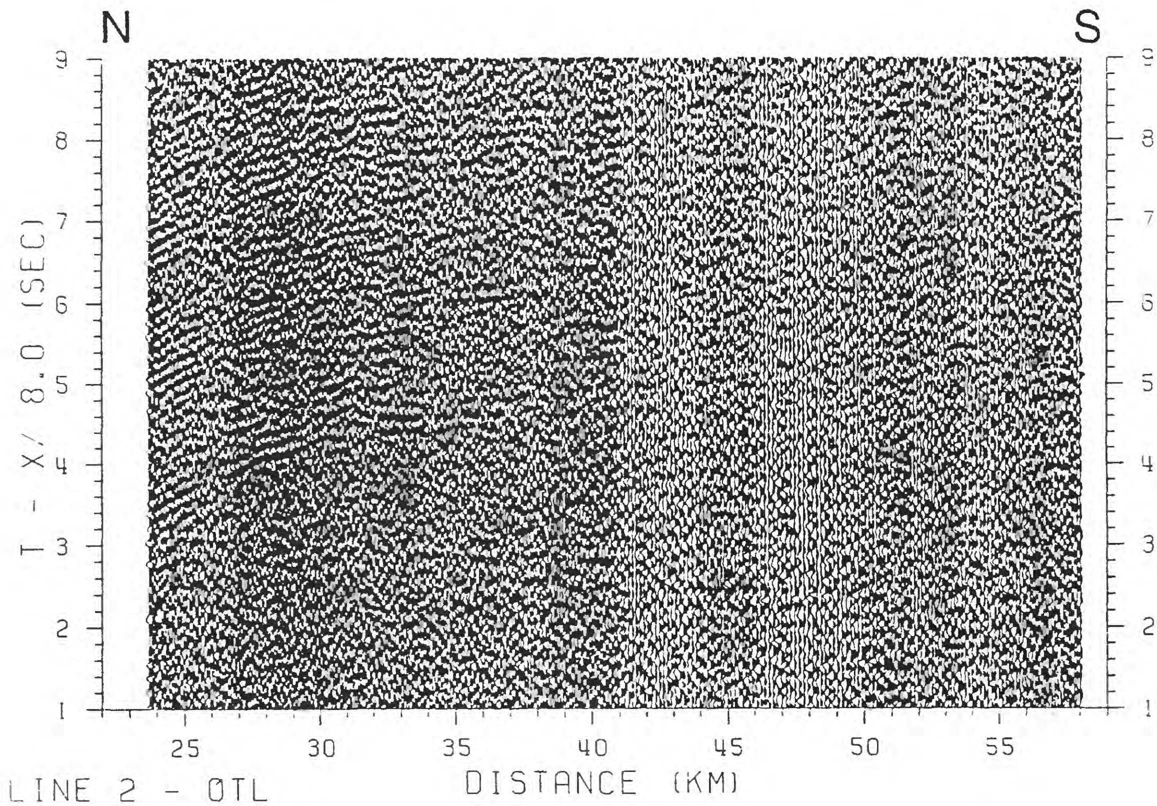

Appendix B.12

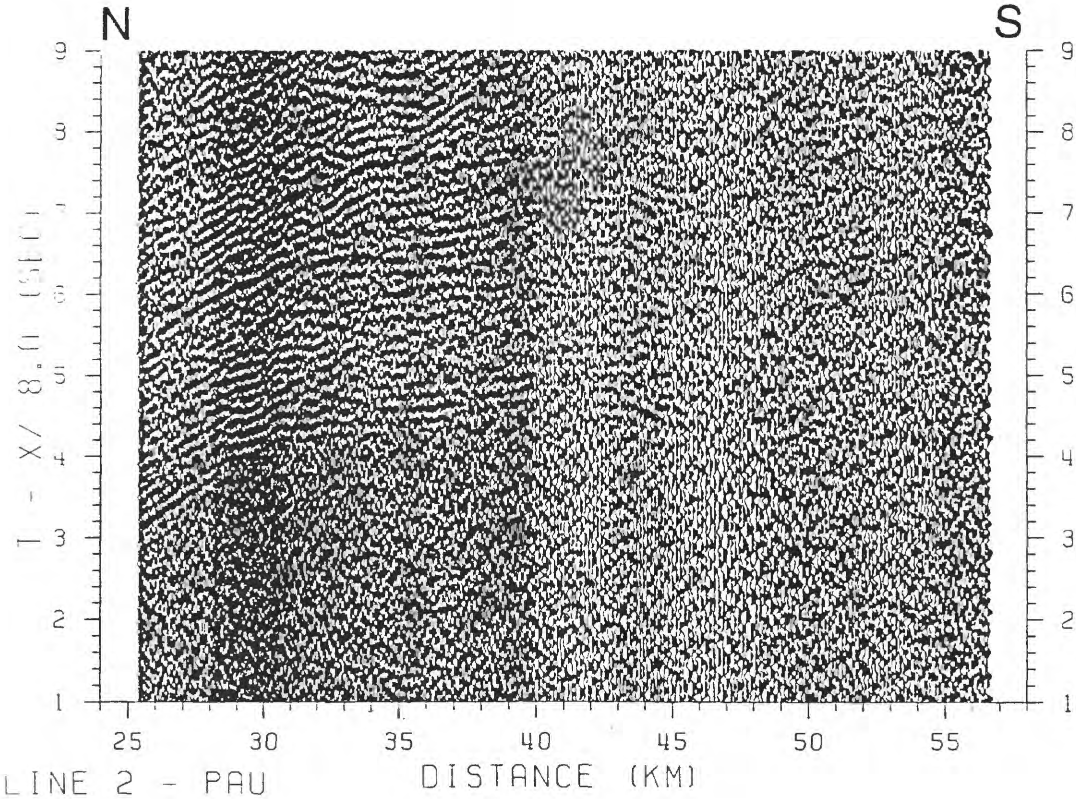

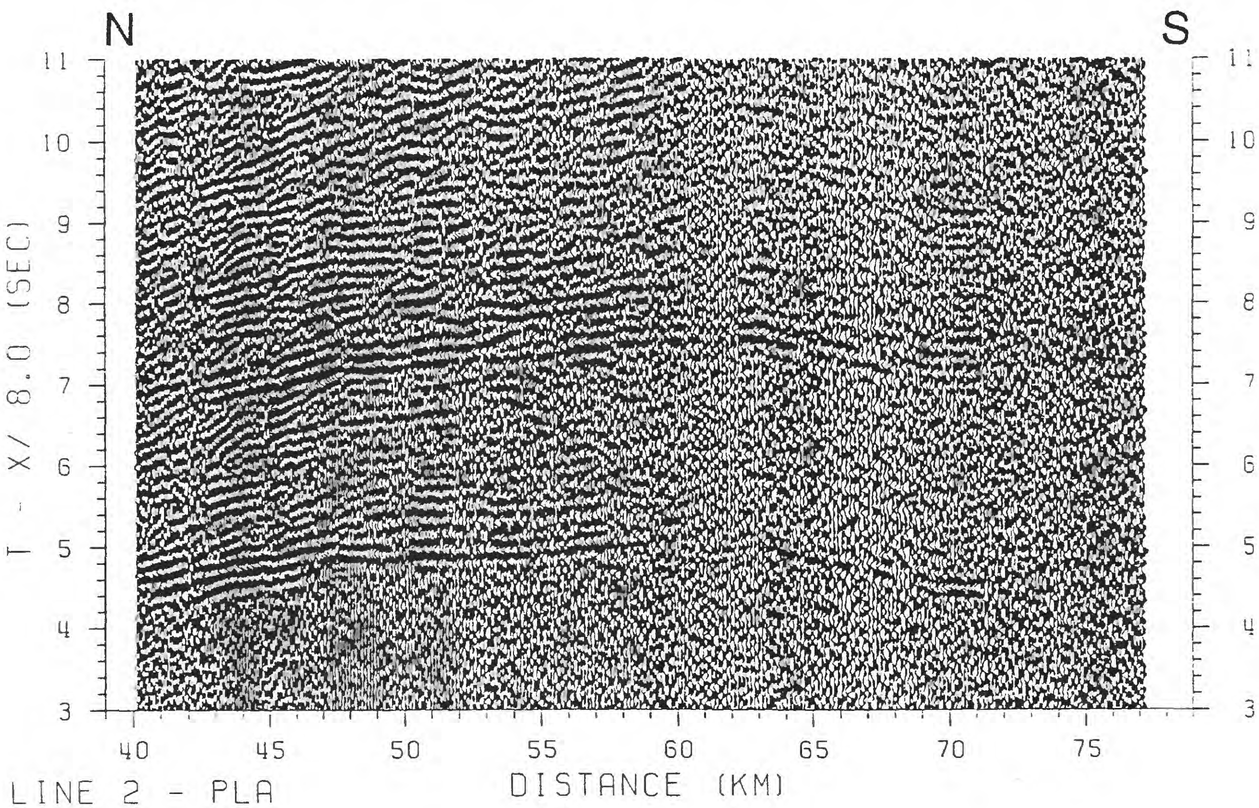

Appendix B.13

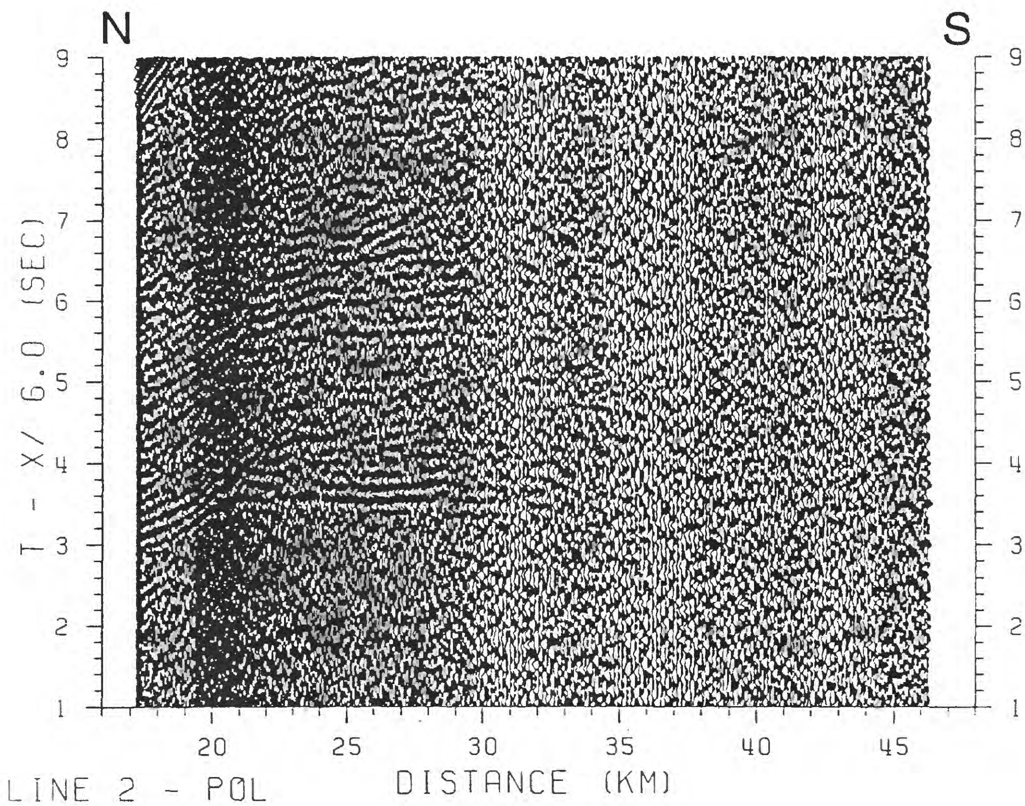

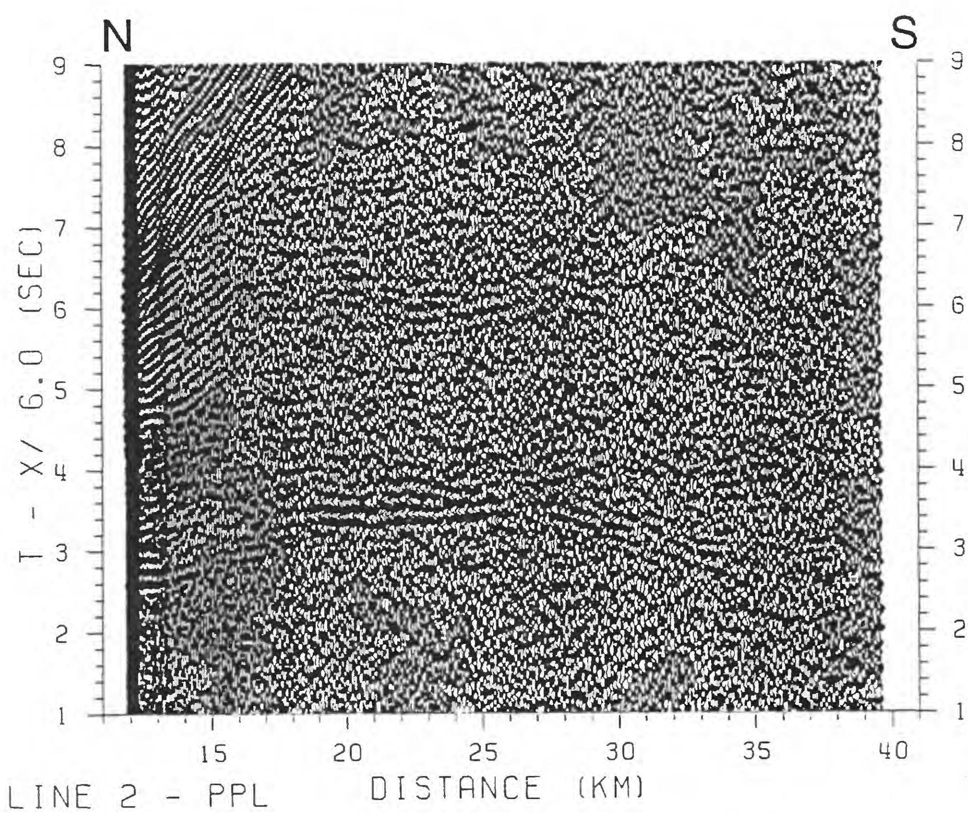

Appendix B.14

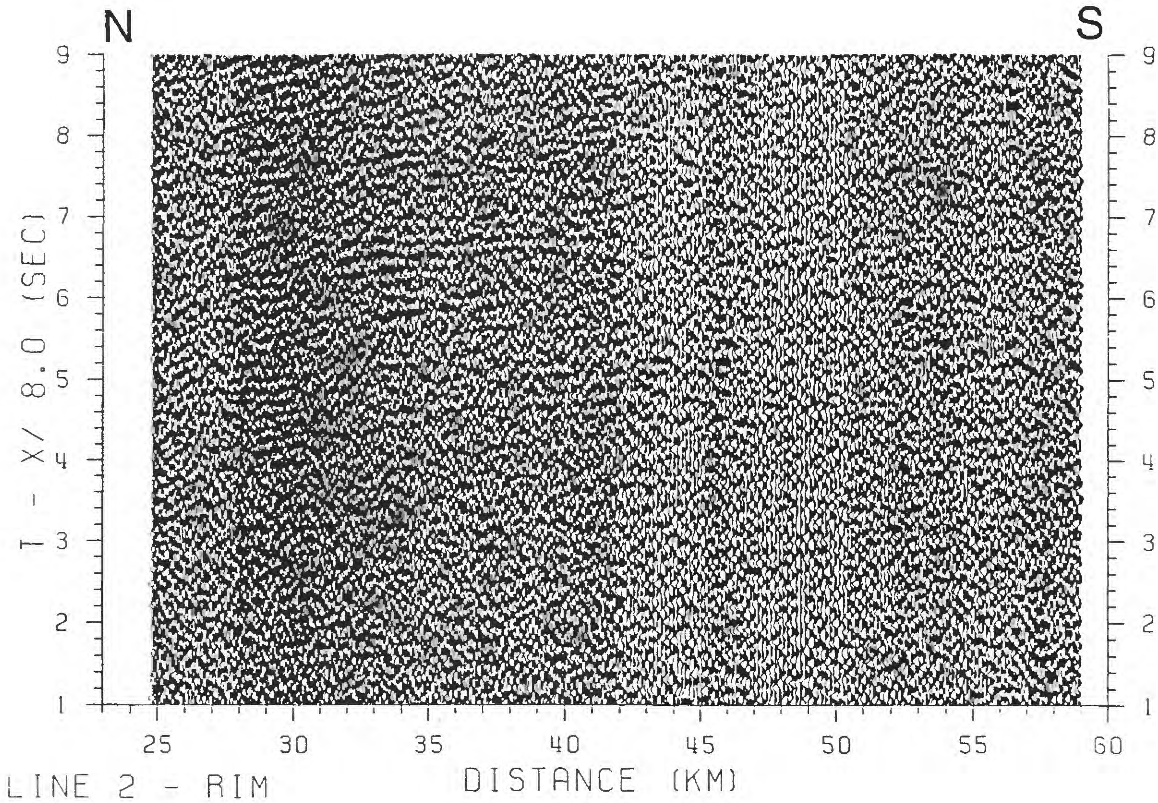

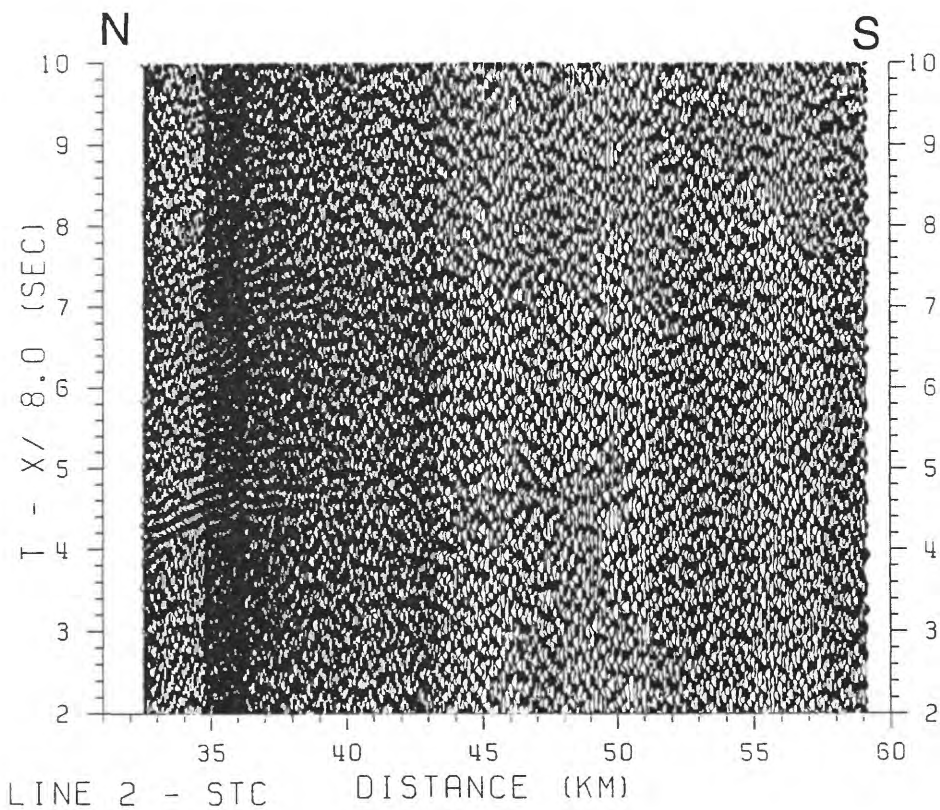

Appendix B.15

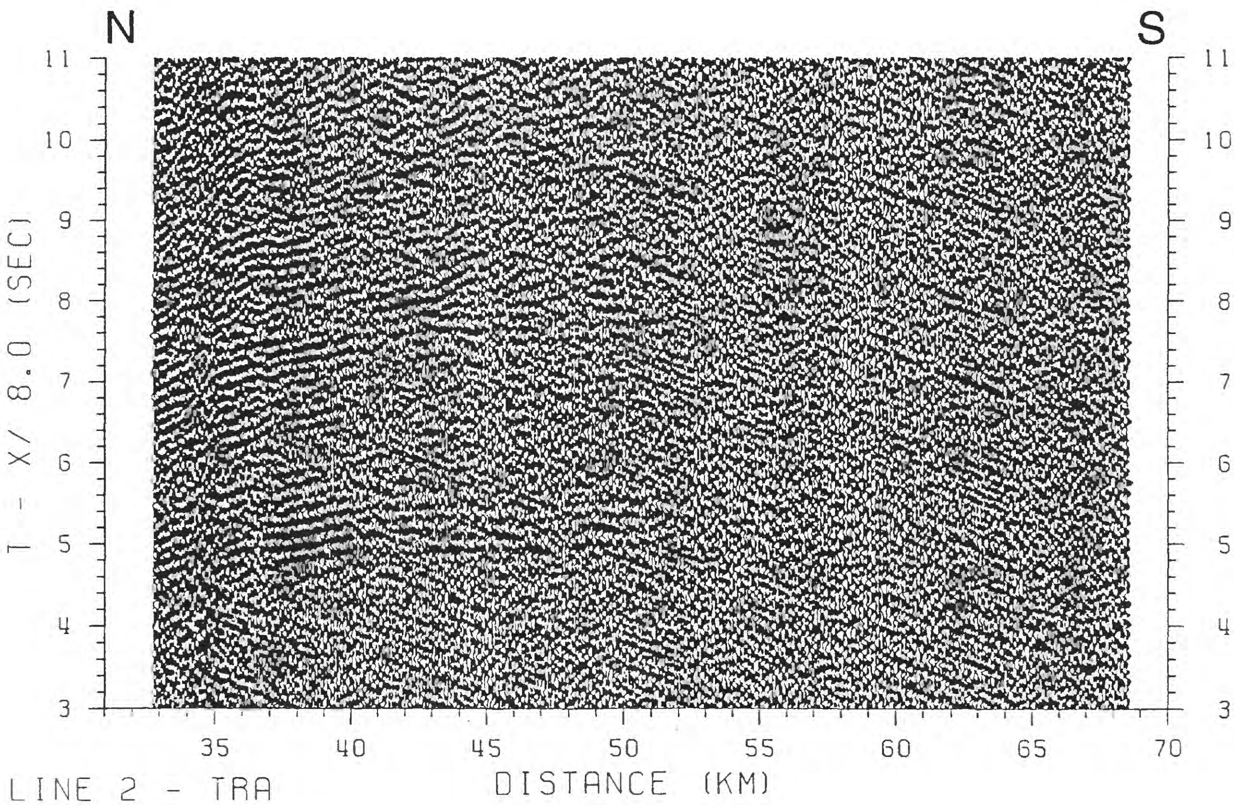

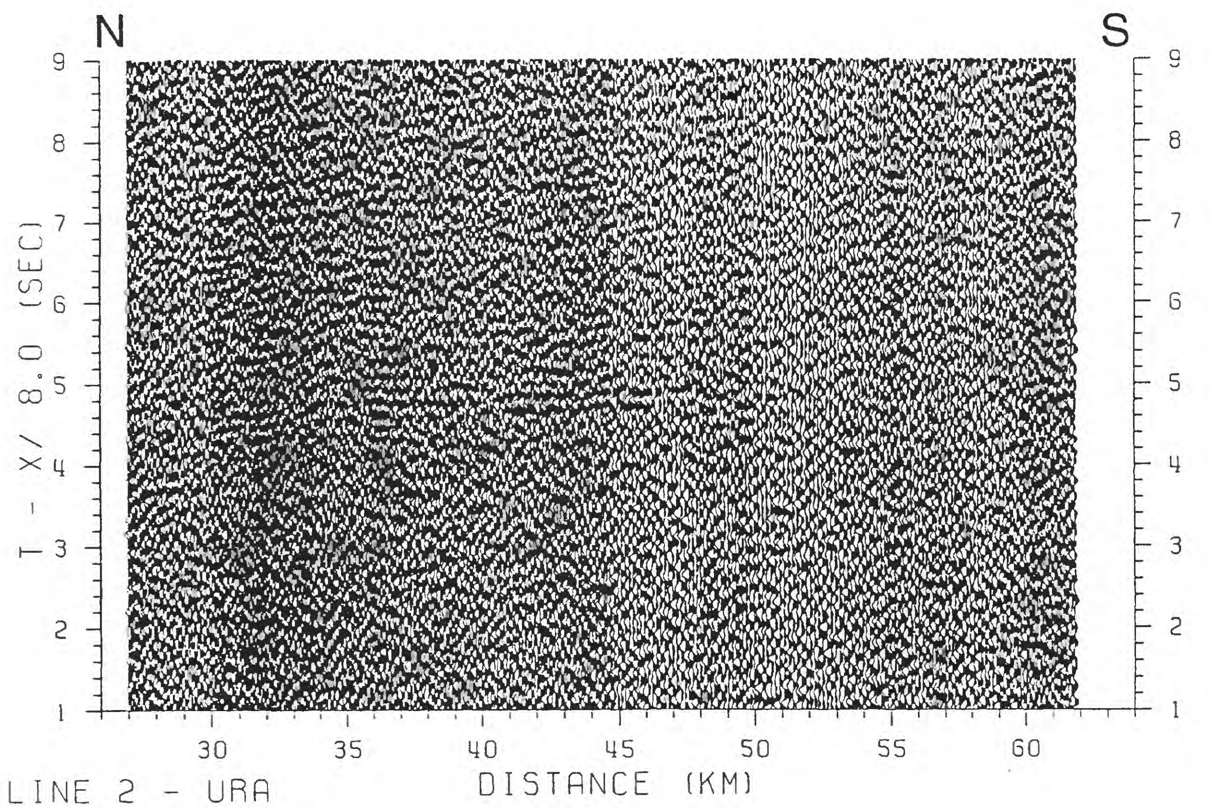

Appendix B.16

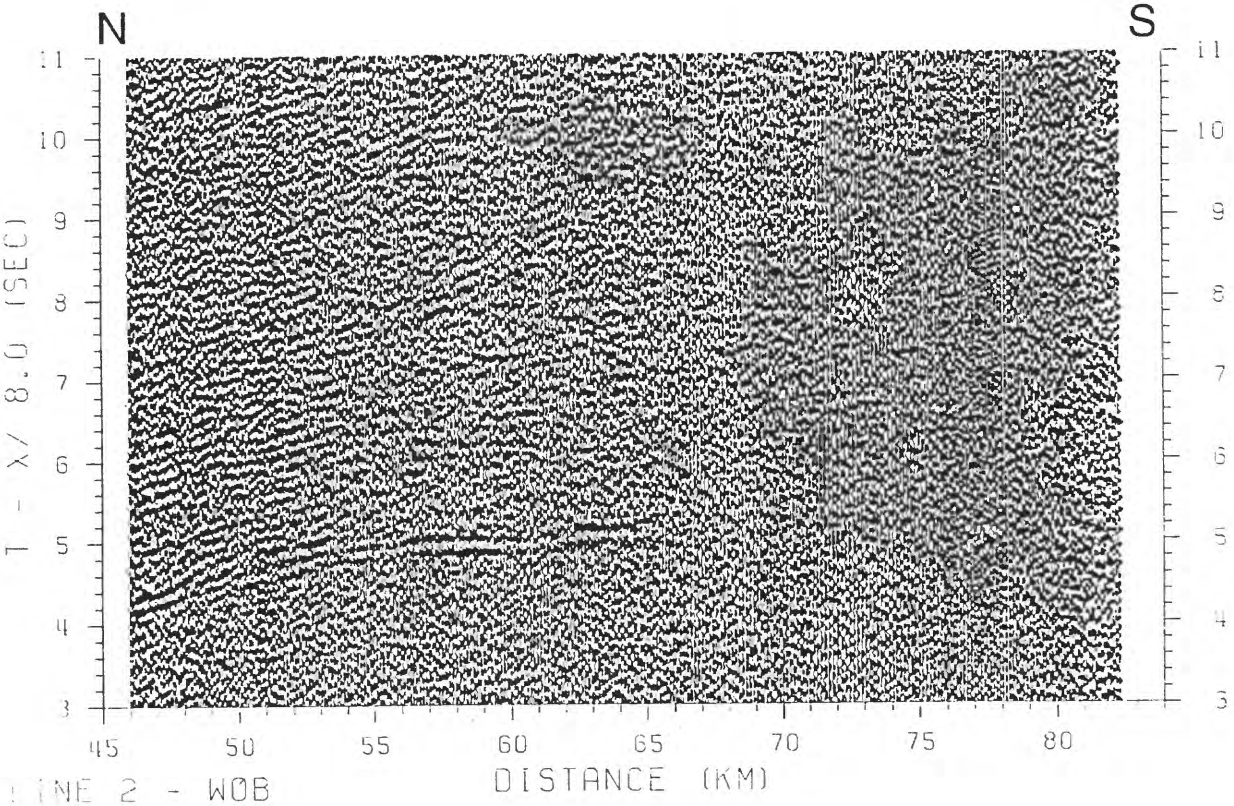

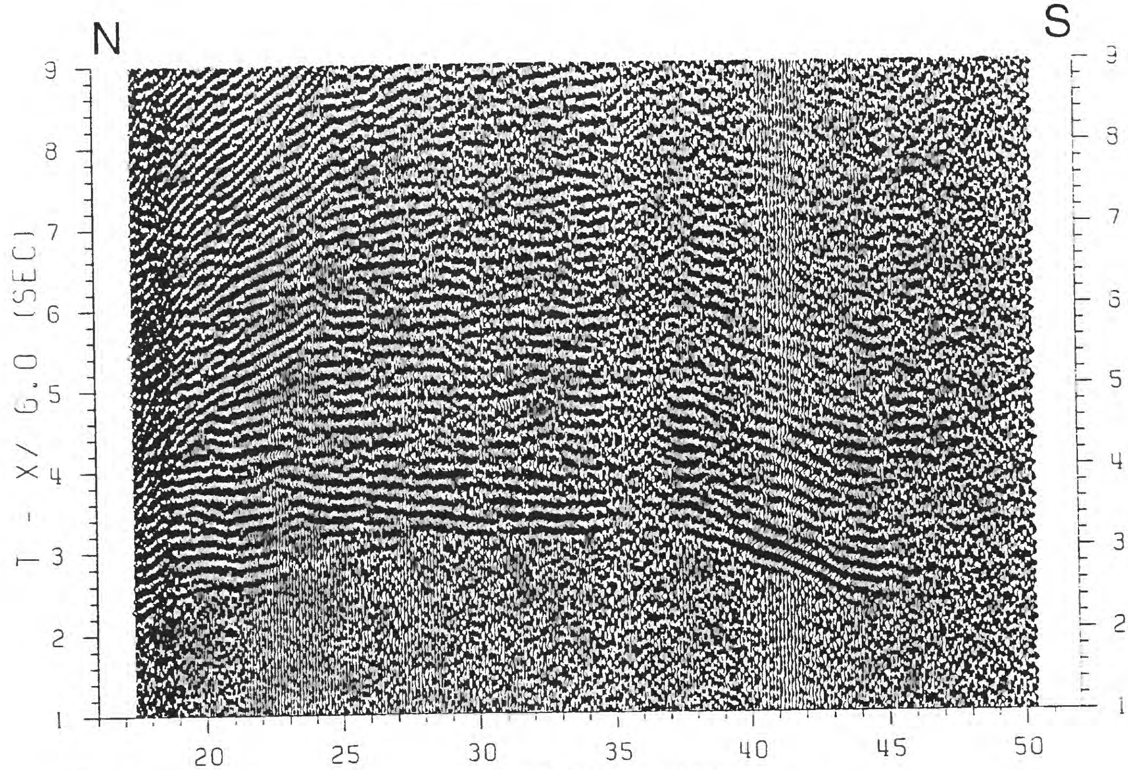

Appendix B.17

APPENDIX C. RECORD SECTIONS FROM LINE 5

Vertical-component record sections for HVO seismic network stations recording seismic phases from Line 5 shots (Figure 5). Data are plotted versus distance or azimuth. Data were bandpass filtered (3 - 10 Hz), and each trace scaled to a uniform maximum amplitude. For time vs. distance plots, data were linearly reduced using velocities of 6 or 8 km/s. Reduction velocities were selected to permit identification of the ranges at which Moho (oceanic crust-mantle boundary) and crustal (volcano-oceanic crust transition) velocities first appear. No topographic or water column corrections have been applied, and the estimated 50 ms firing system delay has not been accounted for in the plots. Shot range is the distance between OHD HVO station locations and WGS 84 shot locations; true ranges, resulting in shifts averaging 445 m in the N140°E direction, are calculated in Table 2.

FIGURE *PAGE*

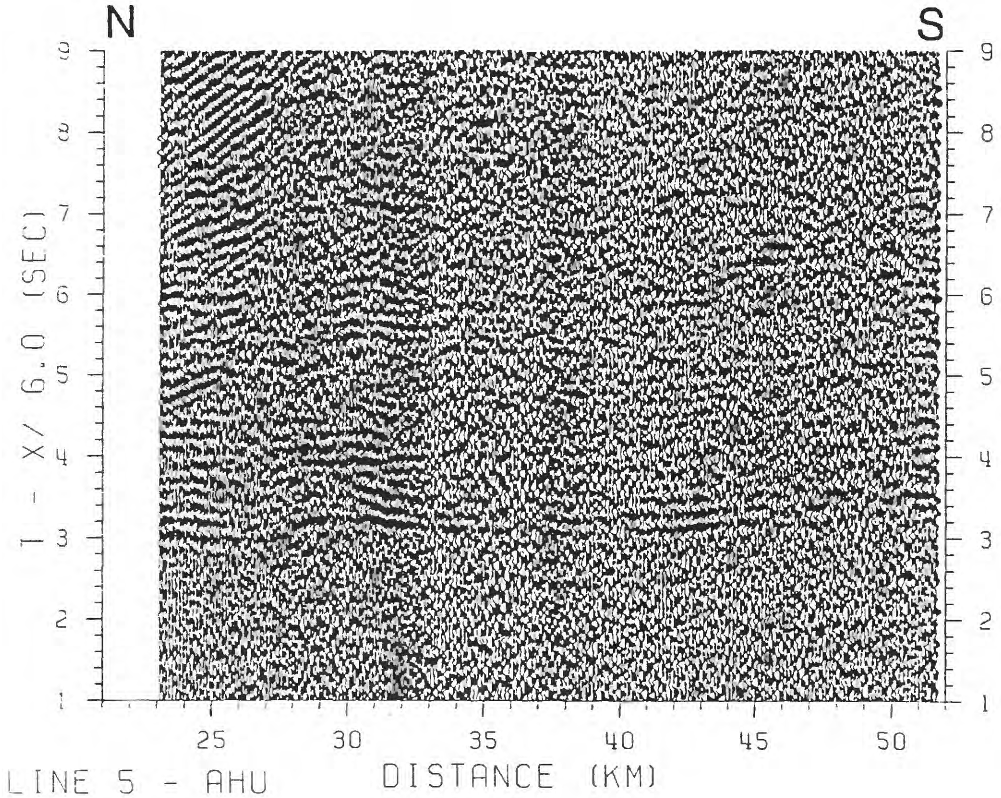
N
S
T - X/ 6.0 (SEC)
1
2
3
4
5
6
7
8
9
25
30
35
40
45
50
LINE 5 - AHU
DISTANCE (KM)

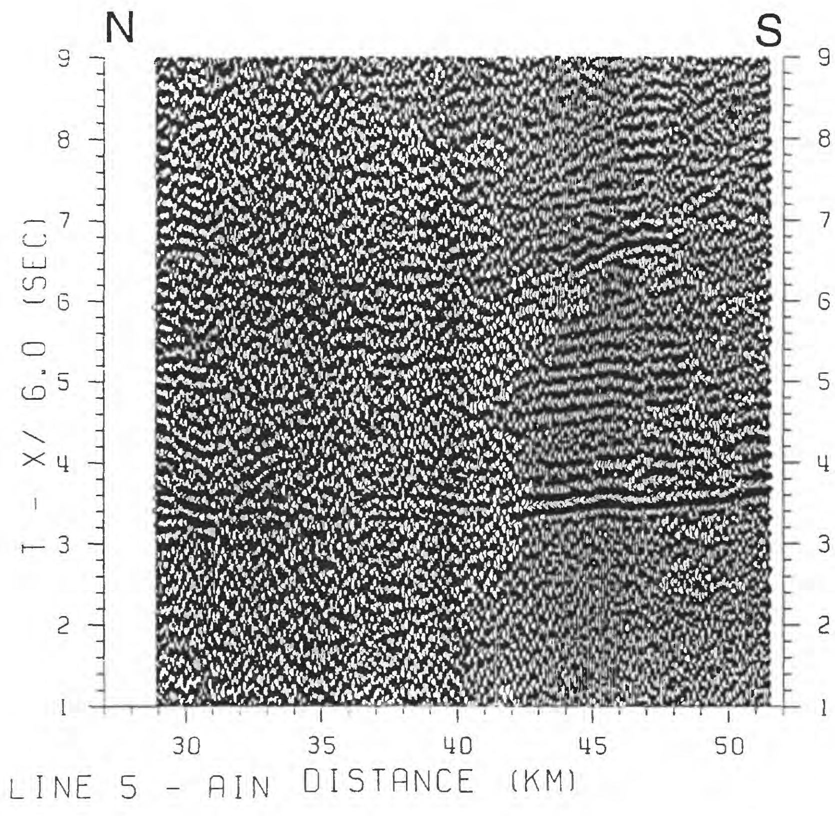
N
S
T - X/ 6.0 (SEC)
1
2
3
4
5
6
7
8
9
30
35
40
45
50
LINE 5 - AIN
DISTANCE (KM)

Appendix C.1

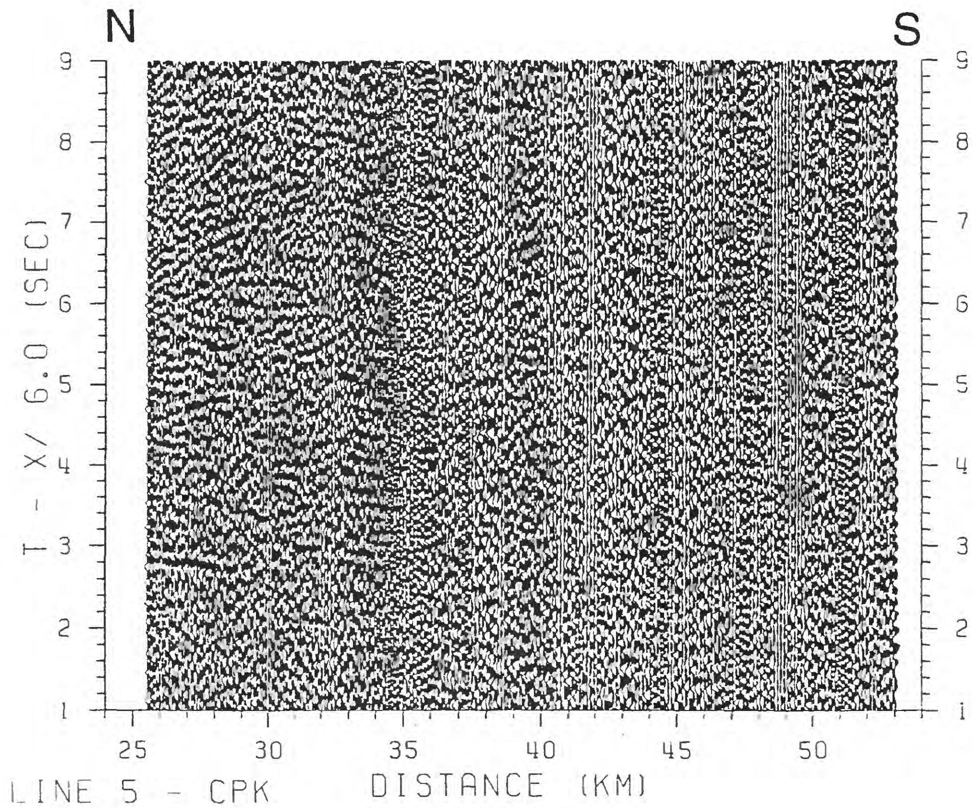
N
S
T - X/ 6.0 (SEC)
1
2
3
4
5
6
7
8
9
25
30
35
40
45
50
LINE 5 - CPK
DISTANCE (KM)

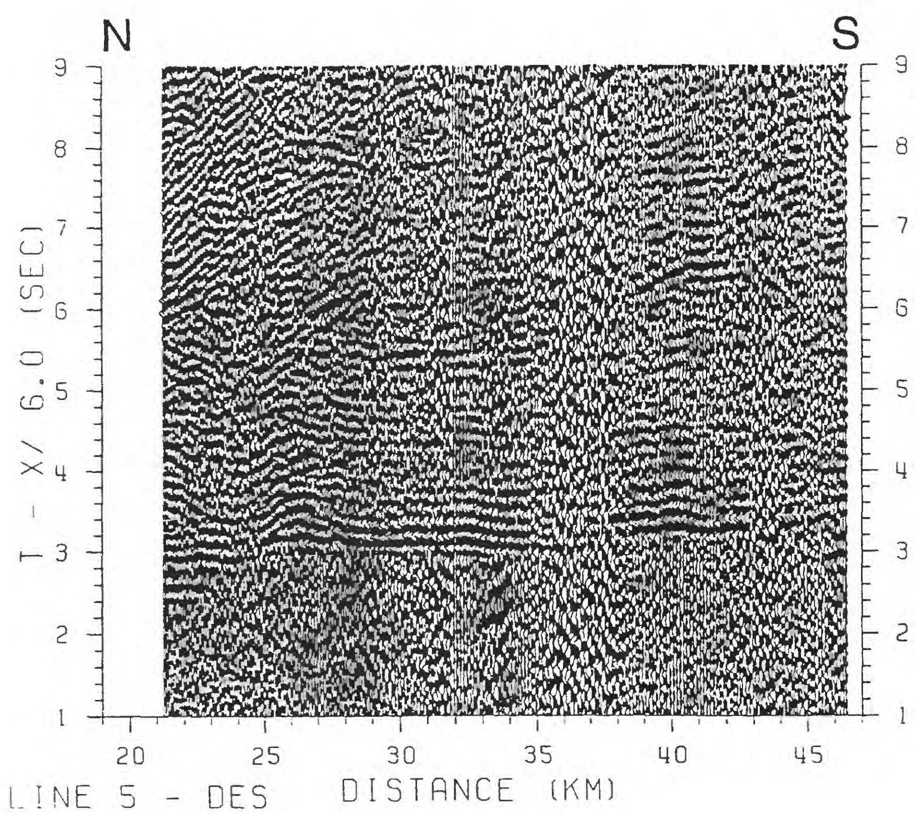
N
S
T - X/ 6.0 (SEC)
1
2
3
4
5
6
7
8
9
20
25
30
35
40
45
LINE 5 - DES
DISTANCE (KM)

Appendix C.2

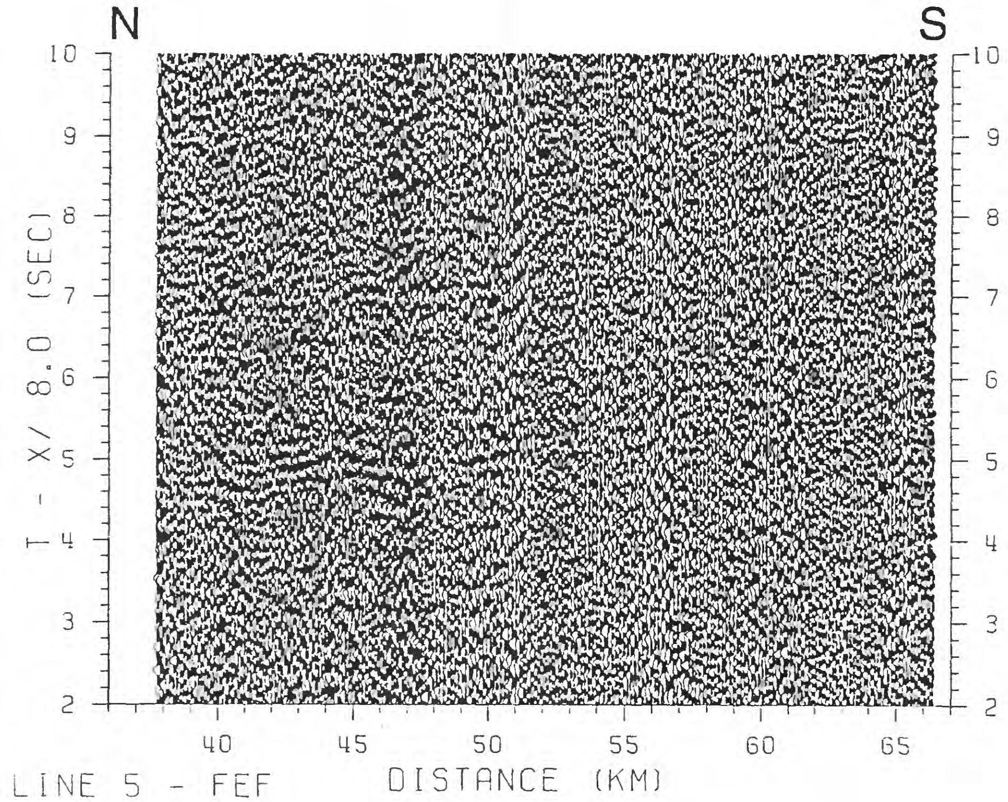
N
S
T - X/ 8.0 (SEC)
10
9
8
7
6
5
4
3
2
40
45
50
55
60
65
LINE 5 - FEF
DISTANCE (KM)

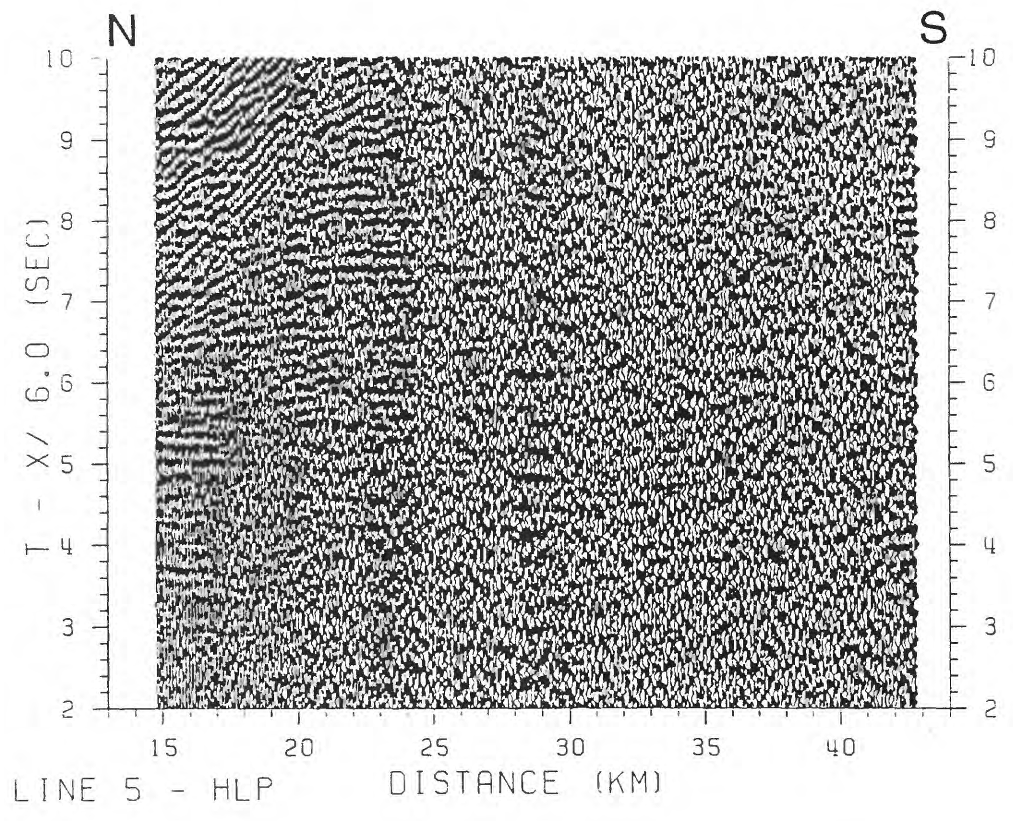
N
S
T - X/ 6.0 (SEC)
10
9
8
7
6
5
4
3
2
15
20
25
30
35
40
LINE 5 - HLP
DISTANCE (KM)

Appendix C.3

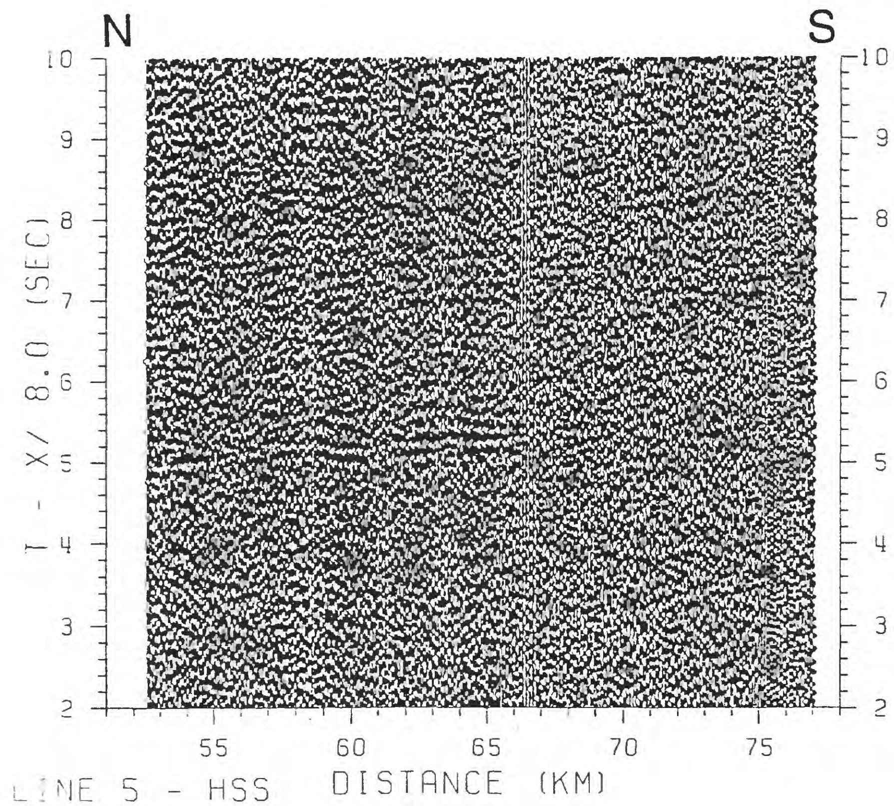

N
S
T - X/ 8.0 (SEC)
10
9
8
7
6
5
4
3
2
55
60
65
70
75
LINE 5 - HSS
DISTANCE (KM)

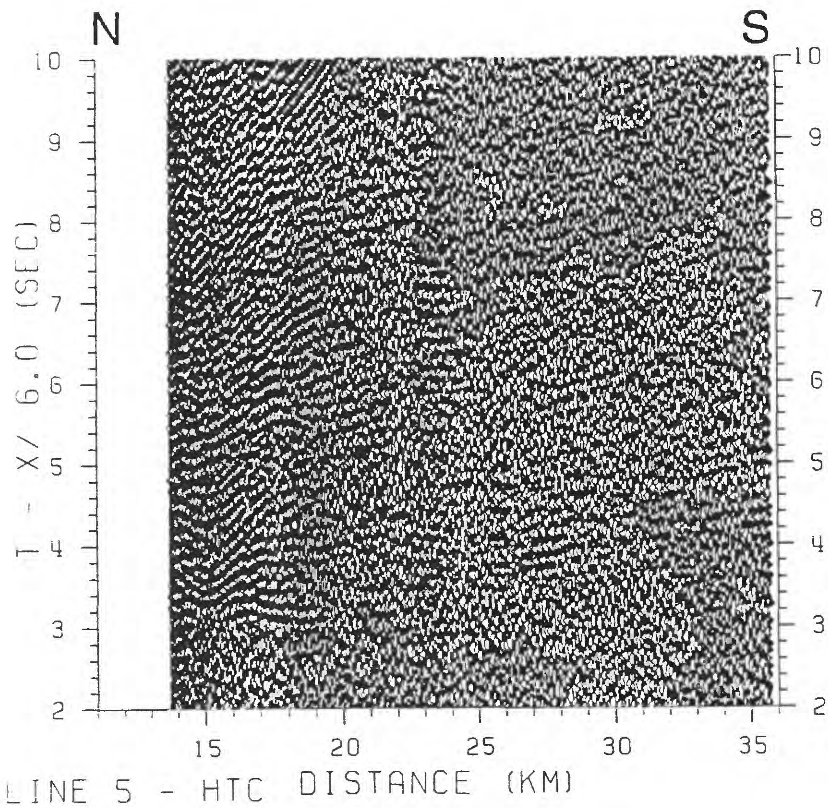

N
S
T - X/ 6.0 (SEC)
10
9
8
7
6
5
4
3
2
15
20
25
30
35
LINE 5 - HTC
DISTANCE (KM)

Appendix C.4

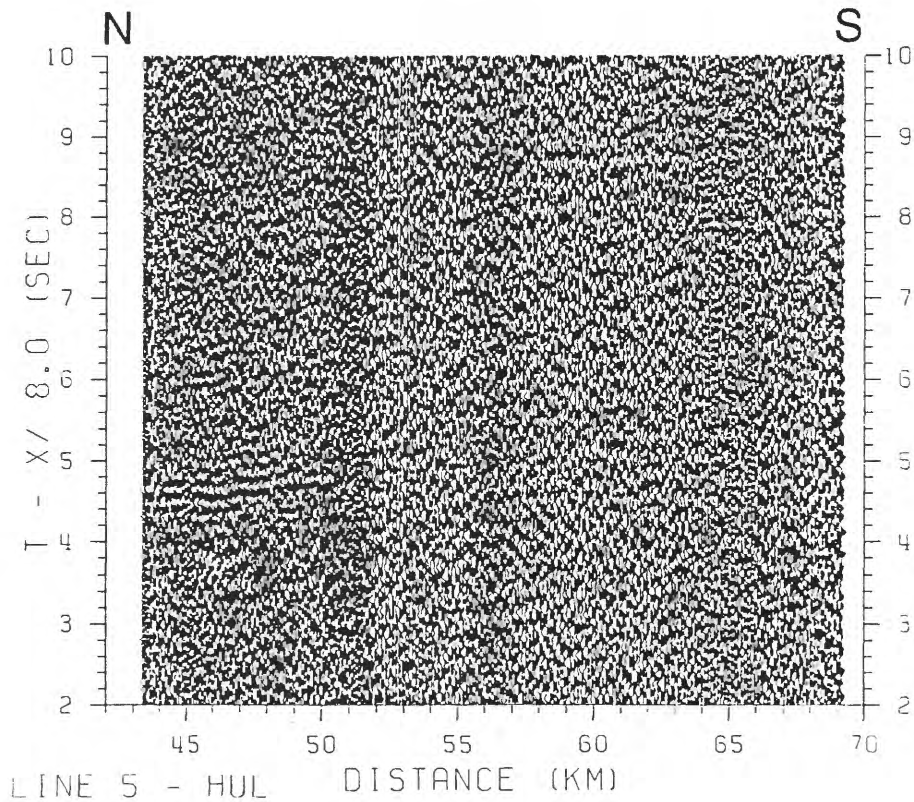
N
S
T - X/ 8.0 (SEC)
10
9
8
7
6
5
4
3
2
45
50
55
60
65
70
LINE 5 - HUL
DISTANCE (KM)

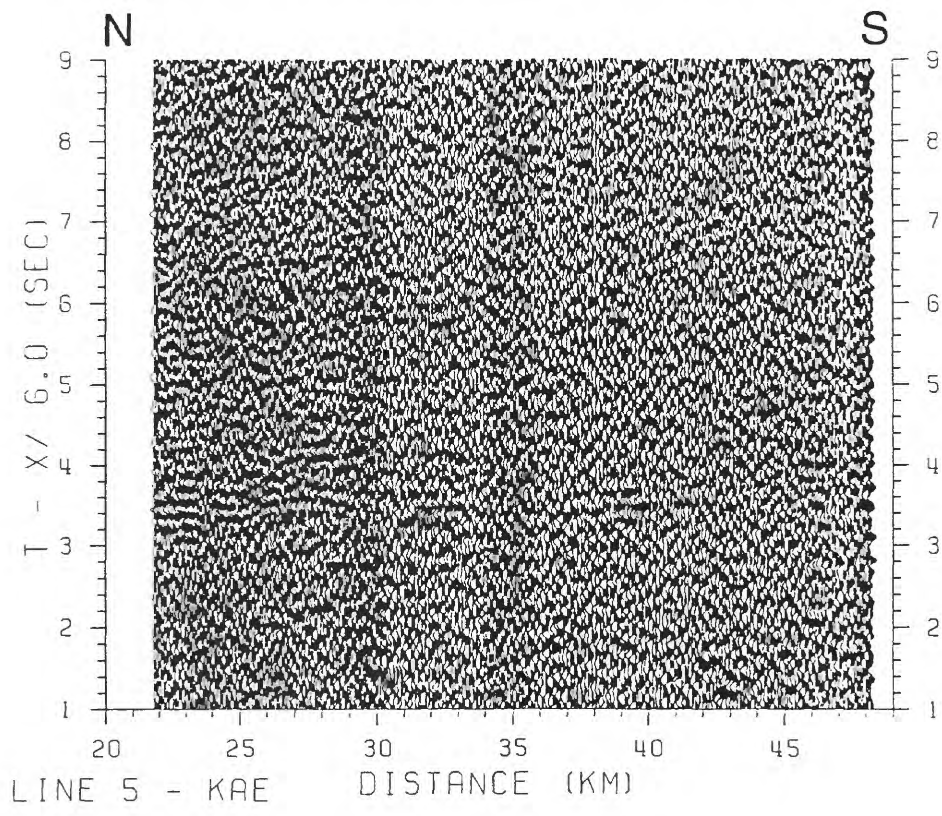
N
S
T - X/ 6.0 (SEC)
9
8
7
6
5
4
3
2
1
20
25
30
35
40
45
LINE 5 - KAE
DISTANCE (KM)

Appendix C.5

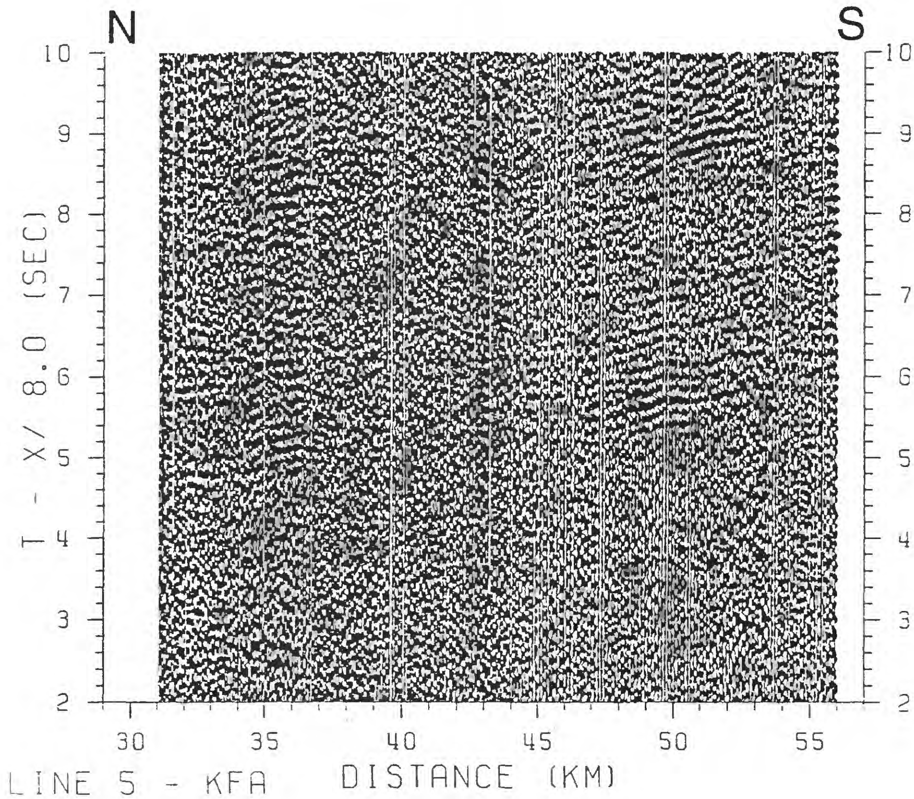
N
S
T - X/ 8.0 (SEC)
10
9
8
7
6
5
4
3
2
30
35
40
45
50
55
DISTANCE (KM)
LINE 5 - KFA

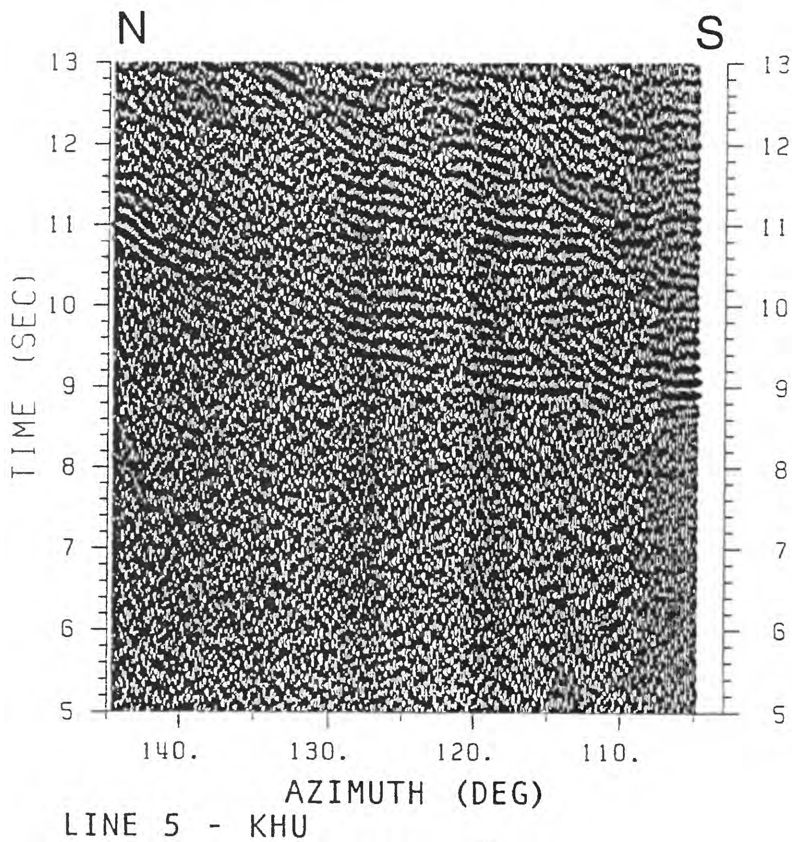
N
S
TIME (SEC)
13
12
11
10
9
8
7
6
5
140.
130.
120.
110.
AZIMUTH (DEG)
LINE 5 - KHU

Appendix C.6

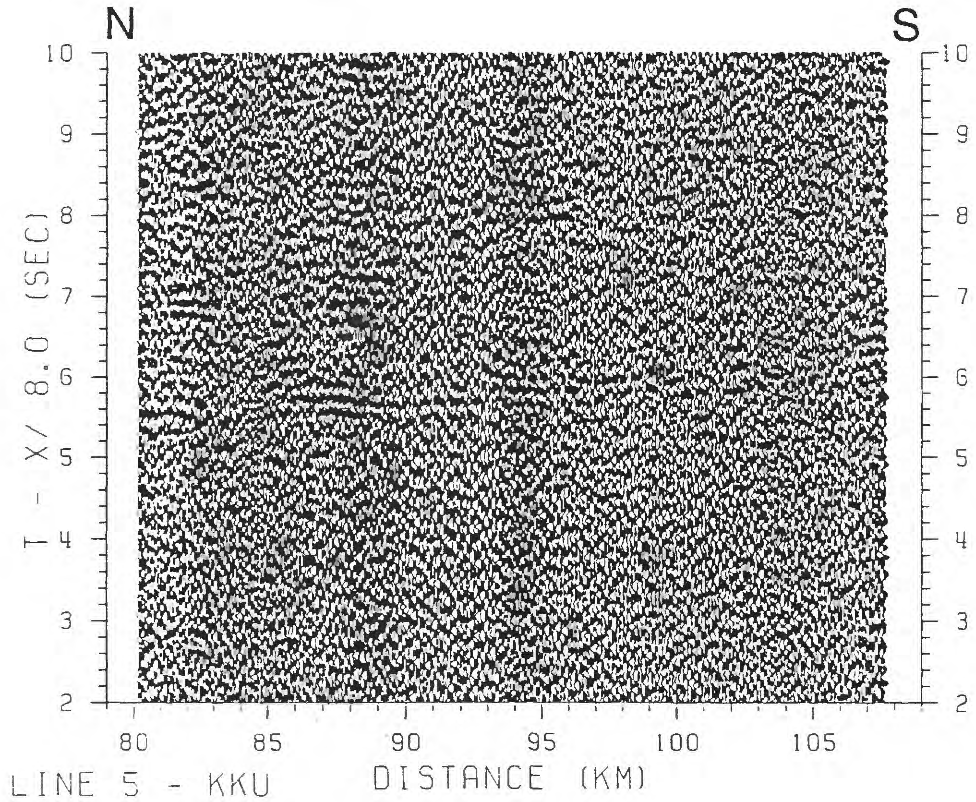
N
S
T - X/ 8.0 (SEC)
DISTANCE (KM)
LINE 5 - KKU

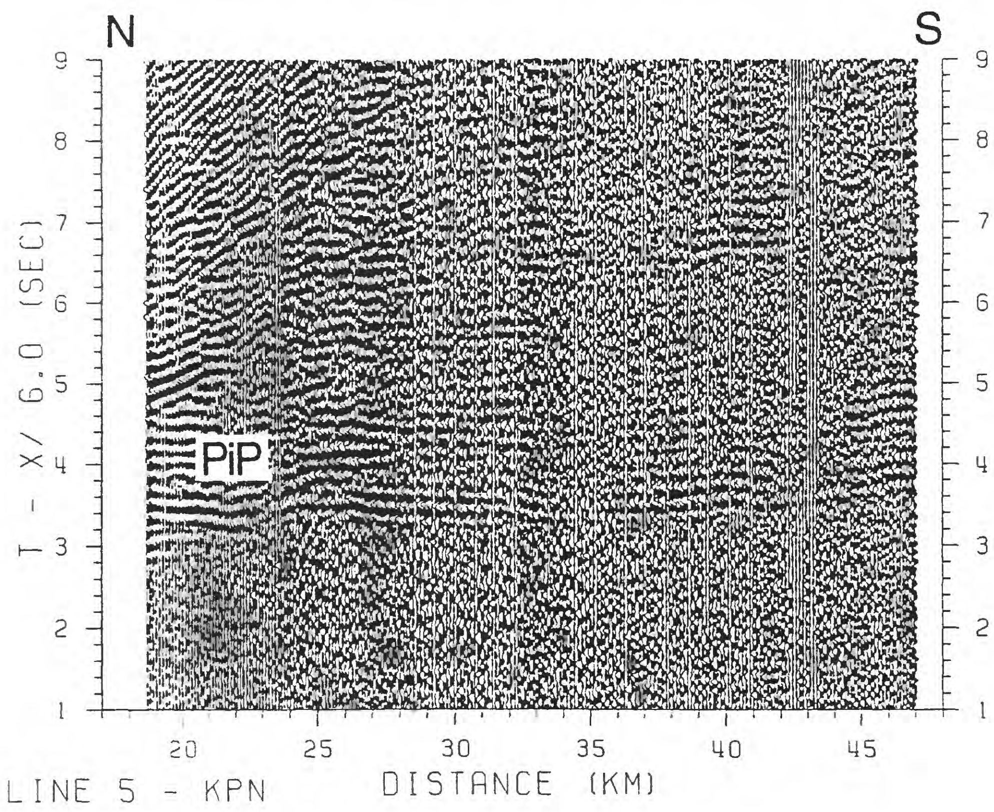
N
S
PiP
T - X/ 6.0 (SEC)
DISTANCE (KM)
LINE 5 - KPN

Appendix C.7

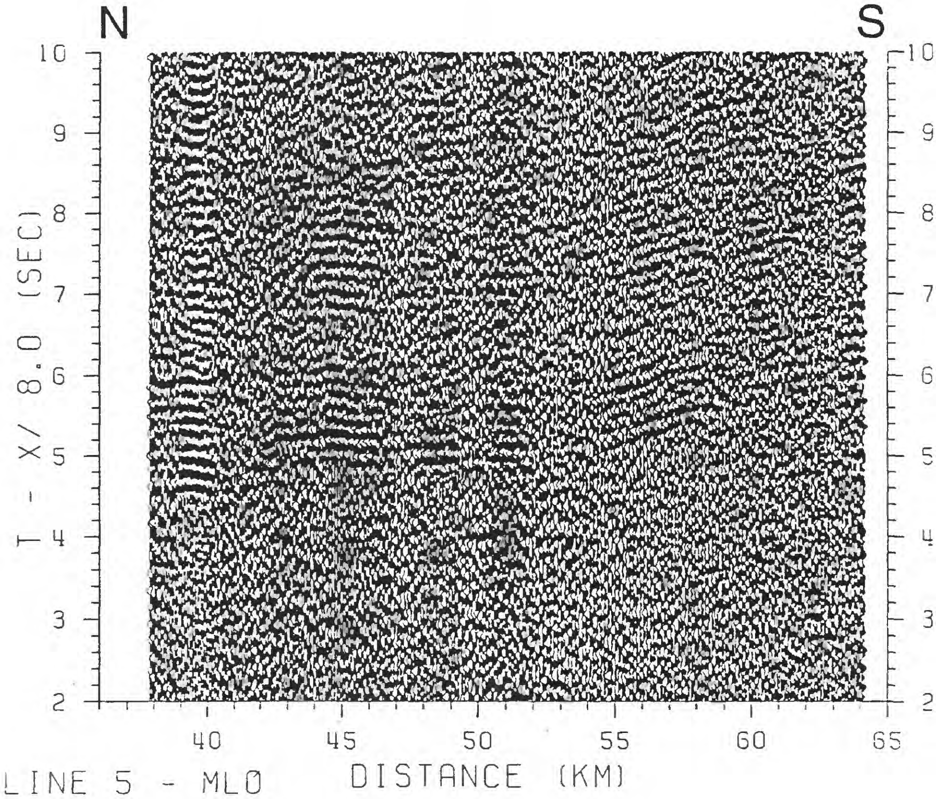

N
S
T - X/ 8.0 (SEC)
10
9
8
7
6
5
4
3
2
40
45
50
55
60
65
LINE 5 - MLO
DISTANCE (KM)

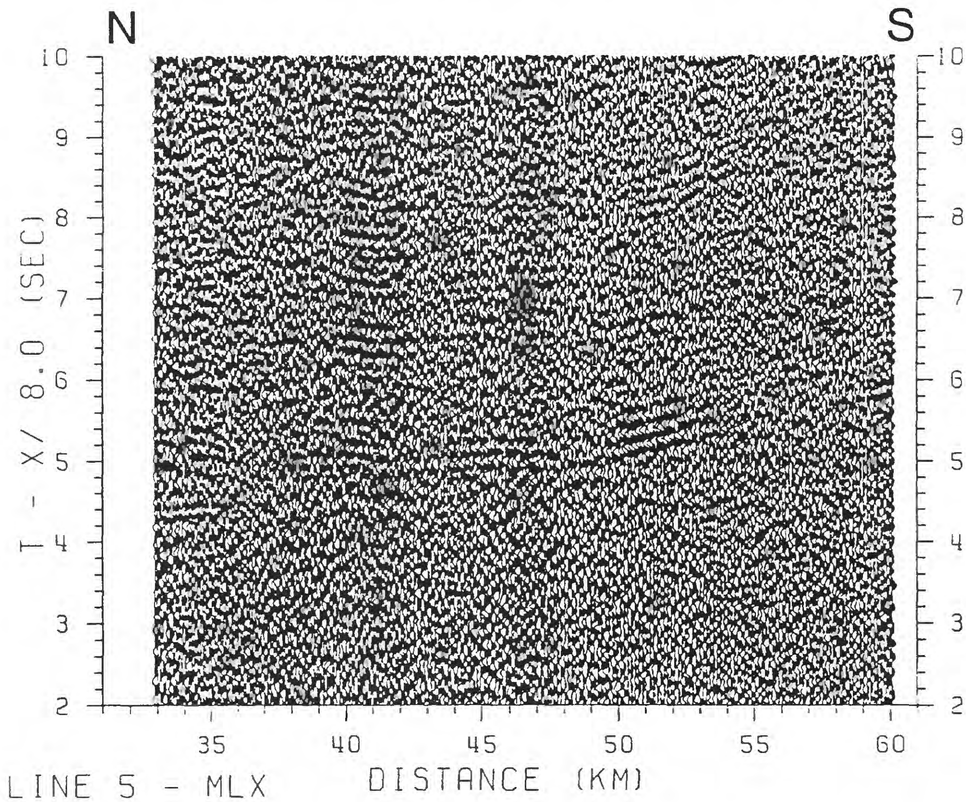

N
S
T - X/ 8.0 (SEC)
10
9
8
7
6
5
4
3
2
35
40
45
50
55
60
LINE 5 - MLX
DISTANCE (KM)

Appendix C.8

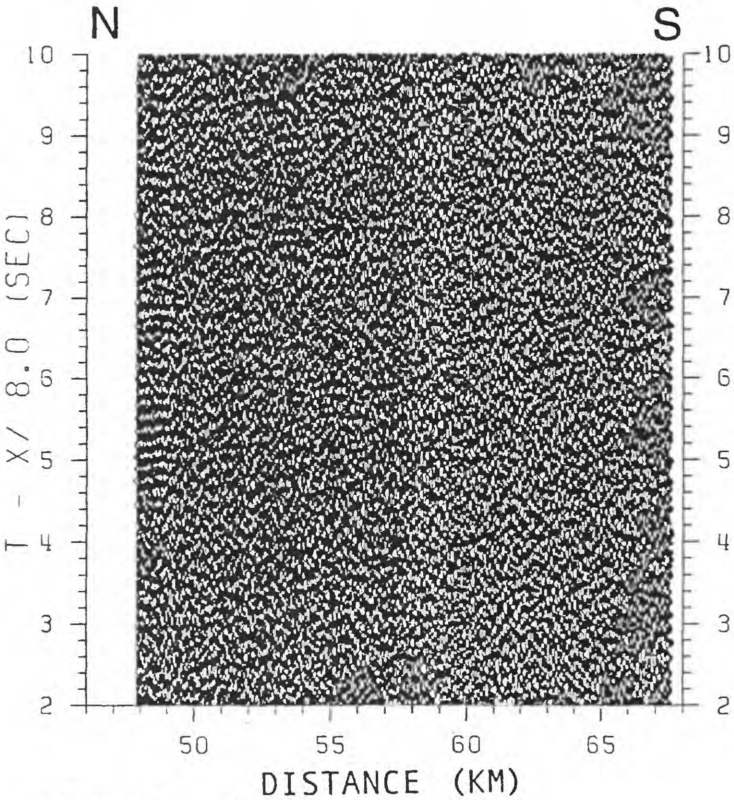

LINE 5 - MOK

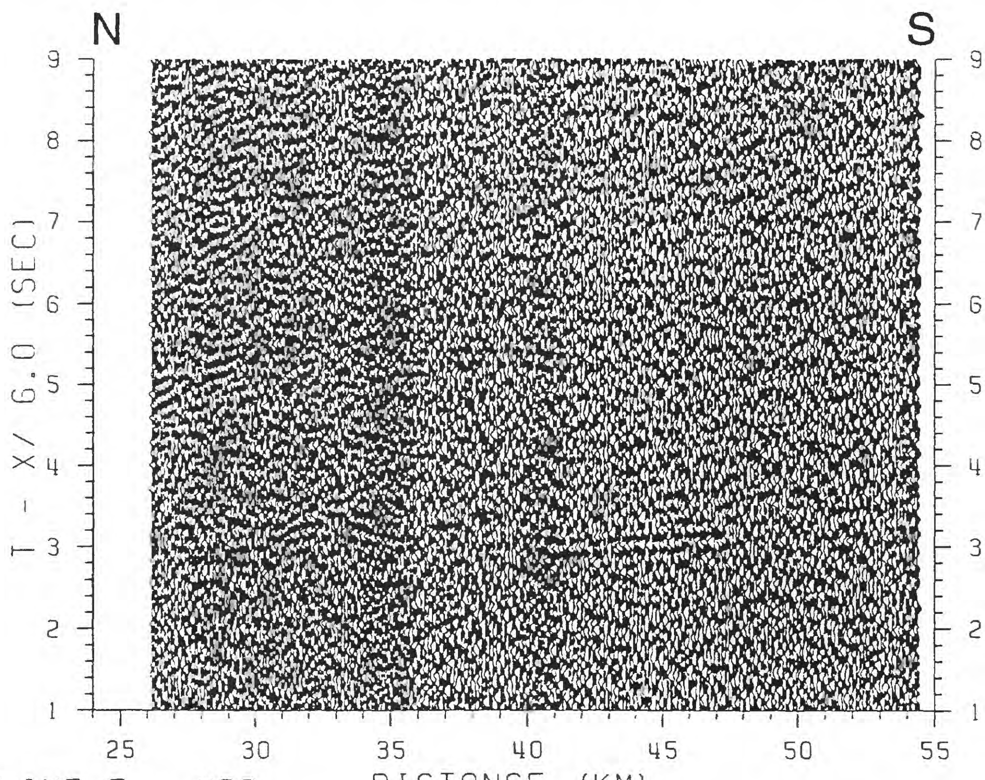

LINE 5 - MPR

Appendix C.9

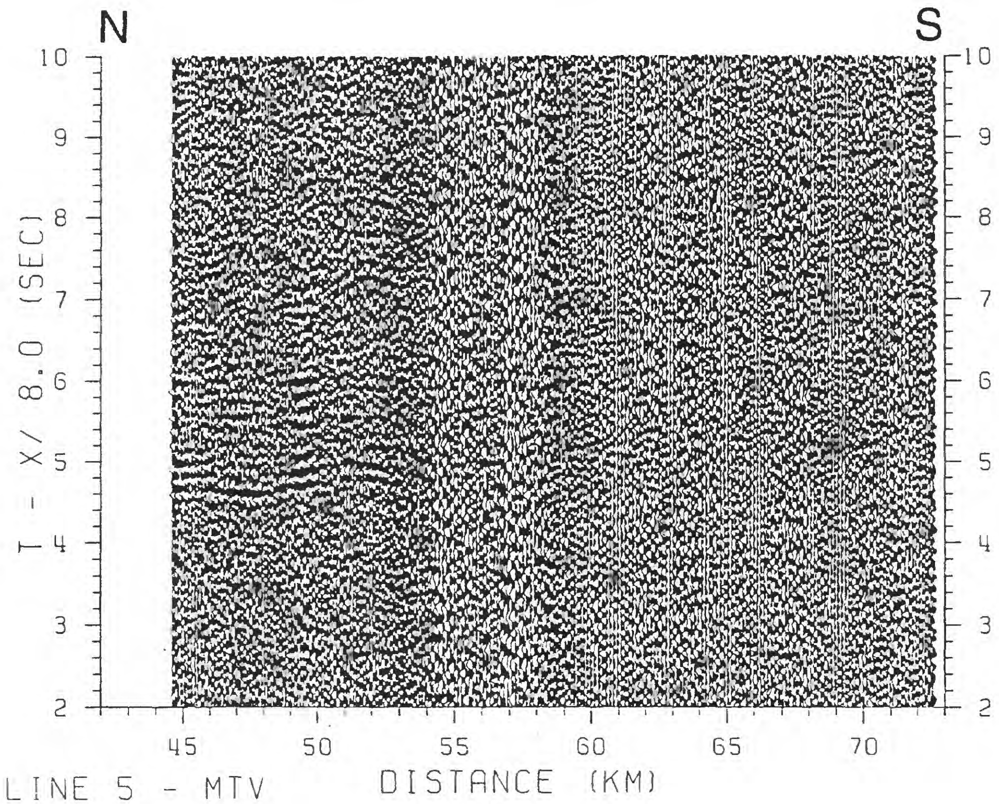

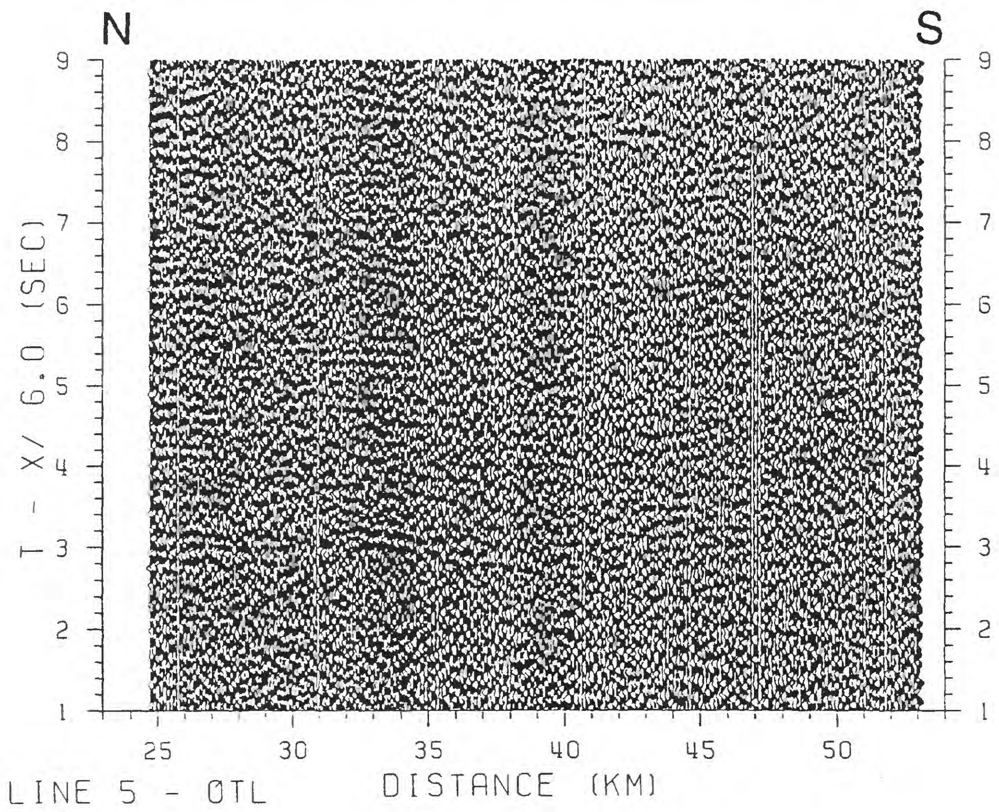

Appendix C.10

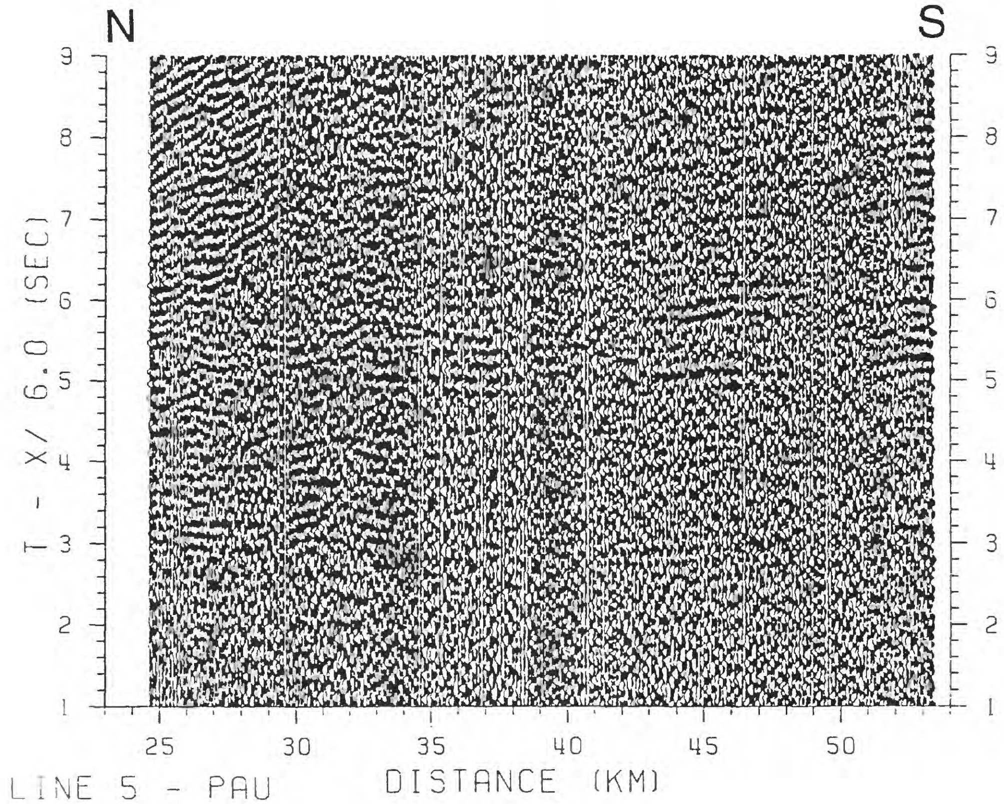

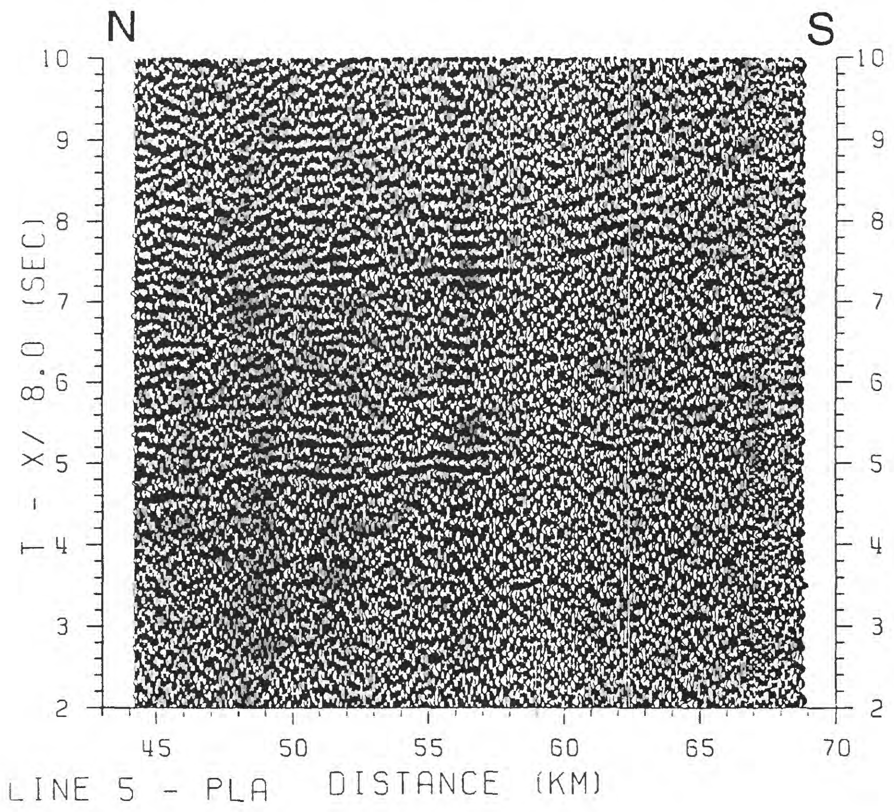

Appendix C.11

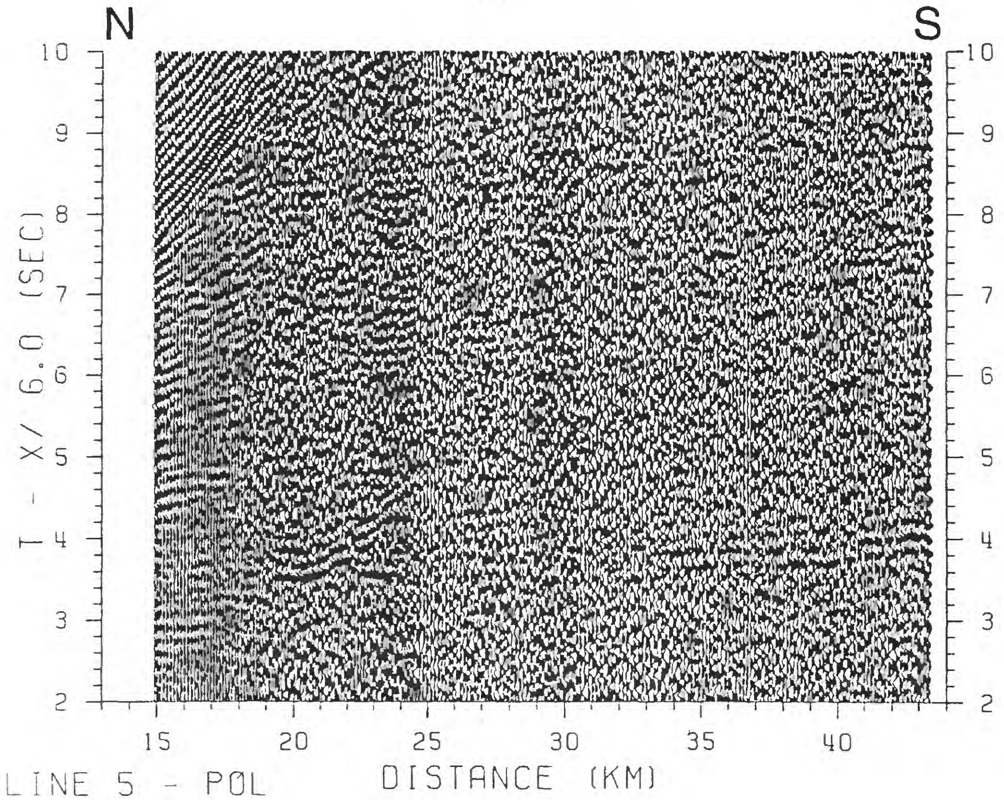

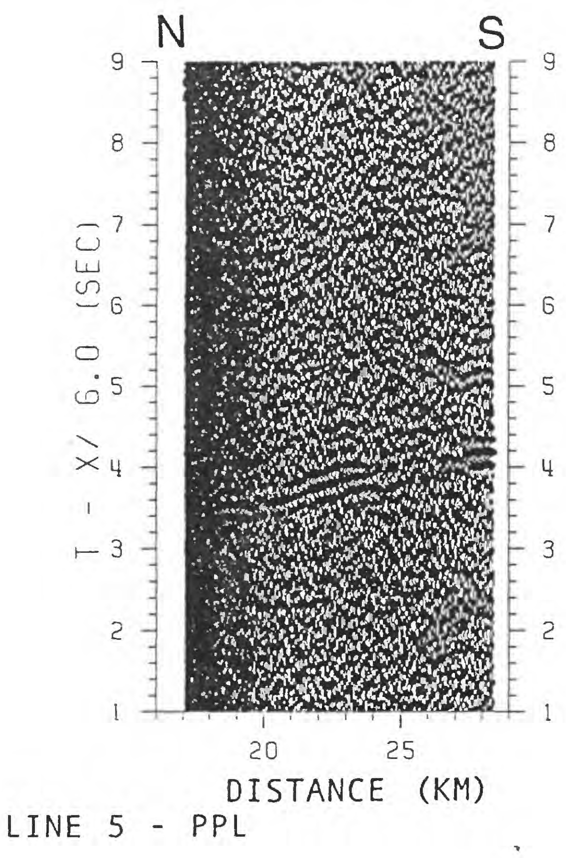

Appendix C.12

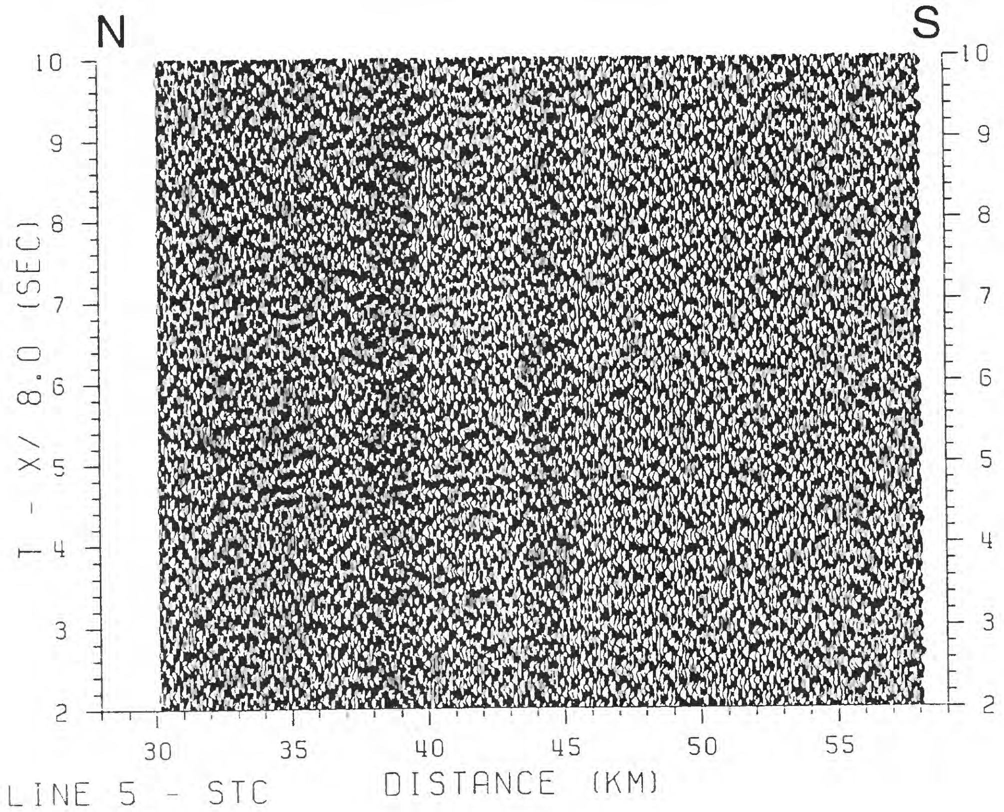

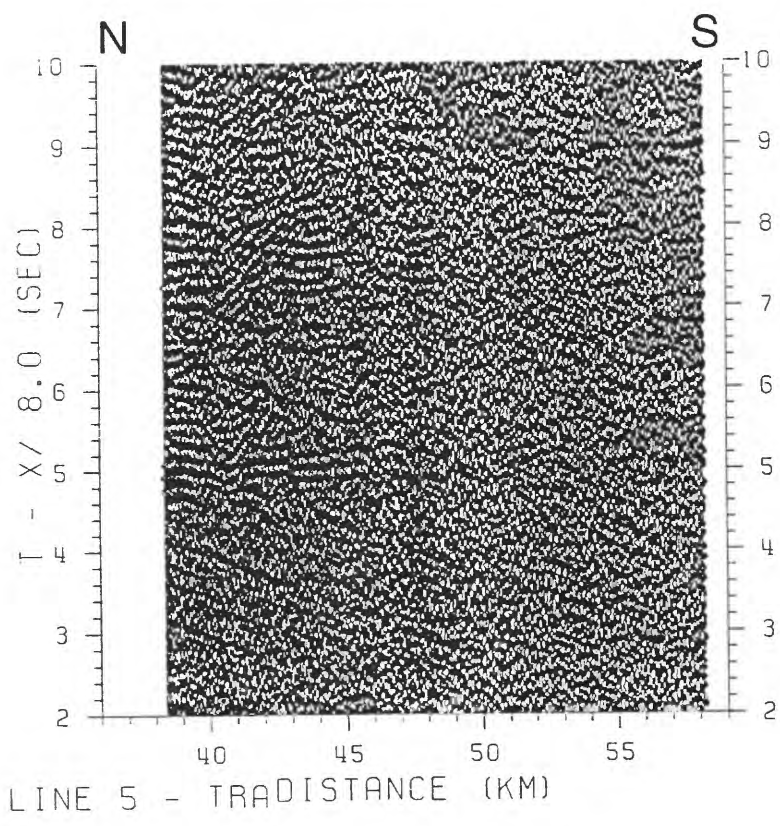

Appendix C.13

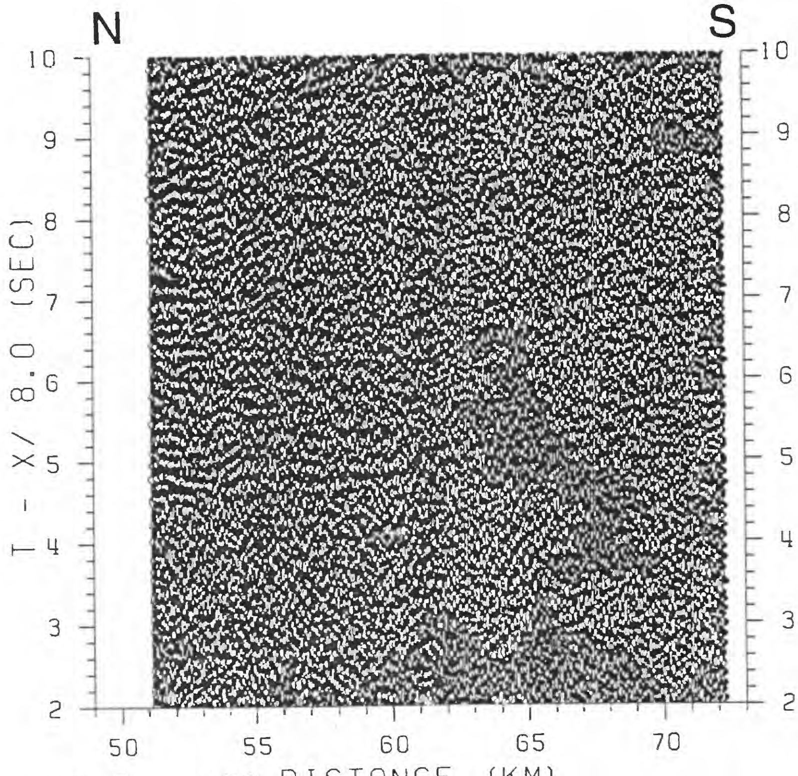

LINE 5 - WØB

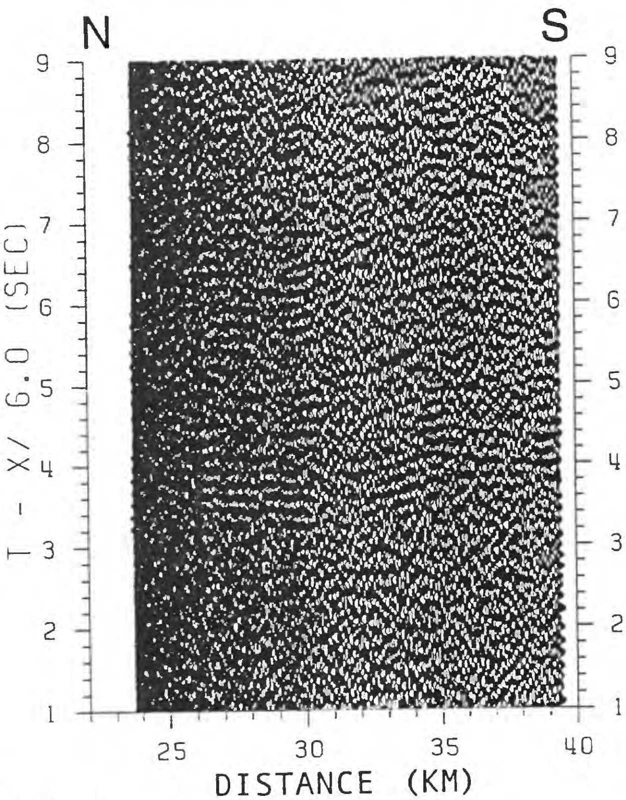

LINE 5 - WOO

Appendix C.14

APPENDIX D. RECORD SECTIONS FROM LINE 6

Vertical-component record sections for HVO seismic network stations recording seismic phases from Line 6 shots (Figure 5). Data are plotted versus distance or azimuth. Data were bandpass filtered (3 - 10 Hz), and each trace scaled to a uniform maximum amplitude. For time vs. distance plots, data were linearly reduced using velocities of 6 or 8 km/s. Reduction velocities were selected to permit identification of the ranges at which Moho (oceanic crust-mantle boundary) and crustal (volcano-oceanic crust transition) velocities first appear. No topographic or water column corrections have been applied, and the estimated 50 ms firing system delay has not been accounted for in the plots. Shot range is the distance between OHD HVO station locations and WGS 84 shot locations; true ranges, resulting in shifts averaging 445 m in the N140°E direction, are calculated in Table 2.

FIGURE *PAGE*

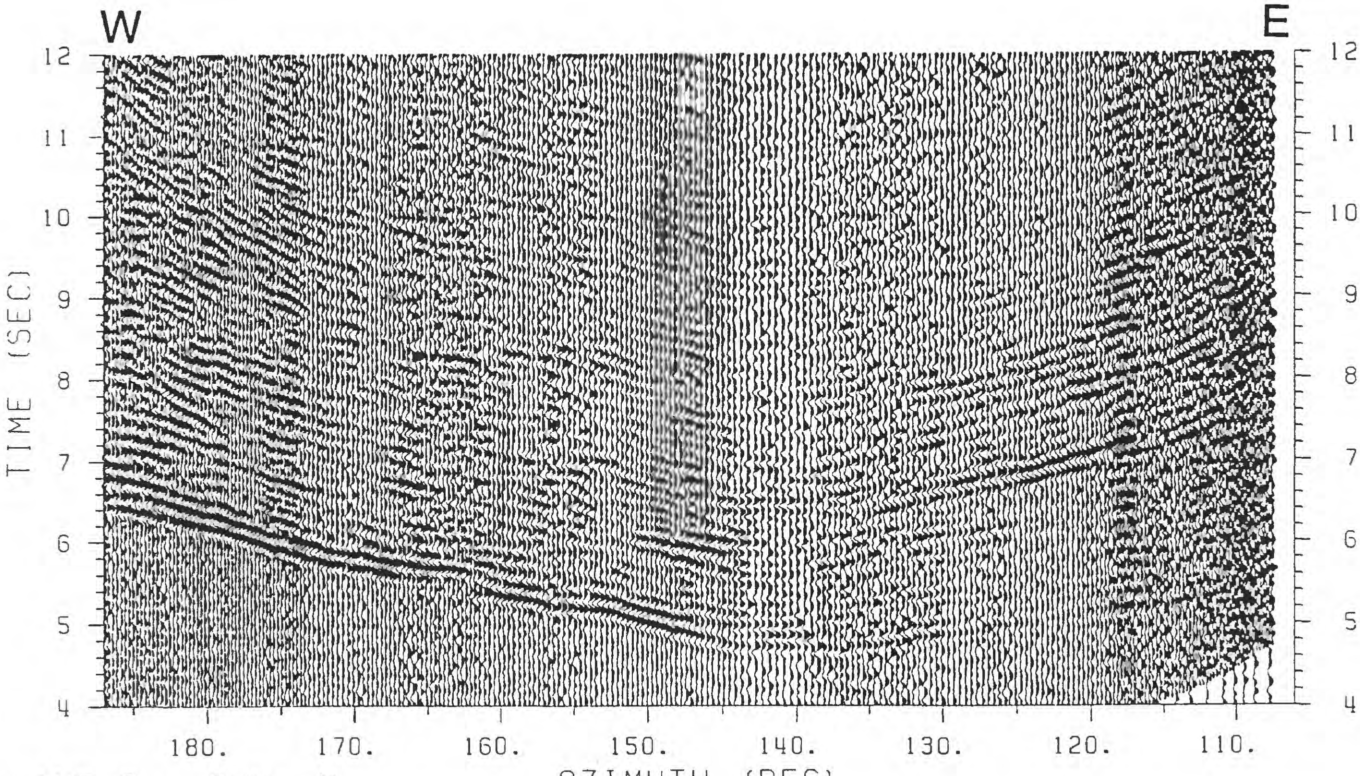

LINE 6 - AHU, V

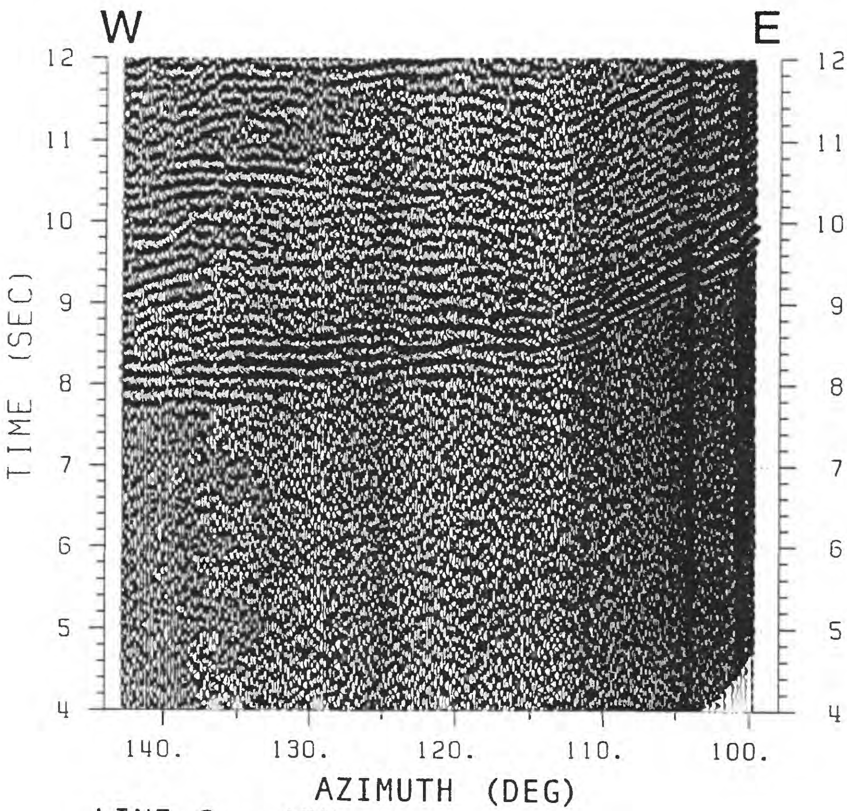

LINE 6 - AIN, V

Appendix D.1

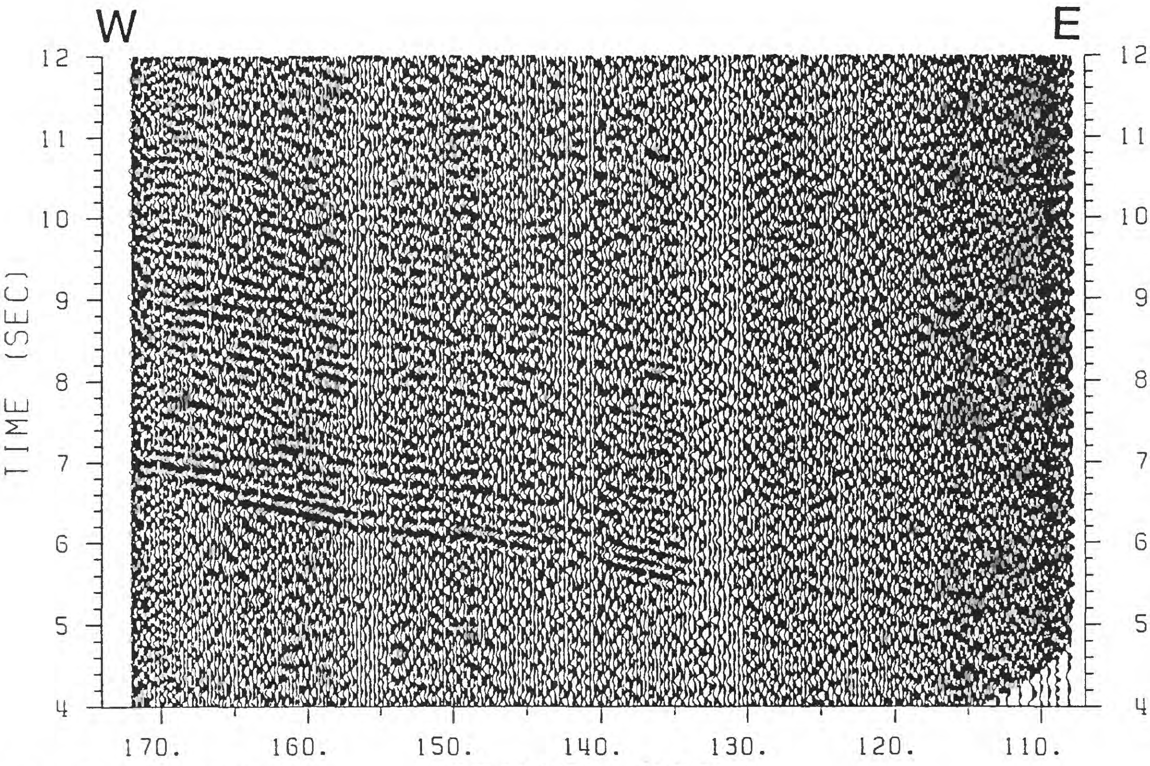

LINE 6 - CPK, V

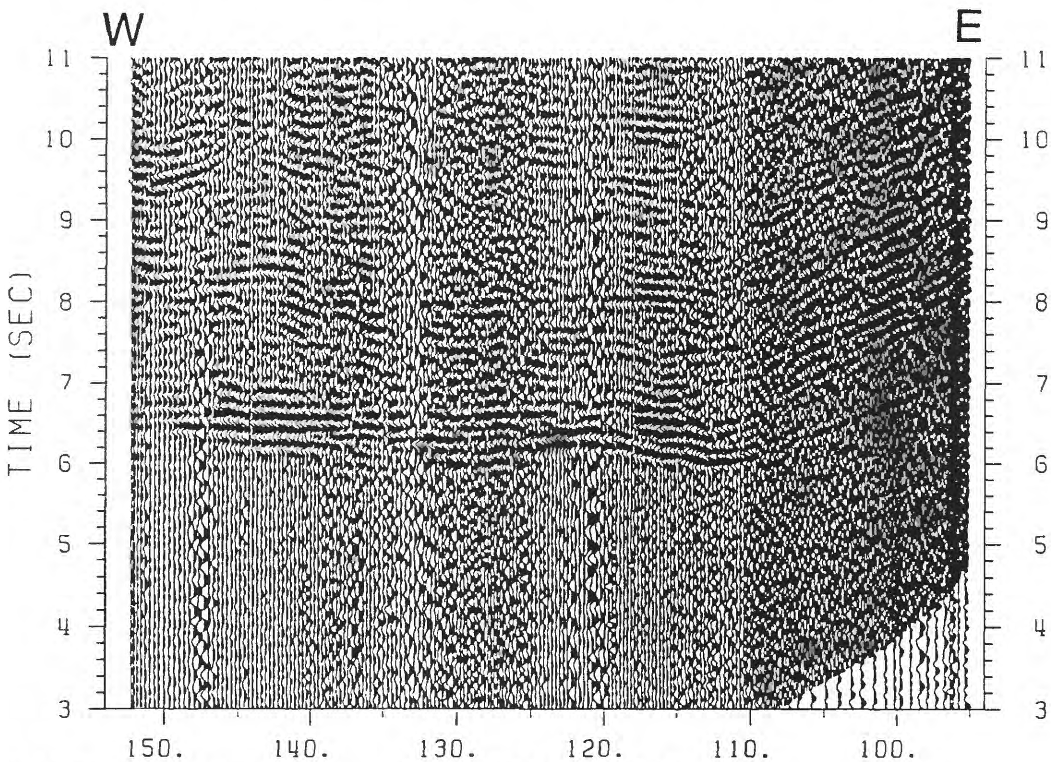

LINE 6 - DES, V

Appendix D.2

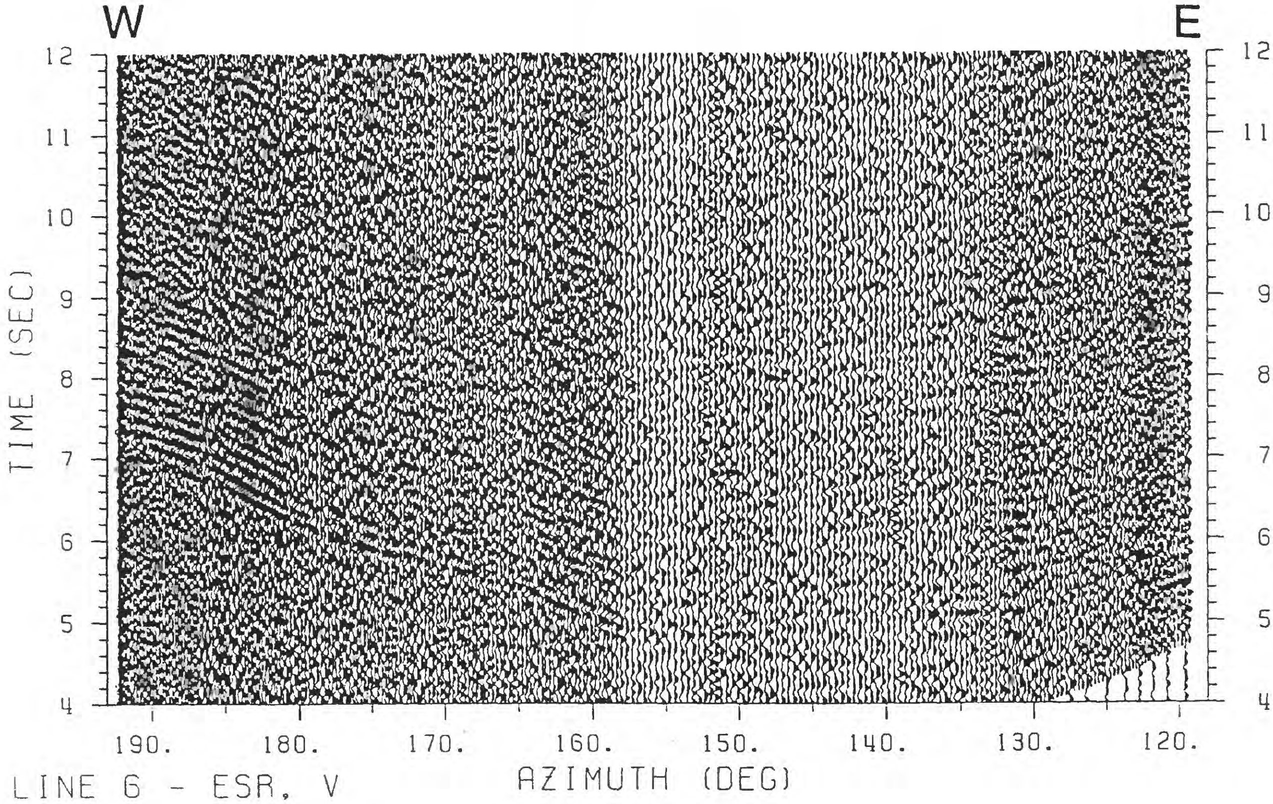
W
E
TIME (SEC)
12
11
10
9
8
7
6
5
4
190.
180.
170.
160.
150.
140.
130.
120.
AZIMUTH (DEG)
LINE 6 - ESR, V

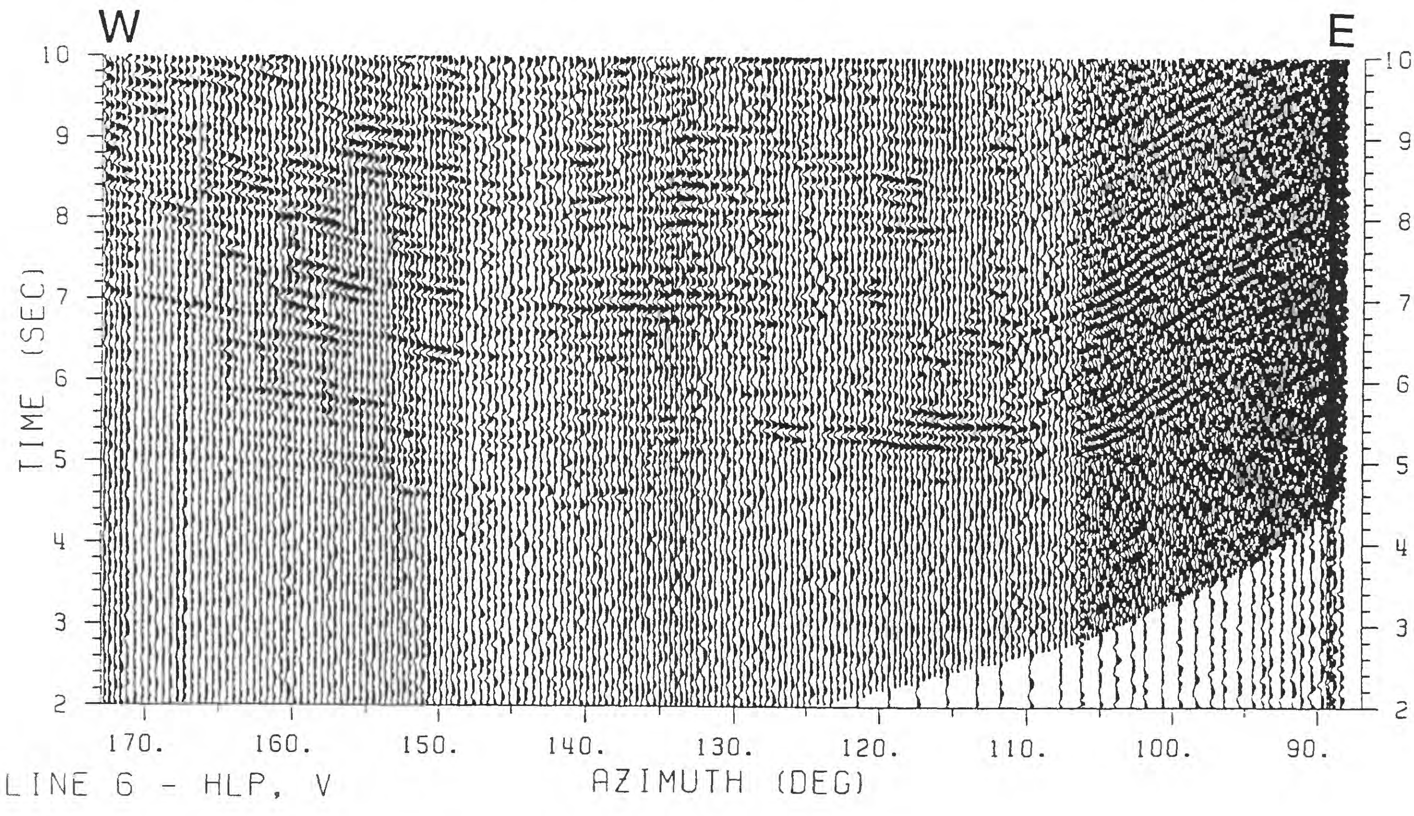
W
E
TIME (SEC)
10
9
8
7
6
5
4
3
2
170.
160.
150.
140.
130.
120.
110.
100.
90.
AZIMUTH (DEG)
LINE 6 - HLP, V

Appendix D.3

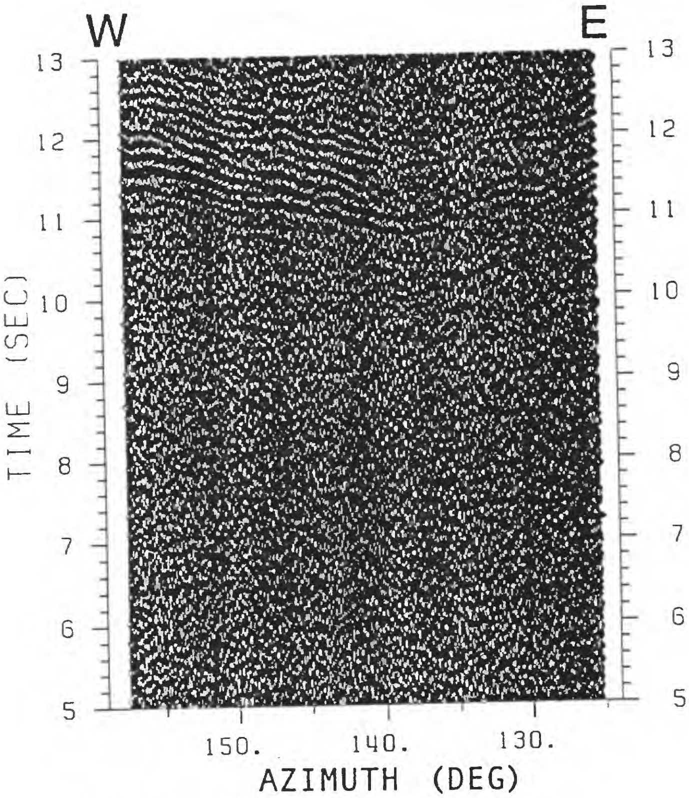

LINE 6 - HSS, V

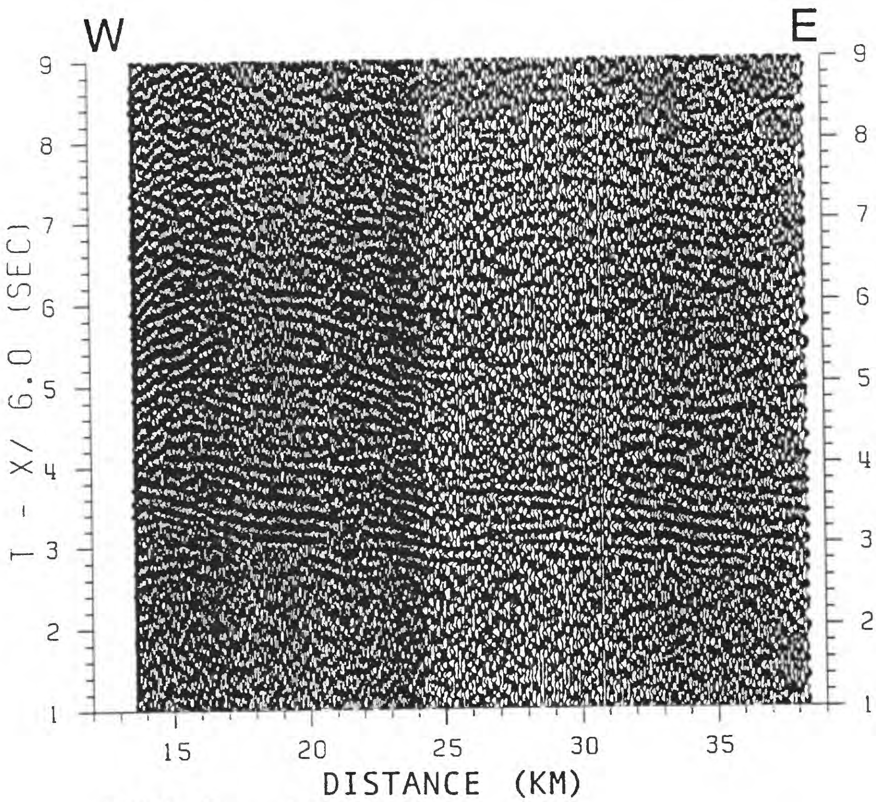

LINE 6 - HTC, V

Appendix D.4

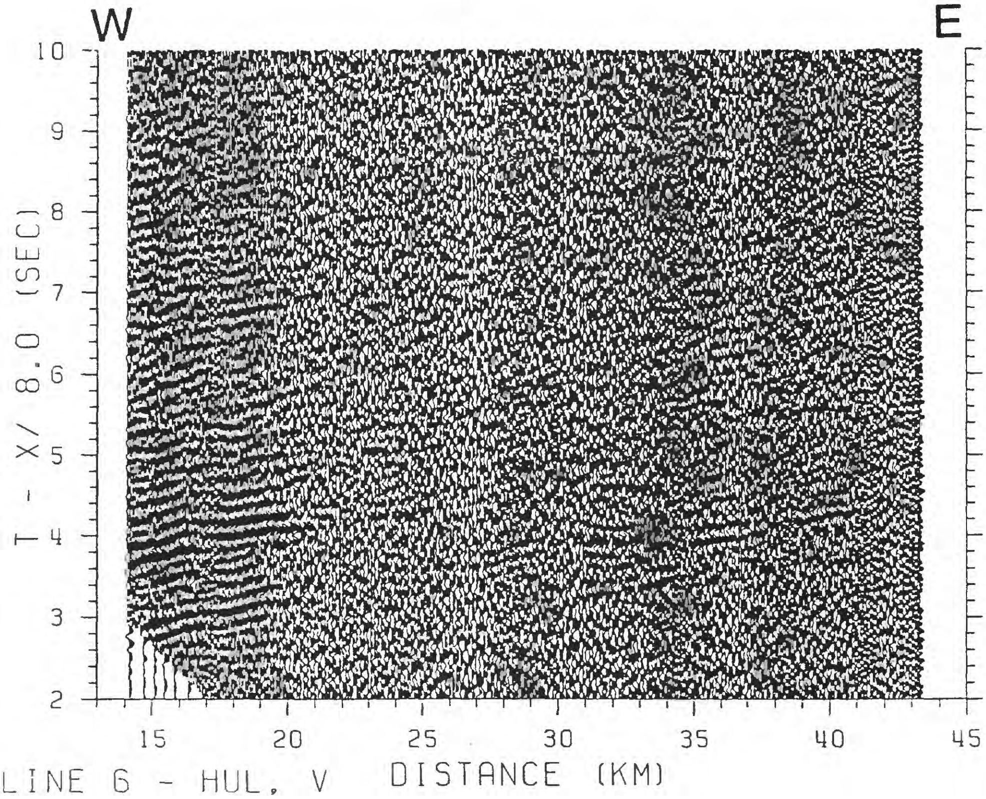

LINE 6 - HUL, V

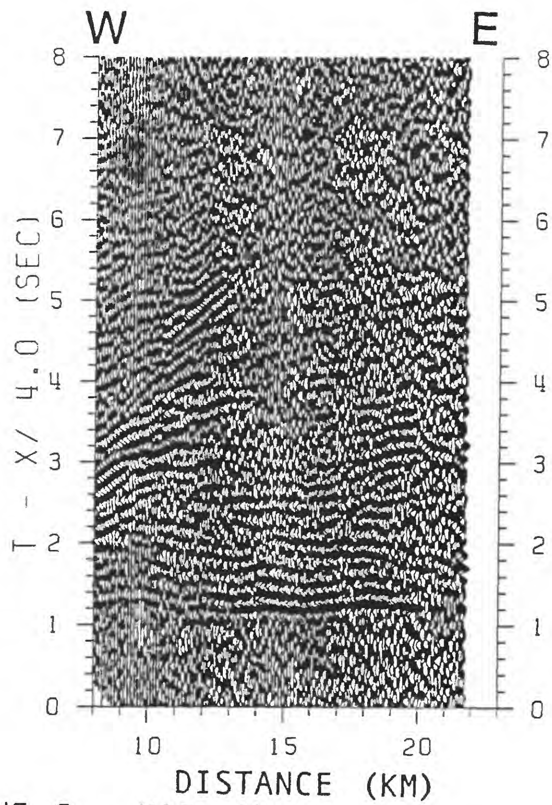

LINE 6 - KAE, V

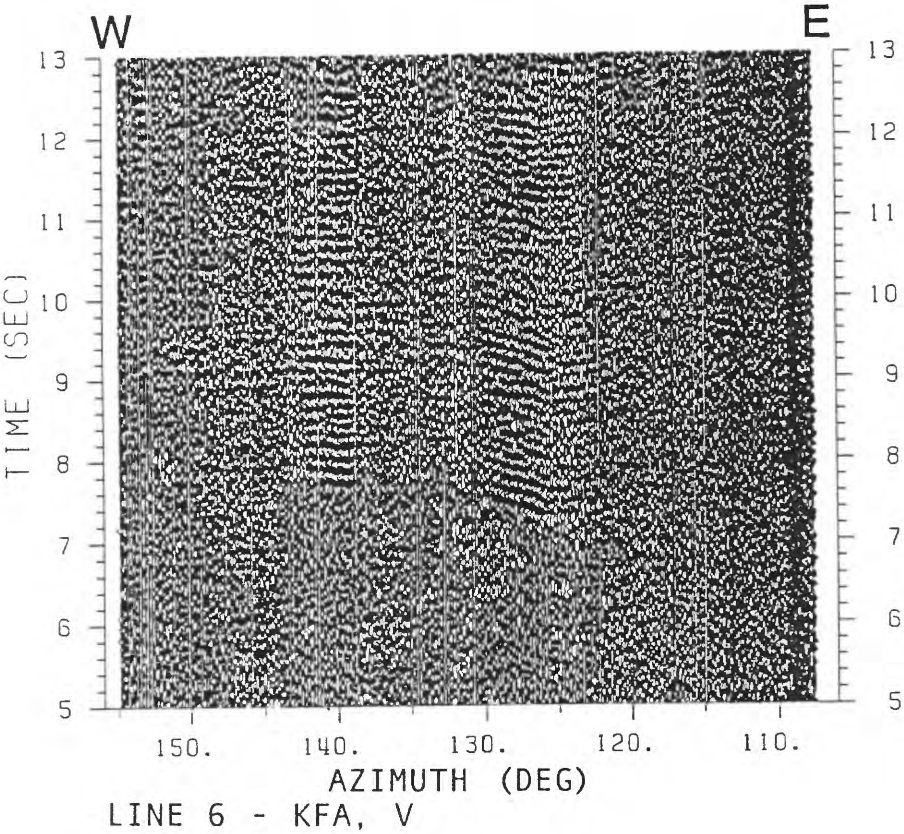
W
E
TIME (SEC)
13
12
11
10
9
8
7
6
5
150.
140.
130.
120.
110.
AZIMUTH (DEG)
LINE 6 - KFA, V

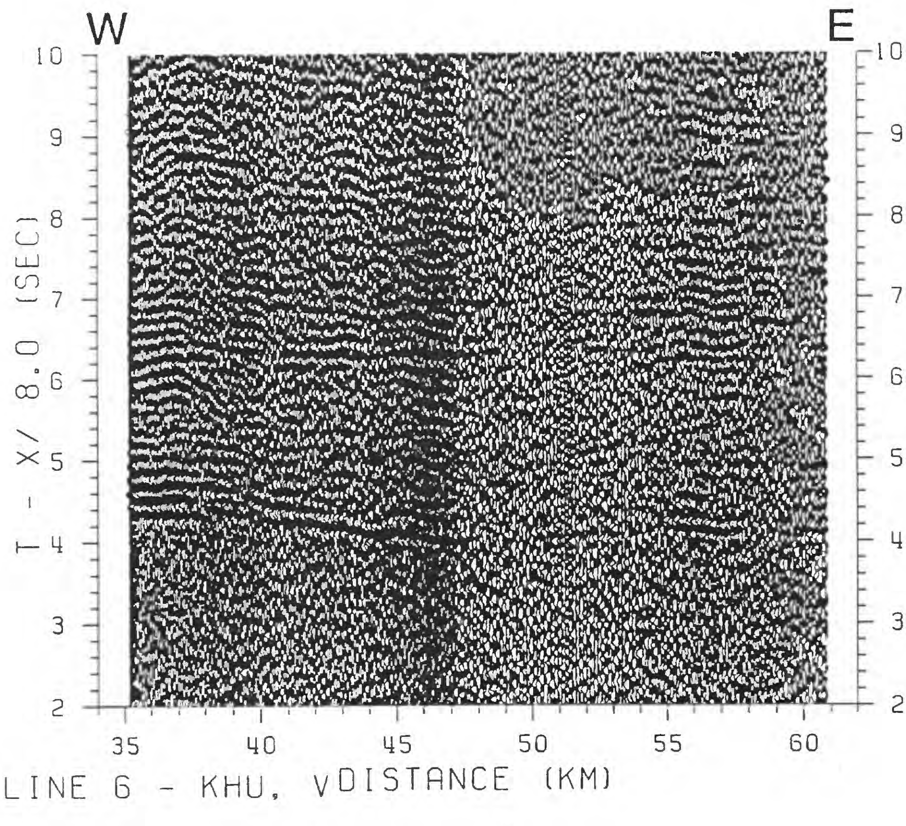
W
E
T - X/ 8.0 (SEC)
10
9
8
7
6
5
4
3
2
35
40
45
50
55
60
LINE 6 - KHU, V
DISTANCE (KM)

Appendix D.6

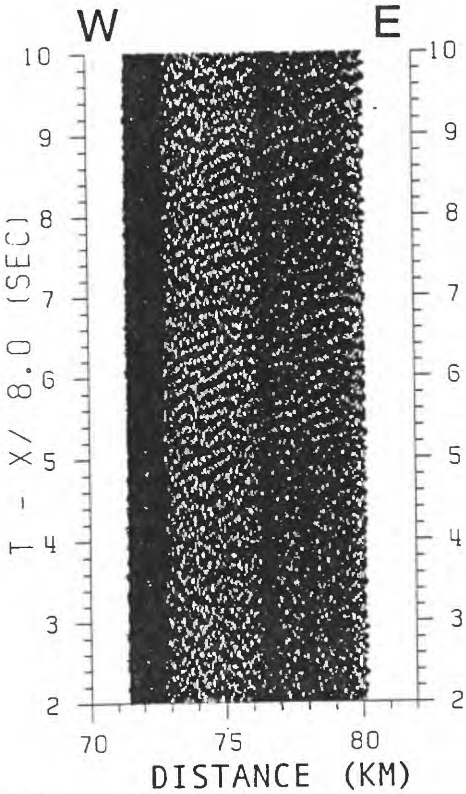

LINE 6 - KKU, V

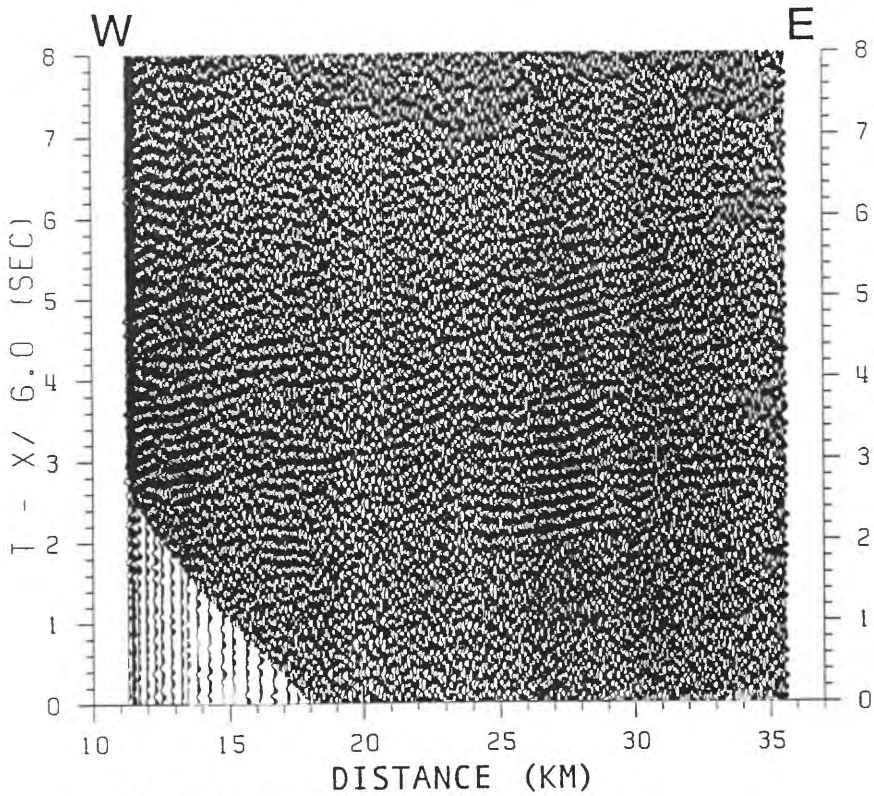

LINE 6 - KLC, V

Appendix D.7

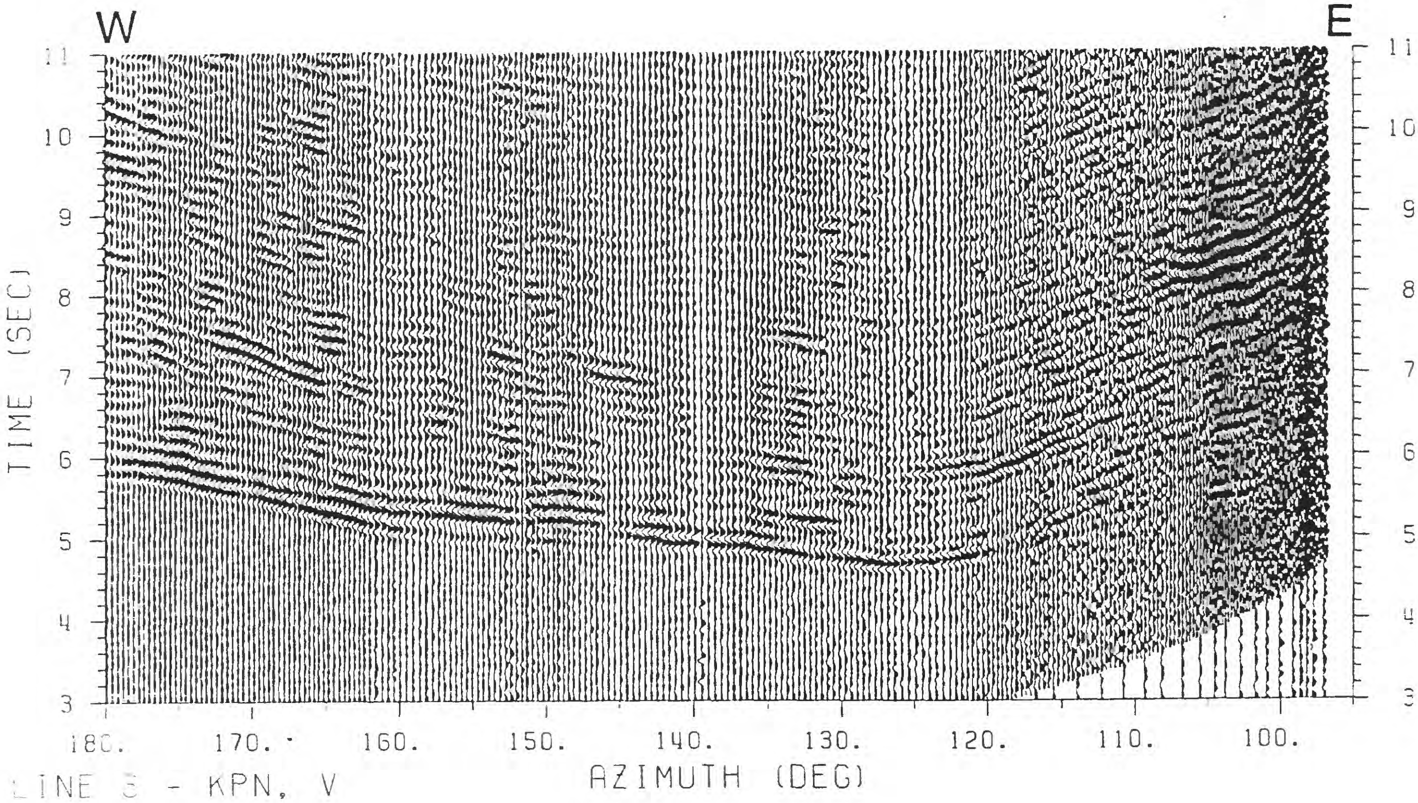

W
E
TIME (SEC)
AZIMUTH (DEG)
LINE 3 - KPN, V

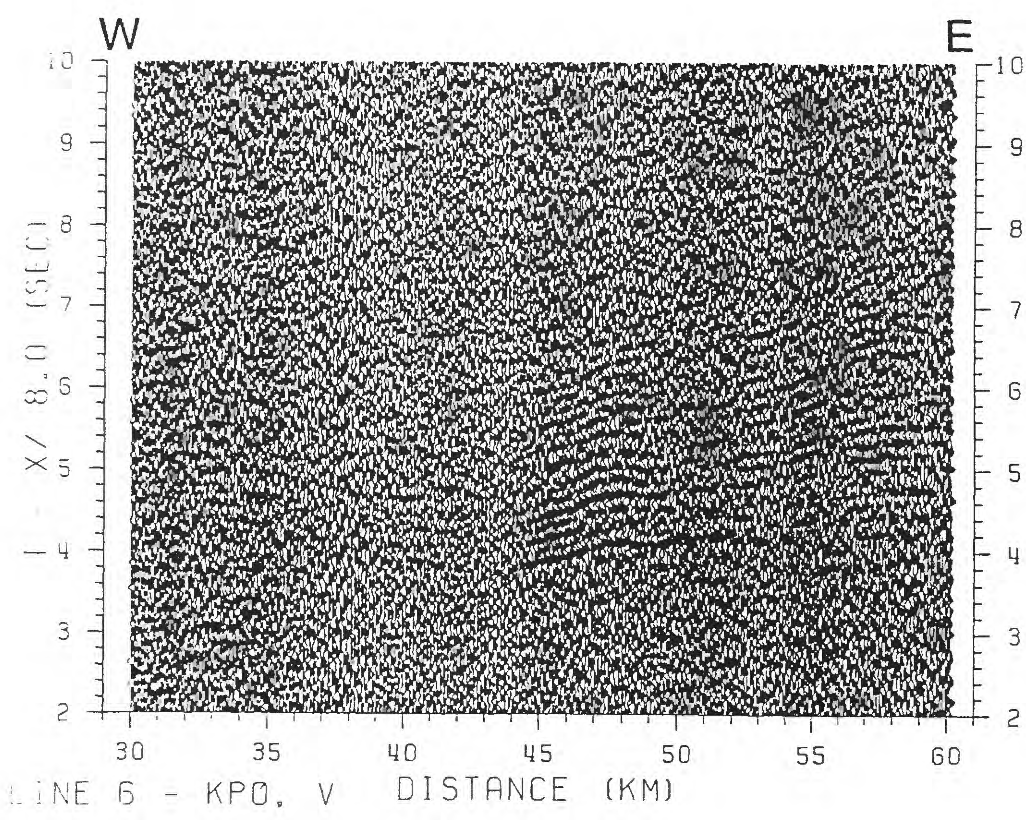

W
E
T - X/ 8.0 (SEC)
DISTANCE (KM)
LINE 6 - KPO, V

Appendix D.8

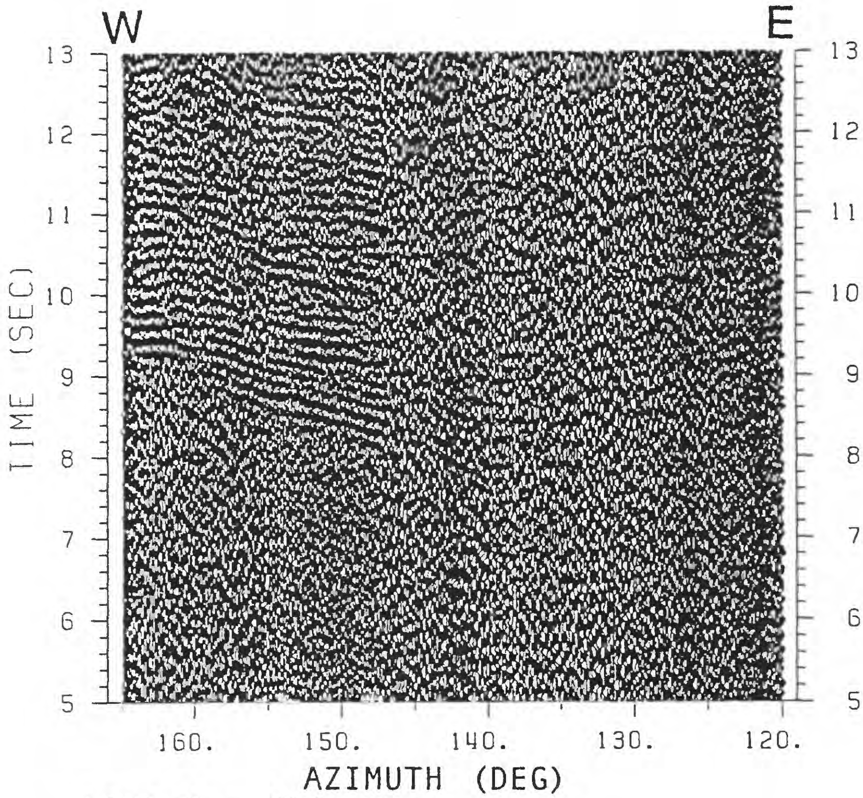

LINE 6 - MLO, V

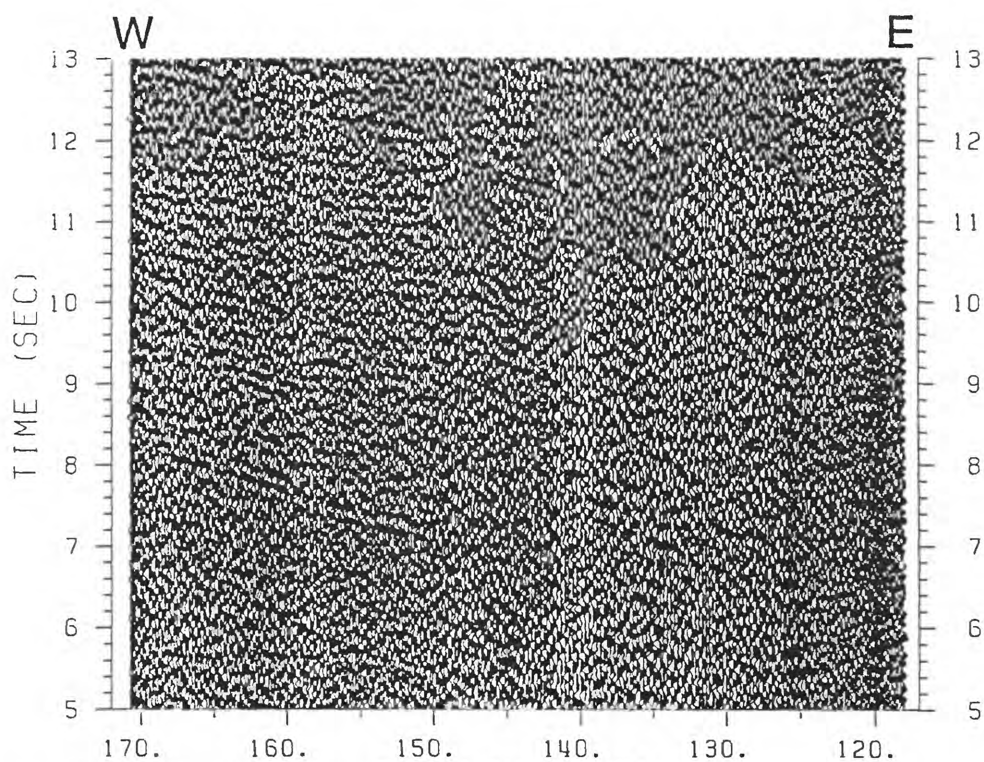

LINE 6 - MLX, V

Appendix D.9

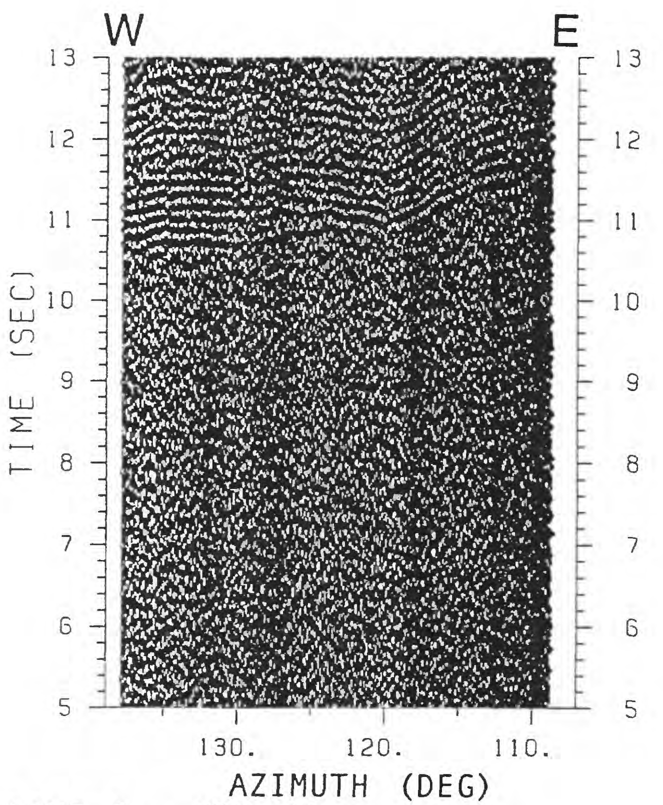

LINE 6 - MOK, V

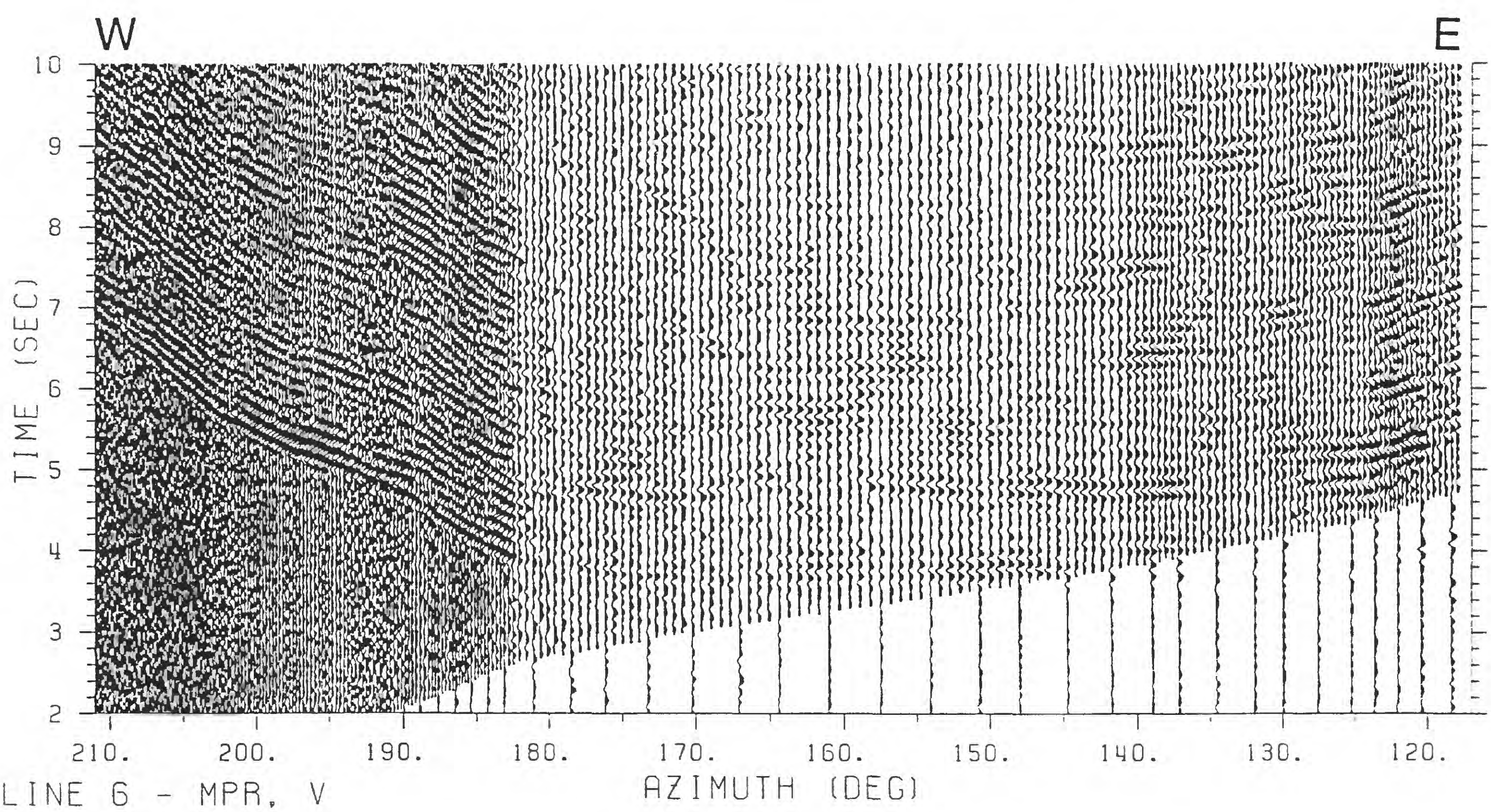

LINE 6 - MPR, V

Appendix D.10

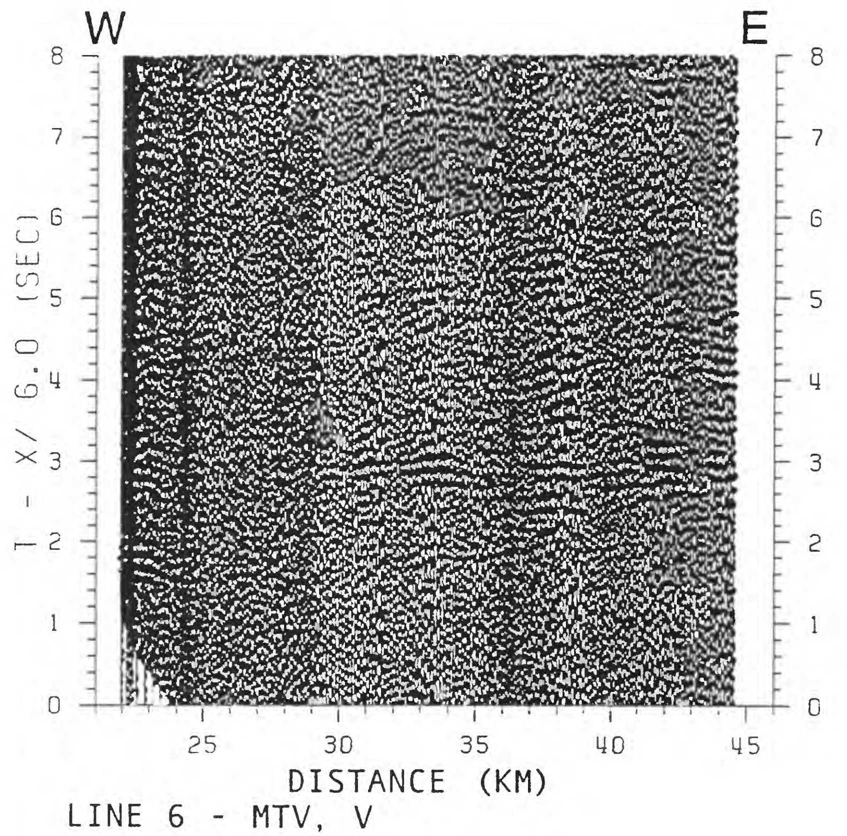

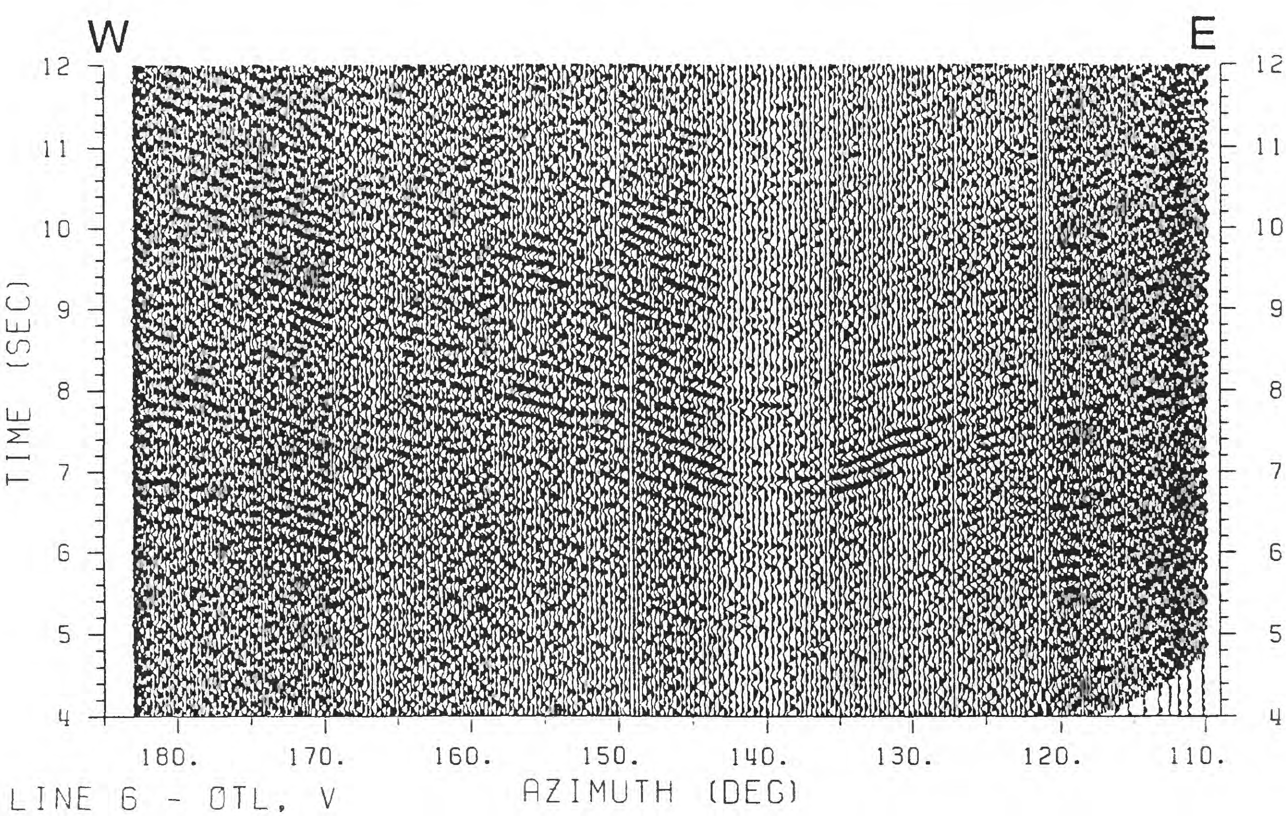

Appendix D.11

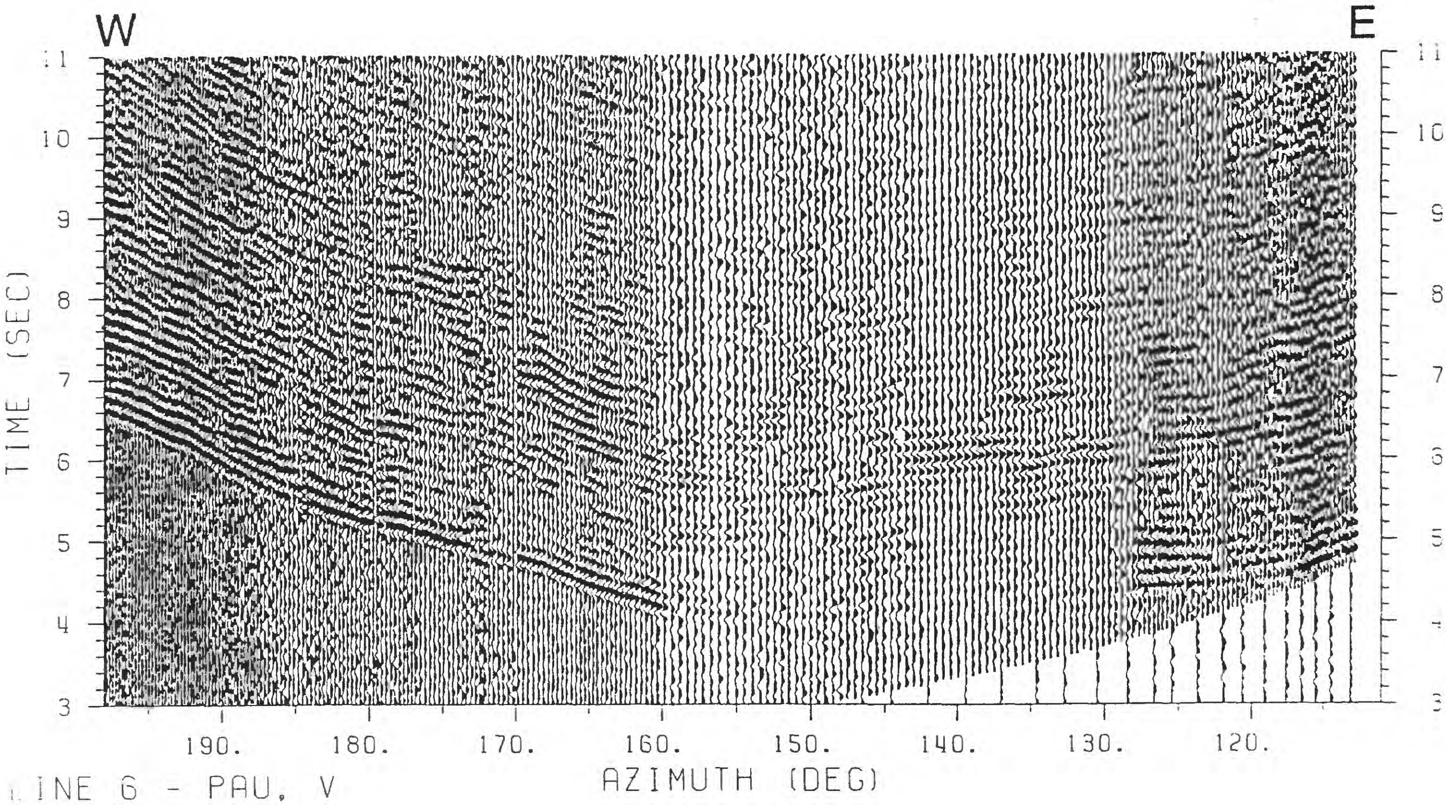
W
E
TIME (SEC)
AZIMUTH (DEG)
190. 180. 170. 160. 150. 140. 130. 120.
LINE 6 - PAU, V

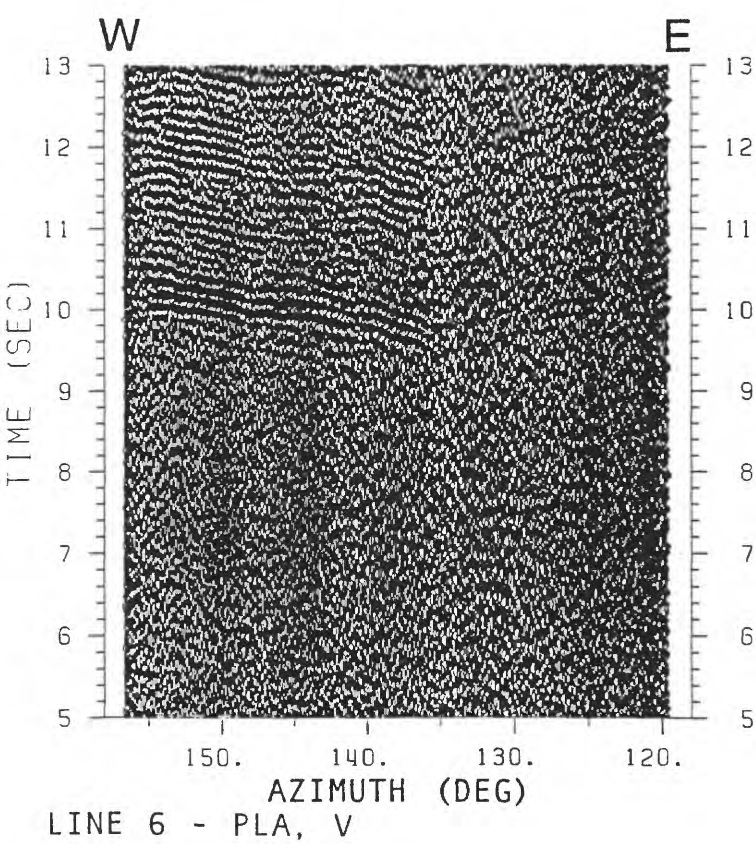
W
E
TIME (SEC)
AZIMUTH (DEG)
150. 140. 130. 120.
LINE 6 - PLA, V

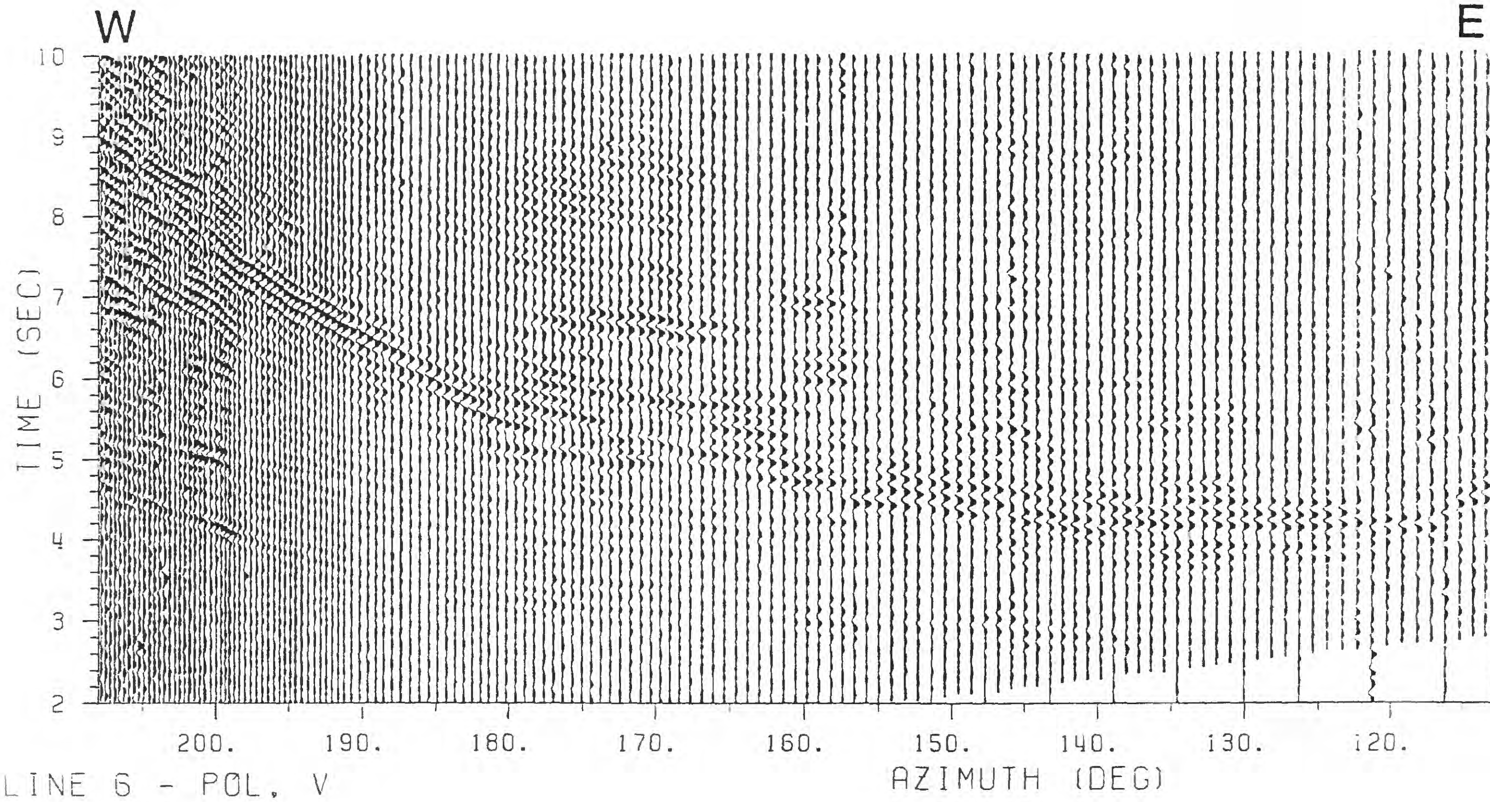

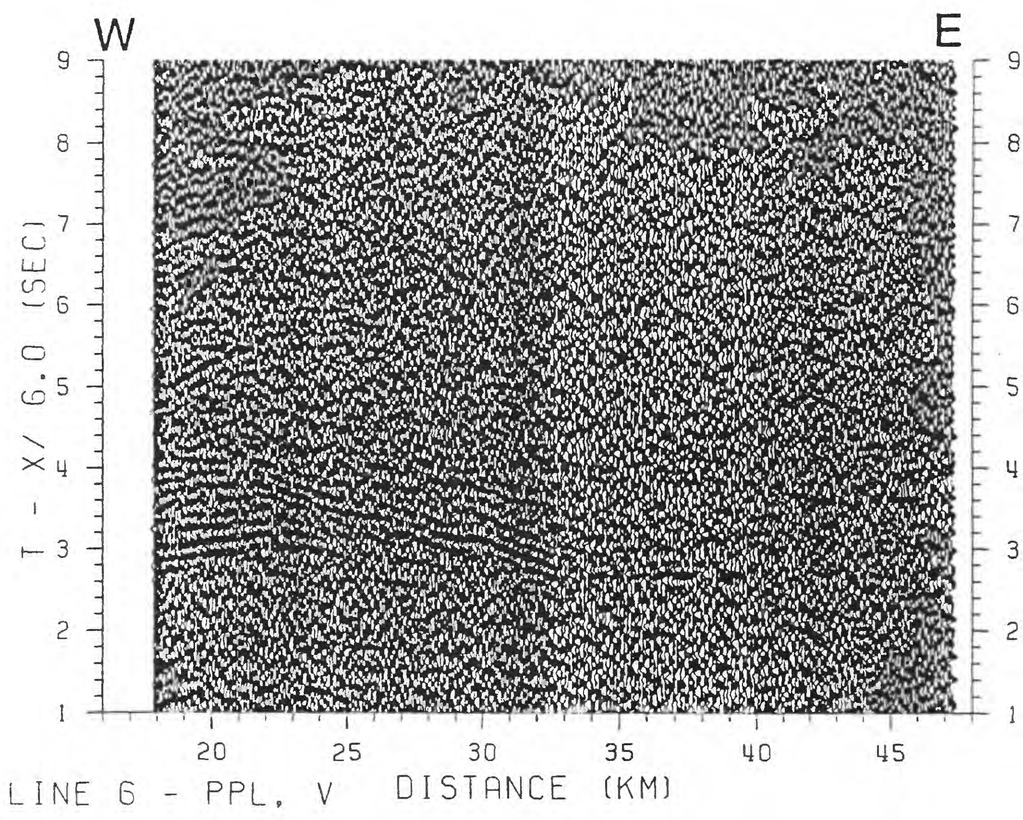

Appendix D.13

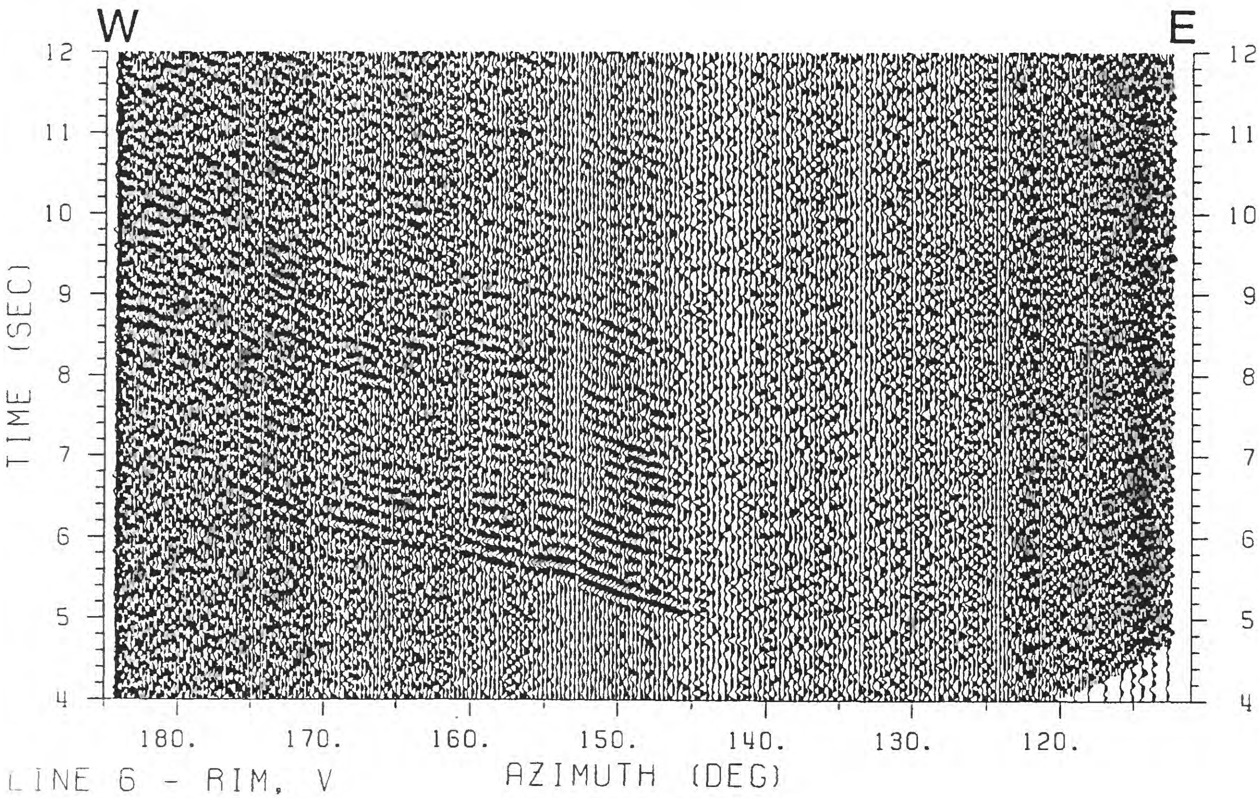

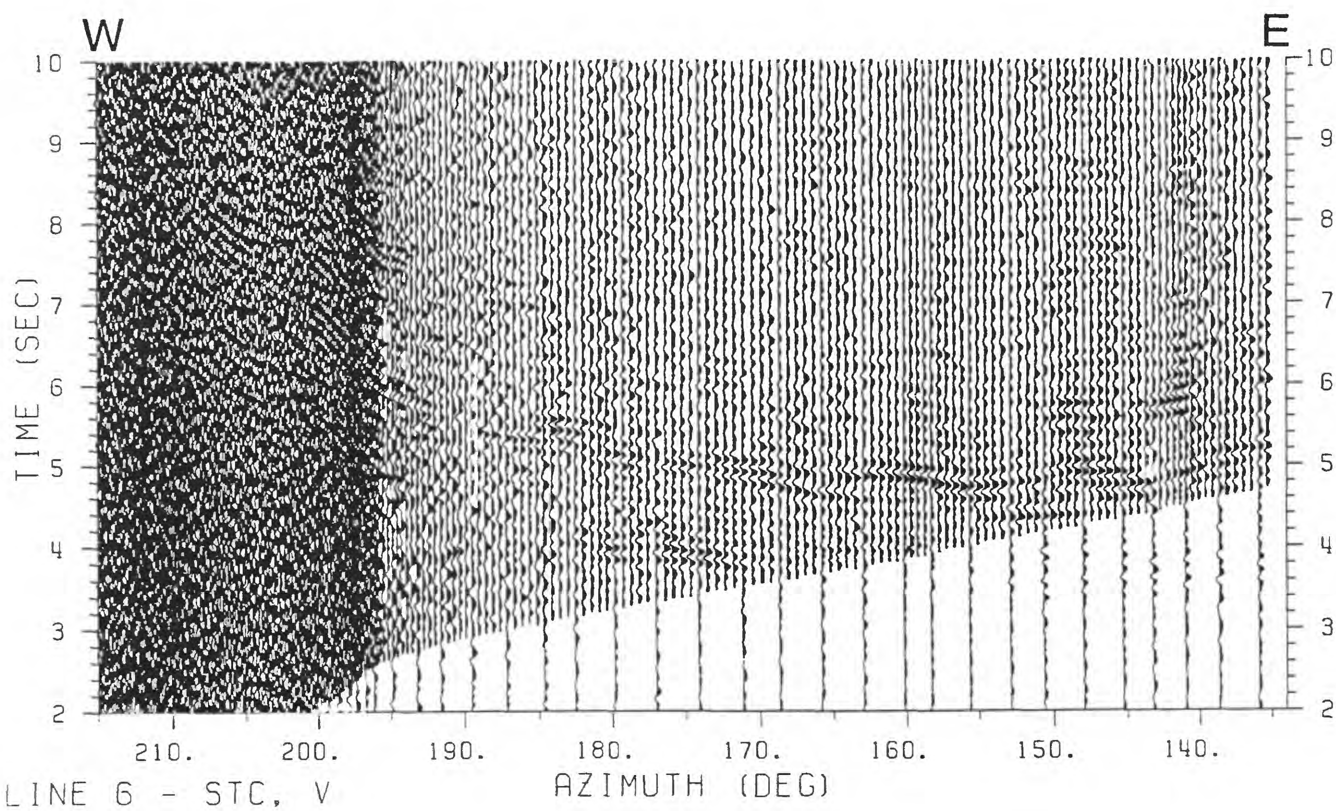

Appendix D.14

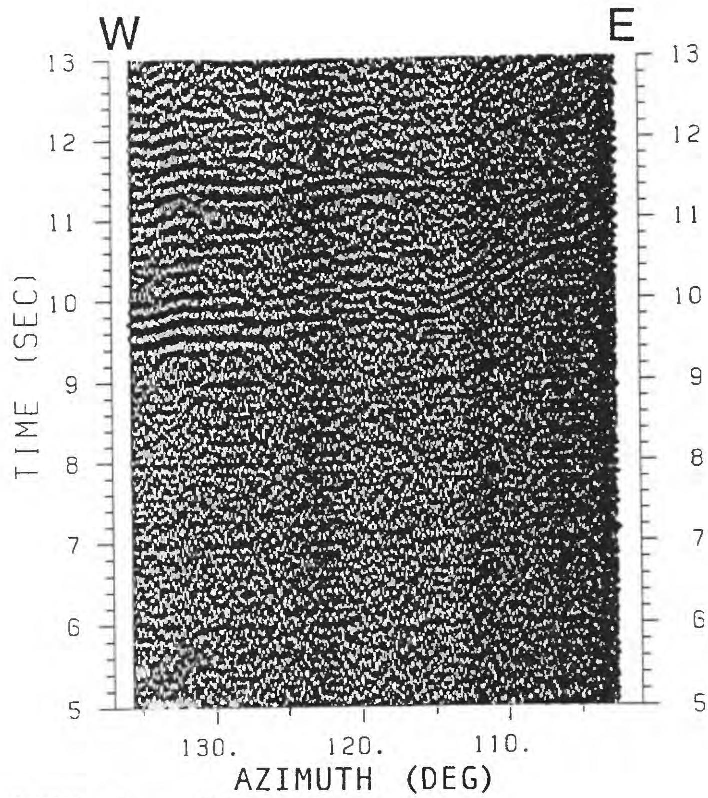

LINE 6 - TRA, V

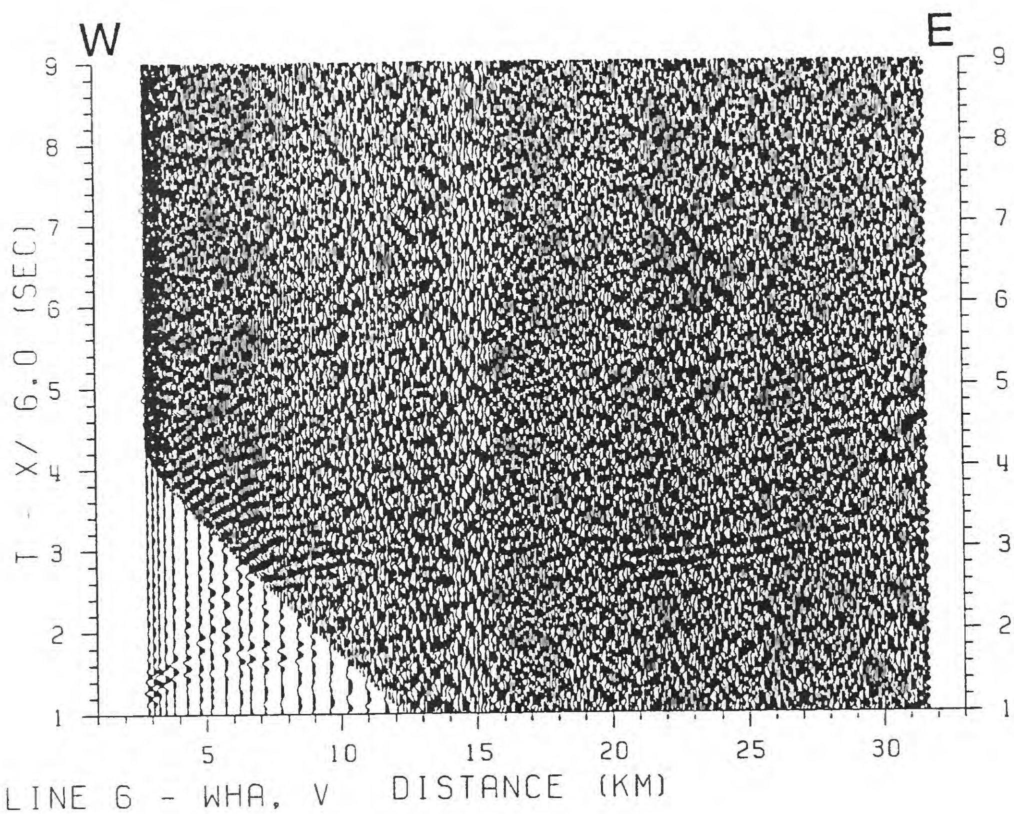

LINE 6 - WHA, V

Appendix D.15

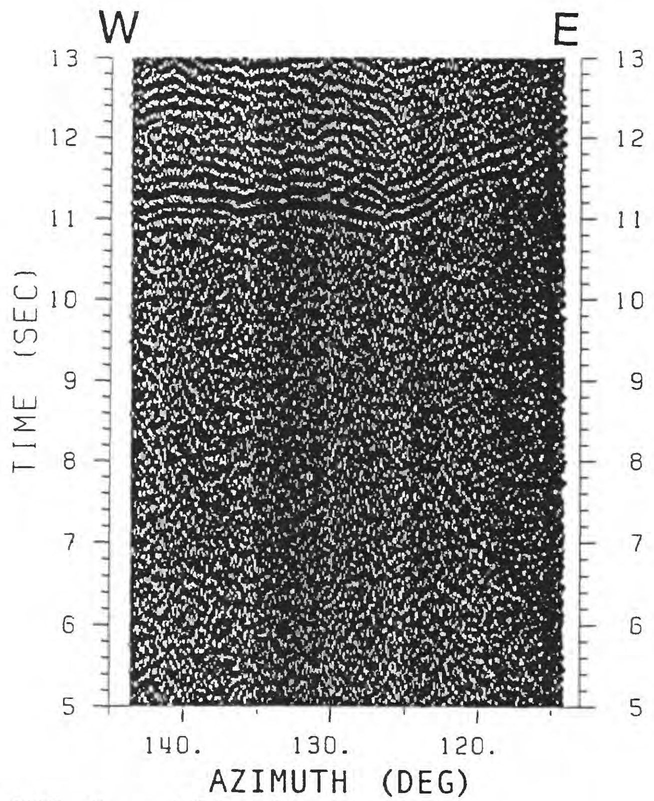

LINE 6 - WOB, V

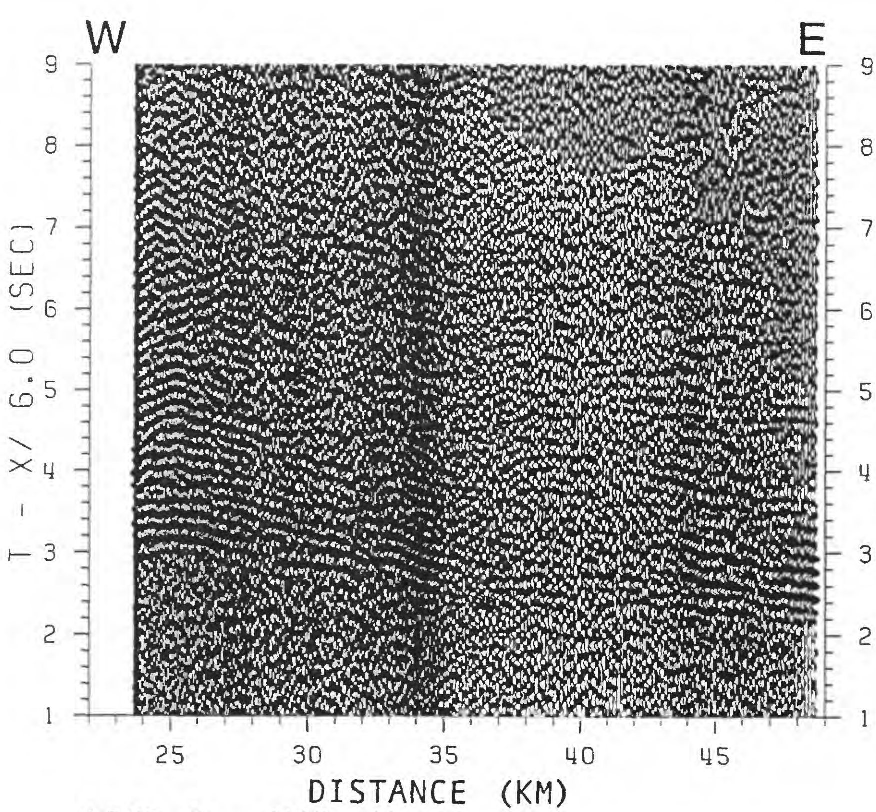

LINE 6 - WOO, V

Appendix D.16

APPENDIX E. RECORD SECTIONS FROM LINE 7

Vertical-component record sections for HVO seismic network stations recording seismic phases from Line 7 shots (Figure 6). Data are plotted versus distance or azimuth. Data were bandpass filtered (3 - 10 Hz), and each trace scaled to a uniform maximum amplitude. For time vs. distance plots, data were linearly reduced using velocities of 6 or 8 km/s. Reduction velocities were selected to permit identification of the ranges at which Moho (oceanic crust-mantle boundary) and crustal (volcano-oceanic crust transition) velocities first appear. No topographic or water column corrections have been applied, and the estimated 50 ms firing system delay has not been accounted for in the plots. Shot range is the distance between OHD HVO station locations and WGS 84 shot locations; true ranges, resulting in shifts averaging 445 m in the N140°E direction, are calculated in Table 2.

FIGURE *PAGE*

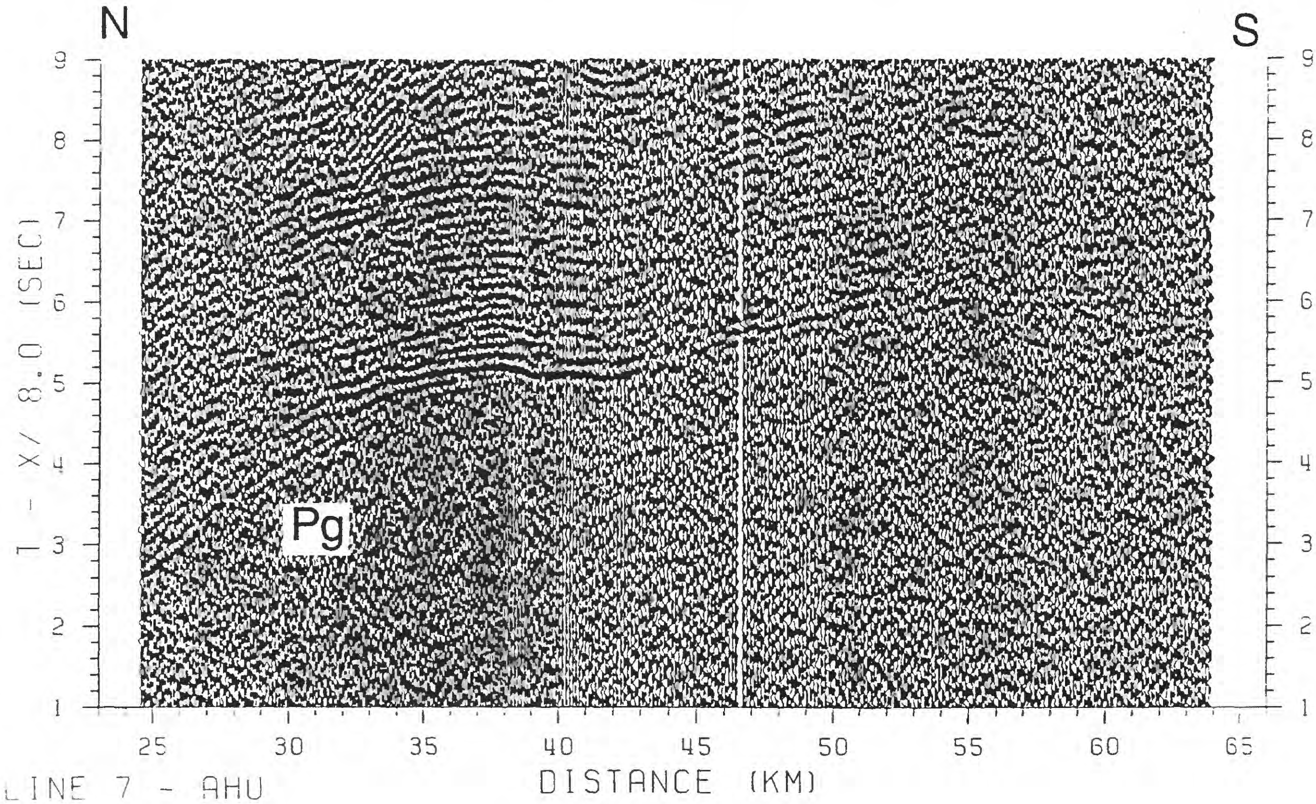
N
S
Pg
T - X/ 8.0 (SEC)
DISTANCE (KM)
LINE 7 - AHU

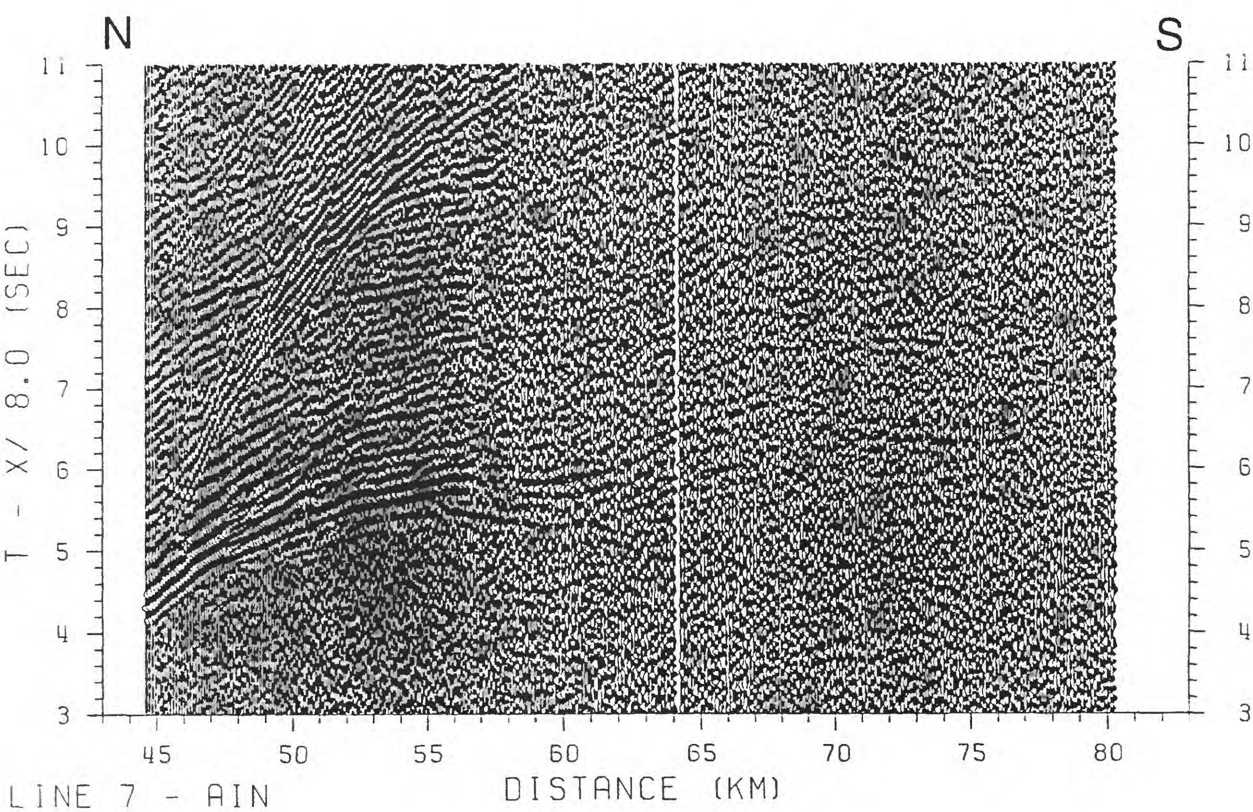
N
S
T - X/ 8.0 (SEC)
DISTANCE (KM)
LINE 7 - AIN

Appendix E.1

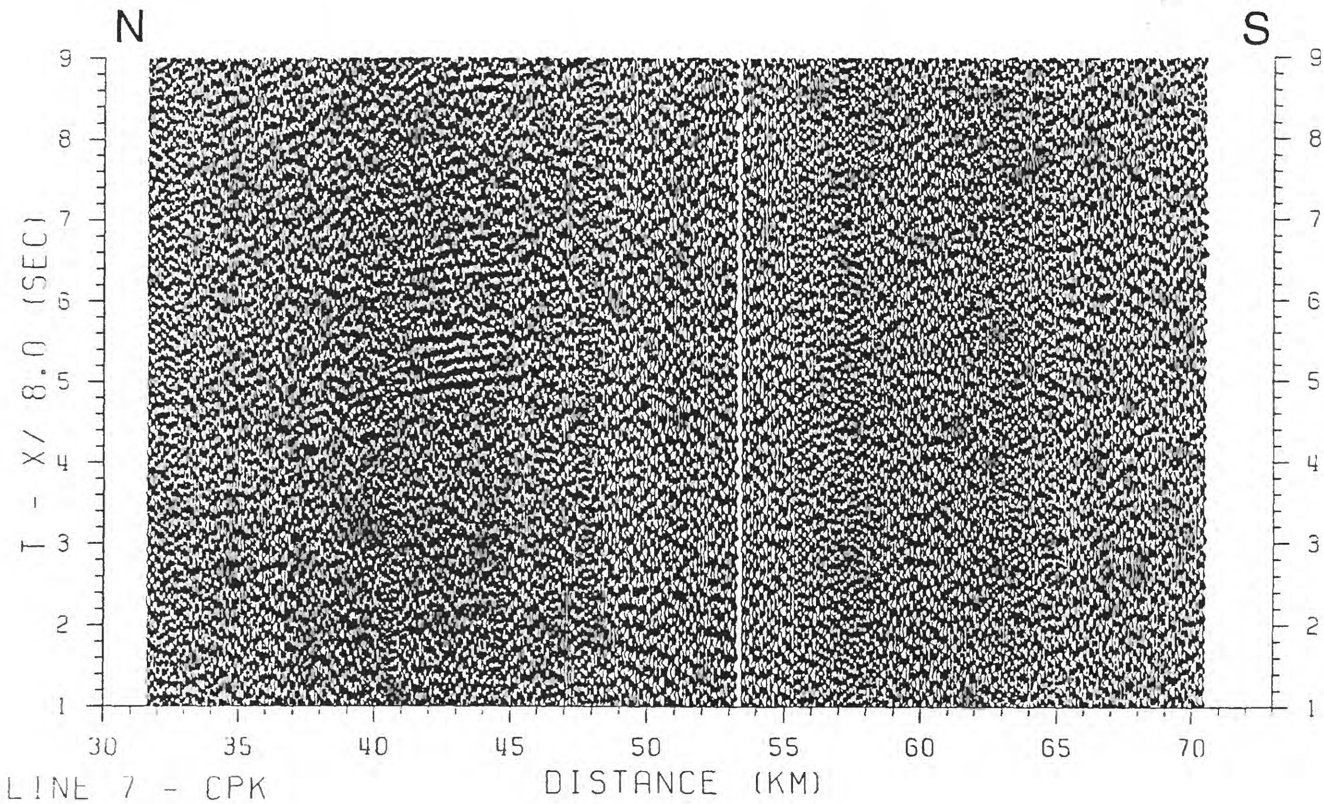
N
S
T - X/ 8.0 (SEC)
9
8
7
6
5
4
3
2
1
30
35
40
45
50
55
60
65
70
LINE 7 - CPK
DISTANCE (KM)

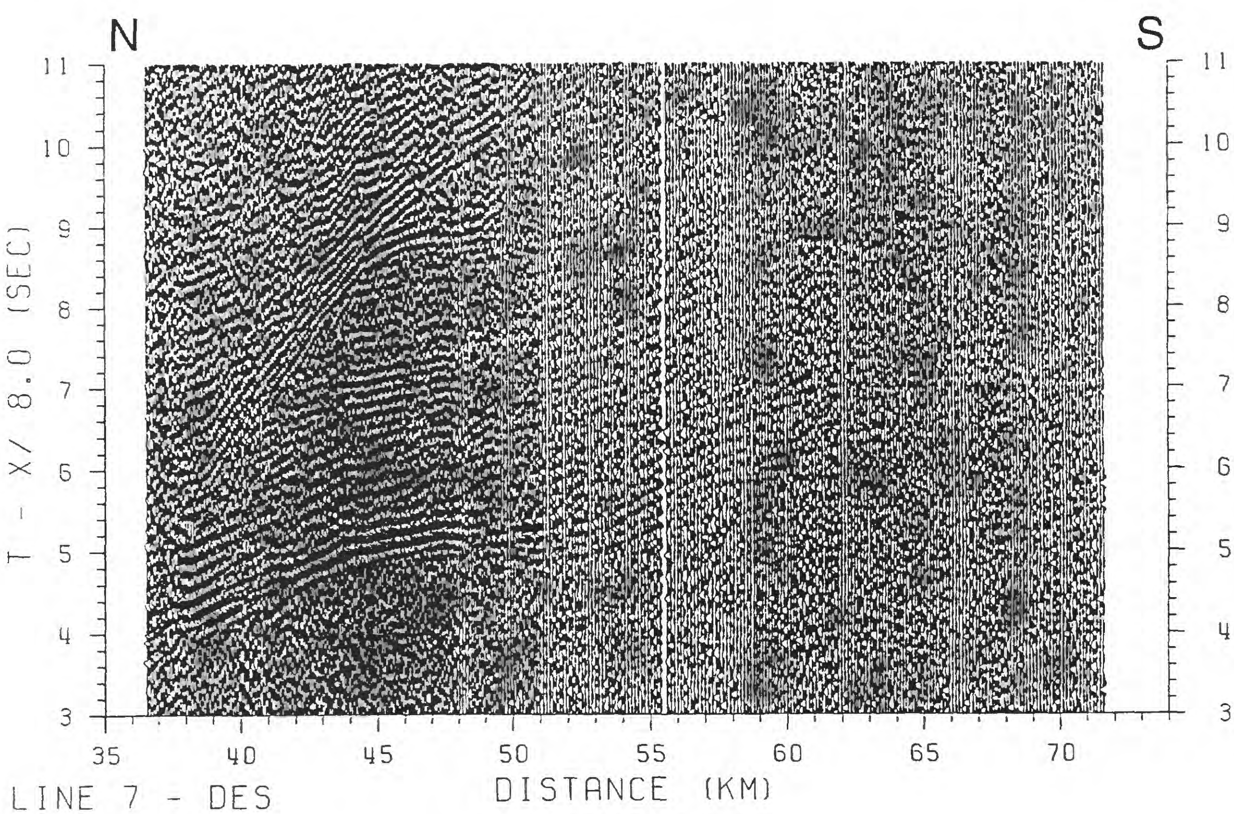
N
S
T - X/ 8.0 (SEC)
11
10
9
8
7
6
5
4
3
35
40
45
50
55
60
65
70
LINE 7 - DES
DISTANCE (KM)

Appendix E.2

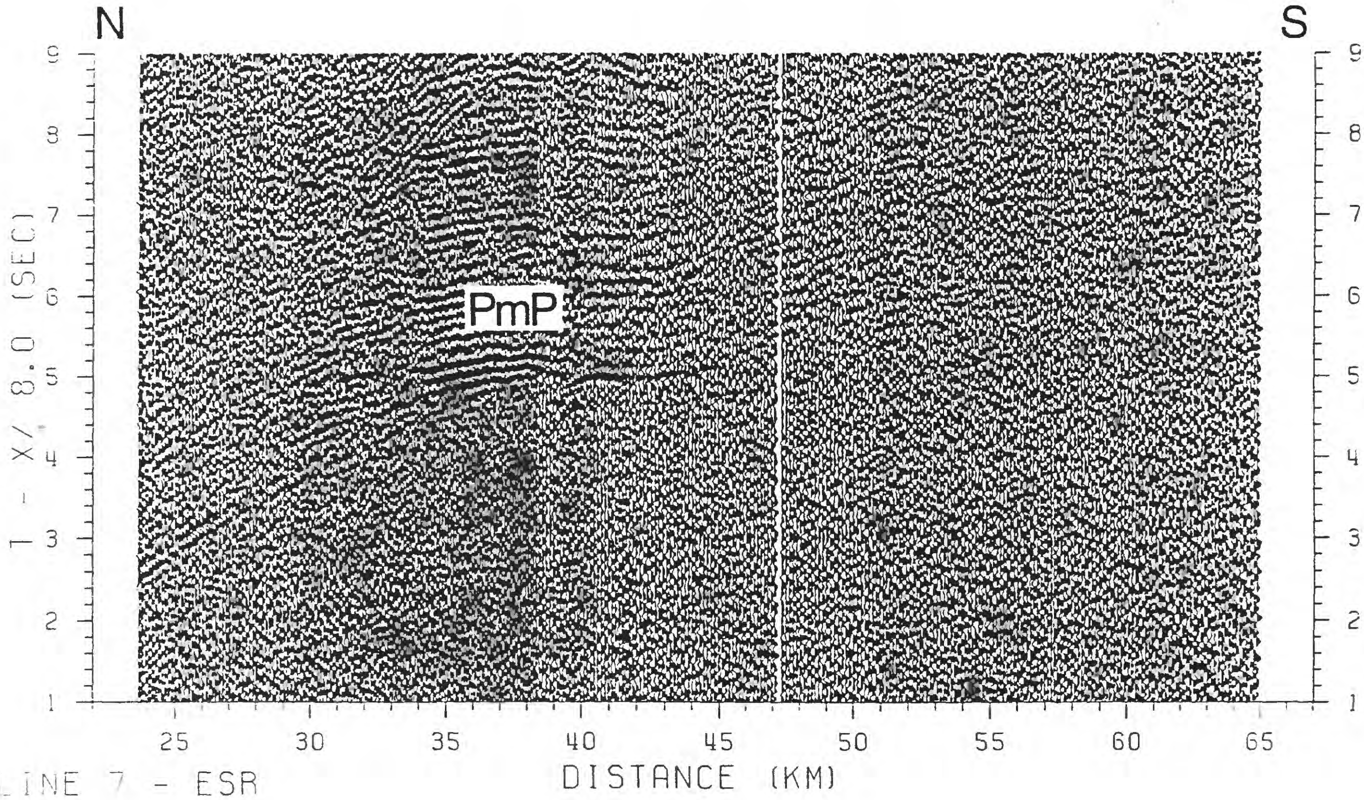

LINE 7 - ESR

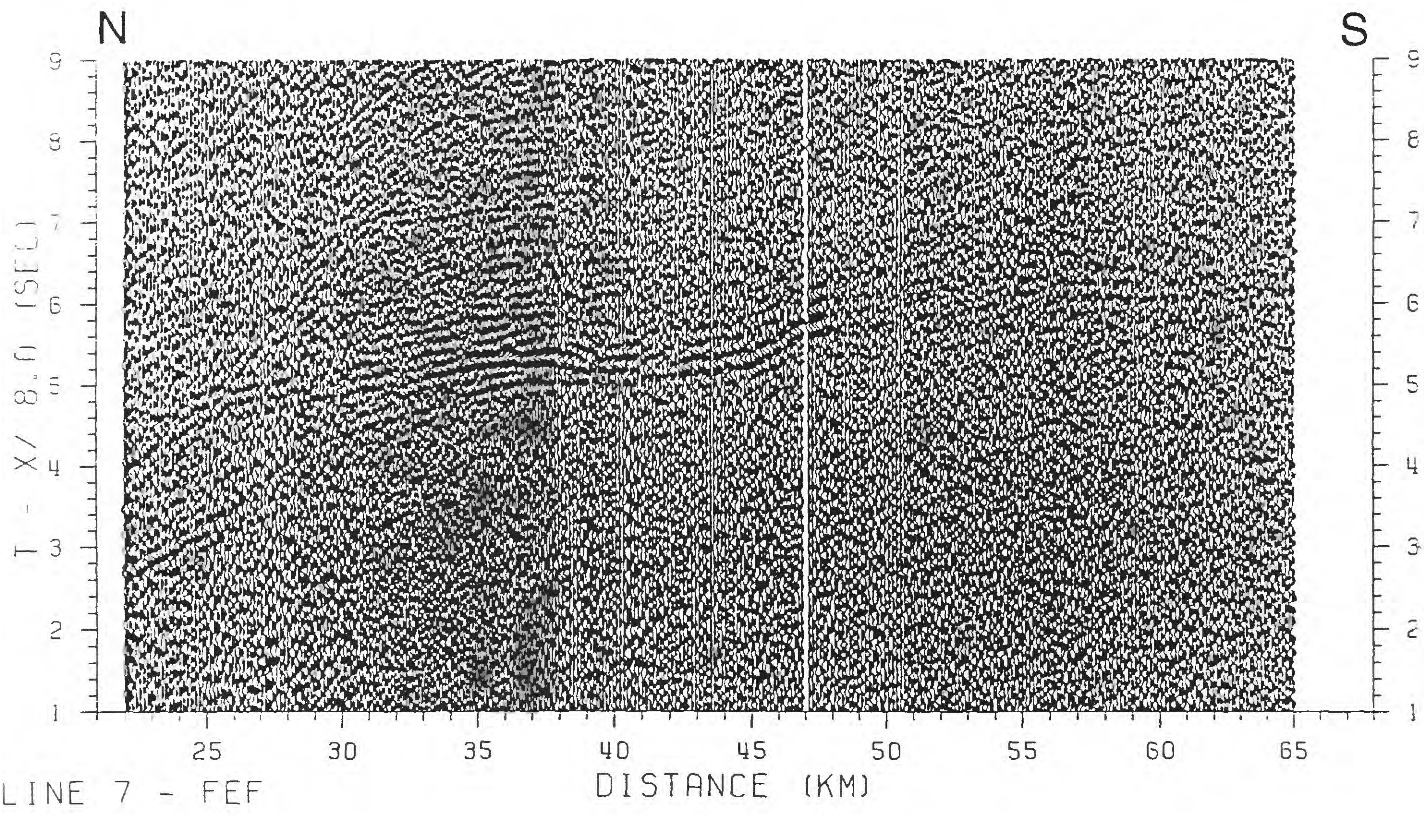

LINE 7 - FEF

Appendix E.3

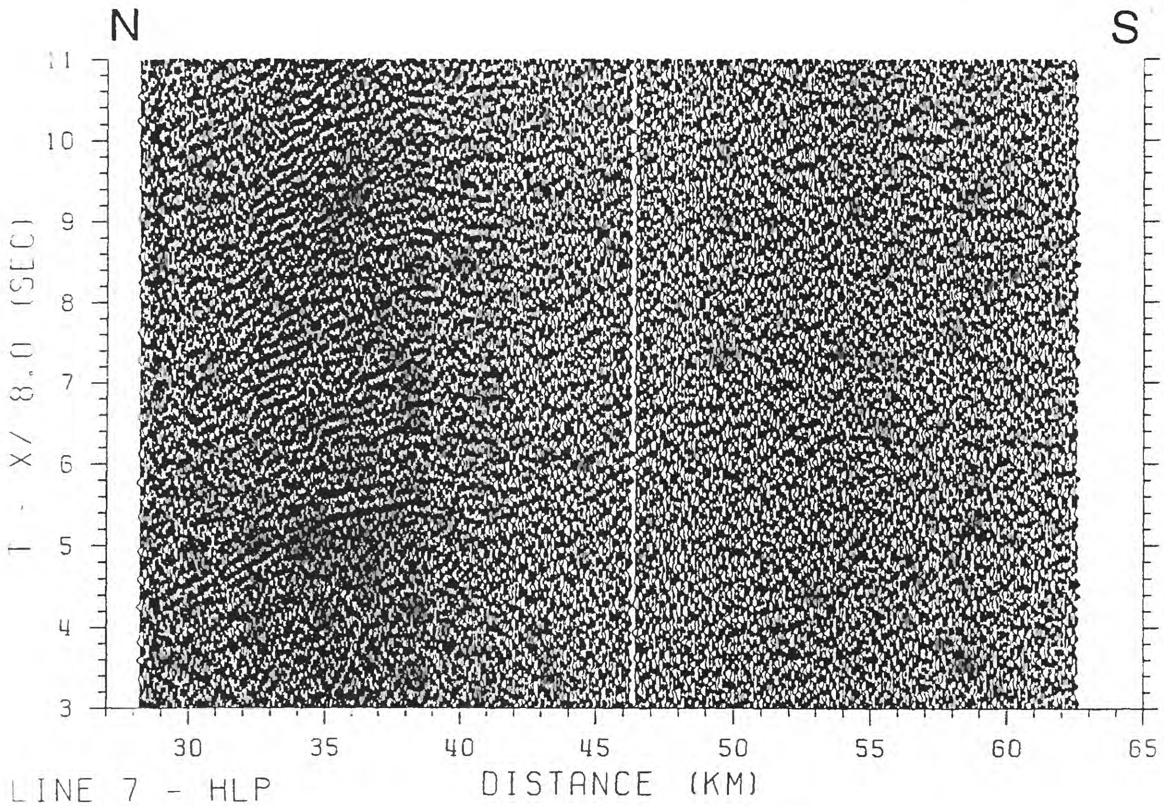
N
S
T - X/ 8.0 (SEC)
DISTANCE (KM)
LINE 7 - HLP

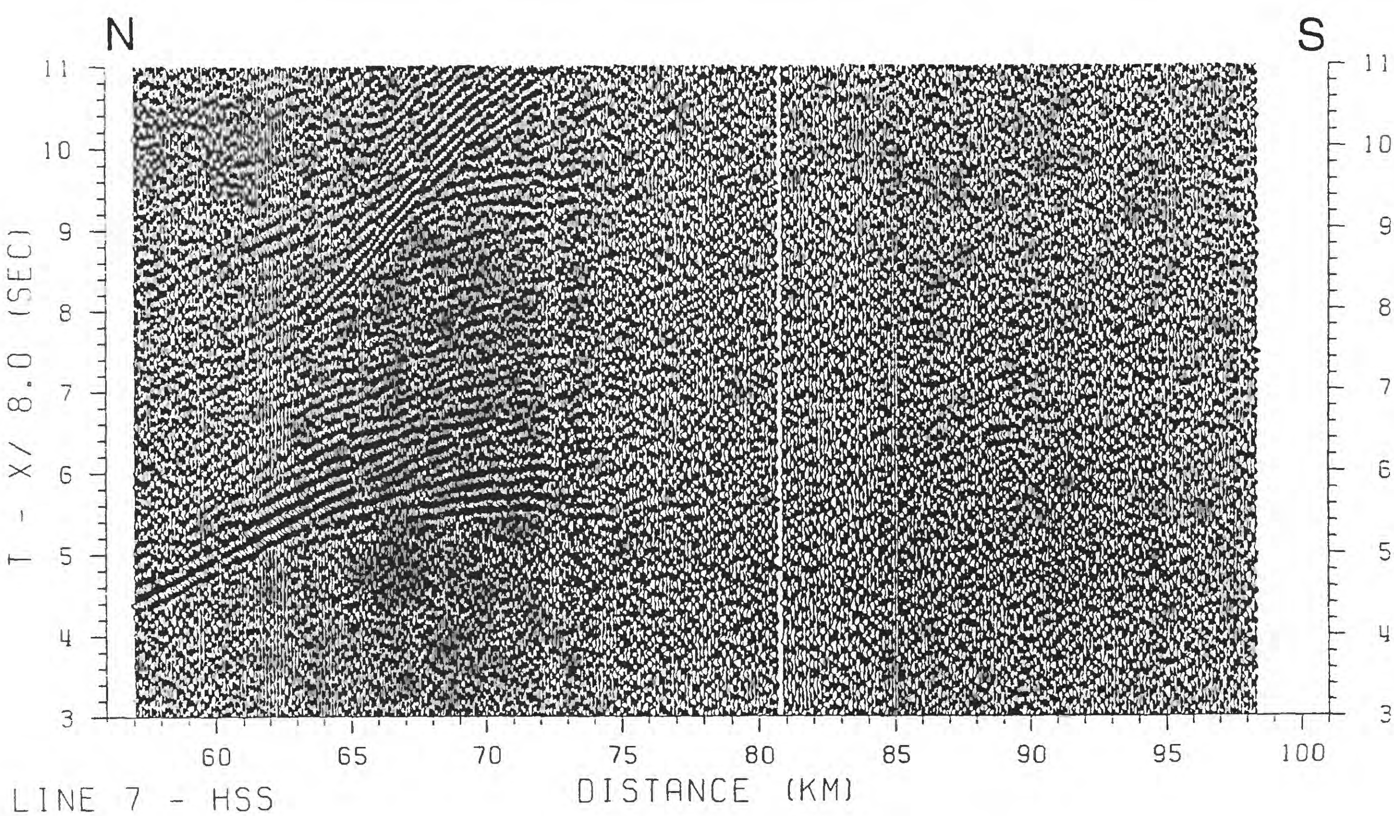
N
S
T - X/ 8.0 (SEC)
DISTANCE (KM)
LINE 7 - HSS

Appendix E.4

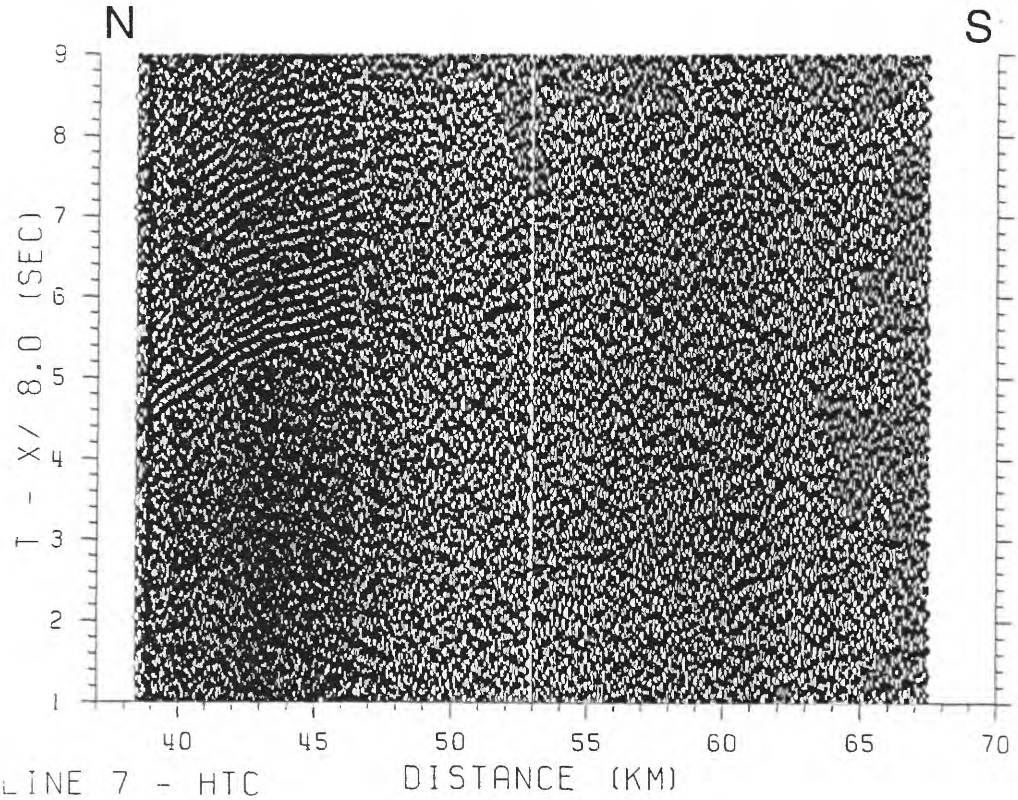
N
S
T - X/ 8.0 (SEC)
1
2
3
4
5
6
7
8
9
40
45
50
55
60
65
70
DISTANCE (KM)
LINE 7 - HTC

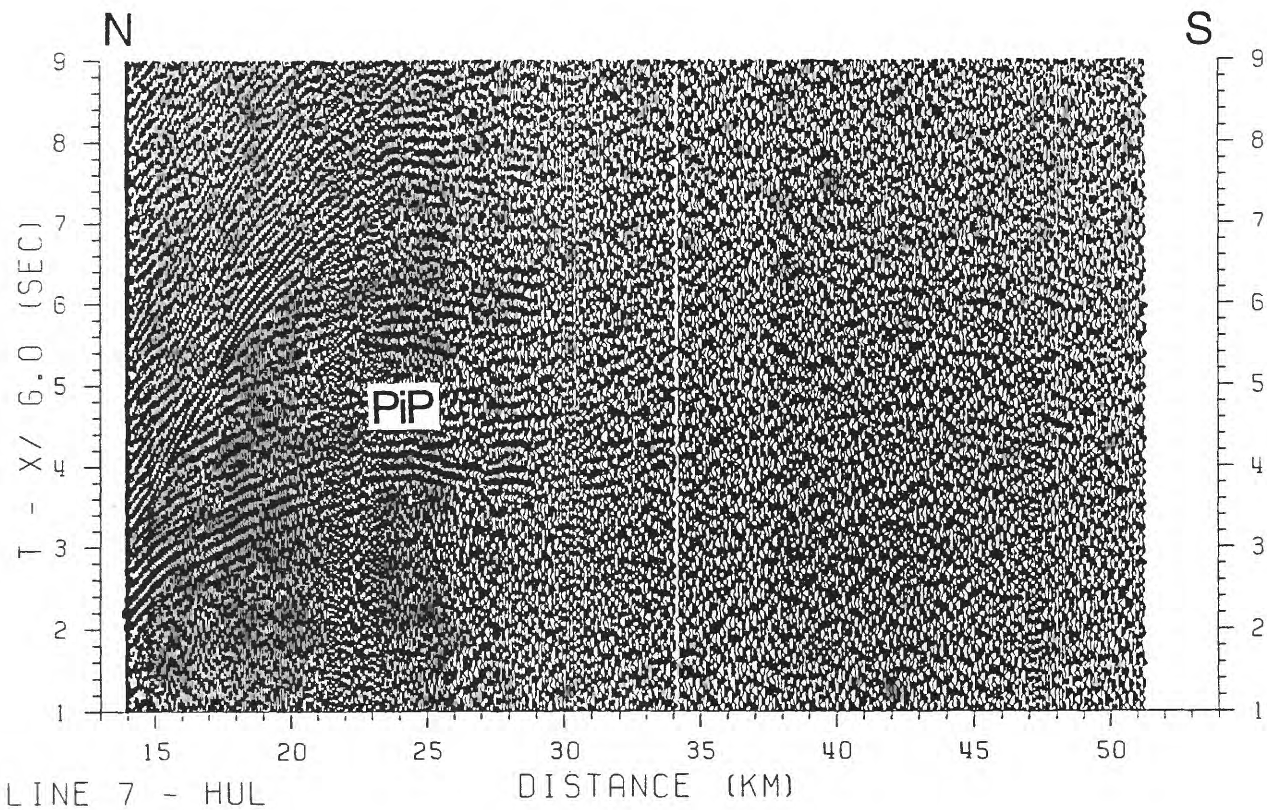
N
S
T - X/ 6.0 (SEC)
PiP
1
2
3
4
5
6
7
8
9
15
20
25
30
35
40
45
50
DISTANCE (KM)
LINE 7 - HUL

Appendix E.5

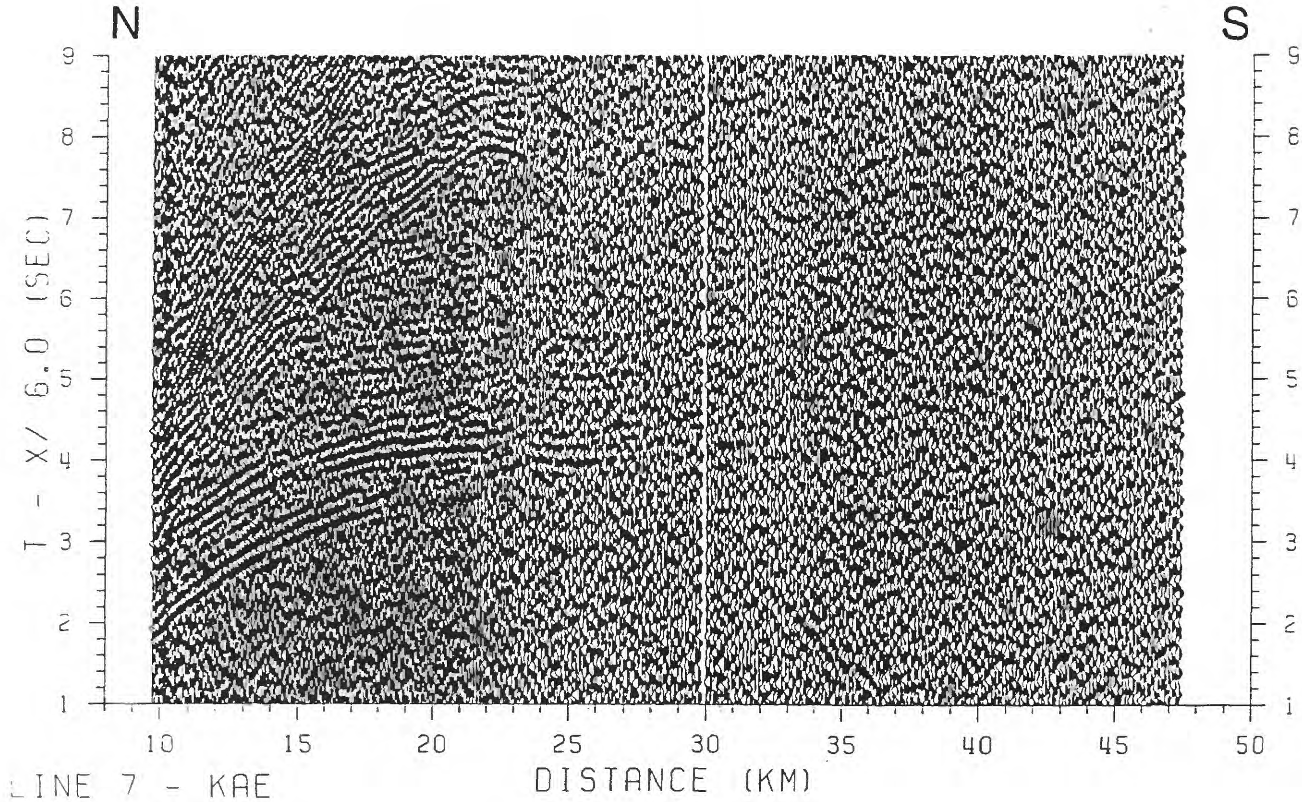
N
S
T - X/ 6.0 (SEC)
DISTANCE (KM)
LINE 7 - KAE

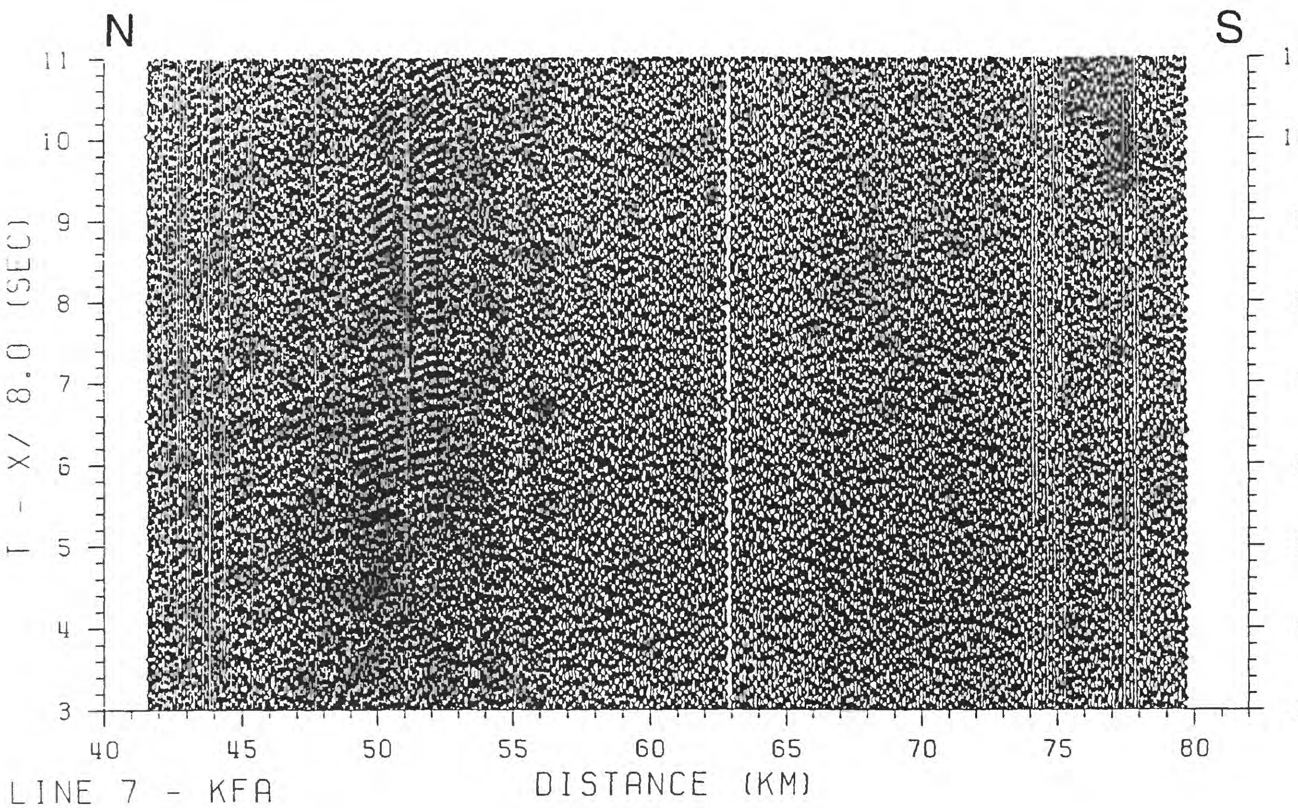
N
S
T - X/ 8.0 (SEC)
DISTANCE (KM)
LINE 7 - KFA

Appendix E.6

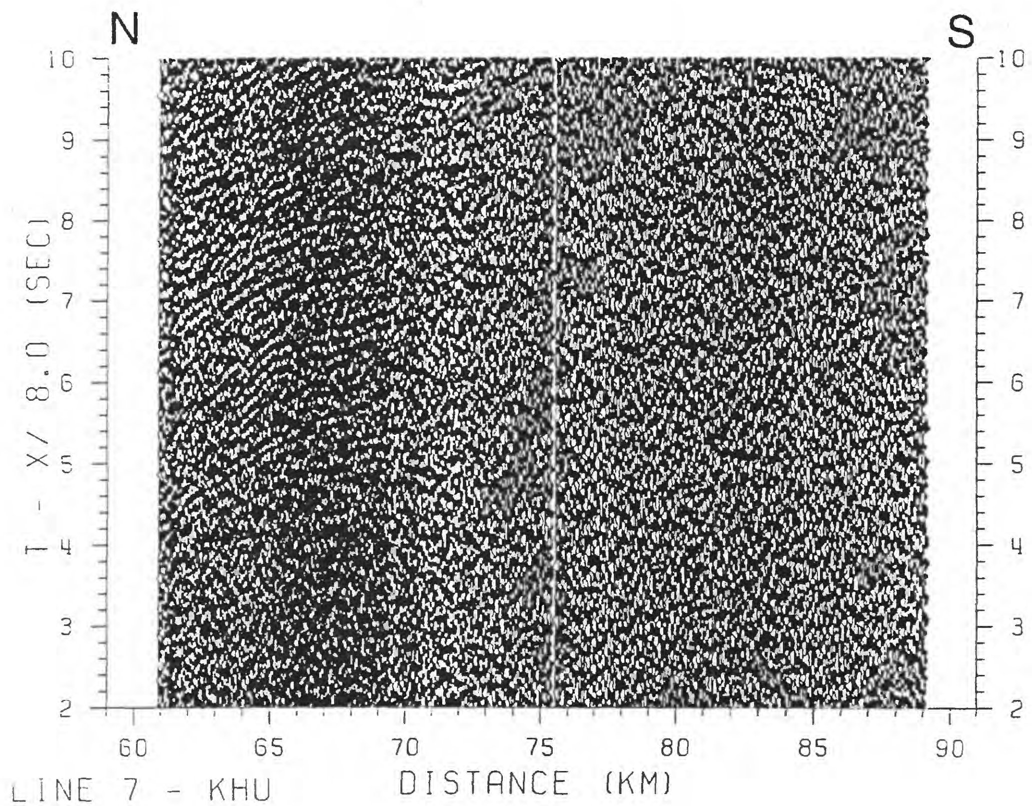
N
S
T - X/ 8.0 (SEC)
DISTANCE (KM)
LINE 7 - KHU

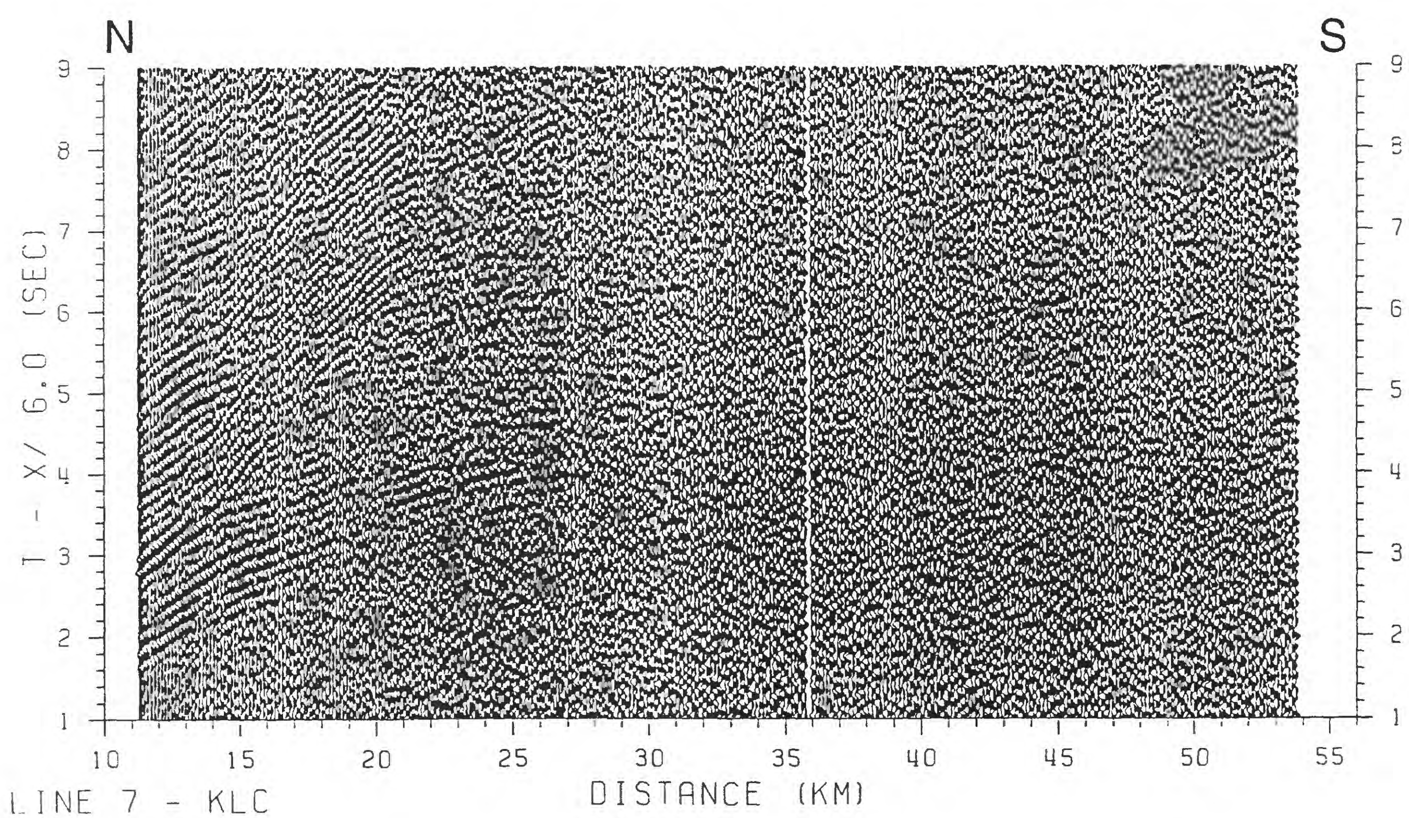
N
S
T - X/ 6.0 (SEC)
DISTANCE (KM)
LINE 7 - KLC

Appendix E.7

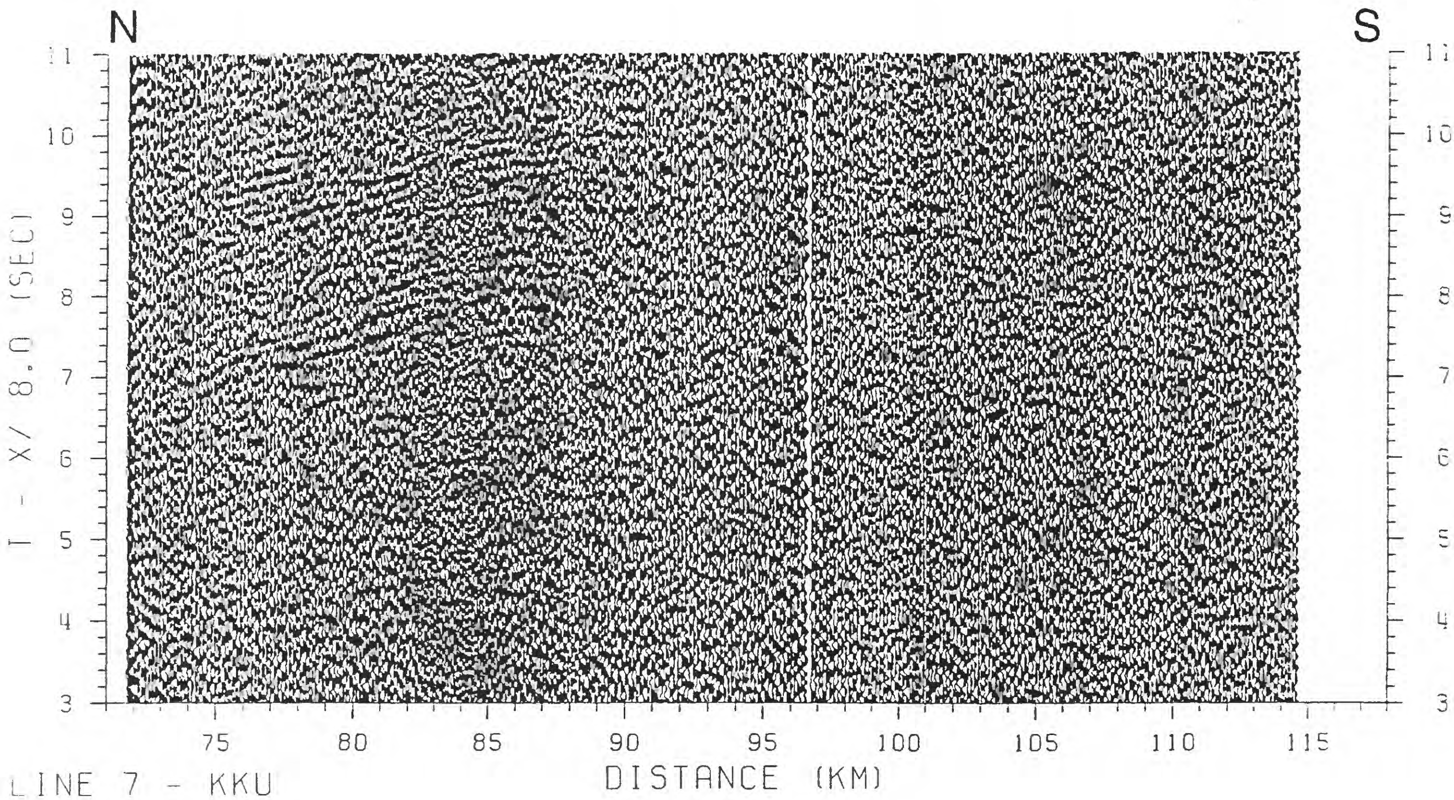
N
S
T - X/ 8.0 (SEC)
11
10
9
8
7
6
5
4
3
75
80
85
90
95
100
105
110
115
DISTANCE (KM)
LINE 7 - KKU

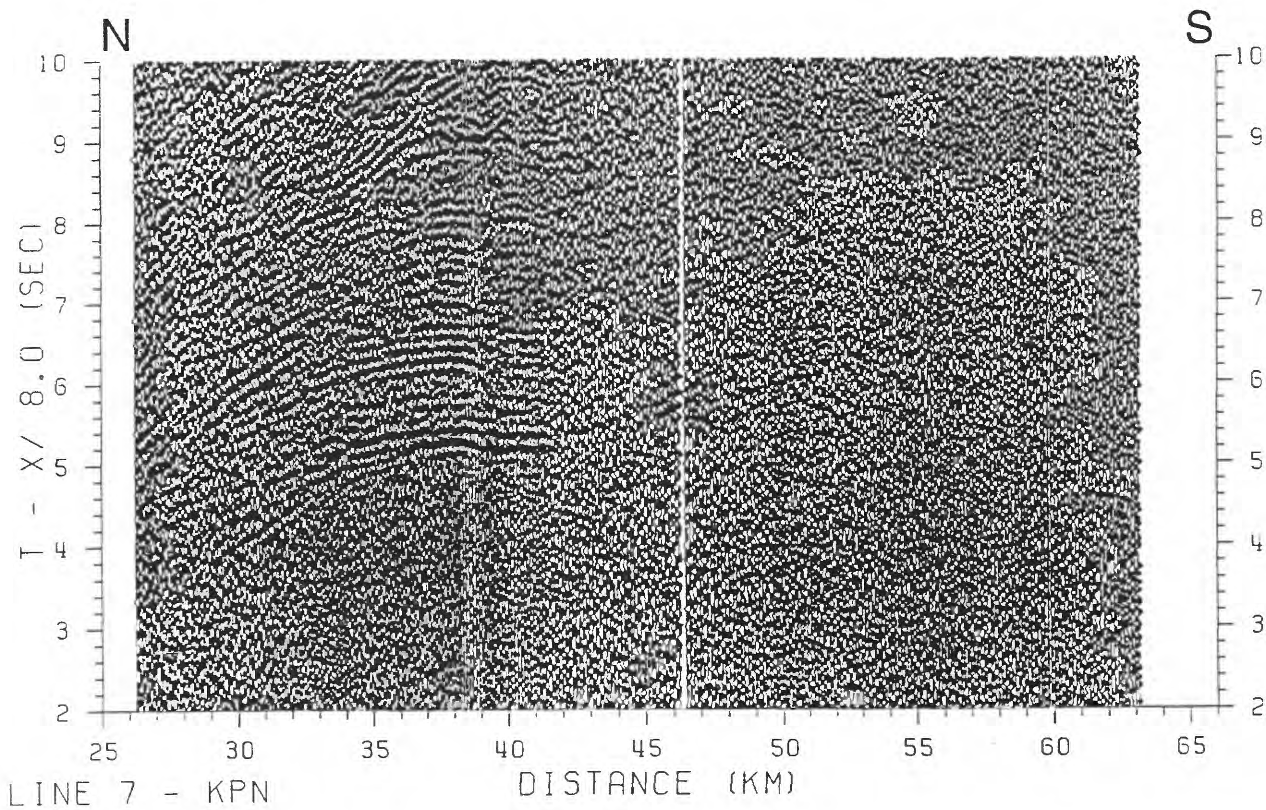
N
S
T - X/ 8.0 (SEC)
10
9
8
7
6
5
4
3
2
25
30
35
40
45
50
55
60
65
DISTANCE (KM)
LINE 7 - KPN

Appendix E.8

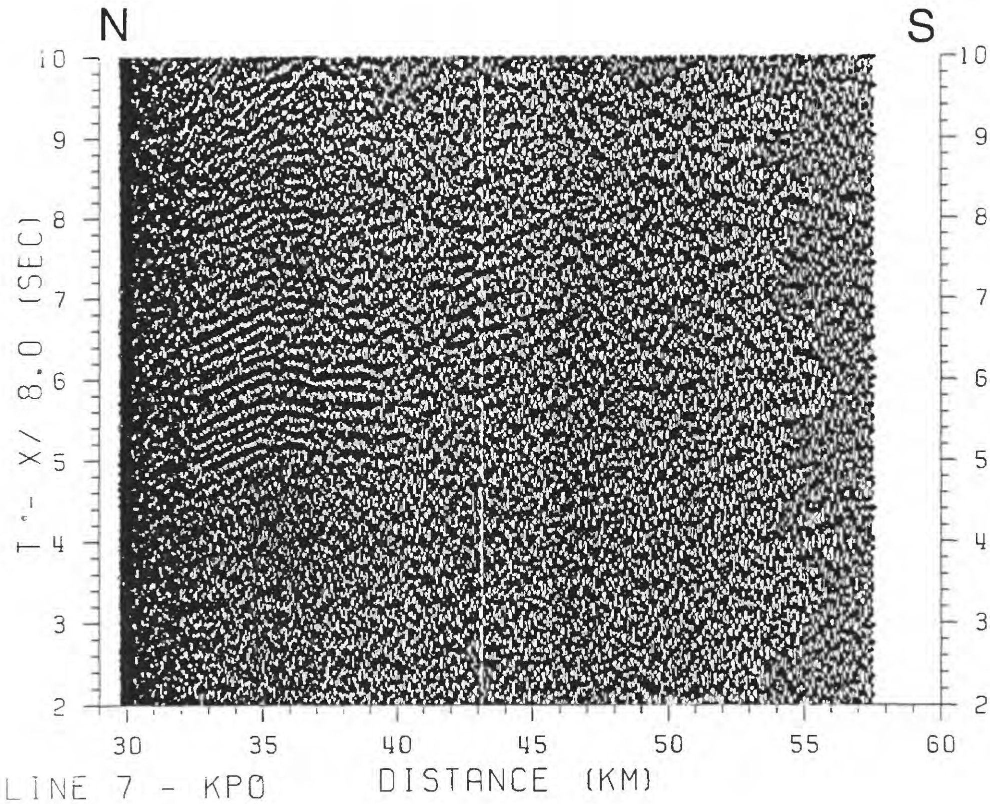
N
S
T - X/ 8.0 (SEC)
10
9
8
7
6
5
4
3
2
30
35
40
45
50
55
60
DISTANCE (KM)
LINE 7 - KPO

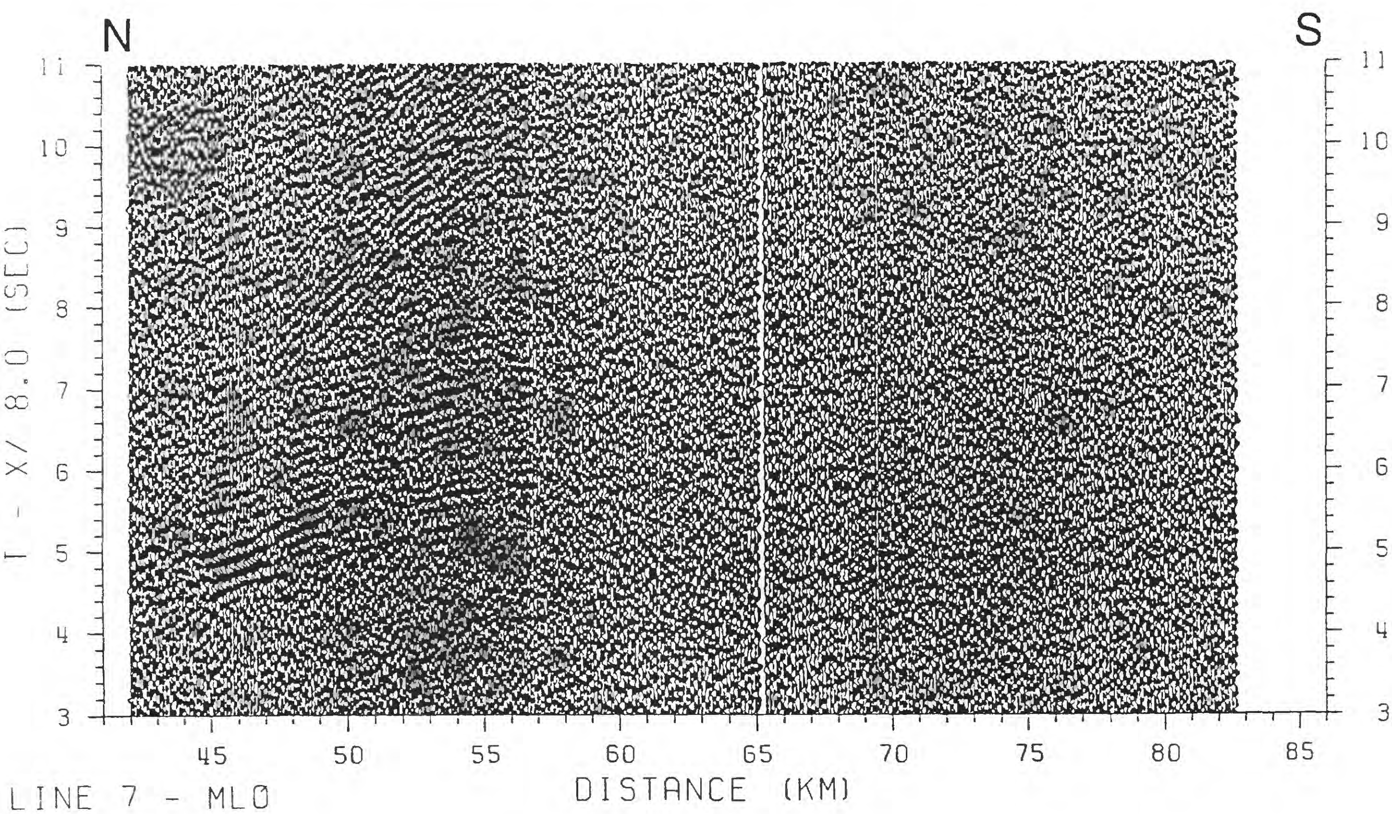
N
S
T - X/ 8.0 (SEC)
11
10
9
8
7
6
5
4
3
45
50
55
60
65
70
75
80
85
DISTANCE (KM)
LINE 7 - MLO

Appendix E.9

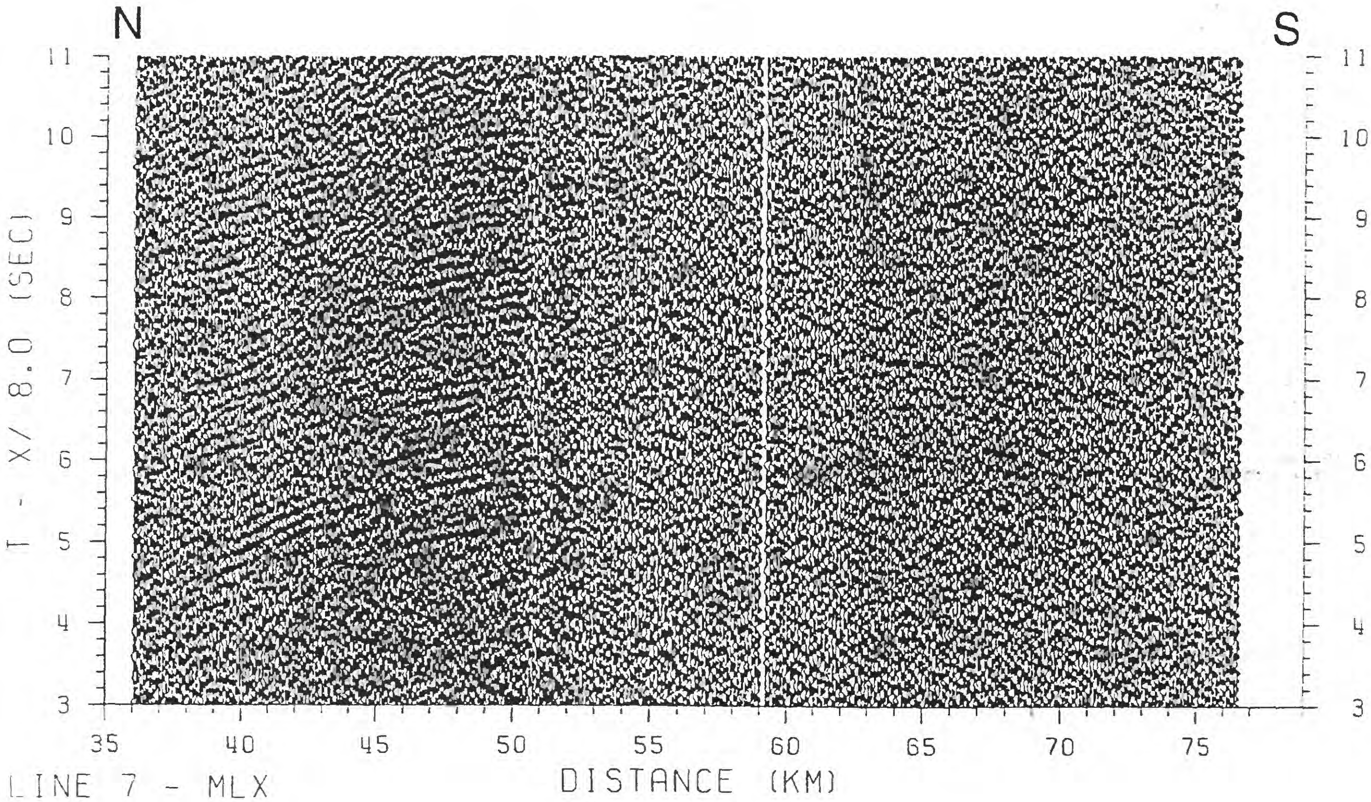

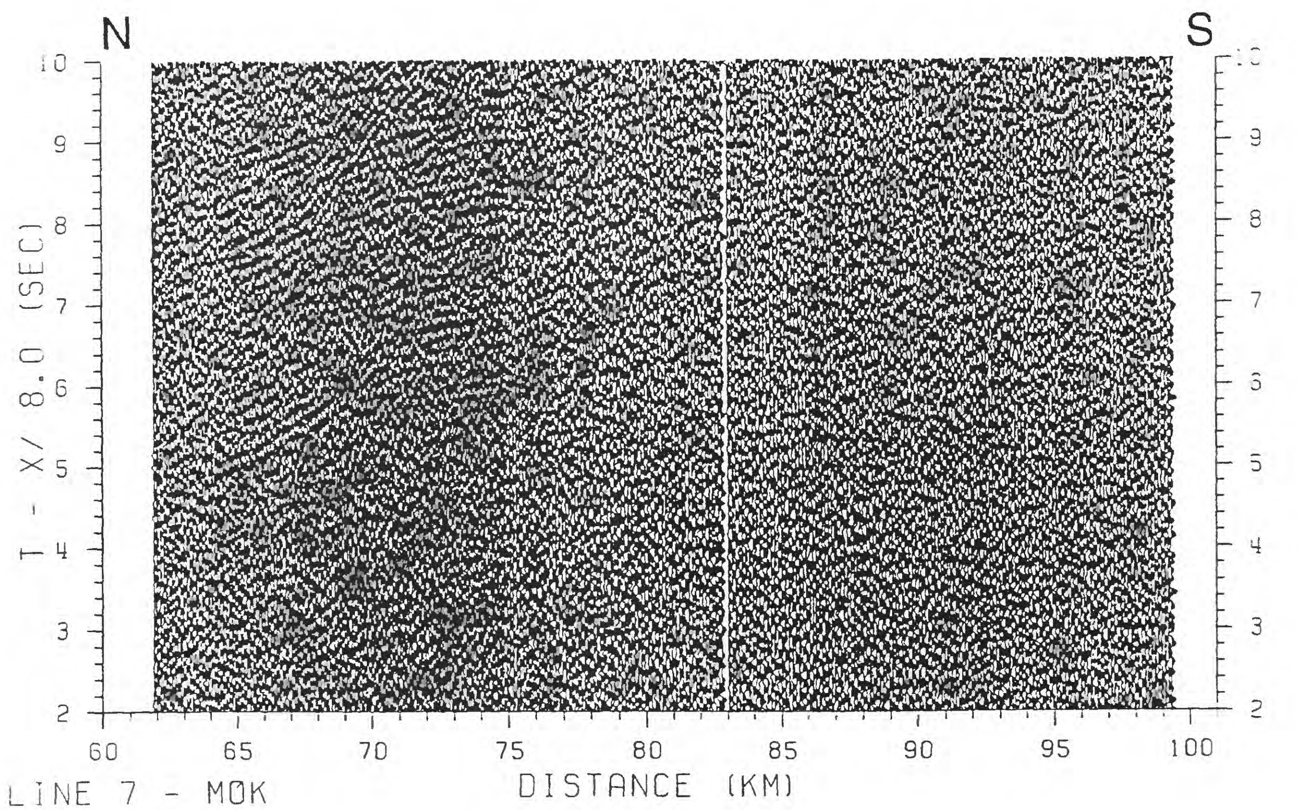

Appendix E.10

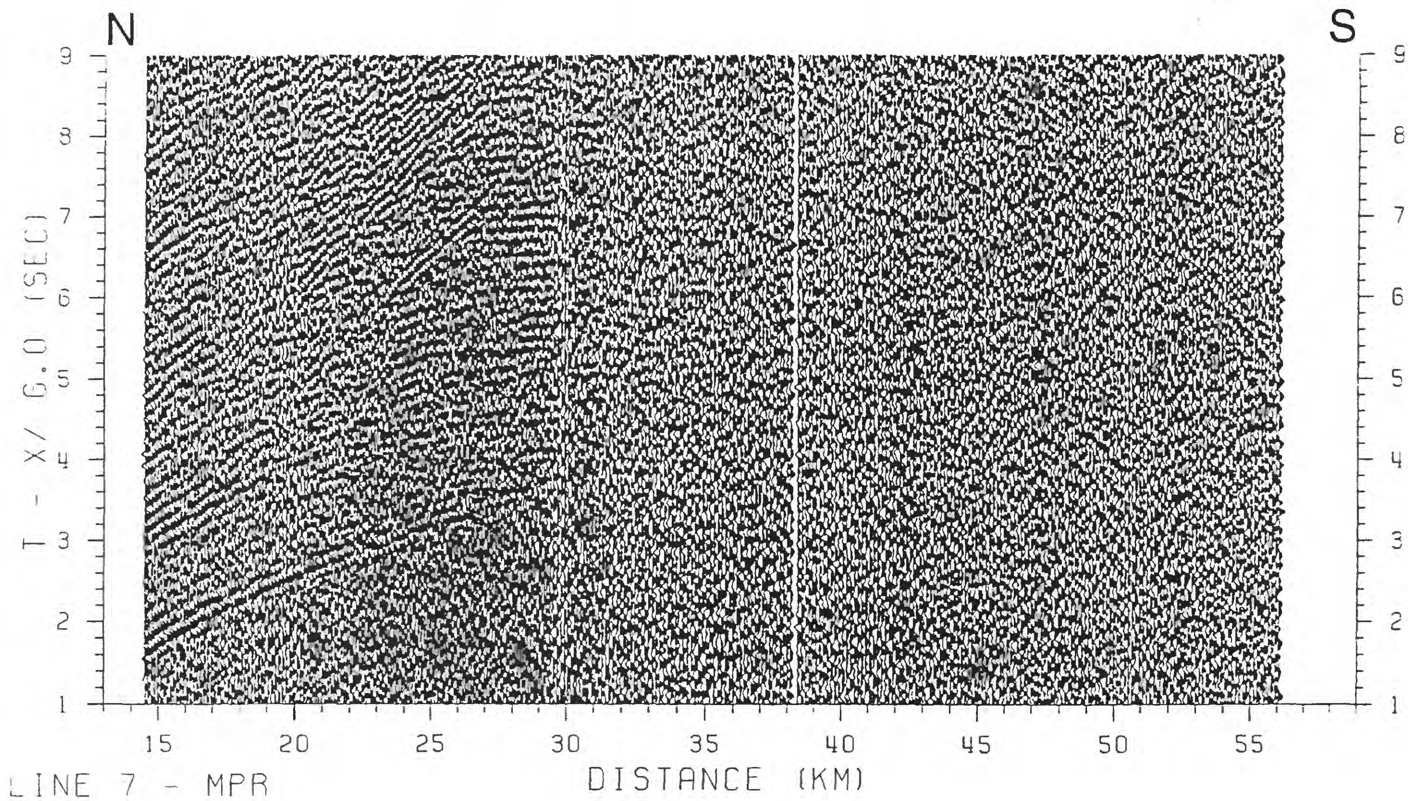
N
S
T - X/ 6.0 (SEC)
DISTANCE (KM)
LINE 7 - MPR

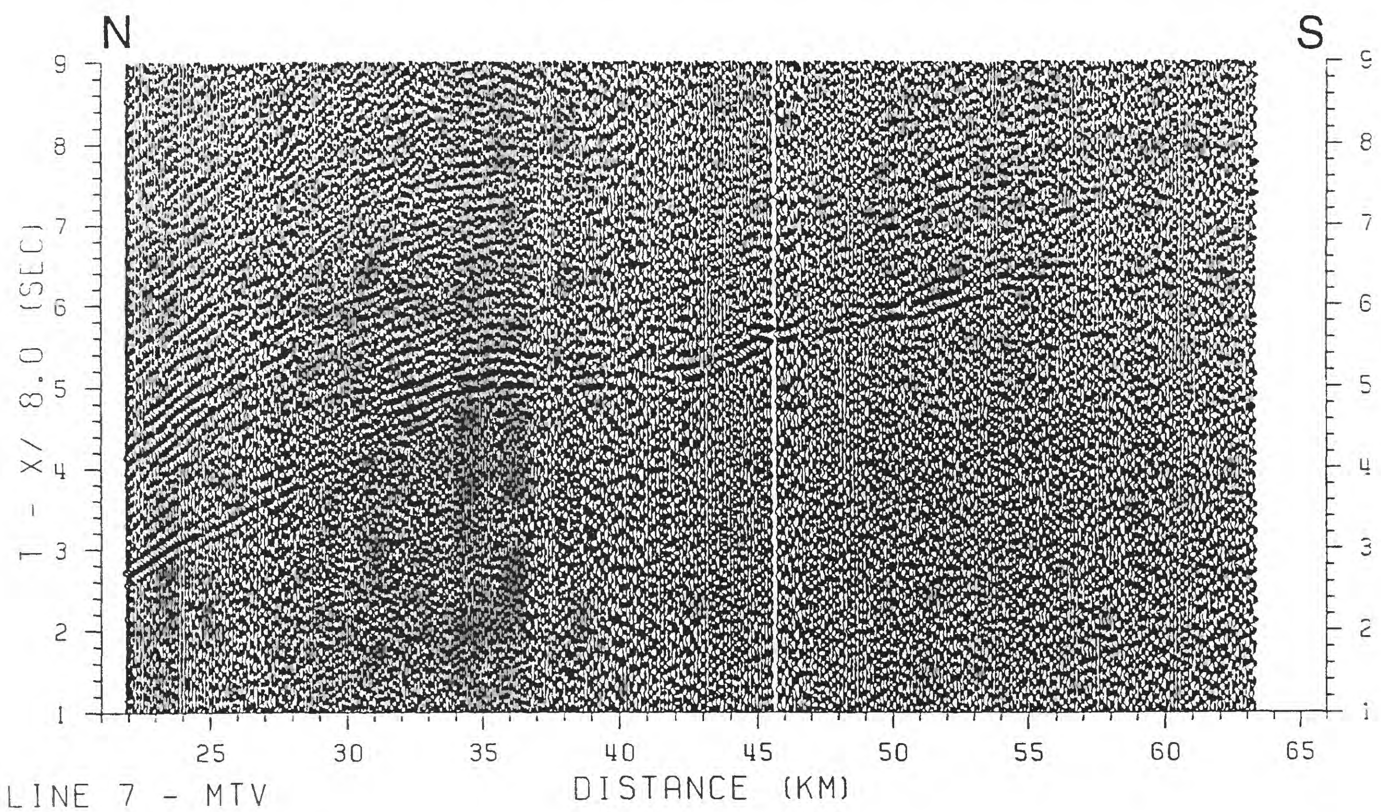
N
S
T - X/ 8.0 (SEC)
DISTANCE (KM)
LINE 7 - MTV

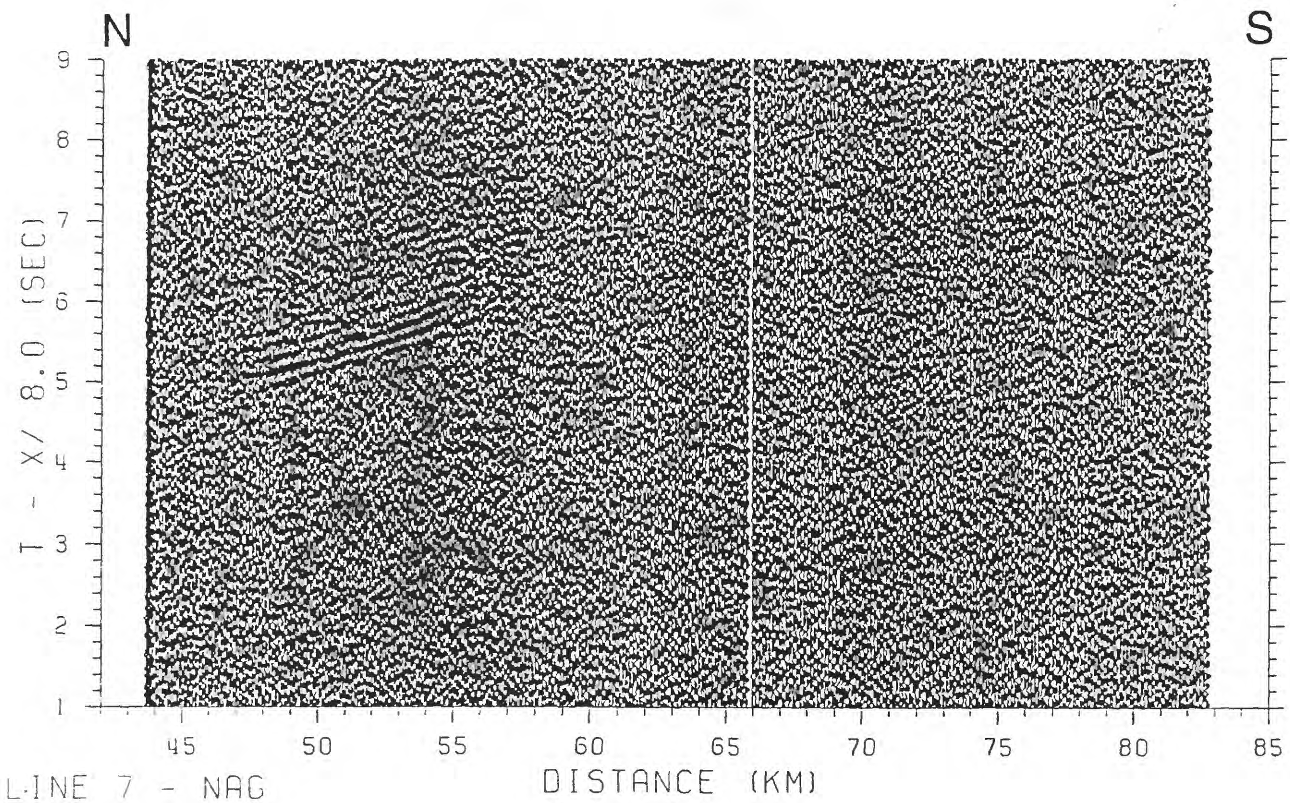

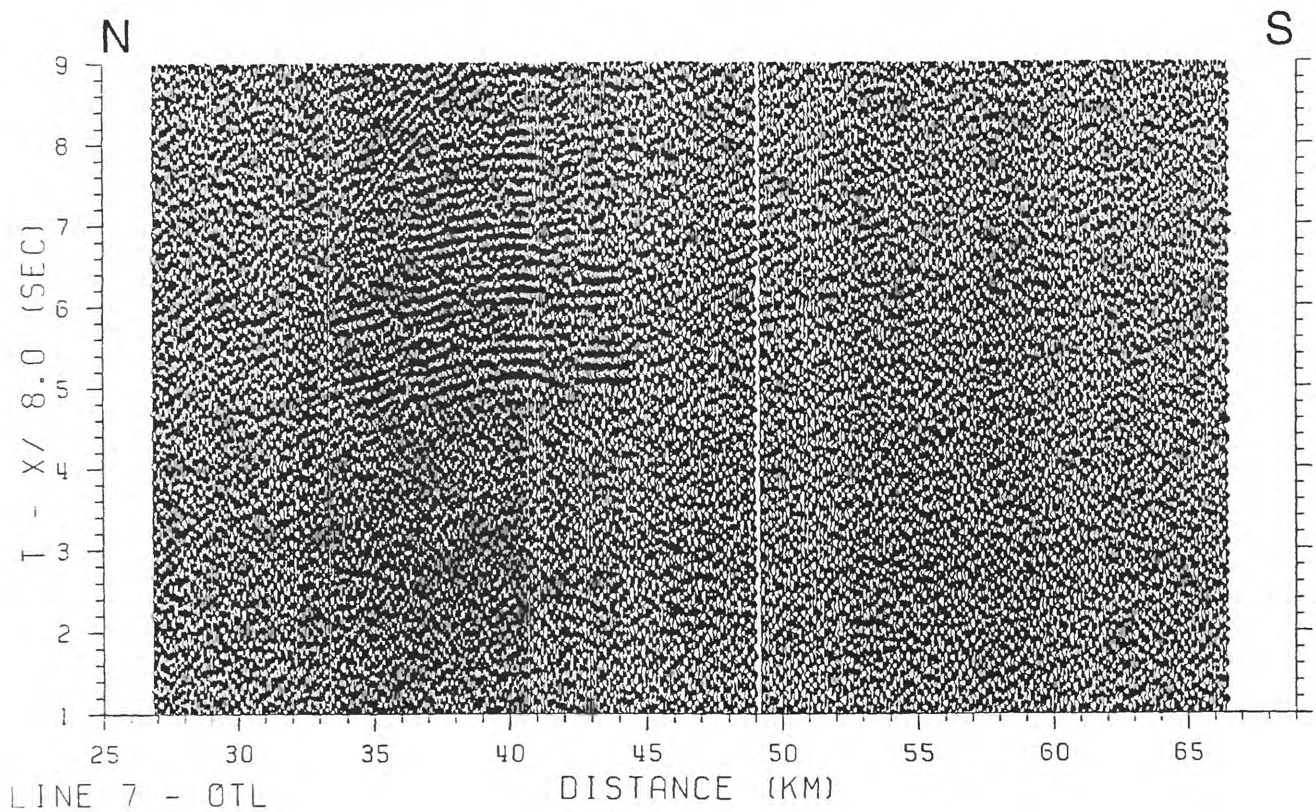

Appendix E.12

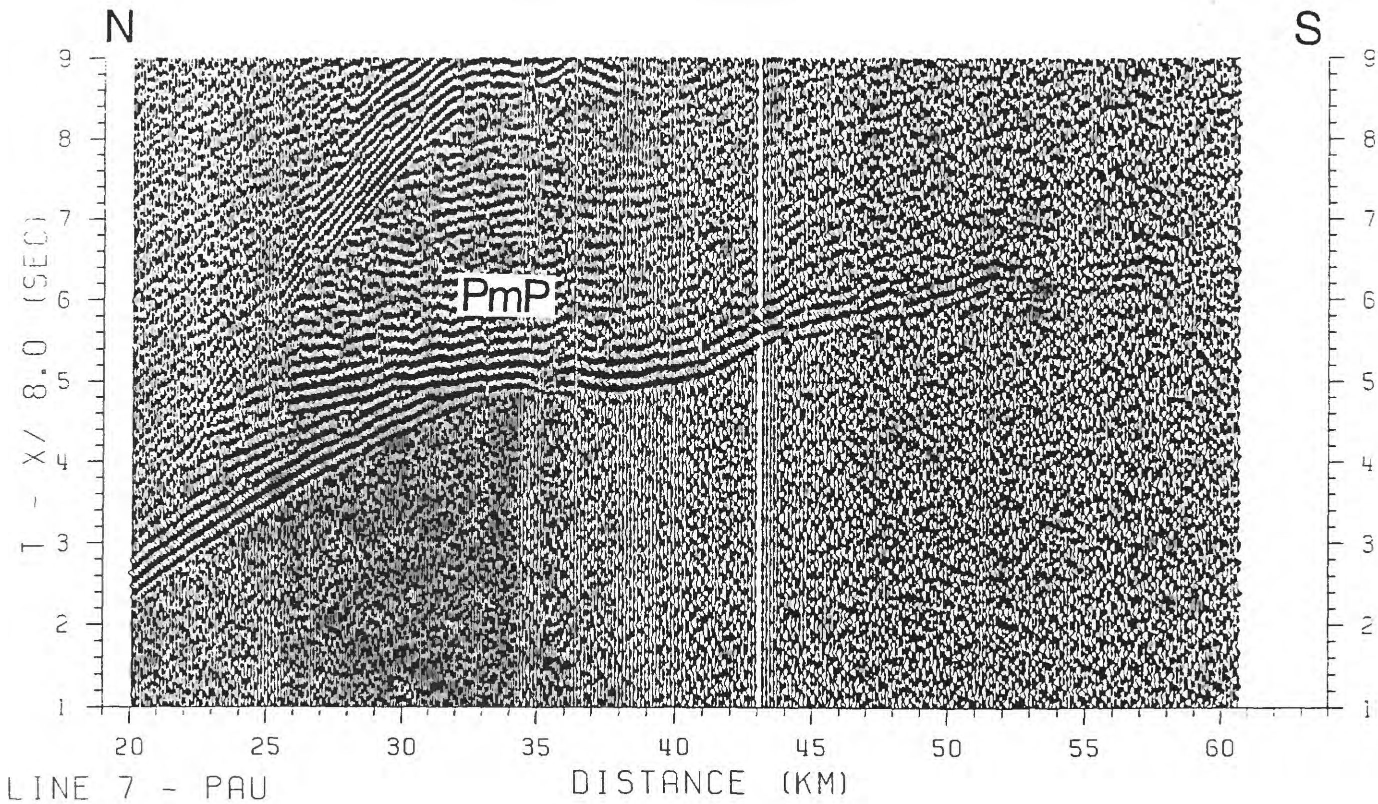

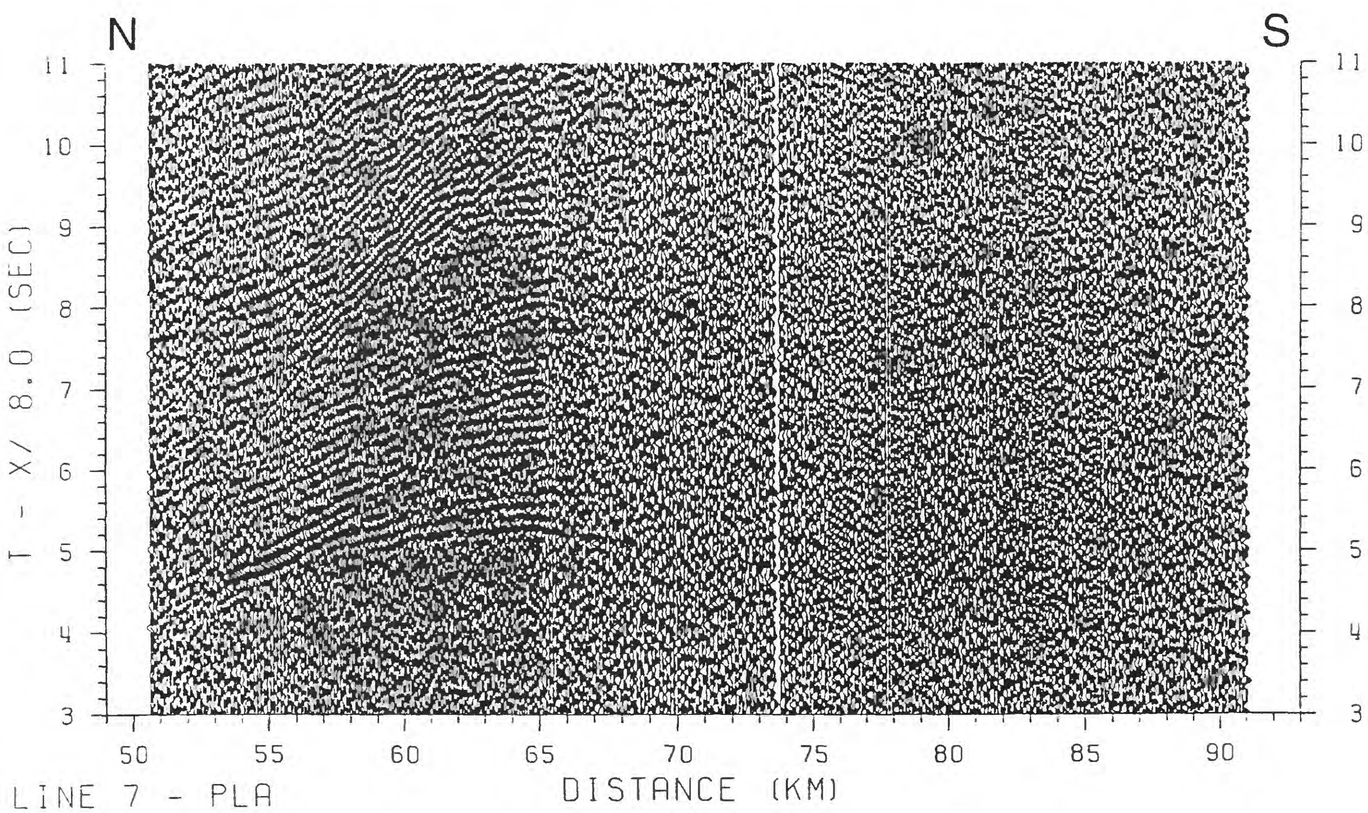

Appendix E.13

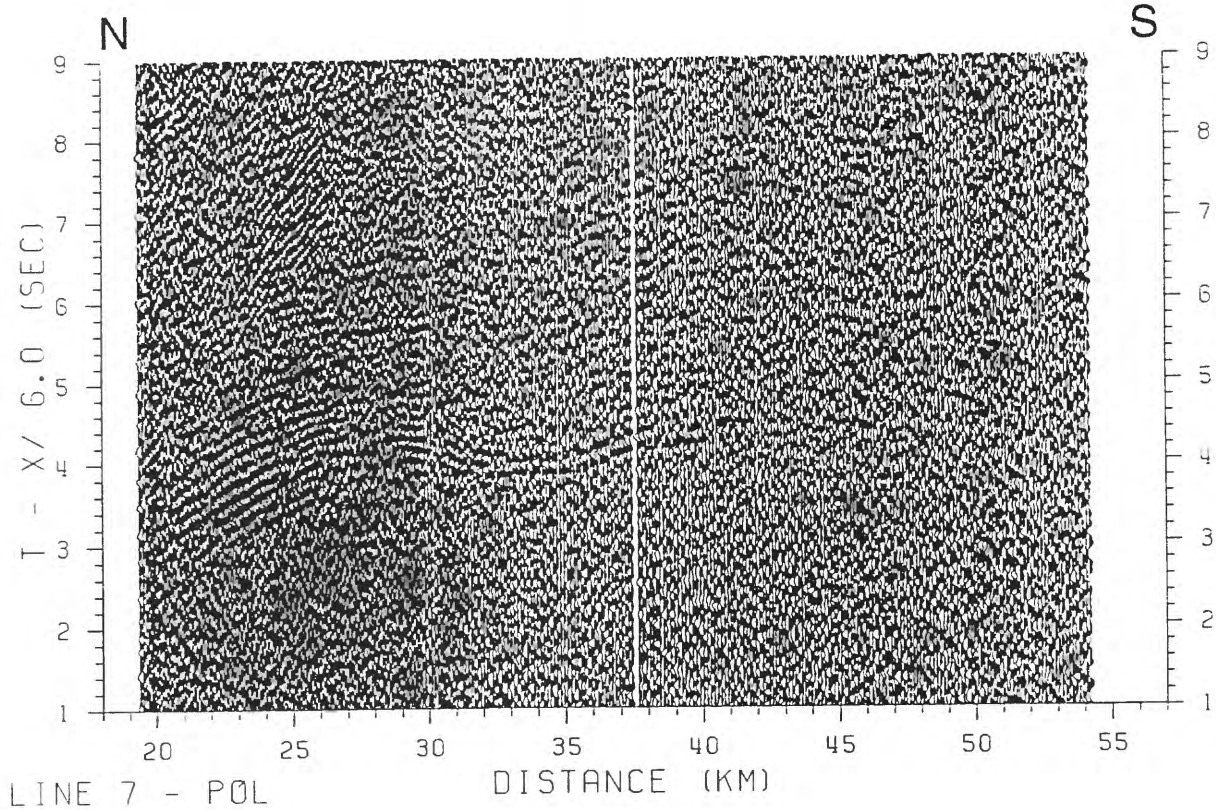

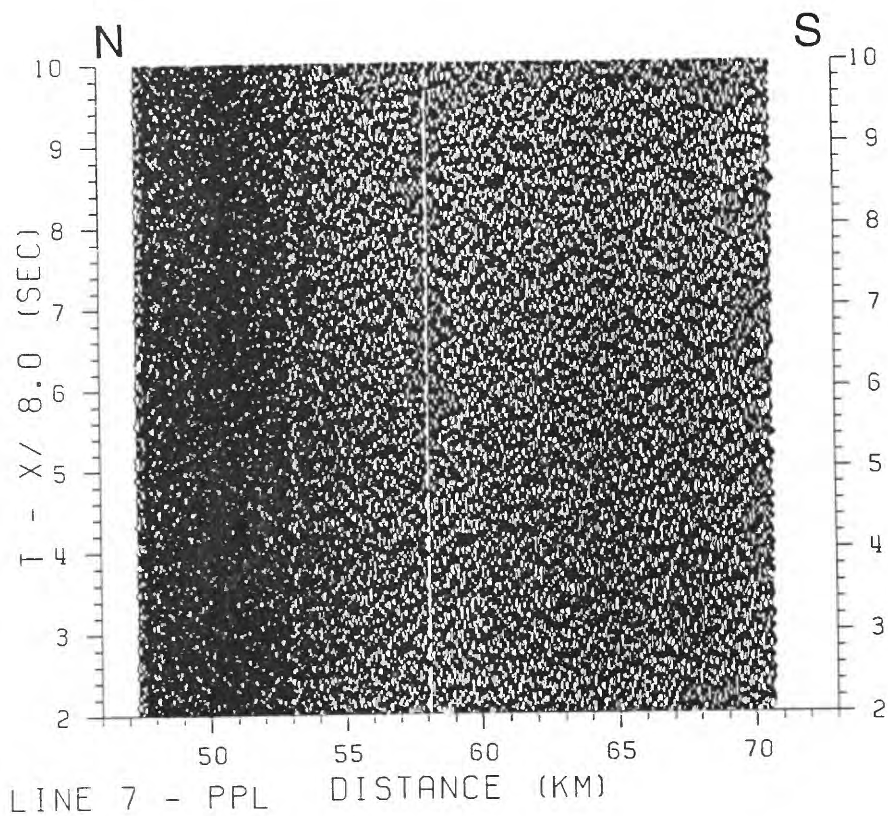

Appendix E.14

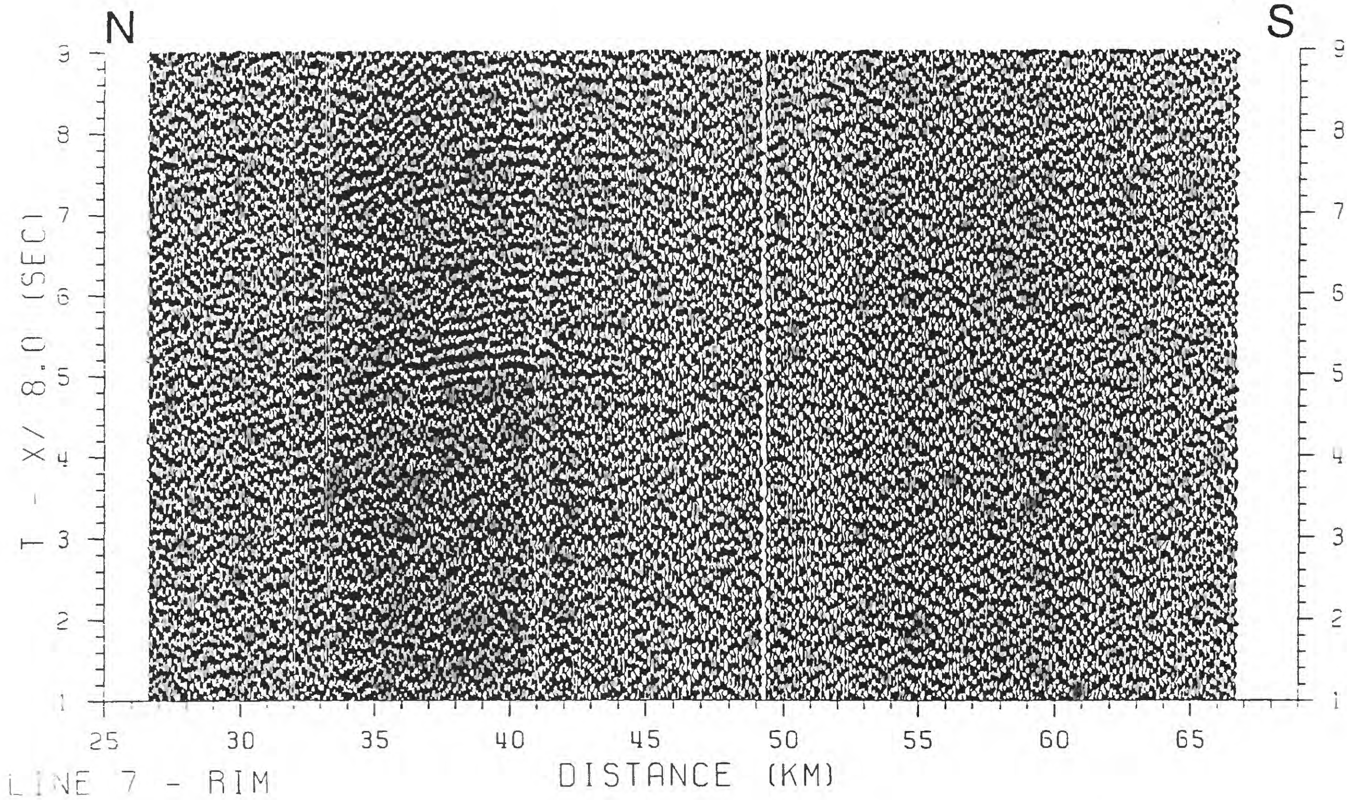

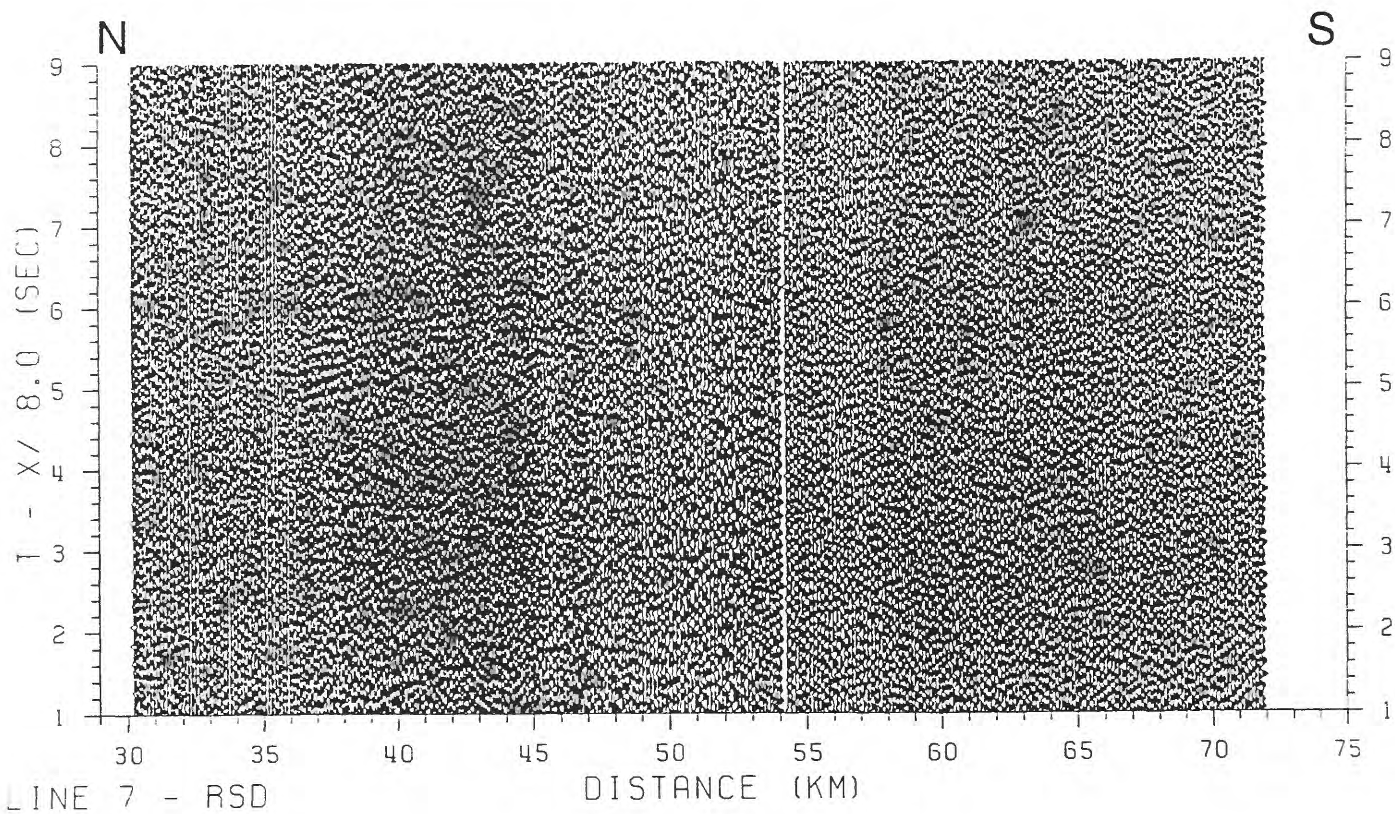

Appendix E.15

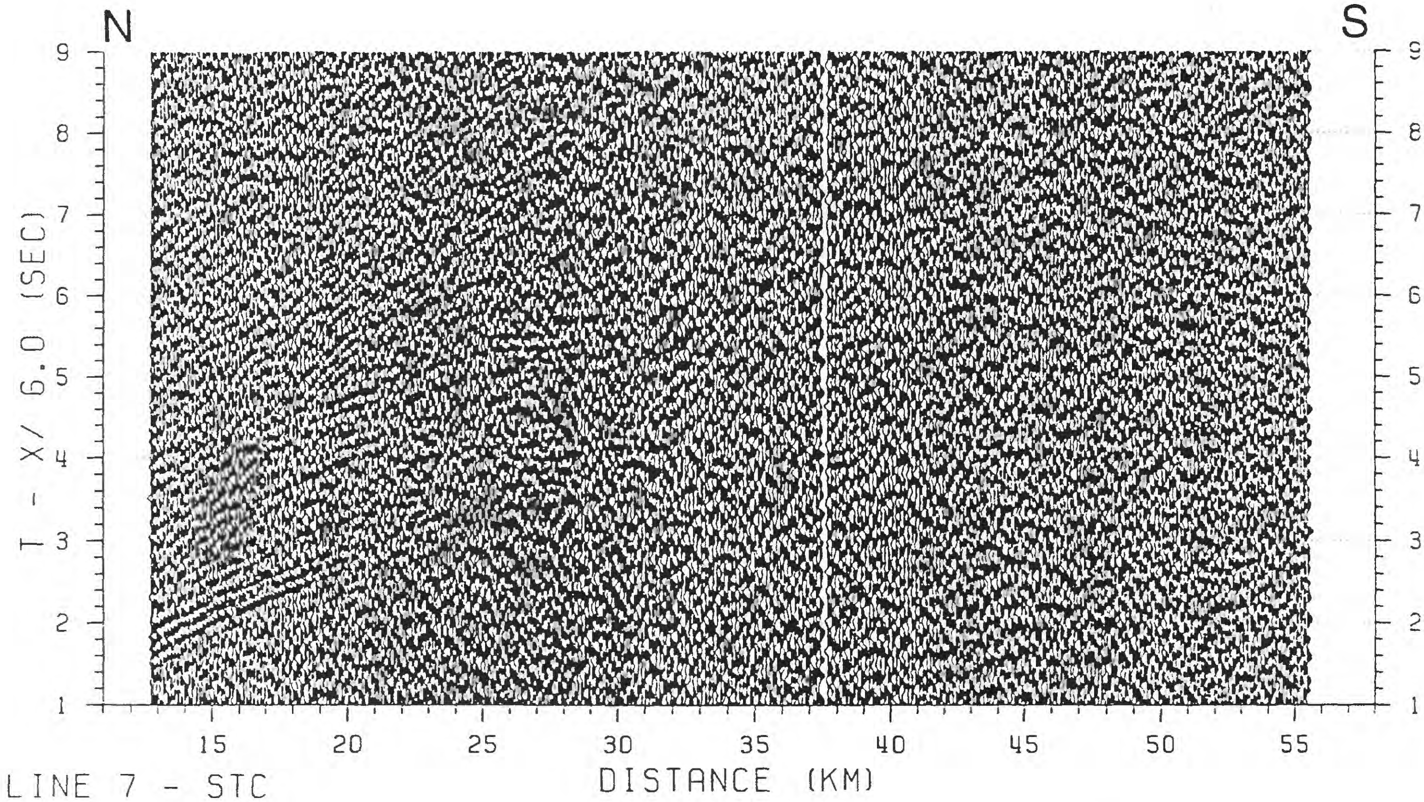

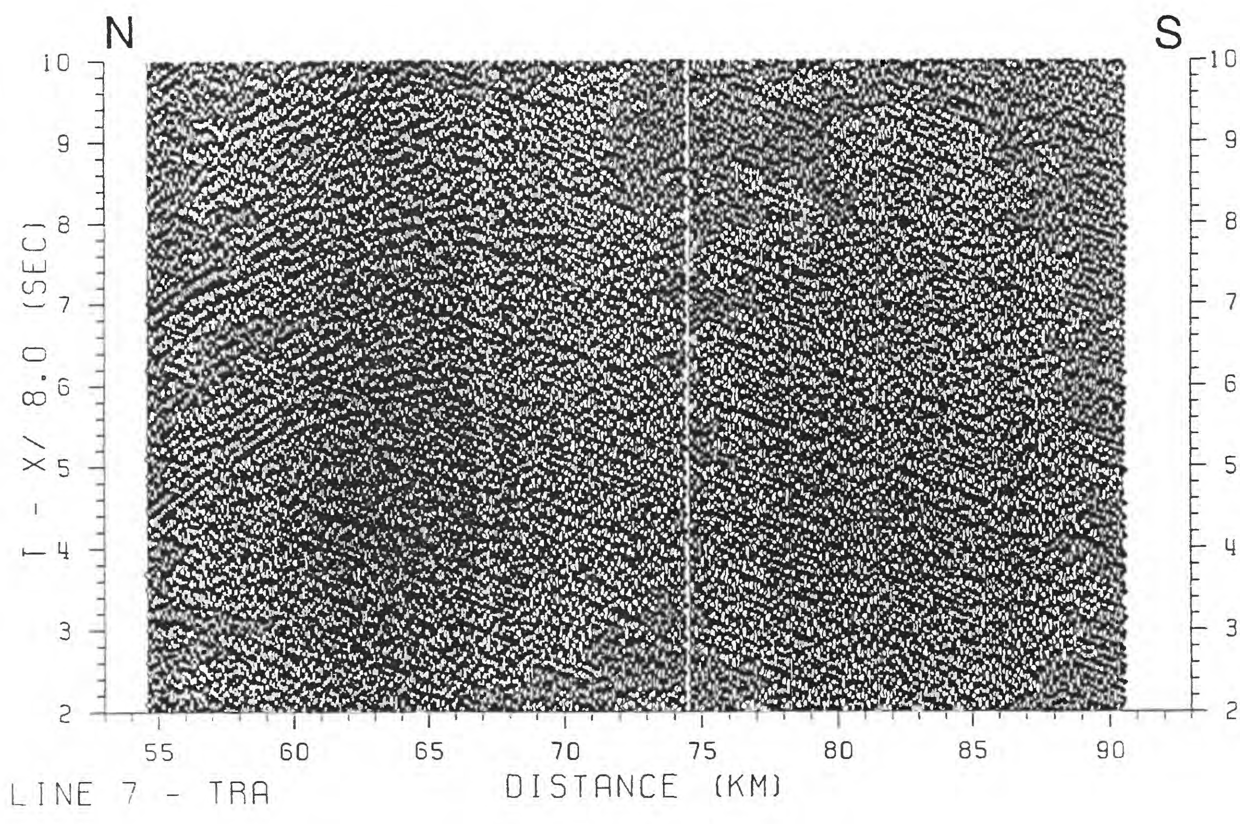

Appendix E.16

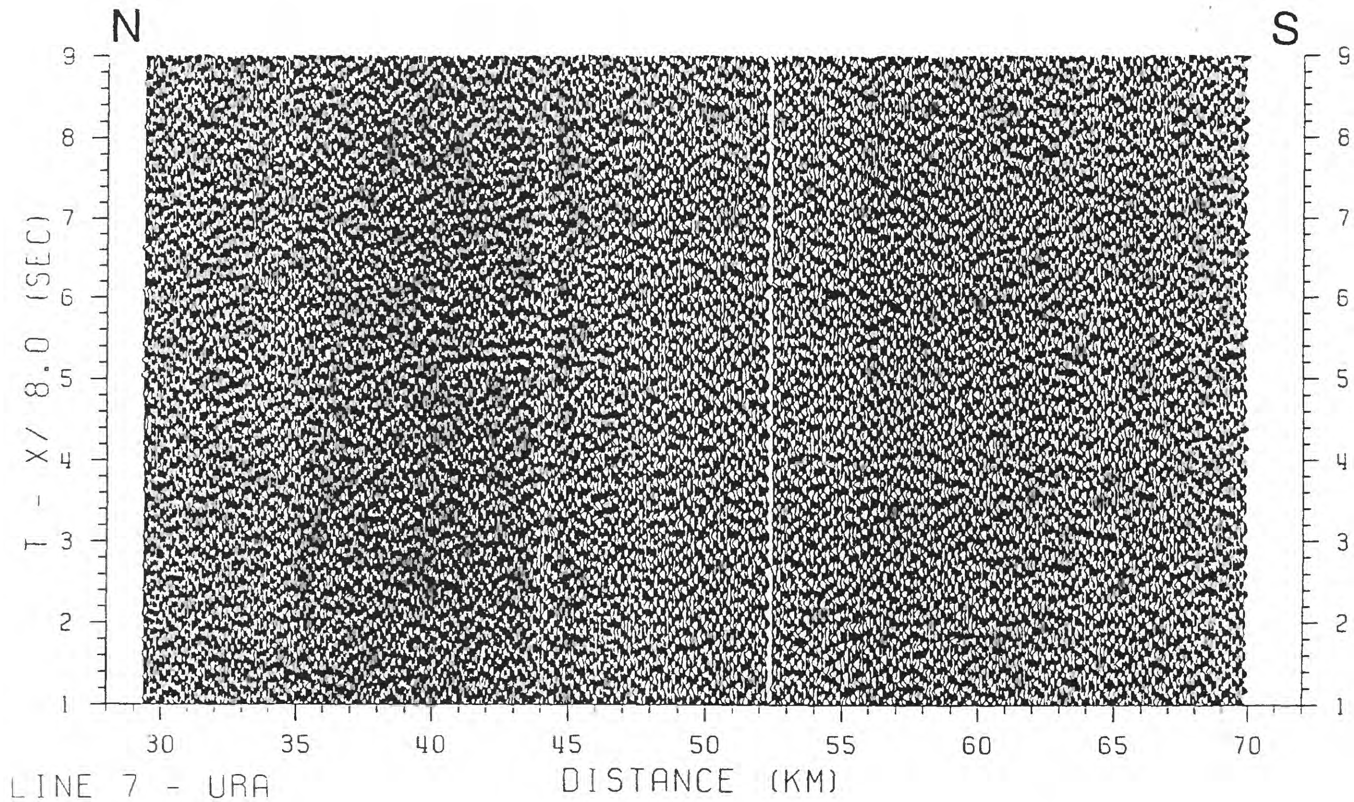

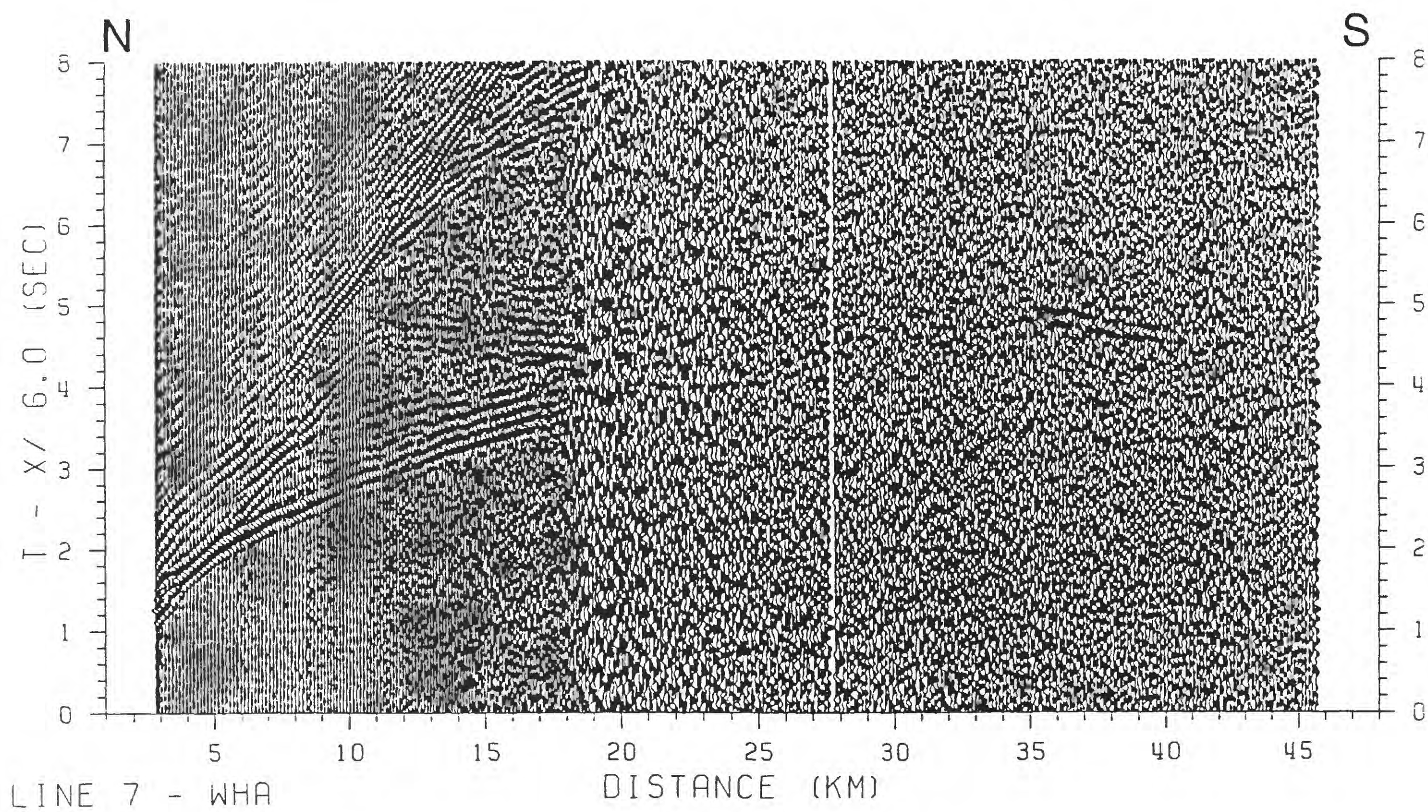

Appendix E.17

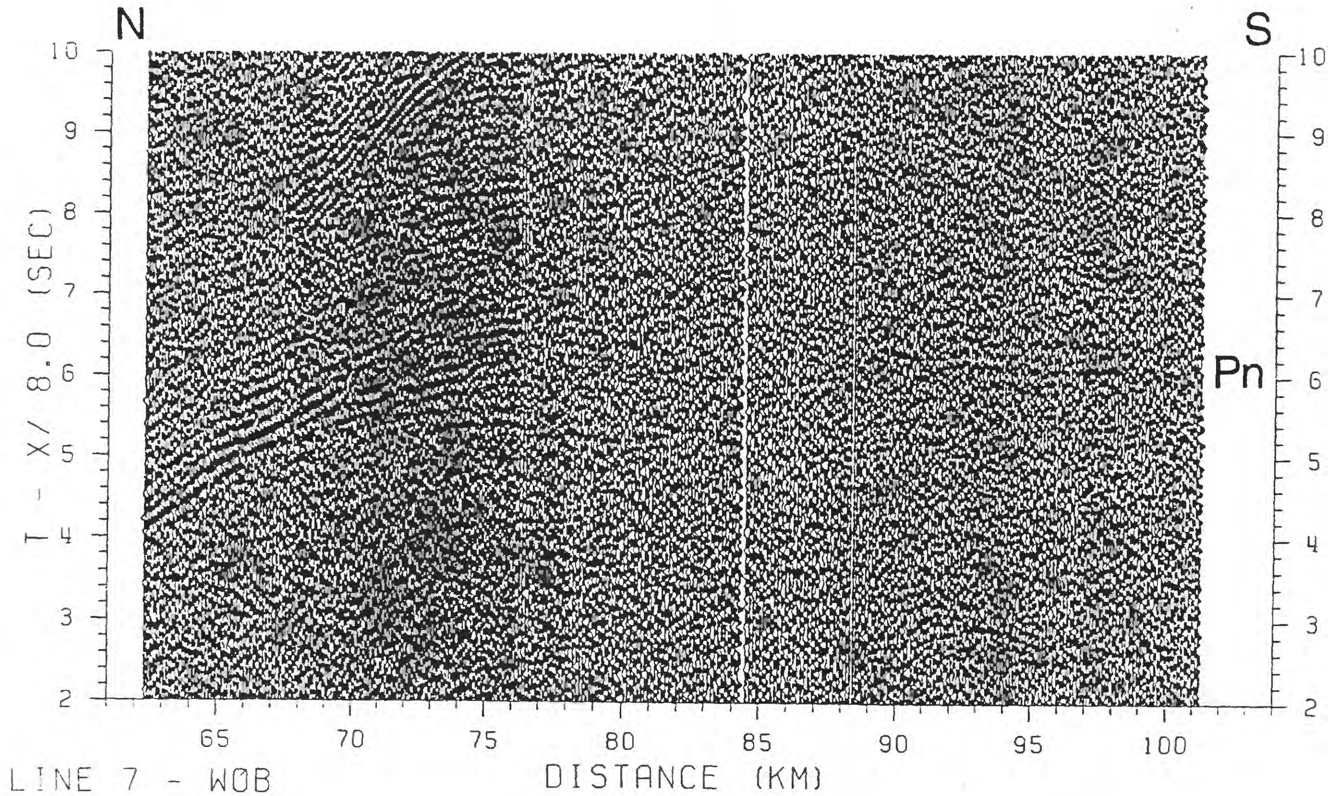

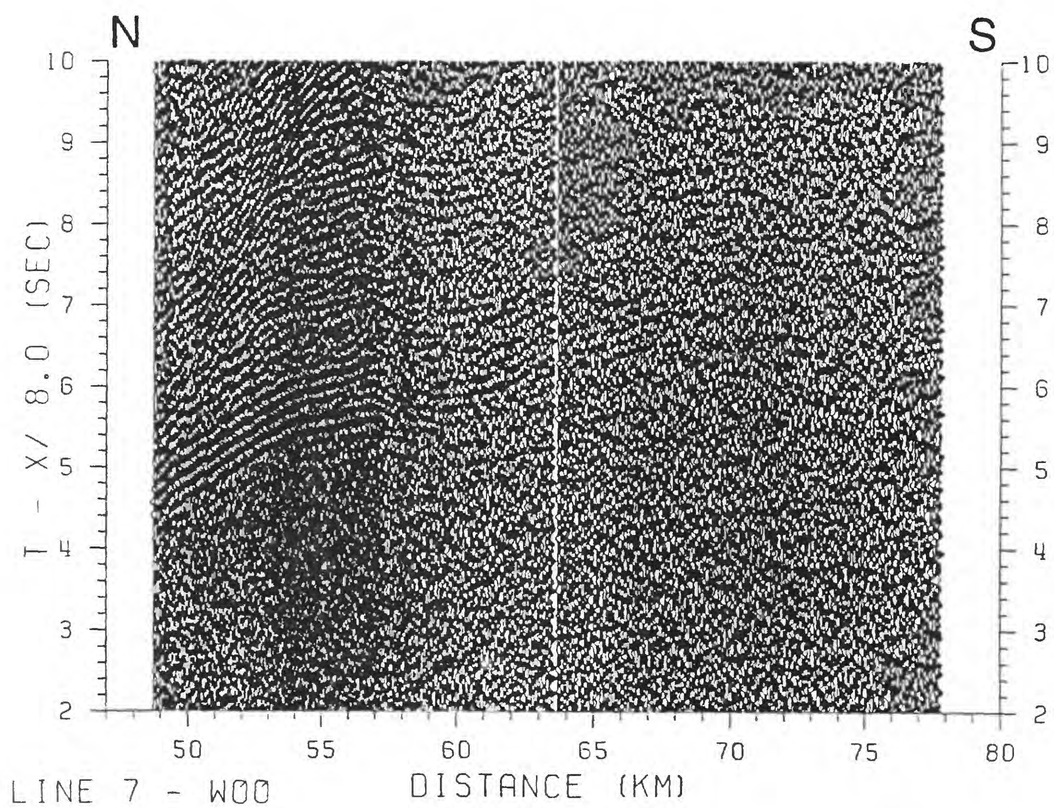

Appendix E.18

REFERENCES

Barry, K. M., D. A. Cravers, and C. W. Kneale, Recommended standards for digital tape formats, *Geophysics*, *40*, 344-352, 1975.

Brocher, T. M., and D.C. Pope, Onshore-offshore wide-angle seismic recordings of the San Francisco Bay Area Seismic Imaging Experiment (BASIX): Data from the Northern California Seismic Network, *U.S. Geol. Surv. Open-File Rept. 94-156*, 123 pp., 1994.

Clague, D. A. and G. B. Dalrymple, The Hawaiian-Emperor volcanic chain. Part I. Geologic evolution, *U. S. Geol. Surv. Prof. Pap.*, *1350*, 5-54, 1987.

Clague, D. A., and R. P. Denlinger, Role of olivine cumulates in destabilizing the flanks of Hawaiian volcanoes, *Bull. Volcanol.*, *56*, 425-434, 1994.

Crosson, R. S., and R. Y. Koyanagi, Seismic velocity structure below the island of Hawaii from local earthquake data, *J. Geophys. Res.*, *84*, 2331-2342, 1979.

Delaney, P. T., R. S. Fiske, A. Miklius, A. T. Okamura, and M. K. Sako, Deep magma body beneath the summit and rift zones of Kilauea volcano, Hawaii, *Science*, *247*, 1311-1316, 1990.

Delaney, P. T., A. Miklius, T. Arnadottir, A. T. Okamura, and M. K. Sako, Motion of Kilauea volcano during sustained eruption from the Puu Oo and Kupaianaha vents, 1983-1991, *J. Geophys. Res.*, *98*, 17801-17820, 1993.

Denlinger, R. P., and P. Okubo, A huge landslide structure on Kilauea volcano, Hawaii, *J. Geophys. Res.*, in press.

Ellsworth, W. L., and R. Y. Koyanagi, Three-dimensional crust and mantle structure of Kilauea Volcano, Hawai, *J. Geophys. Res.*, *82*, 5379-5394, 1977.

Hill, D. P., Crustal structure of the island of Hawaii from seismic-refraction measurements, *Bull. Seism. Soc. Amer.*, *59*, 101-130, 1969.

Hill, D. P., and J. J. Zucca, Geophysical constraints on the structure of Kilauea and Mauna Loa Volcanoes and some implications for seismomagmatic processes, chap. 37 in Decker, R. W., Wright, T. L., and Stauffer, P. H., ed.(s), Volcanism in Hawaii, 2 v., *U.S. Geol. Surv. Prof. Paper 1350*, *2*, 903-917, 1987.

Klein, F. W., Seismic hazards at Kilauea and Mauna Loa volcanoes, Hawaii, *U. S. Geol. Surv. Open-File Rept. 94-216*, 1994.

Kong, L. S. L., P. G. Okubo, W. C. Crawford, J. A. Hildebrand, M. A. Mcdonald, S. C. Webb, F. K. Duennebier, and G. F. Moore, Crustal Imaging of Kilauea Volcano and Loihi Seamount, *EOS, Trans. AGU*, *75*, 645, 1994 (abstract).

Lipman, P. W., J. P. Lockwood, R. T. Okamura, D. A. Swanson, and K. M. Yamashita, Ground deformation associated with the 1975 magnitude-7.2 earthquake and resulting changes in activity of Kilauea Volcano, Hawaii, *U. S. Geol. Surv. Prof. Pap. 1276*, 45 pp., 1985.

Luetgert, J. H., Users manual for RSEC88, Interactive computer program for plotting seismic refraction record sections, *U. S. Geol. Surv. Open-File Rept. 88-262*, 89 pp., 1988.

Luetgert, J., S. Hughes, J. Cipar, S. Mangino, D. Forsyth, and I. Asudeh, Data report for O-NYNEX the 1988 Grenville-Appalachian seismic refraction experiment in Ontario, New York, and New England, *U. S. Geol. Surv. Open-File Rept. 90-246*, 51 pp., 1990.

Moore, J. G., D. A. Clague, R. T. Holcomb, P. W. Lipman, W. R. Normark, and M. T. Torresan, Prodigious submarine landslides on the Hawaiian Ridge, *J. Geophys. Res.*, *94*, 17465-17484, 1989.

Nakamura, K., Why do long rift zones develop in Hawaiian volcanoes? - A possible role of thick oceanic sediments, *Bull. Volc. Soc. Japan*, *25*, 255-269, 1980.

Owen, S., P. Segall, T. Arnadottir, J. Freymueller, and A. Miklius, Rapid displacement of the south flank of Kilauea volcano determined by GPS, *EOS, Trans. AGU*, *74*, 191, 1993.

Rowan, L R., and R. W. Clayton, The three-dimensional structure of Kilauea volcano, Hawaii, from travel time tomography, *J. Geophys. Res.*, *98*, 4355-4375, 1993.

Ryall, A., and D. L. Bennett, Crustal structure of southern Hawaii related to volcanic processes in the upper mantle: *J. Geophys. Res.*, *73*, 4561-4582, 1968.

Swanson, D. A., W. A. Duffield, and R. S. Fiske, Displacement of the south flank of Kilauea volcano: The result of forceful intrusion of magma into the rift zones, *U. S. Geol. Surv. Prof. Pap. 963*, 39 pp, 1976.

Thurber, C. H., Seismic detection of the summit magma complex of Kilauea Volcano, Hawaii: *Science*, *223*, 165-167, 1984.

Tilling, R. I., and J. J. Dvorak, Anatomy of a basaltic volcano, *Nature*, *363*, 125-133, 1993.

Zucca, J. J., and D. P. Hill, Crustal structure of the southeast flank of Kilauea Volcano, Hawaii, from seismic refraction measurements, *Bull. Seism. Soc. Amer.*, *70*, 1149-1159, 1980.

Zucca, J. J., D. P. Hill, and R. L. Kovach, Crustal structure of Mauna Loa Volcano, Hawaii, from seismic refraction and gravity data, *Bull. Seism. Soc. Amer.*, *72*, 1535-1550, 1982.